

DISS. ETH NO. 24934

A Systematic Search for Next Generation Transportation Fuels

A thesis submitted to attain the degree of
DOCTOR OF SCIENCES of ETH ZURICH
(Dr. sc. ETH Zurich)

presented by

Dominik Gschwend
Msc ETH Zurich
born on 24/06/1987
citizen of Altstätten SG

accepted on the recommendation of

Prof. Dr. Alexander Wokaun, examiner
Prof. Dr. Konstantinos Boulouchos, co-examiner
Prof Dr. Frédéric Vogel, co-examiner

2018

Acknowledgements

Dear PROF. DR. ALEXANDER WOKAUN, thank you for the opportunity to write my doctoral thesis on such an interesting and multi-faceted topic at your department at the Paul Scherrer Institut (PSI). In particular I would like to express my gratitude for the productive discussions. A special thanks goes to PROF. DR. KONSTANTINOS BOULOUCHOS for taking on the task of co-examiner of this thesis and sharing his vast knowledge on internal combustion engines. I would like to thank my supervisor PROF. DR. FRÉDÉRIC VOGEL for the freedom he gave me during my dissertation and for his visionary ideas.

This work owes much to DR. PATRIK SOLTIC from Empa especially for his input on engine modeling and more generally for the collaboration – thank you. A special thank you goes belongs to DARIO WÜTHRICH for the countless hours of productive discussions and the time he took to answer all my questions about engines. I would like to thank LUKAS BÄRTSCH for teaching me programming and supporting me whenever I ran into problems with my code. DR. SEBASTIAN MÜLLER, thank you so much for proofreading almost everything I wrote in the past two years and for your invaluable feedback.

Many thanks go to DR. PHILIP EDINGER not only for his collaboration and the effort he put into proofreading the draft of this thesis, but also for all the climbing adventures and conversations we enjoyed together. The readability of this work owes much to DANIEL GSCHWEND, DR. FRANK PILGER, CHRISTOPHER HUNDSTON, DR. ARNIM EYSSLER, DR. SARAH STAUFFER, and PHILIP WISMER for their willingness to proofread the various drafts and for their feedback, thank you so much. I would like to thank CATIA BRUNNENMEISTER for being my personal English helpline and for not letting my climbing training fall short, during the final phase of the thesis. Besides for her effort in proofreading, I would like to thank DR. VERA TSCHEDANOFF for the many coffee breaks and afterwork beers and in particular the accompanying conversations.

To DR. SIMON MAURER: thank you for the collaboration, the support in the past years and all the conversations about everything and nothing. To my friends and co-workers, ERICH DE BONI, TIMON KÄSER, MARTIN KÜNSTLE, DANIEL MEYER, MARTIN WYSS, DR. JOACHIM REIMER, FRANK SCHILLINGER, DAVID SCHOLZ, DR. SINAN TESKE, PATRICK STEIGER and DR. SEBASTIAN VIERECK, thank you for all the support and laughs we shared.

I would like to thank MARTIN ELSENER and DR. ADRIAN MARBERGER for all the time we spent running and enjoying the countryside around PSI. A special thanks goes to MIRJA HARMS, MICHIEL HARTE, BIANCA TETZEL, CORNEL GMÜNDER, CORINNE DÜNNER, ANDREAS MÜLLER and URBAN LACHENMEIER for all the climbing,

mountaineering, skiing and camping expeditions and all the good memories connected to them. It was a huge pleasure and helped to keep me motivated, I look forward to next adventures.

To my parents ROBERT and KARIN as well as my brothers SIMON, DANIEL and FLORIAN, family and all of my friends: thank you for your support and incredible help over the past years.

Villigen, 28/08/2018

Dominik Gschwend

Abstract

The transportation sector is globally the second biggest consumer of energy and is almost exclusively relying on fossil fuels to satisfy its demand. To avoid a global temperature rise of more than 2°C until 2100, CO₂ emissions have to be drastically reduced. Eventually, this requires either alternative propulsion systems or CO₂-neutral fuels. Numerous compounds have already been proposed as potential gasoline replacement. A methodical comparison or systematical design of fuels is hindered by the fact that the specifications of the ideal fuel are unknown. Therefore within the presented thesis a tool was developed to evaluate the performance of possible fuel compounds, either as pure substance or a mixture. Furthermore, a novel algorithm to design molecules for fuel applications is presented, the so-called reverse Group Contribution Method (rGCM).

The influence of fuel properties on engine performance is complex. Universal specifications of the ideal fuel are therefore not available. To overcome this problem, a thermodynamic model of a Spark Ignition (SI) Direct Injection (DI) Internal Combustion Engine (ICE) was developed. The model focuses on fuel-related influences on engine performance and is able to evaluate pure compounds and mixtures. Besides the Research Octane Number (RON), the model requires only readily available properties as input (liquid density, vapor heat capacity, liquid viscosity, vapor pressure, enthalpy of vaporization and elemental composition). The main purpose of the model is to determine the potential of a compound as gasoline replacement. Therefore the efficiency of the engine at 2000 rpm and full load is maximized for each compound by adapting the compression ratio limited by knock and a peak pressure (25 MPa). After this design step, the engine model was used to determine the performance at full and part load and over defined driving cycles.

An extensive literature review identified 34 different biofuels. These compounds were compared to gasoline using the engine model. The evaluated parameters included efficiency, specific CO₂ emissions both at 2000 rpm and full load, as well as consumption and CO₂ emissions over the Worldwide harmonized Light vehicles Test Cycle (WLTC). None of the biofuels result in lower consumption *and* lower CO₂ emissions than gasoline. However, there is a compound superior to gasoline, for each of the measures. Maximum efficiency is achieved by ethyl levulinate with 38.6% compared to 33.7% the efficiency of gasoline. Minimum CO₂ emissions are achieved by *sec*-butanol with 177 g/km *vs.* 193 g/km in the case of gasoline. 2-phenylethanol minimizes consumption (7.21/100 km) which is significantly lower than gasoline (8.21/100 km).

Fast pyrolysis is a well-established process to liquefy lignin. The product is a mixture of mostly aromatic carbons called bio-oil. Due to its properties, this bio-oil is not suited as fuel for SI engines. Therefore, an upgrading step called Hydrodeoxygenation (HDO)

has been proposed in the literature. To model the upgrading process a generalized reaction pathway is presented. The performance of each of the intermediate upgrading products was determined using the engine model. For full HDO, an average of $7 \text{ mol}_{\text{H}_2}/\text{mol}_{\text{oil}}$ is required. The results indicate that with roughly $4 \text{ mol}_{\text{H}_2}/\text{mol}_{\text{oil}}$, well-suited fuels can be produced. Further HDO does not lead to any kind of improved fuels. β -methylstyrene has been identified as the compound resulting from the upgrading process with minimum consumption ($6.91/100 \text{ km}$). 1,2,3-trimethoxy-5-ethylcyclohexane maximizes efficiency (40.2%) and minimizes specific CO_2 emissions (174 g/km).

An algorithm to optimized mixture compositions was developed based on considerations in terms of energy per mole of CO_2 emitted *vs.* volumetric energy density. This mixture optimization algorithm aims to identify biofuel mixtures with both lower consumption *and* lower specific CO_2 emissions than gasoline. However, no such mixtures could be identified. Nonetheless, 82 different mixtures were identified with comparable performance as gasoline. In general, these mixtures consist in average of $34 \text{ mol}\%$ 2-phenylethanol, $7 \text{ mol}\%$ methyl valerate as well as butanol and pentanol isomers in varying compositions and to different extents.

A novel Computer Aided Molecular Design (CAMD) method was developed by combining the ICE model with Group Contribution Methods (GCMs) from the literature and a pattern search optimization algorithm. Two different scenarios were evaluated: firstly, an unrestricted search for the perfect liquid fuel, and secondly, an upper limit to the boiling point (at the cylinder wall temperature 470 K) was introduced. The unrestricted search led to the identification of three sets of isomers with almost identical performance. They provide a full load efficiency at 2000 rpm of 40.7% , a consumption of $6.51/100 \text{ km}$ and specific CO_2 emissions of 157 g/km over the WLTC. The second run including the boiling point limitation identified the following four compounds: 2,2,3,3,4,4-hexamethylpentane, β -methylstyrene, 3,5,6,7-tetramethyloctan-2-one and 3-methyl-2-buten-2-ol. 2,2,3,3,4,4-hexamethylpentane and 3,5,6,7-tetramethyloctan-2-one are superior to all discussed fuels (including gasoline) with respect to all investigated parameters, but inferior to the results of the unrestricted search. β -methylstyrene results in minimum consumption at the costs of increased CO_2 emissions. 3-methyl-2-buten-2-ol leads to maximum efficiency but shows increased consumption when compared to gasoline. Overall, the compounds of the boiling point limited search resulted in efficiencies of 36.2% to 39.5% at 2000 rpm and full load, specific CO_2 emissions of 166 g/km to 211 g/km and consumptions in the range of $6.91/100 \text{ km}$ to $8.51/100 \text{ km}$ over the WLTC.

In a nutshell it can be concluded that fuels superior to gasoline exist and that the presented CAMD method is able to identify them. Furthermore, the ICE model provides a versatile tool to investigate the suitability of molecules and mixtures as gasoline replacement. To share the model with the scientific community it was made publicly available at <http://fuel-simulation.psi.ch>.

Zusammenfassung

Weltweit ist der Transportsektor der zweitgrösste Energieverbraucher und basiert weitgehend auf fossilen Energieträgern. Um den weltweiten Temperaturanstieg in Folge des Klimawandels auf maximal 2°C bis zum Jahr 2100 zu begrenzen, müssen die CO₂-Emissionen stark reduziert werden. Demzufolge müssen entweder alternative Antriebskonzepte oder CO₂-neutrale Treibstoffe zur Anwendung kommen. Es wurden bisher zahlreiche alternative Treibstoffe in die Diskussion eingebracht. Einem methodischen Vergleich dieser Treibstoffe oder gar einer systematischen Suche nach dem idealen Treibstoff steht das Fehlen allgemeingültiger Spezifikationen im Weg. In dieser Dissertation wurde deshalb ein Modell entwickelt, um die Eignung eines Stoffes (Reinstoff oder Mischung) als Benzinersatz zu evaluieren. Darauf aufbauend wurde eine neuartige systematische Suche nach dem idealen Treibstoff entwickelt, die sogenannte reverse Group Contribution Method (rGCM).

Der Einfluss des Treibstoffes auf das Verhalten des Motors sind komplex. Dementsprechend sind allgemeingültige Spezifikationen des idealen Treibstoffes nicht ableitbar. Um dieses Problem zu umgehen, wurde ein thermodynamisches Modell eines fremdgezündeten, direkteinspritzenden Verbrennungsmotor entwickelt. Das Modell legt speziellen Wert auf den Einfluss des Treibstoffes auf den Motor und akzeptiert sowohl Reinstoffe als auch Mischungen. Neben der Oktanzahl bedingt das Modell nur gut verfügbare Eigenschaften als Eingabeparameter: Dichte (flüssig), Wärmekapazität des Dampfes, Viskosität (flüssig), Dampfdruck, Verdampfungsenthalpie sowie elementare Zusammensetzung. Die Hauptaufgabe des Modells ist es, das Potenzial eines Stoffes als Benzinersatz zu ermitteln. Dazu wird das optimale Verdichtungsverhältnis für den jeweiligen Stoff ermittelt. Das optimale Verdichtungsverhältnis ist definiert durch den maximalen Wirkungsgrad bei 2000 rpm und unter Vollast — unter der Voraussetzung, dass weder die Druckobergrenze (25 MPa) überschritten wird, noch Klopfen auftritt. Nach diesem Designschritt wird das Motorenmodell verwendet, um die Leistungsfähigkeit des Stoffes bei Voll- und Teillast sowie über bestimmte Fahrzyklen zu studieren.

Durch eine umfangreiche Literaturstudie konnten 34 Biotreibstoffe identifiziert werden. Diese Stoffe wurden mit Hilfe des Modells mit Benzin verglichen. Als Vergleichsparameter wurden Wirkungsgrad und CO₂-Emissionen bei 2000 rpm und unter Vollast sowie der Verbrauch und CO₂-Emissionen über den WLTC verwendet. Keiner der untersuchten Stoffe ist Benzin in allen Kriterien überlegen. Jedoch gibt es für jedes einzelne Kriterium einen Treibstoff, welcher besser als Benzin ist. So wird der Wirkungsgrad von Benzin (33.7%) von Ethyllevulinat mit 38.6% übertroffen. Die niedrigsten CO₂ Emission wurden für *sec*-Butanol (177 g/km) ermittelt, gegenüber Benzin mit 193 g/km. Minimalen Verbrauch wurde durch 2-Phenylethanol mit 7.21/100 km erreicht, im Vergleich dazu liegt der Verbrauch von Benzin bei 8.21/100 km.

Ein kostengünstiger Weg zur Verflüssigung von Biomasse ist die Pyrolyse: Wird mit diesem Prozess Lignin verflüssigt, entsteht eine Mischung aus hauptsächlich aromatischen Verbindungen, genannt Bioöl. Die Eigenschaften dieses Bioöls stehen einer direkten Verwendung als Treibstoff in einem Ottomotor entgegen. In der Literatur wurde deshalb die Hydrodeoxygenation (HDO) als Aufbereitungsprozess vorgeschlagen. Dieser Aufbereitungsprozess wurde anhand eines verallgemeinerten Netzwerks von Reaktionen modelliert. Anschliessend wurde jedes einzelne Zwischenprodukt mit Hilfe des Motorenmodells auf seine Eignung als Treibstoff untersucht. Durchschnittlich werden für vollständige HDO $7 \text{ mol}_{\text{H}_2}/\text{mol}_{\text{Oil}}$ benötigt. Die Resultate zeigen jedoch, dass die am besten geeigneten Treibstoffe mit etwa $4 \text{ mol}_{\text{H}_2}/\text{mol}_{\text{Oil}}$ hergestellt werden können. Eine weiterführende HDO führt in keiner Weise zu besser geeigneten Treibstoffen. Als Treibstoff mit minimalem Verbrauch ($6.91/100 \text{ km}$) wurde β -Methylstyren identifiziert. 1,2,3-Trimethoxy-5-Ethylcyclohexan führt zu minimalen spezifischen CO_2 -Emissionen (174 g/km) und dem maximalen Wirkungsgrad von 40.2% .

Ein Algorithmus zur Optimierung von Mischungen wurde basierend auf einem Vergleich von Energie pro ausgestossenen Mol- CO_2 und volumetrischer Energiedichte entwickelt. Die Aufgabe des Algorithmus war es, aus den bestehenden 34 Biotreibstoffen Mischungen zu identifizieren, welche einen niedrigeren Verbrauch *und* niedrigere CO_2 -Emissionen als Benzin aufweisen. Es war nicht möglich solche Mischungen zu identifizieren. Es wurden jedoch 82 Mischungen mit vergleichbarer Leistungsfähigkeit wie Benzin identifiziert. Im Allgemeinen bestehen diese Mischungen im Durchschnitt aus $34 \text{ mol}\%$ 2-Phenylethanol, $7 \text{ mol}\%$ Methylvalerat sowie Butanol- und Pentanolisomeren in wechselnder Zusammensetzung.

Durch die Kombination des Motorenmodells mit Gruppenbeitragsmethoden (GCM) aus der Literatur und einem Optimierungsalgorithmus entstand eine neuartige CAMD Methode, mit deren Hilfe der optimale Treibstoff für zwei verschiedene Szenarien gesucht wurde: Erstens wurde eine unbeschränkte Suche durchgeführt und zweitens wurde eine Obergrenze für den Siedepunkt eingeführt (entsprechend der Zylinderwandtemperatur von 470 K). Die unbeschränkte Suche identifizierte drei Sets von Isomeren mit identischer Leistungsfähigkeit. Bei 2000 rpm und unter Volllast erreichen sie einen Wirkungsgrad von 40.7% . Über den WLTC kommt es zu einem Verbrauch von $6.51/100 \text{ km}$ und einem CO_2 -Ausstoss von 157 g/km . Im zweiten Szenario wurden vier Moleküle gefunden: 2,2,3,3,4,4-Hexamethylpentan, β -Methylstyren, 3,5,6,7-Tetramethyloctan-2-on und 3-Methyl-3-buten-2-ol. Die Moleküle, welche im unbeschränkten Szenario gefunden wurden, zeigen eine bessere Leistungsfähigkeit als jene des siedepunktlimitierten Szenarios. 2,2,3,3,4,4-Hexamethylpentan sowie 3,5,6,7-Tetramethyloctan-2-on sind allen bisher diskutierten Treibstoffen (inklusive Benzin) in Bezug auf alle Parametern überlegen. β -Methylstyren führt zu minimalem Verbrauch verbunden mit einem Anstieg der CO_2 -Emissionen. 3-Methyl-3-buten-2-ol maximiert den Wirkungsgrad, führt allerdings zu einem grösseren Verbrauch als Benzin. Die Zielmoleküle des siedepunktlimitierten Szenarios resultieren in einem Wirkungsgrad zwischen 36.2% und 39.5% bei 2000 rpm und Volllast. Über den WLTC wurde ein Verbrauch von $6.91/100 \text{ km}$ bis $8.51/100 \text{ km}$, sowie ein CO_2 -Ausstoss im Bereich von 166 g/km bis 211 g/km ermittelt.

Zusammenfassend kann gesagt werden, dass besser geeignete Treibstoffe als Benzin

existieren und die hier vorgestellte CAMD-Methode in der Lage ist, diese zu identifizieren. Des Weiteren stellt das Motorenmodell ein vielseitiges Werkzeug dar, um die Eignung von Reinstoffen oder Mischungen als Benzinersatz zu untersuchen. Das Modell wurde daher der wissenschaftlichen Gemeinschaft unter <http://fuel-simulation.psi.ch> zugänglich gemacht.

Contents

Acknowledgments	iii
Abstract	v
Zusammenfassung	vii
Glossary	xv
1 Introduction	1
1.1 Motivation	1
1.2 Objective of the Project	2
2 Theoretical Background	5
2.1 Biofuels	5
2.2 Internal Combustion Engines	11
2.2.1 Theory	11
2.2.2 Knocking	14
2.2.3 Modeling Approaches	15
2.3 Fuel – Engine Interaction	16
2.4 Property Estimation	17
2.5 Computer Aided Molecular Design	18
3 Modeling	21
3.1 Engine Modeling	21
3.1.1 Process Description	21
3.1.2 Input Parameters and Derived Fuel Properties	21
3.1.3 Intake	23
3.1.4 Fuel Injection and Evaporation	23
3.1.5 Compression and Expansion	26
3.1.6 Combustion	27
3.1.7 Knock Model	30
3.1.8 Friction	31
3.1.9 Gas Exchange	31
3.1.10 Adaptation of ϵ_{CR}	32
3.1.11 Model Output	33
3.1.12 Further Influences	34
3.2 Validation	34
3.2.1 Experimental Validation	34

3.2.2	Extended Validation	36
3.3	Sensitivity Analysis	38
3.3.1	Method	38
3.3.2	Convergence	39
3.3.3	Results and Discussion	39
3.4	Model Extensions	41
3.4.1	Driving Cycle Modeling	41
3.4.2	Mixtures	42
3.4.3	Hybrid Powertrains	46
4	Review of the Performance of Pure Fuels	49
4.1	Introduction	49
4.2	Results and Discussion	51
4.2.1	Loss Analysis	51
4.2.2	Single Load Points	52
4.2.3	Cycle Operation	57
4.2.4	Hybrid Powertrains	58
4.3	Summary	59
5	Fuel Design based on Lignin Pyrolysis Oil	61
5.1	Introduction	61
5.2	Upgrading	62
5.3	Method	68
5.4	Results and Discussion	68
5.4.1	Compliance with Boundary Conditions	68
5.4.2	Group Influences	68
5.4.3	Optimized Selections	69
5.4.4	Single Compounds	72
5.4.5	Influence of Selected Groups	72
5.5	Conclusion	75
6	Optimization of Mixtures of Established Fuels	77
6.1	Introduction	77
6.2	Algorithm	78
6.3	Results and Discussion	80
6.4	Conclusions	85
7	Systematic Fuel Design using the reverse Group Contribution Method	87
7.1	Concept	87
7.2	Adaptations	89
7.2.1	Group Matching	89
7.2.2	Aromatic Rings	89
7.3	Algorithm	90
7.3.1	Group Classification	90
7.3.2	Iteration Procedure	90

7.3.3	Validity	93
7.3.4	Grading	97
7.3.5	Processing of Results	99
7.4	Results	99
7.5	Conclusions	104
8	Summary, Conclusions and Outlook	105
8.1	Summary	105
8.2	Conclusions	106
8.3	Outlook	109
8.3.1	Modeling	109
8.3.2	Established Fuels	109
8.3.3	The reverse Group Contribution Method (rGCM)	110
	Bibliography	111
	List of Figures	129
	List of Tables	133
	Curriculum Vitae	135
	List of Publications	137
	Appendix	138
A	Internal Combustion Engine	141
A.1	Thermodynamic Modeling Constants	141
A.2	Heat Transfer – Compound dependence	141
A.3	Engine Testbench Configuration	144
B	Established Fuels	145
B.1	Correlation RON–dCN	145
B.2	Results	146
C	Fuel from Pyrolysis Oil	149
D	Mixtures	151
E	The reverse Group Contribution Method	157
E.1	List of Groups	157
E.2	Structure Optimization Results	160

Glossary

AAE	Average Absolute Error
AFR	Air-to-Fuel Ratio
ARE	Average Relative Error
BDC	Bottom Dead Center
<i>bmep</i>	break mean effective pressure
CADC	Common Artemis Driving Cycle
CAMD	Computer Aided Molecular Design
CFD	Computational Fluid Dynamics
CI	Compression Ignition
CN	Cetane Number
dCN	derived Cetane Number
DI	Direct Injection
diB	diisobutylene
DMF	2,5-dimethylfuran
EE	Elementary Effect
EGR	Exhaust Gas Recirculation
EL	ethyl levulinate
Empa	Swiss Federal Laboratories for Materials Science and Technology
ETBE	ethyl <i>tert</i> -butyl ether
FFA	furfuryl alcohol
<i>fmep</i>	friction mean effective pressure
GCM	Group Contribution Method
GSA	Global Sensitivity Analysis
GVL	γ -valerolactone
HDO	Hydrodeoxygenation

HHV	Higher Heating Value
ICE	Internal Combustion Engine
<i>imep</i>	indicated mean effective pressure
ipE	diisopropyl ether
LCA	Life Cycle Analysis
LH	Latin Hypercube
LHV	Lower Heating Value
2-MF	2-methylfuran
ML	methyl levulinate
MON	Motor Octane Number
MTBE	methyl <i>tert</i> -butyl ether
2-MthF	2-methyltetrahydrofuran
3-MthF	3-methyltetrahydrofuran
NEDC	New European Driving Cycle
OI	Octane Index
ORC	Organic Rankine Cycle
PM	Particulate Matter
QPPR	Quantitative Property–Property Relation
QSPR	Quantitative Structure–Property Relation
rGCM	reverse Group Contribution Method
RMSE	Root Mean Square Error
RON	Research Octane Number
SA	Sensitivity Analysis
SI	Spark Ignition
TDC	Top Dead Center
TMED	2-ethyl-2,4,5-trimethyl-1,3-dioxolane
WLTC	Worldwide harmonized Light vehicles Test Cycle

Nomenclature

Symbols

A	area	[m ²]
a	activity coefficient	[-]
aC	aromatic carbon	
B	bore	[m]
c	specific heat capacity	[J/(mol K)]
c	consumption	[l/100 km]
c_m	mean piston velocity	[m/s]
c_D	drag coefficient	[-]
d	diameter	[m]
E	energy	[J]
e	emission	[kg]
F	force	[N]
h	specific enthalpy	[J/mol]
K	constant	
k	thermal conductivity	[W/(m K)]
k_1	knock index	[-]
M	molar mass	[kg/mol]
m	mass	[kg]
N	revolution speed	[rpm]
Nu	Nusselt number	[-]
n	number	[-]
P	power	[W]
p	pressure	[Pa]
Pr	Prandtl number	[-]
Q	heat	[J]
Re	Reynolds number	[-]

S	stroke	[m]
s	entropy	[J/(mol K)]
T	temperature	[K]
T_{auto}	autoignition temperature	[K]
T_{boil}	boiling point	[K]
T_{melt}	melting point	[K]
t	time	[s]
u	flow velocity	[m/s]
V	volume	[m ³]
v	number of nitrogen atoms	[-]
v	velocity	[m/s]
W	work	[J]
We	Weber number	[-]
w_i	mass fraction of compound i	[-]
x	number of carbon atoms	[-]
x_i	mole fraction of compound i	[-]
x	property	
y	number of hydrogen atoms	[-]
y_i	volume fraction of compound i	[-]
z	number of oxygen atoms	[-]
α	heat transfer coefficient	[W/(m ² K)]
β	fitting constant	
δ	constant	
ε_{tot}	total energy input	[J/mol]
ε_{CR}	compression ratio	[-]
η	efficiency	[-]
κ	heat capacity ratio	[-]
μ	dynamic viscosity	[Pa s]
μ	friction coefficient	[-]
ν	kinematic viscosity	[m ² /s]
ξ	combustion progress	[-]
Π	pressure ratio	[-]
ρ	density	[kg/m ³]
σ	surface tension	[N/m]

ς	group contribution	[-]
τ_{ig}	ignition delay	[s]
φ	crank angle	[rad]
χ	grading criteria	[-]
χ^N	normalized grading criteria	[-]

Constants

g	gravitational acceleration	= 9.81 m/s ²
R	gas constant	= 8.314 J/(mol K)

Subscript

0	initial
ac	after cooler
acc	acceleration
amb	ambient
b	burnt
bt	turbine backpressure
c	compressor
circ	circular
cyc	cycle
cyl	cylinder
D	displacement
d	droplet
diss	dissipative
est	estimation
ex	exhaust
f	fuel
FL	full load: 2000 rpm, 2 bar charging pressure
fric	friction
g	gaseous

h	heating
hp	hybrid powertrain
in	intake, input
inj	injection
L	liquid
mech	mechanical
mix	mixture
out	output
p	pump
PL	part load: 2000 rpm, 6.6 kW brake power
r	recuperation
ref	reference
req	required
t	turbine
tc	turbocharger
tot	total
ub	unburnt
vap	vapor
w	wall

1 Introduction

1.1 Motivation

It is well-established that environmental disturbances due to global climate change lead to irreversible transformations of the planet and the ecosystem [1]. The Paris Agreement (COP 21, 2015) aims to limit this by keeping the global temperature rise well below 2 °C until the end of the century. To achieve this, less than 2900 Gt of CO₂ should be emitted in this time span, of which up to now about 1900 Gt have already been emitted [1].

On a global scale, the transportation sector is the second largest energy consumer (29% in 2015 [2]) and is almost exclusively based on fossil fuels (95.8% in 2015 [3]). A detailed overview of the shares of energy consumption and the energy mix of transportation is given for both the World and Switzerland in Fig. 1.1.

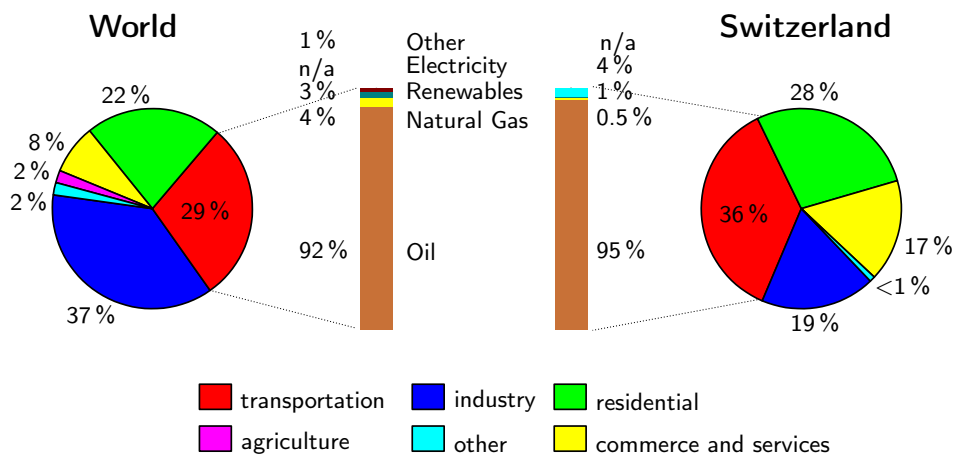


Figure 1.1: Overview of the total energy consumption by sectors globally and for Switzerland including the energy sources used in transportation. Adapted from [2–4], values given for 2015.

In Switzerland the energy demand due to transportation sums up to 36% of the total energy demand in the same period [4]. This accounts for roughly one third of the Swiss CO₂ emissions (about 70% of that is due to passenger cars [5]). If Switzerland wants to fulfill the Paris Agreement, CO₂ emissions per kilometer have to be reduced by 65% until 2040 and reach zero by 2060 [6]. Thus, two different approaches are envisaged: reduced consumption and alternative fuels. The consumption may be reduced by

technological measures, e.g. increased efficiency, reduced car weight and electrification. It is also affected by customer requirements and behaviors which either enhance or diminish the effect of technological measures. Nowadays, there are two alternatives for fossil fuels on the market: ethanol (to replace gasoline) and biodiesel (to replace diesel fuel). Ethanol for fuel applications is mainly produced from sugarcane and maize, triggering a competition between fuel and food production. Further research on other fuels or different production pathways to utilize other feedstocks is therefore inevitable. It has been stated that Internal Combustion Engines (ICEs) will remain dominant in surface transportation by 2030 with a share above 80 % [7]. This implies the quest for alternatives.

The discussion includes alternatives to the ICE as well as a small number of compounds as alternative fuels for ICEs [8–10]. For a biofuel to be considered as “drop-in” it must fulfill all current fuel standards and to be compatible with the infrastructure in place. A comprehensive review on generally discussed compounds will be given in Section 2.1. However, the requirements for the optimal fuel/propulsion pair are numerous, ranging from sustainable production, over ease of handling to zero emissions. Sustainability combines the environmental burdens of production, usage and disposal. It is generally assessed using Life Cycle Analysis (LCA). Due to the contribution of production the sustainability of a fuel not only depends on its performance, but also on the feedstock and the production pathway.

The most common approaches to identify alternative fuels are the following: Either as the output of well-established production processes or as compounds with similar properties to the existing ones. Neither approach is expected to give ideal results by design. Although the ICE has been optimized for gasoline or diesel over the last 100 years, there are hopeful indications that better fuels can be found. Increases in efficiency have been shown for example by replacing gasoline with ethanol [11–14].

In this light, there is probably no single perfect solution, but numerous optimal solutions for different applications. One example is aviation where fuel specifications are strictly regulated, and safety considerations are important. Thus, it is expected that only drop-in biofuels stand a chance. Another example is short distance travel which might be dominated by battery powered cars in the near future.

1.2 Objective of the Project

The aim of this thesis was to identify the most suitable alternative to gasoline. A novel combination of Computer Aided Molecular Design (CAMD) techniques and ICE modeling was applied to obtain this target. A graphical overview of the structure of this thesis is given in Fig. 1.2.

This approach allowed the design of molecules optimized for the application as gasoline alternatives. The project was divided into several sub-projects. First, a model of a Spark Ignition (SI) ICE focusing on fuel influence was developed which allowed for fast and efficient comparison between different compounds (Chapter 3). Second, the compounds proposed to replace gasoline were reviewed using the model (Chapter 4).

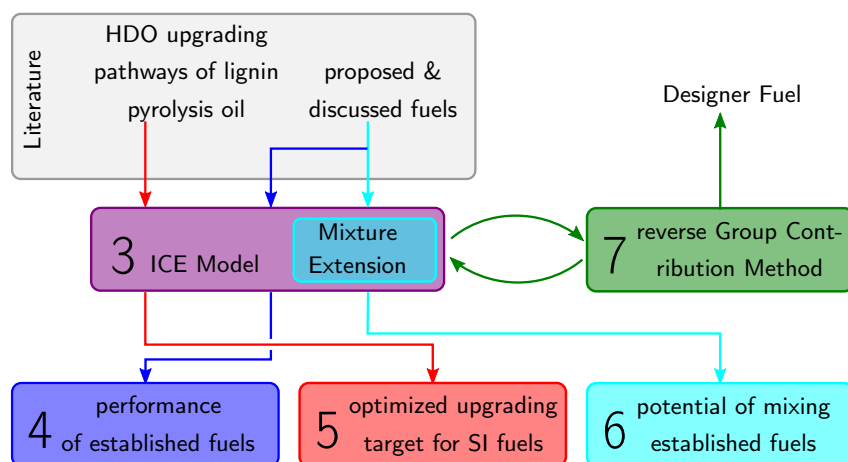


Figure 1.2: Graphical overview of the structure of this thesis. Numbers related to the respective chapters.

Third, the versatility of the model was assessed using different upgrading products of lignin pyrolysis oil (Chapter 5). Furthermore, the model was extended to fuel mixtures with the aim of obtaining the fuel mixtures superior to gasoline (Chapter 6). Finally, an algorithm was developed to optimize the structure of a molecule for its performance as fuel (Chapter 7).

The tasks of the different sub-projects are the following:

- Development of an SI engine model able to judge the performance of pure compounds and mixtures without experimental input (Chapter 3).
- Critical review of the performance of currently discussed fuels using the engine model (Chapter 4).
- Studying the Hydrodeoxygenation (HDO) upgrading process of lignin pyrolysis oil to determine the best-suited fuels derivable from it (Chapter 5).
- Attempts to overcome the shortcomings of discussed biofuels by mixing to identify mixtures with superior performance than gasoline (Chapter 6).
- Developing the reverse Group Contribution Method (rGCM) to design the perfect SI fuel (Chapter 7).

An overall summary and conclusions will be given in Chapter 8 including suggestions for further work on the different topics.

2 Theoretical Background

2.1 Biofuels

The discussion about fuels for ICEs is about as old as the engine itself. The famous Ford Model T launched in 1908, for example ran on ethanol [16]. However, the availability of cheap petroleum displaced ethanol rapidly. Ever since, the discussion about fuel alternatives has frequently reappeared, either due to reduced petroleum availability (e.g. oil crisis) or due to environmental considerations. The scientific community is still far from having reached a consensus on the fuel best-suited as gasoline replacement. As the requirements for fuels range from sustainable production over engine performance to environmental impact, it is difficult to identify *a priori* the optimal biofuel for all purposes. This difficulty is reflected by the fact that so far a wide range of compounds has been proposed and discussed. Different compounds are commonly theoretically assessed based on their properties. Experimental studies are most often limited to one or two of the most well-known compounds in comparison with gasoline on a given engine. In this section an overview of discussed biofuels shall be given. A compound is considered as soon as experimental values for either Research Octane Number (RON) or derived Cetane Number (dCN) are available. Compounds lacking this key fuel parameter are not considered, as these compounds lack the most basic experimental considerations. Thereby they have been proposed, but have not entered the discussion.

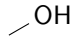
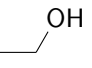
Currently, the most commonly used alternative liquid fuel for SI engines is ethanol, one of the reasons being its well-established production process from carbohydrate fractions of biomass. Other compounds frequently discussed include methanol, *n*-butanol, and more recently 2-methylfuran (2-MF) and 2,5-dimethylfuran (DMF) [17–19]. An extensive review of the suitability of *n*-butanol as gasoline replacement concluded that the usage of *n*-butanol may overcome many of the drawbacks of ethanol [20]. However, empirically an excessive oil dilution of up to 24 % of the injected fuel was noticed. Thus pure *n*-butanol is not suited as fuel [21]. Recently, Raman *et al.* [22] proposed to use α -pinene as a gasoline replacement because its energy content is similar to gasoline and therefore a similar driving range is expected. The application of CAMD methods led to the identification of 2-butanone, 2-MF, DMF, isobutanol, diisopropyl ether, methyl-isopropyl ketone and isobutyraldehyde as possible alternatives [23]. Another CAMD study listed 2-MF, DMF, 2-butanone, methyl isobutyl ketone, ethyl acetate, ethyl propanoate, propyl acetate and isopropyl acetate as ideal SI fuels to be produced from cellulose and hemicellulose [24]. A review based on pathways starting from furfural revealed 2-MF and ethyl furfuryl ether as best gasoline replacements [19]. Using

Contents of this chapter have been published or submitted: [15]

metabolic engineering, it is possible to produce butanol isomers and 2-phenylethanol from glucose using *Escherichia coli* [25].

In Table 2.1 a list of the frequently discussed biofuels is given, together with findings on their suitability as gasoline replacements from recent studies.

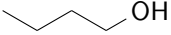
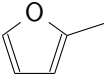
Table 2.1: Comparison between different frequently discussed alternative fuels.

compound	discussion
methanol 	<p>ADVANTAGES: engine: increased combustion efficiency [14, 26]; increased power output [27]; high RON [28]; miscible with gasoline [29] environment: reduced CO, HC, NO_x emissions [14, 26, 27, 30]; biodegradable [31]</p> <p>DISADVANTAGES: engine: corrosive to fuel system [27, 32]; increased specific fuel consumption [14]; high enthalpy of vaporization [33]; cold start problematic [27] environment: completely miscible with water [28, 34]; tendency to increase Particulate Matter (PM) emissions* [26]; increased aldehyde emissions* [30] health and safety: toxic [28]; poor visibility of flame [28, 31]; safety issues due to broad flammability limits [27]</p> <p>STATUS: abandoned — extensive road trials in the US in the 1980s [27]</p>
ethanol 	<p>ADVANTAGES: engine: high RON [11]; increased engine efficiency [11–14, 26]; increased combustion efficiency [14]; broader flammability limits• [28]; increased flame speed• [28]; miscible with gasoline [29, 35] environment: reduced NO_x [21]* [36] and HC emissions• [11, 13]* [36]; reduced CO emissions* [12, 14, 37]; reduced PM emissions*• [36–40]</p> <p>DISADVANTAGES: engine: cold start problems [11]; increased specific fuel consumption [11, 14]; low energy density; corrosive to fuel system [32]; incompatibility with classical seals [32]; increased oil dilution [21] environment: completely miscible with water [32, 34]; increased HC emissions* [37]; increased aldehyde emissions* [39] health and safety: low flame luminosity [28]; toxic [28]</p> <p>STATUS: only liquid renewable gasoline alternative in place today</p>

*: determined for mixtures with gasoline

•: compared to gasoline

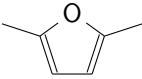
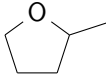
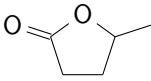
Table 2.1 — *continued*

compound	discussion
<p><i>n</i>-butanol</p> 	<p style="text-align: center;">ADVANTAGES:</p> <p>engine: increased engine efficiency[•] [21, 41, 42]; not hygroscopic [43]; less corrosive than ethanol [43]; possible drop-in fuel [43, 44]; lower tendency to vapor lock (compared to ethanol) [20]; less prone to cold start problems than ethanol [20]; miscible with gasoline [42, 44]</p> <p>environment: reduced NO_x emissions[•] [21, 41][*] [36]; reduced PM emissions[*] [36, 45, 46]; established industrial process from renewable sources (ABE fermentation) [43]</p> <p>health and safety: low volatility [20]</p> <p style="text-align: center;">DISADVANTAGES:</p> <p>engine: low Lower Heating Value (LHV)[•] [20]; increased oil dilution [21]</p> <p>environment: increased HC emissions [21]</p> <p style="text-align: center;">STATUS:</p> <p>well-established — numerous experimental studies (e.g. pure [21, 42, 44] as well as mixed with gasoline [42, 44]; comprehensive review including production pathways [20])</p>
<p>2-MF</p> 	<p style="text-align: center;">ADVANTAGES:</p> <p>engine: improved cold startability (compared to ethanol) [47, 48]; high RON [17, 47]; lower oil dilution than ethanol [47]; increased combustion stability[•] [47]; increased power output^{••} [48]; increased efficiency[•] [17, 49]; miscible with gasoline [48, 50]</p> <p>environment: insoluble in water [34, 35]; decreased CO and HC emissions[*] [48, 50]; lower HC emissions than both gasoline [17, 49] and DMF [17]; decreased PM emissions[•] [17]</p> <p style="text-align: center;">DISADVANTAGES:</p> <p>engine: tendency to polymerize [51]; increased fuel consumption^{••} [48]</p> <p>environment: higher NO_x emissions than both gasoline [17, 49] and DMF [17, 48];</p> <p>health and safety: formation of explosive peroxides upon contact with air [34]; toxic [34]</p> <p style="text-align: center;">STATUS:</p> <p>well-established — numerous experimental studies (e.g. experimentally tested pure [17, 47, 49] and mixed with gasoline [48, 50])</p>

*: determined for mixtures with gasoline

•: compared to gasoline

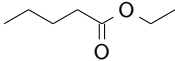
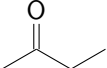
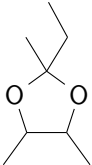
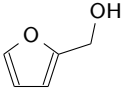
Table 2.1 — *continued*

compound	discussion
DMF 	<p>ADVANTAGES:</p> <p>engine: similar combustion properties • [52, 53]; RON and rate of combustion higher than gasoline [17, 54]; well-suited as pure fuel [53]; miscible with gasoline [55, 56]</p> <p>environment: insoluble in water [35, 57]; similar emission levels • [53, 58]; no significant increase in PM emission* • [38, 56]</p> <p>DISADVANTAGES:</p> <p>engine: gum formation* [55]</p> <p>health and safety: formation of explosive peroxides upon contact with air [34]; toxic [34]</p> <p>STATUS:</p> <p>well-established — numerous experimental studies (e.g. pure [17, 53, 54, 58] as well as mixed with gasoline [56]); detailed kinetic combustion model available [59]</p>
2-MthF 	<p>ADVANTAGES:</p> <p>engine: stable/no tendency to polymerize; miscible with gasoline [51]</p> <p>environment: biodegradable; sustainable production from lignocellulosic biomass [60, 61]</p> <p>DISADVANTAGES:</p> <p>environment: miscibility with water [57]</p> <p>health and safety: forms explosive peroxides upon contact with air [34]</p> <p>STATUS:</p> <p>experimentally tested pure [21]; detailed kinetic model [62]</p>
GVL 	<p>ADVANTAGES:</p> <p>engine: low melting point [63]; 10 % mixture with gasoline shows evaporation properties similar to the respective ethanol–gasoline mixture [63]; miscible with gasoline [63]</p> <p>environment: sustainable production [63]</p> <p>health and safety: easy and safe to store and transport [63]</p> <p>DISADVANTAGES:</p> <p>environment: completely miscible with water [34, 63, 64]</p> <p>health and safety: addictive drug [34]</p> <p>STATUS:</p> <p>proposed by Horváth <i>et al.</i> [63] in 2007</p>

*: determined for mixtures with gasoline

•: compared to gasoline

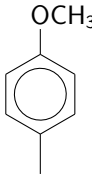
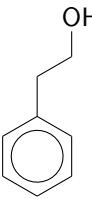
Table 2.1 — *continued*

compound	discussion
ethyl valerate 	<p>ADVANTAGES:</p> <p>engine: no significant change in performance*• [65]; miscible with gasoline [65]; 15 vol% in gasoline led to no measurable changes in engine wear [66]; no increase in oil dilution detected during road trials detected* [66]</p> <p>environment: no significant change in NO emissions*• [65]; low solubility in water [66]; no increase in regulated emissions during road trials* [66]</p> <p>DISADVANTAGES:</p> <p>engine: lower LHV• [66]</p> <p>STATUS:</p> <p>proposed by Lange <i>et al.</i> [66] in 2010 as upgrading product of GVL; experimentally tested, on a testbench [65] as well as on the road [66], mixed with gasoline</p>
2-butanone 	<p>ADVANTAGES:</p> <p>engine: improved cold startability (compared to ethanol) [47]; RON close to ethanol [47]; lower oil dilution than ethanol [47]; increased combustion stability [47]; miscible with gasoline [67]</p> <p>STATUS:</p> <p>proposed by Hoppe <i>et al.</i> [47] in 2016 based on CAMD; experimentally tested pure [47]</p>
TMED 	<p>ADVANTAGES:</p> <p>engine: LHV 34 % higher than ethanol [68]; miscible with gasoline [68]</p> <p>environment: low water solubility [68]; sustainable production from biomass (via 2,3-butanediol) [68]</p> <p>DISADVANTAGES:</p> <p>engine: low RON (= 94) [68]</p> <p>STATUS:</p> <p>proposed by Harvey <i>et al.</i> [68] in 2016</p>
furfuryl alcohol 	<p>ADVANTAGES:</p> <p>engine: enhanced antiknock quality* [50]; miscible with gasoline [50]</p> <p>DISADVANTAGES:</p> <p>engine: limited stability/tendency to polymerize [51, 57]</p> <p>environment: miscible with water [51, 57]</p> <p>STATUS:</p> <p>proposed by Gouli <i>et al.</i> [50] in 1998 as additive; experimentally tested mixed with gasoline [50]</p>

*: determined for mixtures with gasoline

•: compared to gasoline

Table 2.1 — *continued*

compound	discussion
4-methylanisole 	<p>ADVANTAGES: engine: high RON [55]; low melting point [55]; miscible with gasoline [55, 56] environment: low water solubility [55]</p> <p>DISADVANTAGES: engine: potential gum formation [55] environment: increased PM emissions*• [56]</p> <p>STATUS: proposed by McCormick <i>et al.</i> [55] in 2015 as best SI fuel derivable from pyrolysis oil, experimentally tested mixed with gasoline [56]</p>
2-phenylethanol 	<p>ADVANTAGES: engine: increased LHV• [56]; miscible with gasoline [56] environment: production via microbial fermentation possible [25]</p> <p>DISADVANTAGES: engine: high boiling point [56] environment: increased PM emissions* [56]</p> <p>STATUS: proposed by Atsumi <i>et al.</i> [25] in 2008; experimentally tested mixed with gasoline [56]</p>

*: determined for mixtures with gasoline

•: compared to gasoline

Detailed discussions on subsets of the listed compounds with respect to different topics can be found in the literature. An overview of the properties of ethanol, *n*-propanol, isopropanol, *n*-butanol, *sec*-butanol, *tert*-butanol, *n*-pentanol, isopentanol, 2-methyltetrahydrofuran (2-MthF), DMF, 2-MF, ethyl levulinate, butyl levulinate, methyl valerate and γ -valerolactone (GVL) together with an extensive discussion on compliance with current legislation, environmental impact and possible safety hazards has been reported [34]. The effect of mixing ethanol, *n*-propanol, isopropanol, *n*-butanol, *sec*-butanol, isobutanol, *n*-pentanol, isopentanol, methyl levulinate, butyl levulinate, 2-MthF, 2-MF or DMF with gasoline on the adherence to fuel standards has been investigated. Butyl levulinate mixtures failed the boiling range criteria and methyl levulinate separated from gasoline below 0 °C. Furthermore, it was concluded that isobutanol, *sec*-butanol, 2-MF and DMF have a good potential as a future blendstock. For methyl valerate and ethyl levulinate, a reduced potential was determined. Propanol isomers and *n*-pentanol may prove useful in high ethanol blends, whereas for 2-MthF no potential was identified. The argument was that, among other properties, either the water solubility is critically high and/or the RON is too low [35].

In a comprehensive review of the production of fuels from lignocellulosic biomass it was concluded that furans are the most promising compounds [57]. Combining catalytic conversion efficiency and engine requirements, the following candidates were identified:

Furan, 2-MF, DMF, 2-*n*-butylfuran, furfuryl alcohol, tetrahydrofuran, 2-MthF, 3-methyltetrahydrofuran (3-MthF), 2-ethyltetrahydrofuran, 2-*n*-butyltetrahydrofuran.

From this literature review, it becomes evident that the search for a gasoline replacement is far from being concluded. Most studies do not cover a wide range of candidates and use different measures making comparisons between different studies difficult. A further major issue is that the specifications of the “perfect” fuel are still unknown. Even though standards exist for the current fossil fuels, it is unlikely that these historically evolved specifications reflect the “perfect” fuel.

Besides properties that influence the performance of the engine, some less prominent ones exist which might affect the acceptance of a fuel. For example, GVL is discussed as a fuel despite severe issues such as high water solubility [64] and being an addictive drug [34]. The latter fact renders its application in pure form unlikely. A possible solution might be the upgrading of GVL to form alkenes [64]. Methyl *tert*-butyl ether (MTBE) on the other hand was the most commonly used oxygenate additive for gasoline which led, however, to contamination of the ground water. In addition, it is hardly biodegradable. [69, 70].

In summary, it can be stated that a wide variety of different compounds were proposed as gasoline replacement, but no consensus could be achieved so far. The number of regularly-studied compounds is very limited and a large number of not well-studied compounds exist. The performance of these compounds as fuels will be discussed more in-depth in Chapter 4.

A discussion of production pathways was not the aim of this thesis. Interested readers are referred to recent, comprehensive reviews on this subject [51, 71, 72].

2.2 Internal Combustion Engines (ICE)

2.2.1 Theory

This section gives a brief overview of ICEs. Detailed information is provided in textbooks [74, 75].

ICEs in the widest sense of the word are machines that transform chemical energy into mechanical work by combusting a fuel in a combustion chamber inside an engine. More specifically, reciprocating engines are distinguished from continuously operating engines such as e.g. turbines, rocket engines etc. Commonly, ICEs are further classified into SI and Compression Ignition (CI) engines. CI engines inject fuel shortly before Top Dead Center (TDC). The fuel autoignites due to the high temperature within the cylinder. SI engines, on the other hand, compress the fuel and air mixture which is ignited by a spark plug. A further characteristic is the number of strokes. CI or SI engines can be designed for 2- or 4-stroke operation. In a 2-stroke engine, intake and exhaust are combined, thereby completing the cycle within one crankshaft revolution. Conversely, a 4-stroke engine separates intake and exhaust. This work focuses on

Contents of this chapter have been published or submitted: [73]

4-stroke SI engines, as they are the most widespread type of car engine.

In Fig. 2.1 the process of a Direct Injection (DI) SI engine is shown. During the first stroke, the piston moves from TDC to Bottom Dead Center (BDC) sucking in air. At BDC the intake valve closes, and fuel is injected. Afterwards, the second stroke starts during which the fuel/air mixture is compressed. Ignition occurs shortly before TDC. As the fuel is burnt, gas expansion occurs affecting the piston. Around BDC, the exhaust valve opens, and the burnt gases are pushed out of the cylinder as the piston performs the 4th stroke.

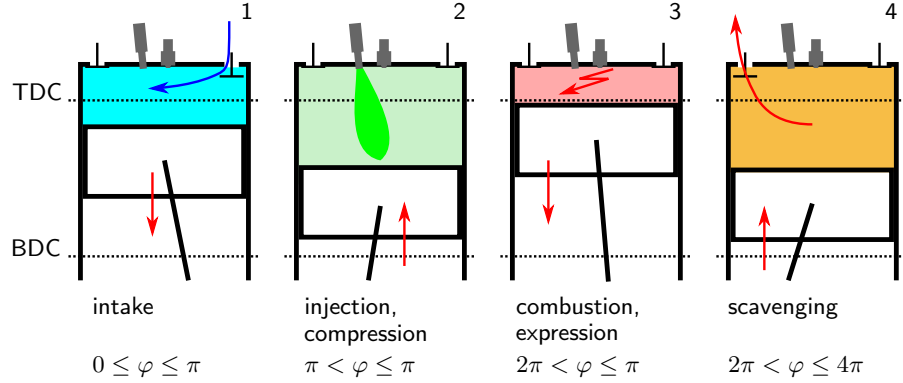


Figure 2.1: Operational scheme of a DI SI engine, showing the different strokes in relation to the crank angle (φ).

The geometrical features of a cylinder are illustrated in Fig. 2.2. The displacement volume (V_D) is the volume displaced by the piston. It is defined by the bore (B) and the stroke (S). An important key figure is the mean piston velocity (c_m), which is used to describe the characteristic flow velocity within the cylinder. The mean piston velocity is calculated based on the stroke and the rotational speed (N) of the engine.

$$c_m = 2SN \quad (2.1)$$

Two different well-established models are commonly used to give an idealized description of the thermodynamic cycle: First, the Otto cycle which assumes isochoric heat addition. Second, the Seilinger cycle, for which the heat addition is divided into an isochoric and an isobaric part. The motivation for the development of the Seilinger cycle was that the pure isochoric heat addition entails an excessive pressure increase. The p - V and T - s diagrams of both cycles are presented in Fig. 2.3 .

The Otto cycle is usually used to describe the maximum efficiency of an SI ICE. The Otto efficiency (η_N) is defined by the compression ratio (ε_{CR}) of the engine and the

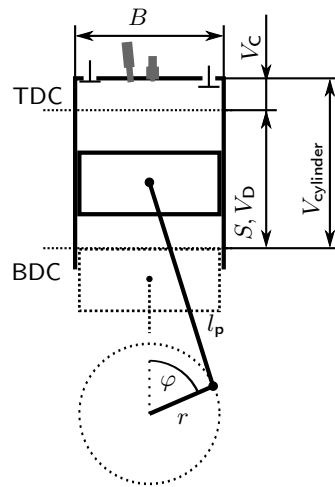


Figure 2.2: Cross section through a cylinder indicating the most important geometrical features (bore B , stroke S , crank angle φ , displacement volume V_D , clearance volume V_C and cylinder volume $V_{cylinder}$).

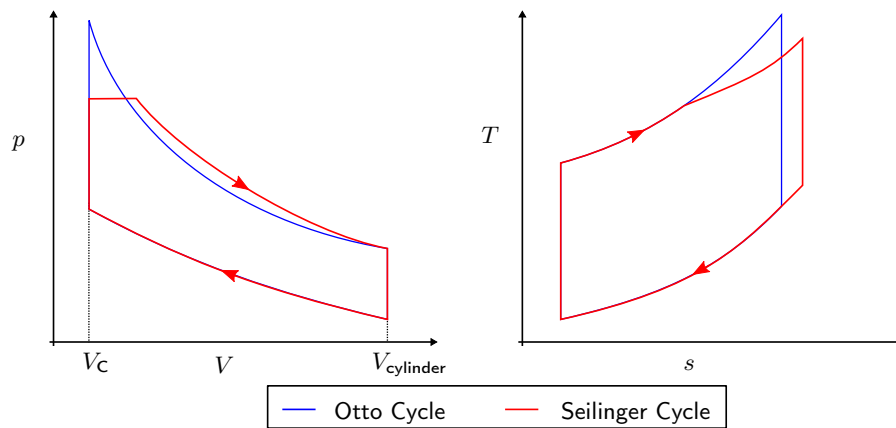


Figure 2.3: Sketch of the p - V and T - s diagrams of the Otto (blue) and Seilinger (red) cycles.

heat capacity ratio (κ) of the working fluid.

$$\varepsilon_{\text{CR}} = \frac{V_{\text{cylinder}}}{V_{\text{C}}} = \frac{V_{\text{C}} + V_{\text{D}}}{V_{\text{C}}} \quad (2.2)$$

$$\eta_{\text{V}} = 1 - \frac{1}{\varepsilon_{\text{CR}}^{\kappa-1}} \quad (2.3)$$

One way to decouple load and engine size is to make use of the concept of mean effective pressure. The mean effective pressure is described as the (constant) pressure at which the same amount of work is performed for the given displacement volume. In general, three different mean effective pressures are defined: indicated mean effective pressure (*imep*), friction mean effective pressure (*fmep*), and break mean effective pressure (*bmep*). The *imep* is defined by the indicated work (W_{I}), which describes the work done without any additional losses.

$$imep = \frac{W_{\text{I}}}{V_{\text{D}}} \quad (2.4)$$

The *fmep* is defined using the friction work instead. The *bmep* describes the work which is available at the crankshaft.

$$bmep = imep - fmep \quad (2.5)$$

Rearranging Eq. (2.4) leads to the following relation between the mean effective pressure (*mep*) and the related power for a four-stroke engine.

$$P = mep V_{\text{D}} N \frac{n_{\text{cyl}}}{2} \quad (2.6)$$

with n_{cyl} the number of cylinders in the engine.

2.2.2 Knocking

Knock describes the uncontrolled ignition of fuel before the flame front can consume it. This process induces pressure fluctuations in the cylinder and can significantly damage the engine. Knocking is a consequence of the operating conditions (T, p) within the cylinder, the tendency of the fuel to ignite and other factors such as possible hotspots within the combustion chamber. Knock-limited operation implies, on a design level, lower compression ratios, and for single load points, delayed ignition timing. Compared to the Otto cycle, both measures lead to lowered efficiencies.

To describe the resistance of a fuel towards autoignition, the octane number was introduced in the 1930s. It is defined as the volumetric fraction of isooctane in a mixture with *n*-heptane with the same knock tendency as the fuel in question at a given load point. Two test procedures were established, the Motor Octane Number (MON) and the RON, which were then the lower and the upper boundaries, respectively.

However, this definition has two major shortcomings: First, there are fuels with a lower knock tendency than isooctane, requiring a different definition. Second, engine design has significantly changed within the past 80 years, so that super charging and downsizing led to operation conditions outside the historic definitions. To overcome the latter, the Octane Index (OI) has recently been introduced, based on the RON, the sensitivity (S) and an engine constant (K) [76].

$$\text{OI} = \text{RON} - K \cdot S \quad (2.7)$$

$$S = \text{RON} - \text{MON} \quad (2.8)$$

The sensitivity is defined as the difference between the RON and the MON. The engine constant (K) depends only on the operating conditions; its value has decreased from about 1 in 1930, to 0 at the turn of the century and is negative today [77–79]. To reach high OI values, a high RON and a low MON is required.

2.2.3 Modeling Approaches

Plenty of studies have been conducted experimentally and theoretically to assess the performance of different fuels. The comparison of two different experimental studies is often hindered by the multiple degrees of freedom in the load, the engine and the testing procedure. One way to overcome that problem is to utilize gasoline as a benchmark [20, 80]. This approach requires knowledge of the influence of each property, complicating quantitative statements. Simulation tools ranging from 0 D thermodynamic approaches to 3 D Computational Fluid Dynamics (CFD) codes might be another solution. The strength of CFD codes lies within the detailed representation of the thermal and fluidic processes within the engine. They are mainly used for engine design purposes. Meanwhile, 0 D thermodynamic models are built primarily for their fast rather than detailed analysis and are, therefore, ideal for the comparison of many different fuels.

Several approaches have been reported in the literature: one model comparing hydrogen, propane, methane and methanol has been presented [81] using 1 D modeling. The combustion part was defined separately, based on empirical correlations for each fuel. Another model focused on emissions and gas dynamic effects [82]. The processes within the engine were studied by a spark ignition engine model using pressure traces obtained empirically [83]. Shen *et al.* [84] published a model to predict the pressure trace during methanol combustion. Ramachandran [85] proposed a fast model including detailed chemical reactions. The model lacks, however, the ability to detect knocking, neglects friction within the engine and is limited to the combustion engine itself. Mehrnoosh *et al.* [86] presented a model for engines running on gasoline and natural gas with a focus on NO_x emissions, combustion rate, and knocking. In numerous publications Caton developed a thermodynamic model of the processes within a cylinder of a SI engine. Their model assumes that the fuel is fully evaporated before entering the cylinder. Thereby it is able to cope with both gaseous and liquid fuels, but does not include an evaporation model. Combustion is modeled by a Wiebe function and knock has been neglected. The model has been applied in the context of an exergy analysis

of different fuels [87–90].

2.3 Fuel – Engine Interaction

The influence of the fuel on the performance of the engine is present in every step of the engine cycle (however, at varying extent). The engine cycle begins with fuel injection (viscosity (ν)), droplet formation (surface tension (σ)), and evaporation (boiling point (T_{boil}), enthalpy of vaporization (h_{vap})). Next, the compression of the air–fuel mixture occurs which is influenced by the heat capacity of the mixture. The latter depends on the vapor heat capacity ($c_{p,g}$) of the fuel and the Air-to-Fuel Ratio (AFR). Around TDC, combustion takes place; the energy content of the mixture determines the peak pressure. The increase in pressure arises from the LHV in conjunction with the AFR. Additionally, the changing number of molecules within the chamber during combustion influences the peak pressure. After combustion, expansion takes place. The temperature levels determine the wall heat losses and are influenced by the heat capacity of the burnt mixture. The heat capacity of the burnt gas is again driven by the elemental composition.

First and Second law efficiencies for different fuels have been studied on an idealized ICE. Both the molar expansion ratio as well as the heat-capacity ratio were found to be of great importance. However, for the studied fuels an inverse correlation was found for both parameters, canceling out the respective effects [Szybist2012].

The efficiency of an ICE depends to a large extent on the compression ratio of the engine. The optimum compression ratio is generally estimated to be in the range of 12 to 14. Increasing the compression ratio above that level entails excessive heat and friction losses.

Whether the optimum compression ratio can be reached by a certain fuel is defined by its resistance to knock under the given operating conditions of the engine. There are two fuel properties which influence a fuel's tendency to knock: firstly, the knock resistance described by the RON, and secondly, the enthalpy of vaporization. The latter defines the amount of charge cooling and thereby the temperature before combustion. The knock resistance defines how long the fuel–air mixture can be exposed to certain temperatures until knock occurs.

Further complicating the situation, the different effects are interlinked with each other. For example, as soon as the RON allows for the optimum compression ratio, a further increase will not lead to a higher efficiency. On the other hand, many fuels are knock-limited and thereby an increase in the RON is beneficial. However, an increase in vaporization enthalpy could also be advantageous since this reduces the temperature at TDC before combustion and thus the requirement of autoignition resistance of the fuel. In conclusion, it is more challenging than expected to give exact specifications of the ultimate fuel.

2.4 Property Estimation

With regard to property estimation of compounds, two main aims can be distinguished: First, reproduction of measured values, and second, extrapolation to unknown compounds. The first mode is widely used to obtain temperature-dependent properties. An example discussed herein is the enthalpy of the gases (except fuel vapor) within the cylinder that are calculated using this technique [92]. These correlations require measurement campaigns or quantum mechanical simulations of the molecule in question and therefore have no extrapolation power. These techniques are a more computer friendly version of the well-known thermodynamic tables.

The second field (extrapolation to unknown compounds) can be divided into three subclasses:

- Quantitative Property–Property Relation (QPPR)
- Quantitative Structure–Property Relation (QSPR)
- Group Contribution Method (GCM)

QPPRs are correlations between known properties and the target property. The Clausius–Clapeyron Equation (Eq. (3.2)), for instance, relates vapor pressure, boiling point and enthalpy of vaporization. Another example is the correlation by Channiwala and Parikh [93] used to predict the LHV based on the elemental composition. In spite of their easy usability, QPPRs reflect statistical correlations and do not necessarily cover the underlying physics. Their field of application must be observed carefully. QSPRs and GCMs directly link the structure of the molecule to the property in question. QSPRs derive parameters from the molecular structure and link those parameters to the target property. A comprehensive review of the subject of QSPRs has been delivered by Katritzky *et al.* [94]. GCMs on the other hand divide the molecule into so-called groups and link the target property to the sum of group increments. The underlying assumption is that the influence of these groups is not affected by their connections to one another.

There are up to three levels of different groups defined within the GCMs. All GCMs include first level groups, to represent a molecule these first level groups are required to cover the whole molecule without any intersections. Whenever conflicts arise and a different combinations of groups can be taken to describe the same part of a molecule, groups with higher molecular weight are preferred. Second and third level groups are not employed by all GCMs. They are used to describe larger fragments of molecules and serve to increase the estimation accuracy for large molecules. In contrast to first level groups, higher level groups are allowed to overlay each other, as long as one group is not fully enveloped by another.

Based on the recommendation of Nieto-Draghi *et al.* [95], the following set of GCMs has been chosen to estimate the required properties of compounds lacking experimental data: Vapor heat capacity [96], liquid density, boiling and melting point, autoignition temperature, enthalpy of vaporization [97], and liquid viscosity [98]. The liquid density is calculated using the GCM for the liquid molar volume. The vapor pressure is

Contents of this chapter have been published or submitted: [91]

calculated based on the estimated boiling point and the enthalpy of vaporization using the Clausius–Clapeyron equation. Table 2.2 gives an overview of the estimation errors (Average Absolute Error (AAE) and Average Relative Error (ARE)), as reported by the respective authors.

Table 2.2: Overview of the chosen Group Contribution Methods in combination with the respective Average Absolute Error and Average Relative Error, as reported by the respective authors.

Property	GCM	AAE	ARE [%]
vapor heat capacity [J/(mol K)]	Joback and Reid [96]	5.9	n/a
molar volume [cm ³ /mol]	Hukkerikar <i>et al.</i> [97]	0.0024	2.03
autoignition temperature [K]	Hukkerikar <i>et al.</i> [97]	13.51	2.09
enthalpy of vaporization [kJ/mol]	Hukkerikar <i>et al.</i> [97]	1.29	3.24
boiling point [K]	Hukkerikar <i>et al.</i> [97]	5.96	1.38
melting point [K]	Hukkerikar <i>et al.</i> [97]	15.99	5.07
kinematic viscosity [mm ² /s]	Nannoolal <i>et al.</i> [99]	n/a	9.2

In the case of viscosity, a slightly less accurate method with the benefit of the group definitions matching the definitions of the other methods was chosen. Although these GCMs use the structure of the molecule to estimate its properties, they are unable to distinguish certain isomers.

2.5 Computer Aided Molecular Design (CAMD)

The field of CAMD is a relatively new field of research as it is closely associated with the arising availability of computers. The first publication on the topic was a study on solvents for liquid extraction based on the UNIFAC method done in 1983 [100]. In 1996, a first summary stating the main aspects and challenges of CAMD has been presented [101]. The possible applications are manifold, including, among others, design of solvents, refrigerants, fuels and pharmaceuticals [102]. The underlying idea of CAMD is to use an algorithm to identify molecules that possess specific desired properties. The easiest way to perform CAMD is to scan a database and compare its entries with the specifications. The main task of this approach is to build up the database. More sophisticated approaches are optimization procedures that optimize the structure of molecules to fulfill the specifications. These algorithms need to be able to modify the molecular structure, then to estimate the properties and finally to compare the specifications with the estimated properties. Another challenge is to ensure that only stable molecules are designed.

In the following, a short review of existing CAMD methods is given. The CAMD proposed by De Vleeschouwer *et al.* [103] uses quantum chemistry simulations to calculate the properties. For instance, the electrophilicity of thiadiazinyl radicals was optimized. The primary fragment was fixed to the thiadiazinyl radical while 21

possible substituents were available for five sites. Combining GCMs and a database, a CAMD tool to design solvents for organic reactions was obtained [104]. Another approach to design solvents for liquid-liquid extractions or gas-adsorption processes included a thermodynamic model of the extraction process [105, 106]. Using a simple fermentation model, biocompatible ethanol extraction solvents were designed as a function of solvent flow rate [107]. Furthermore, solvents for batch distillation were modeled based on the UNIFAC method [108]. In an innovative approach to the design of working fluids for an Organic Rankine Cycle (ORC) has been specified by combining a simple thermodynamic model of an ORC and CAMD [109]. Besides, the performance in the ORC, safety and environmental aspects were taken into account. GCMs have been applied in a design study of refrigerants [110]. Several new candidate molecules to replace dichlorodifluoromethane (R12) were identified. Another application is the design of polymer repeat units [111, 112].

Only a limited number of CAMD studies are related to fuels. Biodiesel additives have been designed using GCMs for melting point and viscosity and a QPPR for the Cetane Number (CN) [113]. Focusing on fuel derivable from biomass eight molecules as possible gasoline alternatives were identified [24]. The method uses QSPRs and a set of specifications (upper and/or lower boundaries) for fuel properties. A similar study focused on CI fuels without the limitation to biomass derivable structures, and found seven compounds [114].

3 Modeling

3.1 Engine Modeling

To evaluate the performance of different liquid fuels, a thermodynamic model of a turbocharged SI DI ICE running at stoichiometric conditions (air–fuel equivalence ratio, $\lambda = 1$) is built. Today, the turbocharged SI DI engine is considered the most promising type of configuration for SI engines [116]. Performance is assessed with respect to engine efficiency at different loads and for three driving cycles, including the specific CO₂ emissions. Other emissions such as NO_x, CO, or soot have not been modeled. Besides the engine, the model includes the following auxiliary systems: turbocharger powered by an exhaust gas turbine, fuel pump and after cooling.

3.1.1 Process Description

Fig. 3.1 shows a schematic overview of the engine model. A list of the modeling constants together with their respective value is given in Table A.1. The process starts with air at ambient conditions (I), the air is then compressed and cooled (III) before entering the cylinder. Intake is followed by compression ($1 \rightarrow 2$); the combustion within the cylinder is modeled according to the T - s diagram approach [117], splitting the combustion into an isochoric ($2 \rightarrow 2a$), an isobaric ($2a \rightarrow 2b$) and an isothermal phase ($2b \rightarrow 3$). Expansion of the burnt gases ($3 \rightarrow 4$) and gas exhaust through the turbine (5, 6) complete the cycle. Frictional losses (P_{fric}) and wall heat losses (\dot{Q}_{wall}) within the cylinder are accounted for.

To obtain a meaningful comparison of the potential of different fuels, the compression ratio is optimized for each fuel. Thereby, it is possible to assess the full potential of a compound as fuel for an SI ICE. Accordingly, the model is split into two different parts: On the one hand, the engine model itself, and on the other hand, an optimization procedure to maximize the efficiency for each fuel and to avoid knocking. The adaptation of the engine to the fuel is achieved by changing the compression ratio ($\varepsilon_{\text{CR}} \in [5, 20]$), while the total cylinder volume (volume at BDC) is kept constant.

3.1.2 Input Parameters and Derived Fuel Properties

As input parameters the chemical composition ($C_xH_yO_zN_v$), the liquid/vapor heat capacities ($\bar{c}_{p,L/g}$), the density (ρ), the surface tension (σ), the liquid kinematic viscosity

Contents of this chapter have been published or submitted: [73, 91, 115]

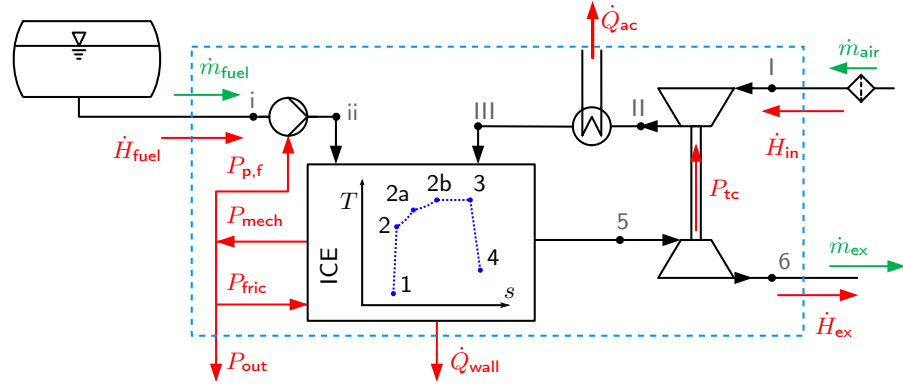


Figure 3.1: Flow sheet representation of all considered engine parts. System boundary as dashed blue line. $P_{p,f}$ power supplied to fuel pump, P_{tc} power transferred from turbocharger turbine to compressor, P_{out} net power output of the engine, P_{mech} mechanical power, P_{fric} friction losses within the engine, \dot{Q}_{wall} wall heat losses, \dot{Q}_{ac} heat transferred by after cooler, \dot{H} , \dot{m} enthalpy stream/ massflow of intake, exhaust or fuel.

(ν), vapor pressure (p_{vap}), enthalpy of vaporization (h_{vap}), and the RON of the fuel are required. To ensure ease of handling and storage only liquid fuels are considered in the following. Therefore, the input to the model is limited to compounds that are liquid at room temperature. LHV is estimated via the correlation for the Higher Heating Value (HHV) presented by Channiwalla and Parikh [93], which leads to Eq. (3.1).

$$\text{LHV} = 418.92x + 95.85y - 165.44z - 21.14v \quad [\text{kJ/mol}] \quad (3.1)$$

The vapor pressure (p_{vap}) at the normal boiling point (T_{boil}) is by definition equal to the ambient pressure (p_{amb}). The vapor pressure, the heat of vaporization (h_{vap}), and the temperature (T) are related by the Clausius–Clapeyron equation. Assuming that the heat of vaporization is independent of the temperature, Eq. (3.2) has been derived:

$$T_{boil} = \left[\frac{1}{T_{ref}} - \frac{R}{h_{vap}(T_{ref})} \ln \left(\frac{p_{amb}}{p_{vap}(T_{ref})} \right) \right]^{-1} \quad (3.2)$$

with the reference temperature (T_{ref}) at which h_{vap} and p_{vap} have been measured and the universal gas constant R . As a GCM to predict the RON was not available, a QPPR relation was developed. Using previously reported experimental data [34, 118–125], the following empirical correlation for the RON based on experimental values for the autoignition temperature (T_{auto}) [126–128], number of hydrogen atoms (y) and the

normal boiling point (T_{boil}) [126, 129] was developed.

$$\begin{aligned} \text{RON} = & 116.44 - 0.26 \exp\left(\frac{2557.48}{T_{\text{auto}}}\right) + 8.13 \times 10^{-5} y^{4.38} \\ & - 1.73 \times 10^{-6} \exp\left(\frac{2557.48}{T_{\text{auto}}}\right) y^{4.36} - 5.94 \times 10^{14} \frac{y^{4.36}}{T_{\text{boil}}^{7.45}} \end{aligned} \quad (3.3)$$

with a residual standard error of 11.2, an R^2 of 0.8251 and an F-statistic of 141.5.

3.1.3 Intake

Prior to intake, the air flows through the compressor of the turbocharger. The ideal after cooler then cools the air stream down to ambient temperature (T_{amb}). Overall, this leads to an increase in pressure by the compression ratio (Π_{tc}), while the temperature remains unchanged.

To describe the intake, compression heating (ΔT_{ch}) and wall heating (ΔT_{wh}) effects are taken into account. It is assumed that no exhaust gas remains in the cylinder. The values for ΔT_{ch} and ΔT_{wh} are defined by the following equations [117]:

$$\Delta T_{\text{ch}} = \frac{\kappa - 1}{\kappa} \frac{K_{p1pIII} - 1 + \delta_{\text{valve,III}}}{K_{p1pIII}} T_{III} \quad (3.4)$$

$$\Delta T_{\text{wh}} = K_{\text{wh}} \frac{\bar{T}_w - T_{III} - \Delta T_{\text{ch}}}{170} \frac{B + 2S}{B \left[\Pi_{\text{tc}} \frac{B}{2} c_m\right]^{0.2}} \quad (3.5)$$

$$T_1 = T_{III} + \Delta T_{\text{ch}} + \Delta T_{\text{wh}} \quad (3.6)$$

where T_1 denotes the in-cylinder temperature after intake, S the stroke, B the bore, c_m the mean piston velocity (defined as $c_m = 2SN$) with the rotational speed (N), \bar{T}_w the mean cylinder wall temperature, T_{III} the temperature prior to intake and κ the heat capacity ratio. The empirical constants K_{p1pIII} , $\delta_{\text{valve,III}}$ and K_{wh} have been chosen according to the recommendations by Boulouchos [117].

3.1.4 Fuel Injection and Evaporation

At the start of the compression, fuel is instantaneously injected, and evaporates during the compression stroke. Any fuel not evaporated at TDC is considered to be incombustible. The initial droplet diameter is estimated based on the nozzle diameter of the fuel injector, the initial droplet velocity, the Weber- and the Reynolds number. Droplet evaporation was modeled according to the d^2 -law as proposed by Godsava [130]

3.1.4.1 Fuel Injection

The initial droplet diameter (d_{d0}) [131] can be estimated based on the nozzle diameter (d_{nozzle}), the Weber (We_d) and the Reynolds number (Re_d).

$$d_{d0} = 3.67d_{\text{nozzle}} (We_d^{0.5} Re_d)^{-0.259} \quad (3.7)$$

$$We_d = \frac{\rho_{\text{fuel}} d_{\text{nozzle}} u_{\text{inj}}^2}{\sigma_{\text{fuel}}} \quad (3.8)$$

$$Re_d = \frac{u_{\text{inj}} d_{\text{nozzle}}}{\nu_{\text{fuel}}} \quad (3.9)$$

The initial droplet velocity (u_{inj}) just after leaving the nozzle is obtained from Bernoulli's equation:

$$u_{\text{inj}} = \sqrt{\frac{2(p_{\text{fuel, inj}} - p_1)}{\rho_{\text{fuel}}}} \quad (3.10)$$

The fuel injection pressure $p_{\text{fuel, inj}}$ is set to 20 MPa.

3.1.4.2 Droplet Evaporation

Neglecting thermal radiation the change in enthalpy of a droplet (ΔH_d) can be described as the difference between the heat supplied to the droplet (ΔQ_d) and the enthalpy stream associated to the vaporization of the fuel.

$$\Delta H_d = \Delta Q_d + \Delta n_d h_g \quad (3.11)$$

$$H_d(t + dt) - H_d(t) = \Delta Q_d + \underbrace{(n_d(t + dt) - n_d(t))}_{=-n_{F, \text{evap}}} (h_{\text{vap}} + h_d(t)) \quad (3.12)$$

The enthalpy can be described in terms of temperature and heat capacity.

$$c_{p,L} n_d(t + dt) (T_d(t + dt) - T_d(t)) = \Delta Q_d - n_{F, \text{evap}} h_{\text{vap}} \quad (3.13)$$

The Nusselt number (Nu) for a sphere within a flow field is given by Eq. (3.14) as a function of the Prandtl (Pr) and Reynolds numbers (Re) [132].

$$Nu = 2 + 0.6Re^{1/2} Pr^{1/3} \quad (3.14)$$

Using the definition of the Nusselt number ($Nu = \alpha d_d k^{-1}$), the heat flow to each droplet (ΔQ_d) can be calculated as follows:

$$\Delta Q_d = \frac{Nu k_{\text{gas}}}{d_d} \pi d_d^2 (T_{\text{gas}} - T_d) dt \quad (3.15)$$

k_{gas} is the thermal conductivity of the surrounding gas mixture while T_{gas} and T_{d} are the temperatures of the gas mixture and the droplet. In Fig. 3.2 the energy balance of an evaporating fuel droplet is shown.

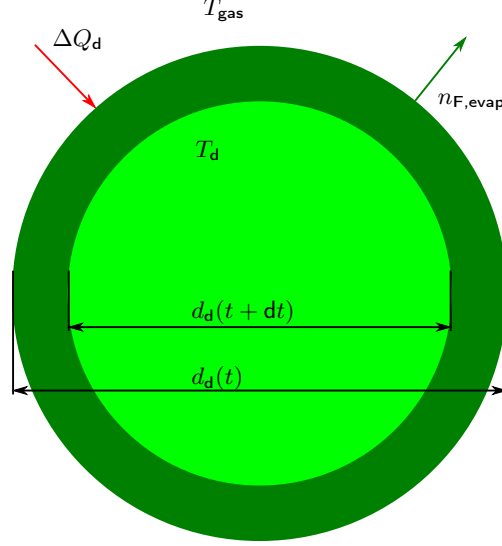


Figure 3.2: Energy balance of an evaporating fuel droplet.

As proposed by Godsave [130] for fuel temperatures below the boiling point, the d^2 -law is applied, to describe the evolution of the droplet diameter (d_{d}) with time.

$$d_{\text{d}}(t) = \sqrt{d_{\text{d}0}^2 - L_{\text{A}}t} \quad (3.16)$$

The evaporation parameter L_{A} is calculated according to Ranz and Marshall [133].

$$L_{\text{A}} = \frac{4k_{\text{gas}}}{c_{V,\text{gas}}\rho_{\text{fuel}}} Nu \log(1 + B_{\text{M}}) \quad (3.17)$$

where

$$B_{\text{M}} = \frac{Y_{1\text{s}}}{1 - Y_{1\text{s}}} \quad (3.18)$$

The mass transfer number $Y_{1\text{s}}$ is defined by Lefebvre [134] as

$$Y_{1\text{s}} = \left[1 + \left(1 - \frac{p}{p_{\text{vap}}(T_{\text{gas}})} \right) \frac{M_{\text{gas}}}{M_{\text{fuel}}} \right]^{-1} \quad (3.19)$$

The vapor pressure is calculated according to the Clausius–Clapeyron Eq. (3.2). In the

present case, the amount of evaporated fuel ($n_{F, \text{evap}}$) can be calculated by the difference in diameter between the current (t) and the next time step ($t + dt$).

$$n_{F, \text{evap}} = \frac{\pi \rho_{\text{fuel}}}{6 M_{\text{fuel}}} \left[d_d(t)^3 - d_d(t + dt)^3 \right] \quad (3.20)$$

In case the fuel temperature reaches the boiling point, the amount of evaporated fuel is determined by the heat supplied divided by the heat of vaporization.

$$0 = \Delta Q_d - n_{F, \text{evap}} h_{\text{vap}} \quad (3.21)$$

$$\Rightarrow n_{F, \text{evap}} = \frac{\Delta Q_d}{h_{\text{vap}}} \quad (3.22)$$

In Fig. 3.3 the mass of droplets with relation to crank angle is shown. Compared are gasoline, ethanol and methanol under engine-like conditions. In this case an initial droplet diameter of $100 \mu\text{m}$ is assumed. For simplicity the wall heat losses are neglected and the dimensions of the engine fixed for all three compounds ($\varepsilon_{\text{CR}} = 10.16$). The engine is running at 2000 rpm, an intake temperature of 298 K and a pressure of 2 bar. The temperature of the fuel droplets is set at 298 K. The crank angle increment is set to $1.8 \times 10^{-5}^\circ$.

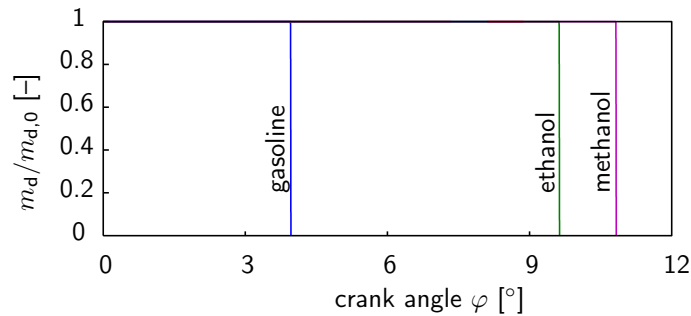


Figure 3.3: Droplet mass during evaporation with relation to crank angle.

As it can be seen from Fig. 3.3 there is a significant difference in the time taken for evaporation between gasoline and methanol. Although in either case the process is finished long before TDC (located at $\varphi = 180^\circ$). Furthermore it can be concluded that due to the size of the droplets evaporation once initiated is completed quickly.

3.1.5 Compression and Expansion

The instantaneous wall heat transfer coefficient (α_w) was initially described by Woschni [135], and later improved by Hohenberg [136]. According to Abedin *et al.* [137], the improved version gives significantly better results. Hohenberg's definition of the heat

transfer coefficient is:

$$\alpha_w = 130V^{-0.06}p^{0.8}T^{-0.4}(1.4 + c_m)^{0.8} \quad (3.23)$$

Based on this equation, the heat losses to the wall can be expressed as:

$$\dot{Q}_w = \alpha_w A_w(\varphi(t))(T - \bar{T}_w) \quad (3.24)$$

Using the first law of thermodynamics, the energy balance, around the complete cylinder volume is described by:

$$n_{\text{mix}} \left(T_{\text{gas}}^{(n+1)} c_V^{(n+1)} - T_{\text{gas}}^{(n)} c_V^{(n)} \right) = W - \left(n_d \dot{Q}_d + \dot{Q}_w \right) \Delta t \quad (3.25)$$

where n_{mix} denotes the total number of molecules within the cylinder, n_d the number of droplets, $*^{(n)}/*^{(n+1)}$ the current/ next iteration, respectively, and W the work done due to compression. The work is defined by

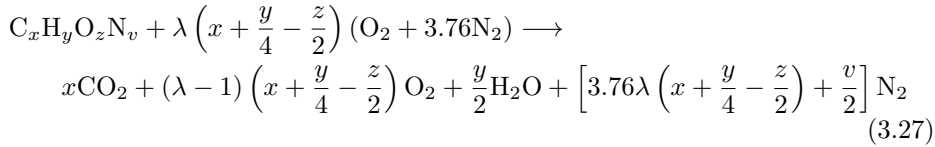
$$W = \frac{1}{1 + \kappa} \left(p^{(n+1)} V^{(n+1)} - p^{(n)} V^{(n)} \right) \quad (3.26)$$

where κ stands for the heat capacity ratio of the gas mixture.

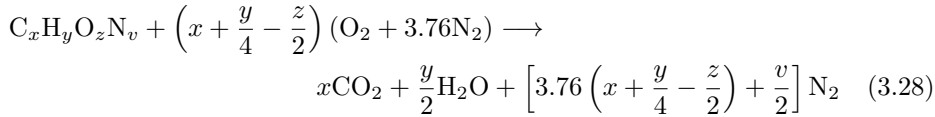
The use of this heat transfer coefficient for fuels other than gasoline is justified by an error estimation presented in Appendix A.2.

3.1.6 Combustion

The general combustion off a hydrocarbon fuel in air can be written as follows:



The equation is limited to equivalence ratios $\lambda \geq 1$. SI engines are designed to operate under stoichiometric conditions ($\lambda = 1$). Thus, Eq. (3.27) then simplifies to Eq. (3.28).



Based on Eq. (3.28) the amount of fuel (n_{fuel}) and the composition of the burnt gas mixture is defined. The amount of fuel to be injected depends on the amount of air

(n_{air}) within the cylinder under intake conditions.

$$n_{\text{air}} = \frac{p_1 (V_D + V_C)}{RT_1} \quad (3.29)$$

$$n_{\text{fuel}} = \frac{n_{\text{air}}}{4.76 \left(x + \frac{y}{4} - \frac{z}{2} \right)} \quad (3.30)$$

Reformulation of Eq. (3.30) leads to the definition of the AFR.

$$\text{AFR} = \frac{m_{\text{air}}}{m_{\text{fuel}}} = 4.76 \left(x + \frac{y}{4} - \frac{z}{2} \right) \frac{M_{\text{air}}}{M_{\text{fuel}}} = \frac{4.76 \cdot 28.97 \left(x + \frac{y}{4} - \frac{z}{2} \right)}{12x + y + 16z + 14v} \quad (3.31)$$

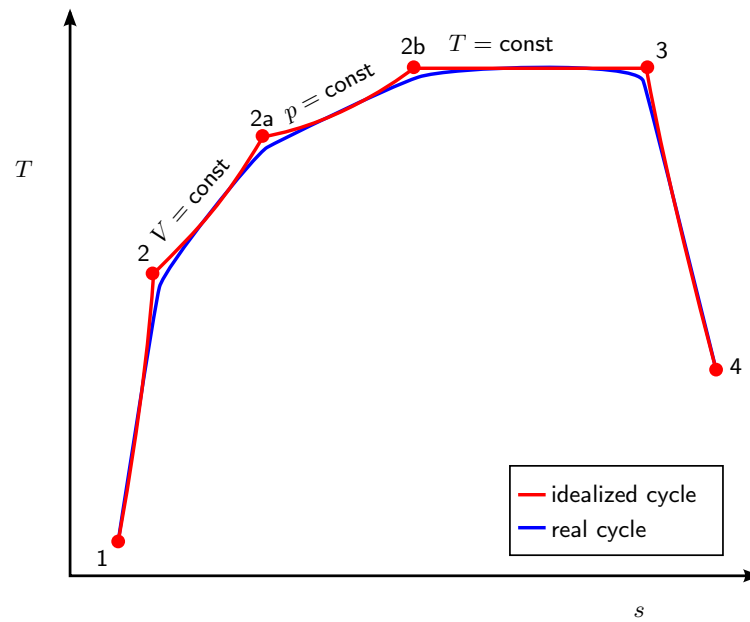


Figure 3.4: Comparison of idealized and real engine cycles, adapted from ref. [117] (red: idealized cycle, blue: real cycle.)

As depicted schematically in Fig. 3.4, the combustion of the evaporated fuel was split into three sequential processes: Firstly, isochoric combustion ($2 \rightarrow 2a$); secondly, isobaric combustion ($2a \rightarrow 2b$); and, thirdly, isothermal combustion ($2b \rightarrow 3$). It is assumed that the properties of the gas mixture in the cylinder depend linearly on the combustion progress (ξ). As an example the number of atoms inside the cylinder (n) is calculated according to Eq. (3.32), other relevant properties are calculated in the same way.

$$n = (1 - \xi)n_{\text{ub}} + \xi n_{\text{b}} \quad (3.32)$$

The total wall heat losses ($Q_{w,tot,0}$) were approximated considering the Reynolds analogy for the heat flux of established turbulent flows:

$$Q_{w,tot,0} = \frac{K_{q,tot}}{[\Pi_{tc} \frac{B}{2} c_m]^{0.2}} \varepsilon_{tot} \quad (3.33)$$

with bore B , charging pressure ratio Π_{tc} , the empirical constant $K_{q,tot}$ and the mean piston speed c_m . The total energy input (ε_{tot}) of the unburnt mixture is calculated based on the LHV, the total number of fuel molecules (n_{fuel}), total number of molecules within the un-/burnt ($n_{ub/b}$) mixture and the enthalpies ($h_{ub/b}$) of the un-/burnt mixtures at a reference temperature of 298 K.

$$\varepsilon_{tot} = \text{LHV} \frac{n_{fuel}}{n_{ub}} + h_b(298 \text{ K}) \frac{n_b}{n_{ub}} - h_{ub}(298 \text{ K}) \quad (3.34)$$

Inspired by the heat transfer correlation of Hohenberg [136], a dependence of the total wall heat losses on the peak pressure (p_{peak}) has been introduced:

$$Q_{w,tot} = Q_{w,tot,0} \left(\frac{p_{peak}}{p_{peak,ref}} \right)^{0.8} \quad (3.35)$$

The dependence of the overall heat losses during combustion on the peak pressure requires an iterative solver as the peak pressure depends on the total heat losses. Therefore, the secant method [138] is employed to find suitable solutions for the peak pressure and the respective heat loss.

The fundamental equations to model the three phases of combustion are:

$$c_{V,2a} T_{2a} - c_{V,2} T_2 = 0.66(\varepsilon_{tot} - Q_{w,tot}) \quad (3.36)$$

$$c_{p,2b} T_{2b} - c_{p,2a} T_{2a} = 0.20(\varepsilon_{tot} - Q_{w,tot}) \quad (3.37)$$

$$T_3 \Delta s_{3,2b} + \Delta h_{3,2b} = 0.14(\varepsilon_{tot} - Q_{w,tot}) \quad (3.38)$$

depending on the heat capacity at constant volume c_V , and constant pressure c_p as well as the entropy difference Δs . Since the heat capacities in Eq. (3.36) to Eq. (3.38) depend on the unknown temperatures at the end of the cycle step. The secant method is applied to find them iteratively. The indices refer to the thermodynamic cycle in a T - s diagram, as shown in Fig. 3.4.

The values 0.66, 0.20, 0.14 have been empirically deduced from fitting the overall efficiency of gasoline *vs.* different loads and rotational speeds, based on measurements from the test bench at Empa. They lie well within the recommended ranges, 0.5 to 0.7, 0.1 to 0.3 and 0.1 to 0.2 respectively [117]. Although different fuels have different flame speeds which would suggest different fractions of the three combustion phases these values are kept constant. Deng *et al.* [139] have shown that the higher flame speed of *n*-butanol does not necessarily lead to a higher combustion rate within an engine. It has been demonstrated that for a well-controlled engine the combustion duration

remains constant [21]. The reason is that for any given SI engine, the engine control will adjust the ignition timing in a way that the main heat release occurs just after TDC. To ensure the mechanical integrity of the engine, a peak pressure limitation has been introduced, imposing an upper limit on the fraction of the isochoric combustion phase. From an efficiency point of view, it is desirable to minimize the isothermal part of combustion. In summary, one should aim at burning under isochoric conditions until the peak pressure limitation is reached, and proceed isobarically until all fuel has been consumed.

3.1.7 Knock Model

Knocking denotes the phenomenon that during combustion a part of the unburnt mixture ignites before being reached by the flame front. It is generally estimated using the knock integral [140]. Its value reaches 1 at the onset of knocking:

$$k_I = \int_2^3 \frac{1}{\tau_{ig}} dt \leq 1 \quad (3.39)$$

$$= \underbrace{\int_2^{2a} \frac{1}{\tau_{ig}} dt}_{=0} + \int_{2a}^{2b} \frac{1}{\tau_{ig}} dt + \int_{2b}^3 \frac{1}{\tau_{ig}} dt \quad (3.40)$$

The assumption of isochoric combustion from $2 \rightarrow 2a$ leads to an infinitely short time span such that $\int_2^{2a} dt = 0$. The ignition delay (τ_{ig}) is approximated by the correlation from Douaud and Eyzat [141].

$$\tau_{ig} = 17.68 \text{ ms} \left(\frac{\text{RON}}{100} \right)^{3.402} \left(\frac{p}{10^5 \text{ Pa}} \right)^{-1.7} \exp \left(\frac{3800 \text{ K}}{T_{ub}} \right) \quad (3.41)$$

where p and T_{ub} are the pressure and the temperature of the unburnt mixture. To obtain these values, the unburnt zone needs to be introduced, leading to a quasi 2-zone model. The following assumptions are made: Firstly, the pressures of the burnt and the unburnt gases are equal and, secondly, the temperature of the unburnt mixture (T_{ub}) is calculated following an isentropic process starting just before combustion:

$$T_{ub} = T_2 \left(\frac{p}{p_2} \right)^{(\kappa-1)/\kappa} \quad (3.42)$$

with the heat capacity ratio (κ) of the unburnt mixture:

$$k_I = \frac{1}{17.68} \left(\frac{\text{RON}}{100} \right)^{-3.402} \left[p_{2a}^{1.7} \exp \left(\frac{-3800}{T_2 (p_{2a}/p_2)^{(\kappa-1)/\kappa}} \right) \Delta t_{2a \rightarrow 2b} \right]$$

$$+ \int_{2b}^3 p^{1.7} \exp\left(\frac{-3800}{T_2 (p/p_2)^{(\kappa-1)/\kappa}}\right) dt \quad (3.43)$$

The application of such a simple knock prediction model has proven useful in practice. Due to the complexity of the phenomenon, higher accuracy has not been achieved with more sophisticated approaches [142].

3.1.8 Friction

Several friction models have been evaluated. The friction model of Chen and Flynn [143] has been chosen due to its simplicity, in terms of input parameters and considerations of the peak pressure (p_{peak}) and the mean piston speed (c_m). This model allows for the accurate calculation of the f_{mep} .

$$f_{\text{mep}} = f_{\text{mep}0} + \beta_0 p_{\text{peak}} + \beta_1 c_m + \beta_2 c_m^2 \quad (3.44)$$

The empirical constants β_0, \dots, β_2 and $f_{\text{mep}0}$ have been deduced from a fit to data measured on a test bench at Empa. The properties of the fit for the f_{mep} are listed in Table 3.1.

Table 3.1: Regression results for the friction mean effective pressure equation. std: standard deviation.

variable		mean	std	p -value
$f_{\text{mep}0}$	[bar]	0.3515315	0.0381548	6.40×10^{-16}
β_0	[-]	0.0054443	0.0002548	$< 2 \times 10^{-16}$
β_1	[bar s/m]	0.0455316	0.0076482	2.24×10^{-8}
β_2	[bar s ² /m ²]	0.0012867	0.0003366	0.000 203

Residual standard error: 0.08661 on 132 degrees of freedom

Multiple R^2 : 0.9632 Adjusted R^2 : 0.9624 p -value: $< 2.2 \times 10^{-16}$

F-statistic: 1151 on 3 and 132 degrees of freedom

3.1.9 Gas Exchange

As a first approximation, the low pressure cycle is modeled using two pressure levels (both are assumed to be constant). The first level is the intake pressure (p_1) which is defined by the charging pressure provided by the compressor. The second level is defined by the back pressure ($p_{4,\text{bt}}$) of the turbocharger turbine. The work needed by the compressor ($W_{\text{c,needed}}$) to deliver the desired charging can be described as follows:

$$W_{\text{c,needed}} = \frac{p_1 V_1}{T_1} \frac{\kappa_{\text{in}}}{\kappa_{\text{in}} - 1} \frac{T_{\text{amb}}}{\eta_c} \left(\Pi_{\text{tc}}^{\frac{\kappa_{\text{in}} - 1}{\kappa_{\text{in}}}} - 1 \right) \quad (3.45)$$

where κ_{in} denotes the heat capacity ratio of air and T_{amb} is the ambient temperature. This leads to the following equation for the turbine back pressure:

$$p_{4,\text{bt}} = p_{\text{amb}} \left[1 - \frac{W_{\text{c,needed}}}{\left(\eta_{\text{t}} p_4 V_4 \frac{\kappa_{\text{ex}}}{\kappa_{\text{ex}} - 1} \right)^{\frac{\kappa_{\text{ex}}}{\kappa_{\text{ex}} - 1}} - 1} \right]^{-1} \quad (3.46)$$

Finally, the power required ($P_{\text{gas,ex}}$) during the low pressure cycle can be described depending on the displacement volume V_{D} , number of cylinders n_{cyl} and the rotational speed N :

$$P_{\text{gas,ex}} = (p_{4,\text{bt}} - p_1) V_{\text{D}} \frac{n_{\text{cyl}}}{2} N \quad (3.47)$$

The efficiencies of the turbine (η_{t}) and the compressor (η_{c}) are 0.65 and 0.70 respectively [144]. To model the throttle valve, for part-load operation, the charge pressure ratio (Π_{tc}) can be reduced to less than 1. Below that value the back pressure is fixed at 107.5 kPa, thereby accounting for pressure losses over the exhaust system. For modeling the decreased turbine efficiency at low rotational speeds of the turbine, the following assumptions are made: Firstly, above an engine rotational speed of 1500 rpm the maximum charge pressure ratio (Π_{tc}) of 2 is achieved; secondly, at 1000 rpm the engine is run as an aspirated engine ($\Pi_{\text{tc}} = 1$) and thirdly, at rotational speeds between 1000 rpm and 1500 rpm the maximum charge pressure ratio is linearly dependent on the rotational speed of the engine. The actual charge pressure ratio can then be chosen either as an input value or such that the required power output is met.

3.1.10 Adaptation of ε_{CR}

The maximum allowable compression ratio is limited by knocking and thus depends on the RON of the fuel. The efficiency increases with the compression ratio until friction losses and wall heat losses become significant enough to reverse this effect. Therefore, an optimum for compression must be determined for each fuel. It has been shown experimentally that the point of the optimal compression ratio differs for different fuels [145]. In Fig. 3.5 the principle of the compression ratio optimization is shown schematically.

For the first run of the model, the compression ratio (ε_{CR}) is set to the minimum value ($\varepsilon_{\text{CR,min}}$) and the engine simulation is performed. If either the knock index ($k_1 < 1$) or the peak pressure limitation (p_{peak}), is violated, the fuel is not suitable, and the procedure is stopped.

As a next step, the maximum allowable compression ratio ($\varepsilon_{\text{CR,max,ok}}$) below the limit ($\varepsilon_{\text{CR,max}}$) is determined by means of the bisection procedure [138]. The maximum efficiency is searched for within the range of $\varepsilon_{\text{CR}} \in [5, \varepsilon_{\text{CR,max,ok}}]$ (Point 1 in Fig. 3.5). This is done by employing Brent's method [146] to find the compression ratio for which the following condition is satisfied: $\frac{\partial \eta}{\partial \varepsilon_{\text{CR}}} = 0$. Once this point has been identified,

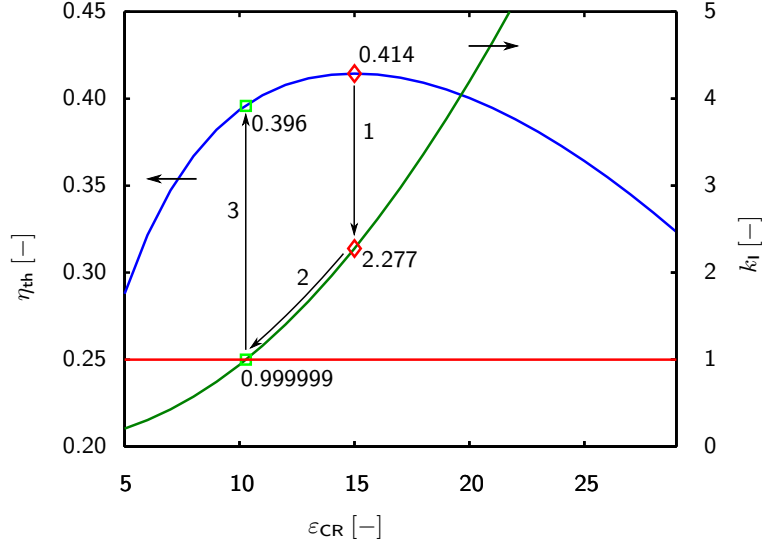


Figure 3.5: Influence of compression ratio (ε_{CR}) on efficiency (η , in blue) and knock (k_1 , in green). Red: boundary above which knock occurs.

knocking and peak pressure limitation are checked. If both parameters are within range, the engine parameters best suited for the fuel in question have been found. Otherwise, the bisection method [138] is used to find the compression ratio that provides a knocking index of $k_1 \leq 0.999999$ (Step 2 in Fig. 3.5).

3.1.11 Model Output

To judge the performance of a fuel, the following values are calculated based on the fuel properties, the engine parameters, and the simulation results: The efficiency (η) at different loads and the specific CO_2 emissions at full load (e_{CO_2}) in g/kWh. Their definitions are given in Equations (3.48) to (3.49).

$$\eta = \frac{P_{\text{out}}}{\dot{n}_{\text{fuel}} \text{LHV}} \quad (3.48)$$

$$e_{\text{CO}_2} = \frac{\dot{m}_{\text{fuel}} M_{\text{CO}_2}}{P_{\text{out}} M_{\text{fuel}}} x \quad (3.49)$$

Results for full load (FL) are reported at 2000 rpm. Part load (PL) is defined as a power output of 6.6 kW at 2000 rpm, which is the power output of the gasoline engine at a *bmep* of 2 bar.

3.1.12 Further Influences

The presented model covers first order effects only. Several other parameters have not been investigated, in particular, flame speed, soot formation, and ignition timing.

In recent years, soot formation became an issue for SI engines too. The paths to soot formation are complex and depend largely on the combustion chemistry of the fuel. As the model is primarily intended as a screening tool for new fuels, these reaction pathways are unknown in most cases, making *a priori* modeling of soot emissions impossible. In any case a good preparation of the mixture may lead to lower soot emissions. If this is not sufficient, particulate filters may provide a solution to the problem.

The flame speed influences the heat release rate and thus the pressure curve. The combustion within an engine is highly turbulent. Therefore the turbulent flame speed is of interest. The latter is a function of the laminar flame speed and the flow field in the cylinder. By assuming the same combustion for all fuels, the turbulence level within the cylinder is adapted to correct for deficiencies of the laminar flame speed. In practice, this is only possible within a limited range, as this may lead to excessive wall heat losses and extinction of the flame.

Ignition timing is considered implicitly in the model: the assumption is that the engine control sets ignition so that the heat release follows the assumed pattern.

In summary, it is important to note that the model focuses on first order effects and is in particular intended to determine the potential as fuel for compounds lacking experimental data.

3.2 Validation

3.2.1 Experimental Validation

The thermodynamic engine model is validated against experimental data of an SI ICE run on commercial gasoline (RON 98) with a displacement of two liters. It has been operated in fully warmed-up conditions on an engine test bench. Table A.3 in the appendix shows the main characteristics of the experimental setup. Validation is discussed in this thesis at an engine speed of 2000 rpm. Passenger car engines are frequently operated at a speed around 2000 rpm, and engines are typically optimized for good efficiency and good driveability in this speed region. Additionally, turbocharged engines typically achieve peak torque around 2000 rpm, and exhaust gas temperatures are not too high such that the engine can safely be operated at $\lambda = 1$. Boosted engines, on the other hand, show clear knock tendencies at 2000 rpm and high load, allowing that the knock model can also be validated at the considered speed.

Fig. 3.6 shows a so-called Willans-type [147] plot for 2000 rpm. This direct representation of input *vs.* output power is a meaningful approach for the analysis of energy

conversion devices at different loads [147–149]. The input power has been calculated as:

$$P_{\text{in}} = \text{LHV} \dot{n}_{\text{fuel}} \quad (3.50)$$

and the output power is the power at the engine’s flywheel. Fig. 3.6 shows that the measured input–output correlation is linear until approximately 50 kW output power (this corresponds to approximately 17 bar *bmep*). At higher loads, the curve bends towards lower efficiencies. The reason for this effect is that the ignition has to be delayed in this load regime to avoid knocking. The model was used to simulate the operating points 2 bar *bmep*, 6 bar *bmep* and full load. Fig. 3.6 shows that the model simulation meets the measured efficiencies very well for the two part-load points. For the full load point, the output power and efficiency are overestimated by the model if knock is not taken into account. However, the model correctly detects knocking at these conditions making it clear that this output power cannot be achieved in reality without adjusting the ignition timing. The reaction of the model is to decrease the compression ratio ε_{CR} as described in Section 3.1.10. In this particular case, the model reduced ε_{CR} from 10 to 7.7. The corresponding result is also plotted in Fig. 3.6. Upon reducing ε_{CR} , the power output declines, matching the measured level. Again, no model parameter was adjusted to the measured data to obtain this match. Thus, ε_{CR} reduction shows a similar effect on power output and efficiency as ignition timing postponement of the real engine.

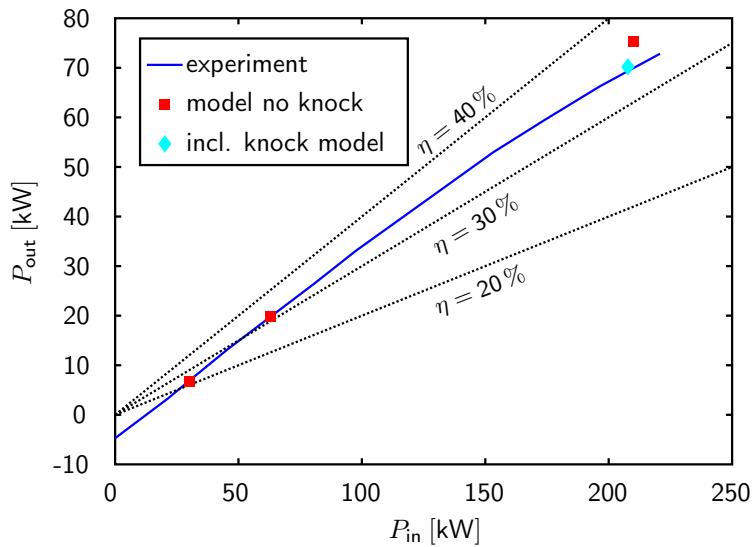


Figure 3.6: Input–output power characteristics for gasoline operation at 2000 rpm, measured engine results *vs.* model results. Blue line: experiment, red squares: modeling results without knock detection (same compression ratio as in the experiments), cyan diamond: modeling result with adapted compression ratio to avoid knock, black dotted lines: lines of constant efficiency.

As described in Section 3.1.6, the model calculates heat release as an isochoric process at TDC, followed by an isobaric process and an isothermal process with constant shares of these phases for all operating points. Fig. 3.7 shows the measured and simulated pressure traces for the operating points shown in Fig. 3.6. The simulation approximates the real behavior well at the 2 bar *bmep* operating point; the deviation is larger for the two other operating points considered. However, the differences appear mainly close to TDC where the volume change is small, and thus the error in *bmep* (or P_{out}) is also small.

In conclusion, the model is able to reflect experimental efficiency and output power results for gasoline operation across a wide range of engine loads. Other fuels could not be experimentally assessed as the engine's fuel system is not compatible with alternative fuels. The validity of the model for alternative fuels is critically discussed in the following sections.

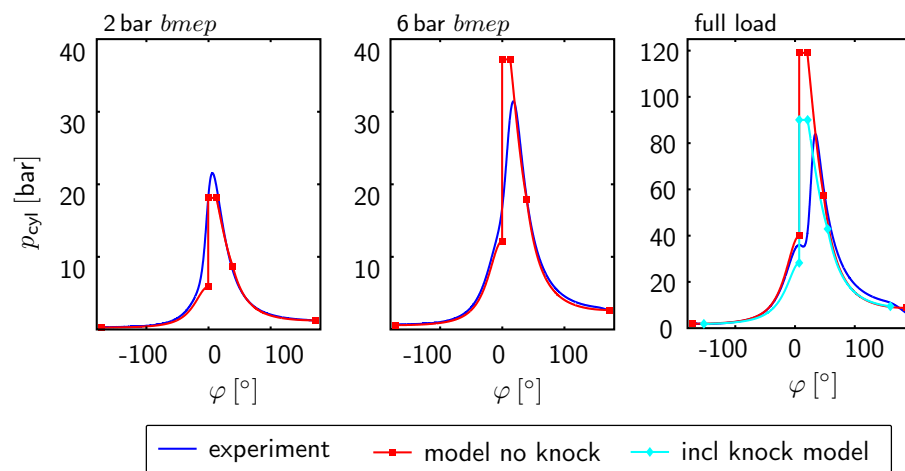


Figure 3.7: Measured and simulated pressure traces, with respect to crank angle (φ), at $N = 2000$ rpm and different loads for gasoline operation. Blue: measurements, red: modeling results without knocking detection, cyan: modeling results with adapted compression ratio to avoid knock.

3.2.2 Extended Validation

Using experimental data from an SI ICE run on gasoline, the model is able to predict the performance of such an engine. The application of the model to fuels other than gasoline is evidenced for *n*-heptane and isooctane: For *n*-heptane, knocking occurred even at the lowest compression ratio of 5. Since *n*-heptane is used as lower benchmark (RON = 0) for the RON, it is expected to be poorly suited as fuel for an SI engine. On the other hand, isooctane (RON = 100) outperforms gasoline slightly, justifying its use as an upper benchmark for the RON.

3.2 Validation

Published data for different fuels and load points [150] is compared to modeling results in Fig. 3.8, values for gasoline, ethanol and *n*-butanol are reported with respect to *imep*. For this comparison the engine geometry was changed according to the reported values. The efficiencies for gasoline and *n*-butanol are overestimated, while the one for ethanol is underestimated. For ethanol at an *imep* of 3 bar, the difference between the model (30.08%) and the experiment (30.2%) diminishes. The ignition for *n*-butanol and gasoline had to be delayed in the experiments for an *imep* of 12 bar, 21 bar and 9.4 bar, whereas the delay for the latter is minor. The model showed knocking for gasoline at an *imep* above 11 bar.

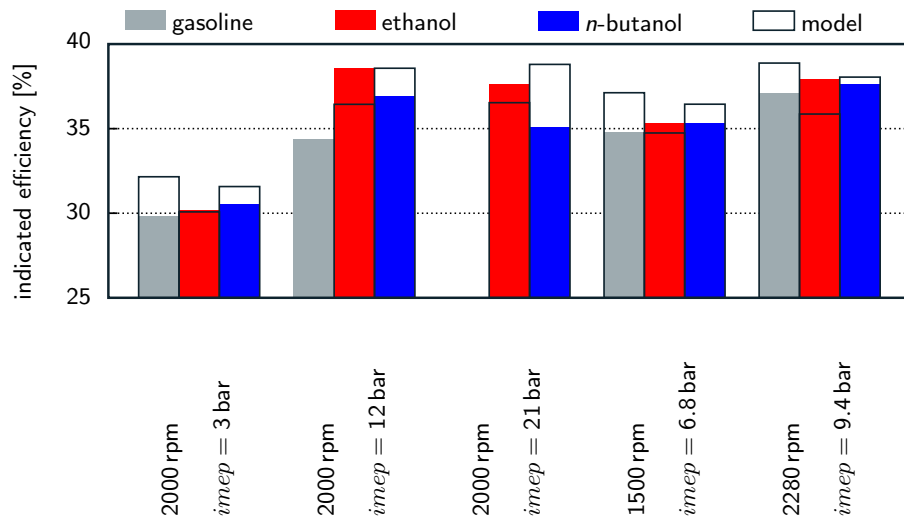


Figure 3.8: Comparison of the model predictions with published data [150] for different fuels and load points. Frames: modeling results, filled shapes: published data: gray gasoline, red ethanol, blue *n*-butanol.

In the following, the simulation results for other fuels than gasoline are compared with experimental studies performed under similar conditions. The simulation trends are in good accordance with the experimental results for ethanol, 2-MF and gasoline [17, 53]. Discrepancies are, however, observed for DMF, for which the simulation yields an efficiency similar to ethanol and significantly higher than both 2-MF and gasoline. The experimental results indicate a similar efficiency for DMF and gasoline. This can be attributed to the fact that in the simulation the optimum compression ratio for each fuel is achieved, while during the experiments the compression ratio is defined by the geometry of the engine. Experimental studies show significantly increased efficiencies at full load for *n*-butanol when compared to gasoline [21, 41, 44], which is in good agreement with the findings of the simulations.

3.3 Sensitivity Analysis

3.3.1 Method

The developed engine model encompasses various parameters, correlations and equations that interact and affect the model output at the same time. To gain more insight into the model, a Global Sensitivity Analysis (GSA) was performed to link the variation in model output γ to the variation of the input factors χ . A popular GSA approach is the Elementary Effects (EEs) method that allows ranking/screening of input factors at low computational cost [151]. The method is based on averaging locally calculated EEs around base points, distributed in the input factor hyperspace. Herein, EE_i^j of the i^{th} input factor χ_i for the j^{th} base point X^j and a perturbation Δ is calculated as

$$EE_i^j = \frac{\gamma(\chi_1^j, \dots, \chi_{i-1}^j, \chi_i^j + \Delta, \dots, \chi_M^j) - \gamma(\chi_1^j, \dots, \chi_{i-1}^j, \chi_i^j, \dots, \chi_M^j)}{\Delta} \quad (3.51)$$

Base points and perturbations were generated by a Latin Hypercube (LH) approach [152, 153]. The mean EE μ_i^* , averaged over n calculated EEs and its normalized form S_i are measures of the total sensitivity of the i^{th} of M input factors [154].

$$\mu_i^* = \frac{1}{n} \sum_{j=1}^n |EE_i^j| \quad S_i = \frac{\mu_i^*}{\max_k \mu_k^*} \quad (3.52)$$

Table 3.2: List of fuel parameters (at 298 K and 0.1 MPa) and their bounds in the Sensitivity Analysis (SA).

Input factor		Units	Bounds in SA
number of C atoms	x	–	[1, 11]
number of H atoms	y	–	[0, 24]
number of O atoms	z	–	[0, 11]
number of N atoms	v	–	[0, 11]
vapor heat capacity	$\bar{c}_{p,g}$	J/(kg K)	[1200, 2000]
liquid heat capacity	$\bar{c}_{p,L}$	J/(kg K)	[1700, 3000]
fuel density	ρ	kg/m ³	[500, 1500]
liquid kinematic viscosity	ν	m ² /s	[2, 100] × 10 ⁻⁷
vapor pressure at 298 K	p_{vap}	Pa	[1.5, 100] × 10 ³
enthalpy of vaporization	\bar{h}_{vap}	J/kg	[2, 12] × 10 ⁵
research octane number	RON	–	[50, 115]
surface tension	σ	N/m	[0.01, 0.1]

The performed SA investigated the effect of 12 input factors (see Table 3.2) on three

model outputs, including η_{FL} , P_{FL} and $e_{\text{CO}_2, \text{FL}}$. Bounds for input factors are listed in Table 3.2 and are based on the parameter ranges as given in Tables 4.1 and 4.2, being representative for a wide choice of fuels. Sensitivity values were obtained after 4.8×10^5 model evaluations ($N = n(M + 1)$, see Fig. 3.9 for convergence).

3.3.2 Convergence

The employed EE method is a sampling-based approach to SA [151]. While a too small of a sample may not yield robust results, an excessively large one may not provide a significant improvement in precision. It is therefore important to investigate how robust the obtained SA results are to changes in sample size.

For this purpose, sub-samples of the original sample were taken and the sensitivity indices (see Eq. (3.52)) and their uncertainty were calculated via the bootstrap technique [155]. Based on the width of the 95% confidence intervals of the individual sensitivity indices, a summary statistic is calculated as

$$\text{Stat} = \max_{i=1 \dots M} (S_i^{\text{ub}} - S_i^{\text{lb}}) \quad (3.53)$$

where S_i^{ub} and S_i^{lb} define the upper and lower bounds of the sensitivity index S_i and M the number of input factors [154].

Figure 3.9 presents the computed statistic for the three model outputs η , P and e_{CO_2} as a function of the number of model evaluations. Herein, convergence is assumed to be reached below a threshold of 0.05 [154]. The sensitivity indices for all three model outputs converge after 1.5×10^5 to 2.7×10^5 model evaluations.

3.3.3 Results and Discussion

The obtained S_i for η_{FL} and P_{FL} show a strong correlation that can be traced back to Eq. (3.48). The SA results can therefore be plotted as S_i for $e_{\text{CO}_2, \text{FL}}$ vs. S_i for η_{FL} and P_{FL} as depicted in Fig. 3.10.

Herein, dotted lines represent the threshold below which factors can be assumed as non-influential [156]. Three input factor groups (i–iii, marked by gray shaded areas) with comparable impact on the model outputs can be discerned. Highly influential factors in group (i) include the fuel composition (x , y , z , v) and the vapor heat capacity $c_{p, \text{g}}$. The importance of the former is related to the effect on the AFR and on the LHV, which defines the amount of fuel within the cylinder and the burnt gas composition. The least influential factors are grouped in (iii) and include parameters that only affect the fuel droplet evaporation rate. Within the varied parameter range, this rate is typically high enough to ensure complete evaporation before reaching TDC. Both parameters might therefore be fixed without changing the variance of the three model outputs. Input factors of intermediate importance are grouped in (ii), including h_{vap} , RON, ν , p_{vap} and ρ .

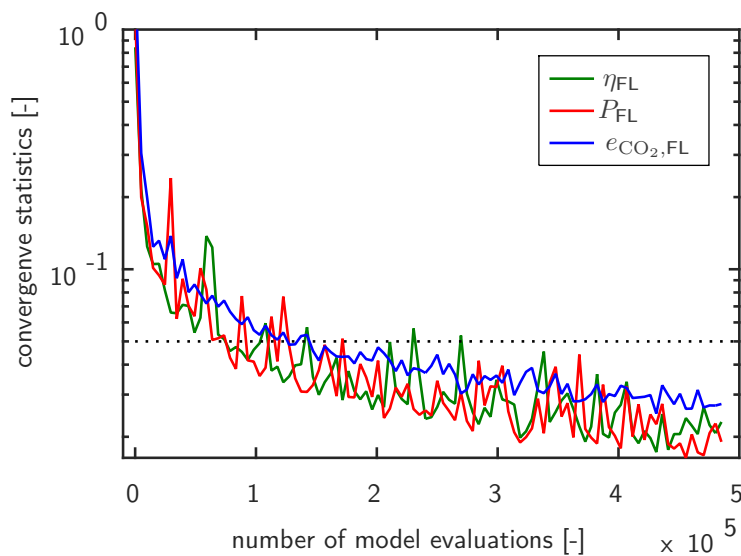


Figure 3.9: Convergence statistics *vs.* number of model evaluations for η , P and $e_{\text{CO}_2, \text{FL}}$. Threshold for convergence is set to 0.05.

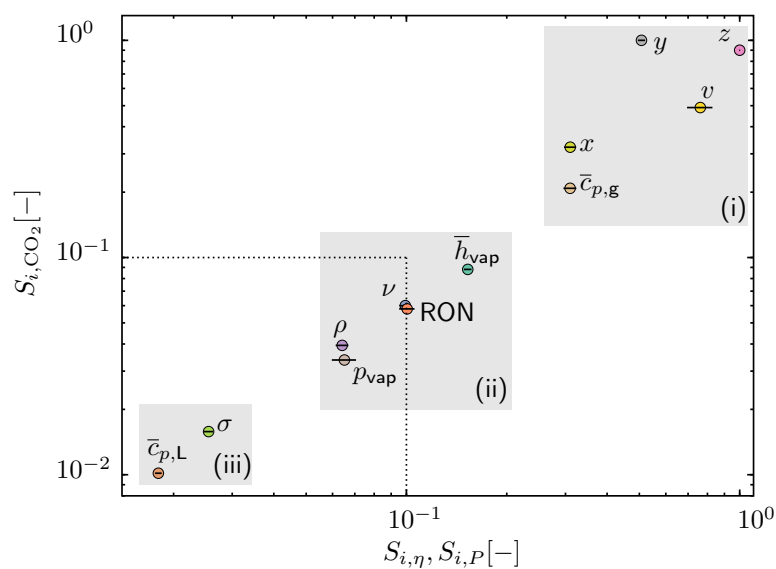


Figure 3.10: Plot of sensitivity index S_i for model output $e_{\text{CO}_2, \text{FL}}$ *vs.* S_i for η_{FL} and P_{FL} (circles represent mean values while lines the respective span). Three gray-shaded areas (i–iii) mark input factor groups of similar importance. The dotted line indicates a threshold below which the factors can be considered non-influential [156].

3.4 Model Extensions

3.4.1 Driving Cycle Modeling

Different car designs are compared by using standardized driving cycles. In the following the Worldwide harmonized Light vehicles Test Cycle (WLTC) [157], the Common Artemis Driving Cycle (CADC) [158] and the New European Driving Cycle (NEDC) [159] are investigated. To be able to predict the performance of a fuel, not only a model of the engine is required but of the whole vehicle. A comparison of different fuels is only meaningful as long as the vehicle remains the same. Therefore, the complexity of the vehicle model is reduced to the minimum. The total force acting upon the vehicle (F_{tot}) is calculated based on the velocity defined by the cycle, considering friction, drag and acceleration forces [160].

$$F_{\text{tot}} = \mu mg + c_D A \frac{\rho_{\text{air}}}{2} v^2 + m C_{\text{acc}} \frac{dv}{dt} \quad (3.54)$$

The values of the constants are listed in Table 3.3. The gearbox is neglected and it is assumed that each point within the engine map can be reached. The whole drivetrain (without the engine) is assumed to have a mechanical transmission efficiency of $\eta_{\text{trans}} = 0.85$. The power required from the engine $P_{\text{eng,req}}$ then becomes:

$$P_{\text{eng,req}} = \frac{F_{\text{tot}} v}{\eta_{\text{trans}}} \quad (3.55)$$

The value off the acceleration coefficient (C_{acc}) is set to 1.05 to reflect the moment of inertia of all the rotating parts (e.g. wheels and the flywheel).

Table 3.3: Constants for vehicle model [160].

property	symbol	value
gravitational acceleration	g	9.81 m/s ²
friction coefficient	μ	8.5×10^{-3}
vehicle mass	m	1500 kg
drag coefficient	c_D	0.3
front area	A	2.2 m ²
air density	ρ_{air}	1.2 kg/m ³
acceleration coefficient	C_{acc}	1.05

To provide a reasonable comparison between the different fuels, the cylinder volume is adjusted such that at 2000 rpm and full load, the engine provides the same power output as the gasoline engine (71 kW). To this end the secant method is applied, while keeping the bore to stroke ratio constant. The model is run as a quasi-stationary simulation, thereby ruling out all dynamic effects of switching gears and acceleration on the performance of the engine. For each required power value, the efficiency is

optimized by adjusting the rotational speed and the charging pressure under the boundary condition that the rotational speed of the engine may not be below 1000 rpm. For each load point (i) the fuel consumption ($\dot{n}_{F,i}$), power output ($P_{F,i}$) and absolute CO₂ emissions ($e_{CO_2,i}$) are determined.

The cycle efficiency (η_{cyc}), the CO₂ emissions with respect to power ($e_{CO_2,P}$) and distance ($e_{CO_2,D}$) and the consumption (c_{cyc}) are defined as follows:

$$\eta_{cyc} = \frac{\sum P_{F,i} \Delta t_i}{LHV \sum \dot{n}_{F,i} \Delta t_i} \quad (3.56)$$

$$e_{CO_2,P} = \frac{\sum e_{CO_2,i} \Delta t_i}{\sum P_{F,i} \Delta t_i} \quad (3.57)$$

$$e_{CO_2,D} = \frac{\sum e_{CO_2,i} \Delta t_i}{\sum v_i \Delta t_i} \quad (3.58)$$

$$c_{cyc} = \frac{\sum \dot{n}_{F,i} M_{fuel} \Delta t_i}{\rho_F \sum v_i \Delta t_i} \quad (3.59)$$

3.4.2 Mixtures

Most fuels are mixtures rather than pure compounds as the production of fuels with high purity is prohibitively expensive. In turn, mixtures allow for additional degrees of freedom in terms of fuel properties. Therefore, the previously presented engine model is extended to mixtures. By considering the mixture as a single compound with the properties of the mixture only minor modifications to the model are required. These properties are deduced using mixing rules presented in the following section. Miscibility of the components is not assessed and it is thereby assumed that the components are miscible at every concentration.

3.4.2.1 Mixing Rules

Vapor heat capacity ($c_{p,g,mix}$) and the enthalpy of vaporization ($h_{vap,mix}$) of the mixture are calculated based on an energy consideration which leads to a linear mixing rule:

$$c_{p,g,mix} = \sum_i x_i c_{p,g,i} \quad [J/(mol K)] \quad (3.60)$$

$$h_{vap,mix} = \sum_i x_i h_{vap,i} \quad [J/mol] \quad (3.61)$$

with x_i as the mol fraction of compound i .

Gmehling *et al.* [161] proposed to estimate the density (ρ_{mix}) of the mixture based on linear mixing of the molar volumes.

$$\rho_{\text{mix}} = \left[\sum_i \frac{w_i}{\rho_i} \right]^{-1} \quad [\text{kg/m}^3] \quad (3.62)$$

The kinematic viscosity (ν_{mix}) is modeled based on the mixing of the dynamic viscosities (μ_i) [161].

$$\nu_{\text{mix}} = \frac{1}{\rho_{\text{mix}}} \prod_i \mu_i^{x_i} \quad [\text{mm}^2/\text{s}] \quad (3.63)$$

To calculate the vapor pressure of the mixture ($p_{\text{vap,mix}}$), the activity coefficient (a) is introduced [162]

$$p_{\text{vap,mix}} = \sum_i x_i a_i(T, x) p_{\text{vap},i} \quad [\text{Pa}] \quad (3.64)$$

The activity coefficients are calculated based on the UNIFAC method [163]. For the sake of simplicity it is assumed that there is no change in composition of the mixture during evaporation.

3.4.2.2 Knock Model

To estimate the RON of a mixture, the concept of blending RON has been introduced. However, the blending RON is not directly related to the RON and depends on the mixture composition. Therefore, a large database of non-readily available, experimental data is required. To overcome this limitation, another approach is chosen instead: As the RON to model the ignition delay, a mixing rule for the ignition delay is introduced. Based on the ignition delay ($\tau_{\text{ig},i}$) of each single compound, and its volume fraction (y_i), the mixing rule calculates the ignition delay of the mixture ($\tau_{\text{ig,mix}}$) [164]:

$$\tau_{\text{ig,mix}} = \frac{\sum_i y_i^\beta}{\sum_i \left[\frac{y_i^\beta}{\tau_{\text{ig},i}} \right]} \quad (3.65)$$

with an empirical coefficient $\beta = 3$ that has been determined based on a mixture of 10 % *n*-heptane, 25 % isooctane, 20 % 1-hexene, 25 % toluene, 10 % ethanol and 10 % butane [164].

Calculating the ignition delays ($\tau_{\text{ig},i}$) of the components based on Eq. (3.41) [141] entails problems with components with very low octane numbers (e.g. *n*-heptane (RON = 0)). According to the applied ignition delay correlation, the ignition delay of *n*-heptane is 0, regardless of the pressure and temperature. That would imply that *n*-heptane ignites instantly upon mixing with oxygen, even at low temperatures. In

combination with Eq. (3.65), this leads to much lower ignition delays than observed in practice for mixtures containing *n*-heptane. To overcome this shortcoming, the RON dependence of the ignition delay has been refitted. The initial correlation is defined for values of RONs between 80 and 100. As opposed to the potential function of the original correlation, an exponential function is proposed since this leads by design to non-zero ignition delays for a RON of 0. As a result, the following equation with parameters $\beta_{0,1,2}$ to be fitted for RONs between 80 and 100 is formulated.

$$\left(\frac{\text{RON}}{100}\right)^{3.402} = \exp\left[\beta_0\left(\frac{\text{RON}}{100}\right)^2 + \beta_1\left(\frac{\text{RON}}{100}\right) + \beta_2\right] \quad (3.66)$$

The parameters are shown within the context of the adapted ignition delay ($\tau_{\text{ig,a}}$) correlation. The fit yields a R^2 value of 0.9999986.

$$\tau_{\text{ig,a}} = 17.68 \exp\left[-5.481 + 7.592\frac{\text{RON}}{100} - 2.112\left(\frac{\text{RON}}{100}\right)^2\right] \frac{\exp\left[\frac{3800}{T_{\text{ub}}}\right]}{p^{1.7}} \quad (3.67)$$

3.4.2.3 Validation

Data for 99 different mixtures, consisting of *n*-heptane, isooctane, toluene, diisobutylene, ethanol, MTBE, 1-hexene and methylcyclohexane (together with their RON) are taken from the literature [165–170]. Their properties as pure compounds are listed in Tables 4.1 and 4.2. This data is used to validate the proposed knock model for mixtures. In Fig. 3.11 the compression ratio for the different mixtures is plotted with respect to their RONs. As a reference, the mixture properties are calculated and, together with the known RON run through the single component model.

The influence of *n*-heptane on the error in compression ratio is presented in Fig. 3.12. The error in compression ratio in relation to the fraction of *n*-heptane is a measure for the sensitivity of the ignition model to compounds with low RON. The initial ignition delay model is sensitive to low levels of *n*-heptane. Thus the error in compression ratio is high regardless of the fraction of *n*-heptane. For high volumetric fractions the level diminishes as the respective mixtures is subject to knock in any case. As expected the adapted ignition delay model reduces the errors. As long as the volumetric fraction of *n*-heptane remains below 10 vol % the error stays below 10 %. Beyond this region the errors raise to similar levels as for the initial model.

Figs. 3.11 and 3.12 show that the adaptation of the ignition delay correlation is beneficial. However, the model has limitations for mixtures containing compounds with low RONs. As in Fig. 3.12 relative error of the compression ratio stays below 10 % for mixtures containing up to 10 % *n*-heptane, which is a significant improvement gained by the adaption.

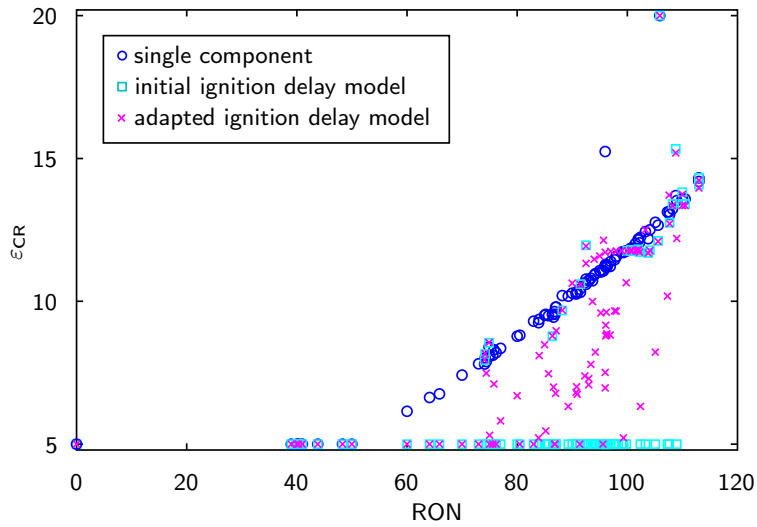


Figure 3.11: Comparison between the different models in terms of compression ratio *vs.* RON. Blue circles: single compound model (Eq. (3.41)), cyan squares: mixture model using the initial ignition delay model (Eqs. (3.41) and (3.65)), pink cross: mixture model using the adapted ignition delay model (Eqs. (3.65) and (3.67)).

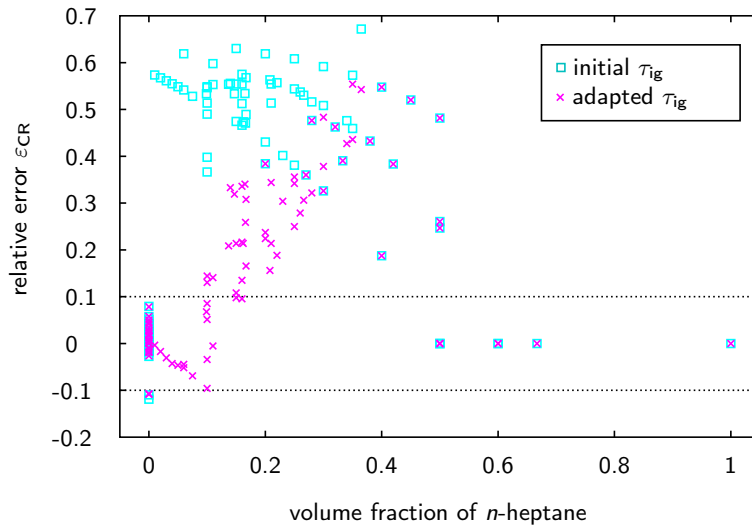


Figure 3.12: Comparison between the two autoignition correlations, in terms of relative error in compression ratio *vs.* volume fraction of *n*-heptane. Cyan squares: initial ignition delay model, pink cross: adapted ignition delay model Eq. (3.67).

3.4.3 Hybrid Powertrains

Hybrid powertrains consist of a combination of electric and internal combustion engines. Hybridization allows reducing consumption due to two mechanisms: Recuperation of brake energy and running the ICE at peak efficiency. The energy required (E_f) for a hybrid powered car over a given driving cycle can be calculated using Eq. (3.68) [171].

$$E_f = \frac{1}{\eta_{FL}} [E_{diss} + (1 - \eta_r) E_{circ}] \quad [\text{MJ/km}] \quad (3.68)$$

with η_r the recuperation efficiency, E_{diss} the dissipative energy demand, and E_{circ} the so called circulating energy (acceleration and potential energy) [171]. Ott *et al.* [171] studied a full parallel hybrid and determined that the recuperation efficiency is almost constant at a value close to 63% independent of the driving cycle. For a given car on a given cycle the equation can be simplified by the introduction of a constant (K_{hp}).

$$E_f = \frac{1}{\eta_{FL}} K_{hp} \quad (3.69)$$

The value of K_{hp} is determined based on the three different cycles introduced in Section 3.4.1 which gives the values listed in Table 3.4.

Table 3.4: Hybrid energy demand for standard driving cycles.

Cycle	K_{hp}	E_{circ}	E_{diss}
CADC	0.56 MJ/km	0.17 MJ/km	0.50 MJ/km
WLTC	0.47 MJ/km	0.16 MJ/km	0.41 MJ/km
NEDC	0.40 MJ/km	0.16 MJ/km	0.35 MJ/km

Rearrangement of Eq. (3.69) in conjunction with the volumetric energy density allows calculating the consumption (c_{hp}). Including the elemental composition leads to the specific CO₂ emissions ($e_{CO_2, hp}$) with respect to the travelled distance:

$$c_{hp} = \frac{100K_{hp}}{LHV\rho\eta_{FL}} \quad [l/100 \text{ km}] \quad (3.70)$$

$$e_{CO_2, hp} = c_{hp}\rho \frac{xM_{CO_2}}{M_{fuel}} \quad [g_{CO_2}/km] \quad (3.71)$$

It is important to note that the presented modeling approach is an idealization. There are several limitations in reality that are difficult to model at this level of detail. A prominent restraint is the fact that batteries impose a limitation on the charging current. Thereby they are limiting the amount of recuperated power, the easiest solution to this problem is to increase the battery size. However, this increases the weight of the vehicle

and thus the energy required. Another limitation is the need for a minimum torque for recuperation that puts a limit to the minimum velocity at which recuperation is feasible.

4 Review of the Performance of Pure Fuels

4.1 Introduction

In the following section the potential biofuels presented in Section 2.1 are discussed and compared to gasoline. As gasoline is a mixture of hundreds of hydrocarbons, a selection of those present in gasoline and used as gasoline surrogate mixture [165, 166, 170, 172–174] is listed in Table 4.1 and used as a reference. The relevant input parameters of the biofuels are listed in Table 4.2. Using the ICE model, their performance as fuel is evaluated and compared to gasoline.

Table 4.1: Gasoline and a selection of its components/additives used as reference including their properties at standard conditions ($T = 298$ K, $p = 0.1$ MPa).

fuel	formula	ρ [kg/m ³]	$c_{p,g}$ [J/(mol K)]	h_{vap} [kJ/mol]	p_{vap} [kPa]	ν [mm ² /s]	RON [-]	LHV [MJ/kg]
gasoline	C ₇ H ₁₄ ^c	748 ^e	154.6 ^f	34.5 ^d	34.3 ^c	0.41 ^d	98 ^b	43.6 ^a
isooctane	C ₈ H ₁₈	689	187.1	35.2	6.5	0.69	100 ^b	44.6 ^a
<i>n</i> -heptane	C ₇ H ₁₆	680	164.3	36.6	6.0	0.58	0 ^b	44.7 ^a
1-hexene	C ₆ H ₁₂	668	133.0	31.3	23.9	0.40	75 ^g	43.6 ^a
diisobutylene	C ₈ H ₁₆	709	181.1	35.8	5.9	0.41	106 ^h	43.6 ^a
cyclohexane	C ₆ H ₁₂	772	107.0	32.9	13.0	1.16	83 ^h	43.6 ^a
methylcyclohexane	C ₇ H ₁₄	764	135.0	35.7	158.4	0.90	75 ^h	43.6 ^a
benzene	C ₆ H ₆	872	82.7	33.9	12.6	0.69	108 ⁱ	39.6 ^a
toluene	C ₇ H ₈	863	105.0	37.9	3.8	0.64	113 ^j	40.2 ^a
MTBE	C ₅ H ₁₂ O	735	135.3	30.1	33.1	0.46	117 ^h	35.0 ^a
ETBE	C ₆ H ₁₄ O	735	156.0	33.0	16.7	0.59	118 ^h	36.2 ^a

^a estimated according to [93]; ^b by definition; ^c [74]; ^d [34]; ^e [175];
^f [176]; ^g [165]; ^h [118]; ⁱ [123]; ^j [165]; ^h [177]

The values given in Tables 4.1 and 4.2 are, if not stated otherwise, taken from the

Contents of this chapter have been published or submitted: [15, 73, 115]

Table 4.2: Investigated fuel molecules and their properties at standard conditions ($T = 298$ K, $p = 0.1$ MPa).

fuel	formula	ρ [kg/m ³]	$c_{p,g}$ [J/(mol K)]	h_{vap} [kJ/mol]	p_{vap} [kPa]	ν [mm ² /s]	RON [-]	LHV [MJ/kg]
methanol	CH ₄ O	789	44	37.5	16.7	0.68	109 ^b	19.9 ^a
ethanol	C ₂ H ₆ O	785	65	42.6	7.9	1.38	109 ^c	27.1 ^a
<i>n</i> -propanol	C ₃ H ₈ O	798	85	47.9	2.8	2.45	104 ^c	31.0 ^a
isopropanol	C ₃ H ₈ O	781	90	46.1	5.7	2.64	106 ^c	31.0 ^a
<i>n</i> -butanol	C ₄ H ₁₀ O	805	110	52.5	0.9	3.53	98 ^c	33.4 ^a
isobutanol	C ₄ H ₁₀ O	796	110	52.0	1.4	4.21	105 ^c	33.4 ^a
<i>sec</i> -butanol	C ₄ H ₁₀ O	801	113	50.4	2.3	3.85	105 ^c	33.4 ^a
<i>tert</i> -butanol	C ₄ H ₁₀ O	781	114	46.6	5.5	5.90	105 ^c	33.4 ^a
<i>n</i> -pentanol	C ₅ H ₁₂ O	811	130	57.1	0.3	4.27	78 ^c	35.0 ^a
isopentanol	C ₅ H ₁₂ O	806	131	56.4	0.4	4.55	94 ^c	35.0 ^a
2-MF	C ₅ H ₆ O	913 ^c	90 ^d	29.4 ^d	18.5 ^d	4.00 ^e	103 ^c	30.5 ^a
DMF	C ₆ H ₈ O	889 ^f	135 ^d	32.0 ^d	7.1 ^d	0.65 ^g	119 ^c	32.4 ^a
2-MthF	C ₅ H ₁₀ O	847	106	33.6	12.7	0.56	86 ^c	33.6 ^a
GVL	C ₅ H ₈ O ₂	1048	131	53.0	0.1	2.28	100 ^c	25.3 ^a
methyl valerate	C ₆ H ₁₂ O ₂	895 ^c	159 ^h	43.1 ^c	1.0 ^c	0.76 ^h	105 ^c	28.7 ^a
ethyl valerate	C ₇ H ₁₄ O ₂	882 ⁱ	182 ^h	49.2 ^h	0.6 ⁱ	0.96 ^h	89 ^{j,k}	30.3 ^a
methyl levulinate	C ₆ H ₁₀ O ₃	1020 ⁱ	159 ^h	50.4 ^d	0.1 ^d	1.16 ^h	100 ^{j,k}	22.9 ^a
ethyl levulinate	C ₇ H ₁₂ O ₃	1007	176	58.9	0.02	1.70	110 ^c	24.9 ^a
butyl levulinate	C ₉ H ₁₆ O ₃	974 ^c	228 ^h	47.7 ^c	0.01 ⁴	1.37 ⁱ	98 ^c	28.0 ^a
α -pinene	C ₁₀ H ₁₆	855 ^l	173	35.6 ^l	6.4 ^l	1.74	85 ^l	42.1 ^a
2-butanone	C ₄ H ₈ O	798	103	34.5	12.2	0.50	117 ^m	31.6 ^a
methyl-isopropyl ketone	C ₅ H ₁₀ O	798	112	36.4	6.9	0.54	117 ^{m,k}	33.6 ^a
diisopropyl ether	C ₆ H ₁₄ O	719	157	31.6	19.7	0.45	105 ⁿ	36.2 ^a
ethyl furfuryl ether	C ₇ H ₁₀ O ₂	986 ⁱ	151 ^h	46.3 ^h	1.5 ⁱ	0.92 ^h	89 ^{j,k}	28.3 ^a
isobutyraldehyde	C ₄ H ₈ O	782	99	33.9	20.9	0.67	84 ^j	31.6 ^a
methyl isobutyl ketone	C ₆ H ₁₂ O	795	148	40.8	2.6	0.69	88 ^{o,k}	35.0 ^a
ethyl acetate	C ₄ H ₈ O ₂	893	114	35.7	12.3	0.48	99 ^{o,k}	24.0 ^a
ethyl propanoate	C ₅ H ₁₀ O ₂	882	133	39.5	4.9	0.57	91 ^{o,k}	26.7 ^a
propyl acetate	C ₅ H ₁₀ O ₂	881	136	39.7	4.4	0.63	91 ^{o,k}	26.7 ^a
isopropyl acetate	C ₅ H ₁₀ O ₂	868	131	36.8	8.0	0.57	106 ^{o,k}	26.7 ^a
TMED	C ₈ H ₁₆ O ₂	870 ⁱ	179 ^h	47.6 ^h	1.6 ⁱ	1.55 ⁱ	94 ^p	31.6 ^a
furfuryl alcohol	C ₅ H ₆ O ₂	1127	118	56.8	0.1	4.30	106 ^j	23.9 ^a
4-methylanisole	C ₈ H ₁₀ O	969	141	39.0	0.5 ^q	0.84	113 ^{r,k}	34.0 ^a
2-phenylethanol	C ₈ H ₁₀ O	1016	141	60.6	0.1	0.80	111 ^{j,k}	34.0 ^a

^a estimated according to [93]; ^b [178]; ^c [34]; ^d [129]; ^e [49]; ^f [53];
^g [179]; ^h estimated by GCM; ⁱ [180]; ^j [181]; ^k estimated via dCN; ^l [22];
^m [182]; ⁿ [177]; ^o [24]; ^p [68]; ^q estimated by Clausius–Claperyon equation;
^r [55]

DIPPR database [126]. For recently proposed or less well-established compounds, values for the RON are not always available. As the dCN is less complicated to measure, data for a wider range of compounds is readily available. The dCN is inversely correlated to the RON, which is reflected in the correlation presented in Appendix B.1. It is used to estimate the RON if needed, marked in Table 4.2 by ^k.

4.2 Results and Discussion

4.2.1 Loss Analysis

An overview of the energy distribution for a selection of fuels is depicted in Fig. 4.1. Interestingly, the output power (P_{out}), the overall wall heat losses (\dot{Q}_{wall}) and the enthalpy of the exhaust gas (\dot{H}_{ex}) account for about 95% of the total energy input.

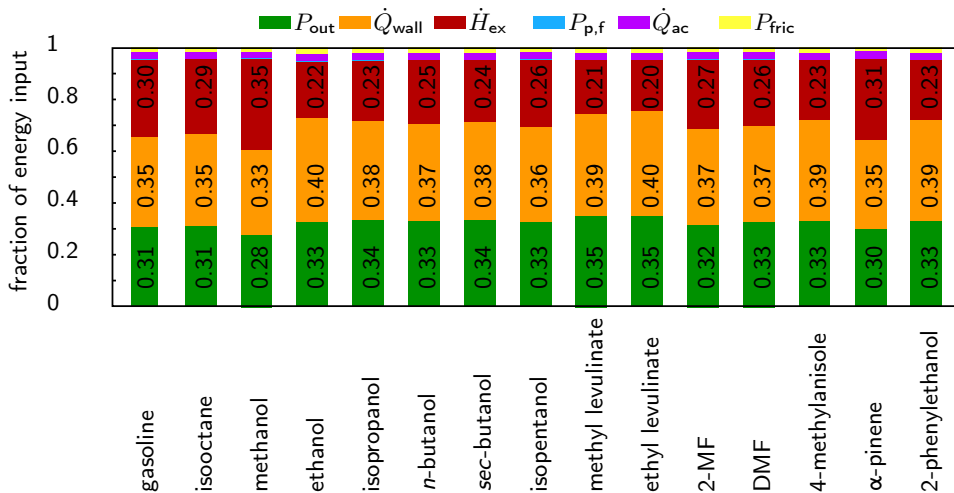


Figure 4.1: Distribution of total energy input at full load. $P_{\text{p,f}}$ power supplied to fuel pump, P_{out} net power output of the engine, P_{fric} friction losses within the engine, \dot{Q}_{wall} wall heat losses, \dot{Q}_{ac} heat transferred by after cooler, \dot{H}_{ex} enthalpy of the exhaust stream.

As shown in Fig. 4.2, the wall heat losses and the power output generally increase with the compression ratio, while the exhaust enthalpy decreases. The peak pressure is a direct function of the compression ratio, and the pressure governs the wall heat losses. The decrease in exhaust enthalpy can be explained by the increased expansion in high compression ratio engines. A broad optimum exists around a compression ratio of about 14. Two compounds are outside of the general trend: butyl levulinate (BL) and methanol. Since several of the properties of methanol are extreme in comparison with the other fuels, it is difficult to pinpoint the main effect. Butyl levulinate shows a very low volatility, and non-evaporated fuel remains at the time of ignition. This fraction of non-evaporated fuel remains unburnt. Thus, only a fraction of the injected

fuel contributes to the output power. According to Eq. (3.48) this leads to a reduced efficiency.

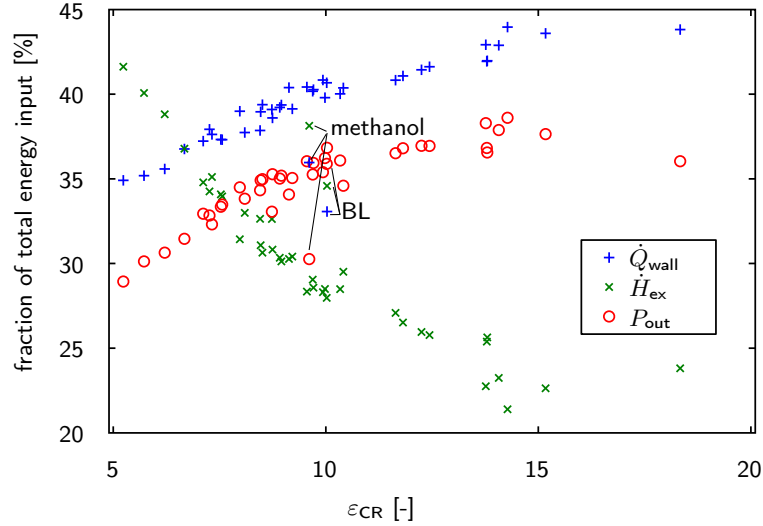


Figure 4.2: The three main energy flows, wall heat losses (\dot{Q}_{wall}), exhaust enthalpy (\dot{H}_{ex}) and power output (P_{out}) with respect to the compression ratio (ε_{CR}).

As expected, friction shows a strong dependence on the compression ratio (Fig. 4.3). An increase in compression ratio is connected with a higher peak pressure, which requires, among others, more robust bearings. Fuel pump power and after cooler heat flow can be considered independent of the compression ratio (Fig. 4.3). Overall, the friction losses show the biggest relative change over the whole compression ratio range.

Friction losses are 29% higher for ethanol and 8% lower for DMF than for *n*-butanol. The other shares vary less than 2% (again compared to *n*-butanol). Overall, this leads to a power output fraction of 33.3% for *n*-butanol, followed by ethanol (32.9%) and DMF (32.7%).

4.2.2 Single Load Points

In Table 4.3, efficiency, power output, compression ratio, and specific CO₂ emissions of the studied fuels are listed for different load points and the WLTC. Further results including values for the other driving cycles (NEDC and CADC) are given in Appendix B.2.

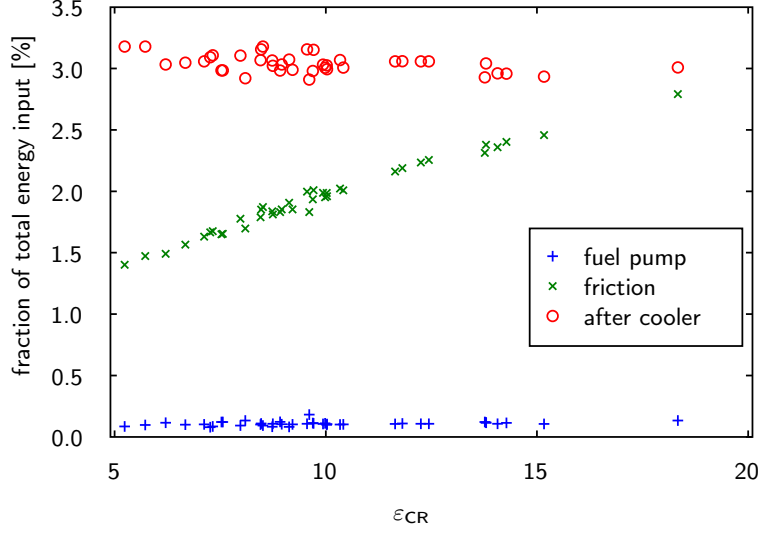


Figure 4.3: Minor energy flows, fuel pump power, friction losses and after cooler with respect to the compression ratio (ε_{CR}).

Table 4.3: Overview of the performance of all fuels. η_{FL} efficiency at full load, η_{PL} efficiency at 2000 rpm and $P_{out} = 6.6$ kW, P_{FL} power output at full load, e_{FL} specific CO₂ emissions, ε_{CR} compression ratio, η_{cyc} cycle efficiency, e_D CO₂ emissions per distance and c consumption over the WLTC.

fuel	label	η_{FL}	η_{PL}	P_{FL}	e_{FL}	ε_{CR}	η_{cyc}	e_D	c
		[%]	[%]	[kW]	[kg/kWh]	[-]	[%]	[g/km]	[l/100km]
gasoline		33.7	20.8	70.8	0.77	7.7	21.1	193	8.2
isooctane	iO	34.5	21.2	74.2	0.72	8.0	21.5	182	8.6
<i>n</i> -heptane					<i>knocking</i>				
1-hexene	Hx	30.1	19.1	63.2	0.86	5.7	19.4	210	10.0
diisobutylene	diB	35.0	21.4	73.5	0.74	8.5	21.7	187	8.4
cyclohexane	ch	32.3	20.1	69.4	0.80	7.3	20.3	201	8.3
methylcyclohexane	mch	28.9	18.6	60.7	0.90	5.2	18.8	216	9.0
benzene		33.1	20.3	72.0	0.93	8.7	20.6	234	7.9
toluene	T	34.1	20.8	74.1	0.88	9.1	21.1	223	7.7
MTBE		35.7	21.6	75.6	0.72	9.4	22.1	183	9.9
ETBE		36.0	21.9	76.2	0.71	9.6	22.3	181	9.5
methanol		30.3	18.3	69.4	0.82	9.6	18.6	209	19.3
ethanol		36.0	22.0	80.1	0.70	18.3	22.5	177	11.8

Table 4.3 - *continued*

fuel	short	η_{FL}	η_{PL}	P_{FL}	e_{FL}	ε_{CR}	η_{cyc}	e_D	c
		[%]	[%]	[kW]	[kg/kWh]	[-]	[%]	[g/km]	[l/100km]
<i>n</i> -propanol	n3	36.6	22.0	80.3	0.70	13.8	22.6	178	10.1
isopropanol	i3	36.8	22.1	80.9	0.69	13.8	22.7	176	10.3
<i>n</i> -butanol	n4	36.5	22.0	79.8	0.70	11.6	22.5	179	9.3
isobutanol	i4	36.9	22.3	80.7	0.69	12.4	22.8	177	9.3
<i>sec</i> -butanol	s4	37.0	22.3	80.7	0.69	12.3	22.8	177	9.3
<i>tert</i> -butanol	t4	36.8	22.2	80.4	0.70	11.8	22.7	177	9.5
<i>n</i> -pentanol	n5	34.3	20.9	74.7	0.75	8.5	21.3	189	9.3
isopentanol	i5	36.1	21.8	78.5	0.71	10.3	22.3	181	9.0
2-MF	MF	34.6	21.0	76.8	0.91	10.4	21.4	232	9.5
DMF		35.9	21.7	79.2	0.85	10.0	22.1	216	8.8
2-MthF	MthF	31.5	19.6	68.9	0.87	6.7	19.9	217	10.0
GVL		37.9	22.8	85.5	0.83	14.1	23.4	210	9.1
methyl valerate	MV	36.2	22.1	80.5	0.79	10.0	22.9	195	9.6
ethyl valerate	EV	35.3	21.5	77.9	0.80	8.7	22.0	201	9.6
methyl levulinate	ML	38.3	23.0	87.4	0.83	13.8	23.7	212	10.2
ethyl levulinate	EL	38.6	23.2	87.2	0.80	14.3	23.9	203	9.4
butyl levulinate	BL	36.8	22.2	82.2	0.81	10.0	22.8	204	9.1
α -pinene		32.8	20.4	70.9	0.84	7.3	20.6	211	7.6
2-butanone	B	35.3	21.3	79.0	0.79	9.7	21.8	200	10.3
methyl-isopropyl ketone	MIK	35.4	21.4	78.0	0.77	9.9	21.9	197	9.6
diisopropyl ether	ipE	34.9	21.3	73.8	0.74	8.5	21.7	186	10.0
ethyl furfuryl ether	EFE	35.0	21.3	78.3	0.89	9.2	21.7	225	9.3
isobutyraldehyde	IBA	30.6	19.3	67.4	0.91	6.2	19.5	224	11.7
methyl isobutyl ketone	MibK	32.9	20.5	71.9	0.82	7.1	20.6	207	9.8
ethyl acetate	EA	33.8	20.7	77.3	0.89	8.1	21.0	224	12.5
ethyl propanoate	EP	33.4	20.6	74.6	0.87	7.5	20.8	219	11.5
propyl acetate	PA	33.5	20.7	74.9	0.87	7.6	20.8	219	11.5
isopropyl acetate	IA	35.0	21.3	78.4	0.83	8.9	21.7	210	11.2
TMED		35.2	21.5	77.5	0.79	9.0	21.8	200	9.4
furfuryl alcohol	FFA	37.6	22.6	85.7	0.90	15.2	23.3	228	9.0
4-methylanisole	MA	36.3	22.0	80.0	0.84	11.6	22.5	213	7.6
2-phenylethanol	PE	36.5	22.0	80.4	0.84	12.0	22.6	212	7.2

Levulinates show the highest efficiencies: peak efficiency is reached by ethyl levulinate with 38.6%, followed by methyl levulinate with 38.3%. Compression ratios are between about 7 to 14, which lies in the range of today's SI engines and reflects the tendency

towards higher compression ratios. The compression ratio of ethanol is significantly higher than the values for all other fuels. It is rather in the range of a Diesel engine than in the range of an SI engine. These findings are in line with experimental studies that report the possibility to significantly increase the compression ratio of engines running on ethanol [11, 21, 183–185]. First tests to exploit this potential have already been conducted by converting a Diesel engine to SI operation [186].

Thewes *et al.* [21] further determined the optimum compression ratio between 7 to 13.5 for gasoline, ethanol, *n*-butanol and 2-MthF. As shown in Table 4.4 experimental and model values agree well.

Table 4.4: Comparison between experimentally optimized compression ratios and model predictions.

Fuel	Experiment [21]	Model (this work)
gasoline	8.5	7.7
<i>n</i> -butanol	10.0	11.6
2-MthF	<7.0	6.7
ethanol	>13.5	18.3

DMF and ethanol are two frequently discussed biofuels and show high efficiencies and similar power outputs. Although DMF has a RON of 119 and ethanol of 109, the optimum compression ratio is much lower for DMF than for ethanol. This observation suggests that other fuel properties also affect the optimum compression ratio. The maximum compression ratio is limited by the onset of knocking. According to the knock-model, the temperature at TDC is one of the governing factors influencing the occurrence of knock. Besides the compression ratio, the enthalpy of vaporization, the vapor heat capacity as well as the air to fuel ratio influence the temperature (T_2) at TDC. In the case of DMF and ethanol, both $c_{p,g}$ and h_{vap} have very different values. Therefore different temperature and pressure curves are expected.

The results at the full load point are presented in Fig. 4.4. The alcohols, excluding methanol, *n*-pentanol (n5) and furfuryl alcohol (FFA), show the best overall performance followed by ethyl *tert*-butyl ether (ETBE) and MTBE. Diisopropyl ether (ipE), *n*-pentanol, isooctane and diisobutylene (diB) outperform gasoline to a lower extent. If CO₂ emissions are climate-neutral, ethyl levulinate (EL), methyl levulinate (ML), GVL and furfuryl alcohol (FFA) would be of interest as they show maximum efficiency.

To better distinguish between the different alcohols in Fig. 4.5 the dependence between chain length and efficiency is shown. The optimum for butanol is interesting as it shows a trade-off between RON and elemental composition effects. The RON decreases with increasing chain length, while AFR, LHV, and related properties increase.

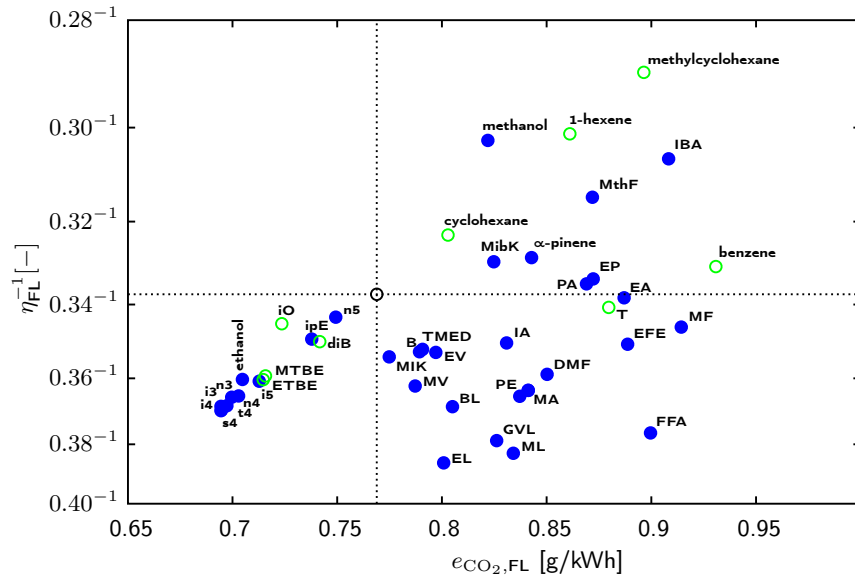


Figure 4.4: Comparison of the different fuels with respect to CO₂ emissions and efficiency at full load. Blue: biofuels, green: gasoline components, black: gasoline.

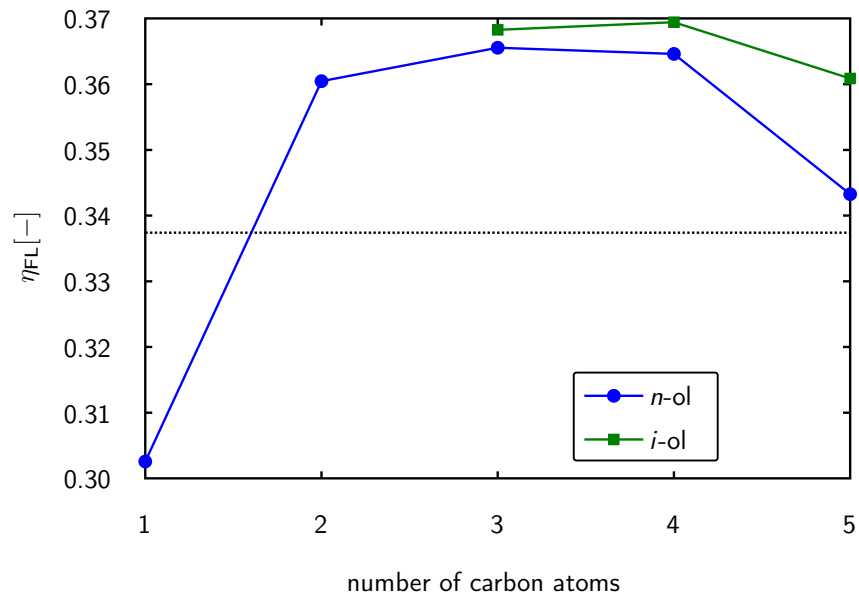


Figure 4.5: Influence of carbon chain length on efficiency at full load for alcohols.

4.2.3 Cycle Operation

The performance of all fuels over three different driving cycles, the WLTC, the CADC and the NEDC, is evaluated. The results are similar for all three cycles, only the values over the WLTC are listed in Table 4.3. The interested reader is referred to the Appendix B.2 for the full list.

In Fig. 4.6, the results for the WLTC are summarized regarding CO₂ emissions per distance and consumption. No compound is superior to gasoline for both metrics. 2-phenylethanol, 4-methylanisole, benzene, toluene, and α -pinene are the only fuels with lower consumption than gasoline. Lower CO₂ emissions at the cost of higher consumption is achieved by alcohols (except methanol and FFA), ethers (MTBE, ETBE and diisopropyl ether), isooctane and diisobutylene. The other fuels perform worse than gasoline with respect to both criteria, with a staggering consumption of almost 20l/100 km for methanol. In the literature reported methanol consumption values are roughly twice that of gasoline [187].

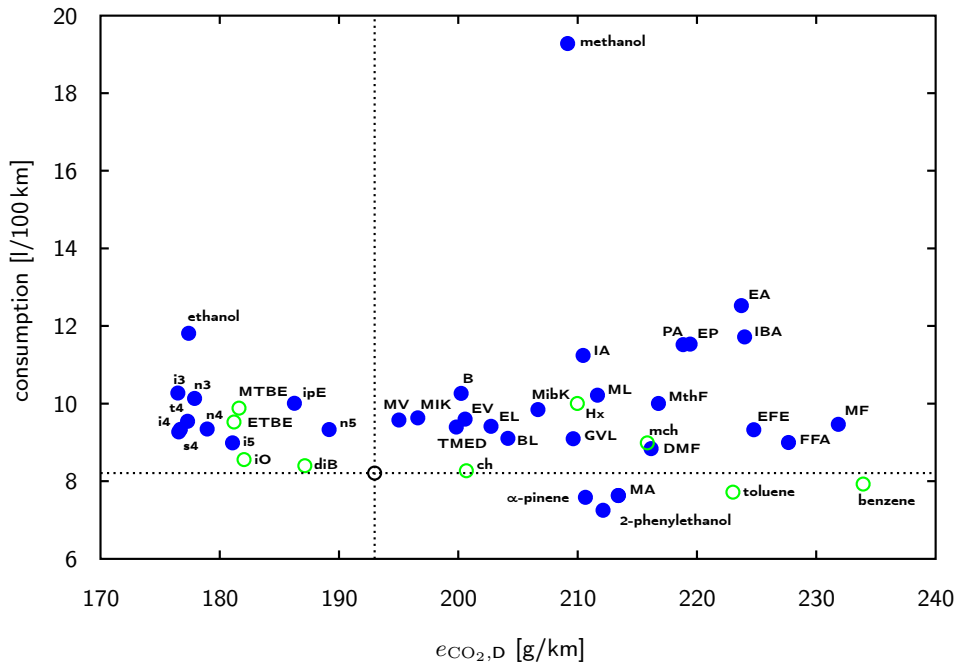


Figure 4.6: Comparison of the different fuels with respect to consumption and CO₂ emissions over the WLTC. Blue: biofuels, green: gasoline components, black: gasoline.

The different results in terms of efficiency at full load (η_{FL}) and consumption arise from two different reasons: firstly, volumetric consumption includes density and LHV besides the efficiency, and secondly, due to high shares of part load over a driving cycle the full load efficiency is not necessarily directly linked to the cycle efficiency.

Based on these findings, the fuel choice depends on the criteria to be applied:

sec-butanol followed by the other butanol isomers and isopropanol are most promising with regard to CO₂ emissions. From a consumer's perspective, consumption is a particularly interesting parameter. 2-phenylethanol together with α -pinene and 4-methylanisole outperform the other biofuel candidates.

4.2.4 Hybrid Powertrains

According to Eq. (3.71), the specific CO₂ emissions depend only on the consumption and the amount of carbon in the fuel. Therefore, the only way to reduce the emissions is to lower the consumption or changing the fuel. Thus, the reduction potential for a given fuel is the same for consumption and CO₂ emissions. In Fig. 4.7, the reduction potential for CO₂ emissions and consumption are shown for the different driving cycles. Depending on the driving cycle 40% to 60% \pm 0.8% to 2.0% reduction can be expected, regardless of the fuel.

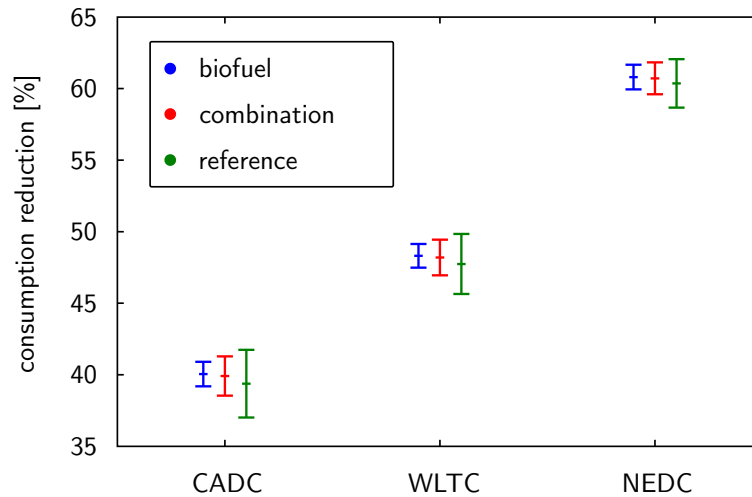


Figure 4.7: Representation of the reduction potential (consumption and CO₂ emissions) for hybrid powertrains over different driving cycles. Blue: biofuels, green: gasoline and its components, red: all studied fuels.

Toyota claims a consumption of down to 31/100 km for its Prius IV [188]. Comparing this value to the modeling results for a gasoline car, this is a reduction of 63% that is in the order of the predictions for the NEDC. Values given by car manufacturers are in general optimistic and therefore might compensate for the idealization in modeling. Another unknown parameter is the exact specifications of the Prius. Therefore, no adjustments to the weight, cross sectional area or the drag coefficient could be made.

4.3 Summary

The presented model has been used to review the performance of different biofuels in pure form with relation to gasoline. Depending on the relevance of certain parameters, different fuels can be recommended. If reduction of CO₂ emissions is most important, butanol and propanol isomers are most promising. The use of *sec*-butanol leads to CO₂ emissions of only 177 g/km (−8%), while increasing the consumption by 13% from 8.21/100 km (gasoline) to 9.31/100 km. Minimum consumption is achieved by 2-phenylethanol (7.21/100 km) with a reduction of 12% compared to gasoline and at the expense of an increase in CO₂ emissions to 212 g/km (10%). Suitability criteria not linked to performance, such as oil dilution, cold start behavior or emissions, have not been assessed and need further investigation. To judge the sustainability of a fuel additionally to its performance in an engine, production needs to be taken into account.

The loss analysis showed that the major influencing factor is the compression ratio, showing a broad optimum around 14.

Regardless of the fuel chosen, a significant reduction of both CO₂ emissions and consumption is achieved by employing hybrid powertrains. The reduction potential for the considered idealized case is in the order of 40 to 60%. Although the issue of climate change cannot be solved by that measure alone, it allows reducing the CO₂ emissions by a factor of about 2. It also reduces the consumption by the same factor and eventually the required biomass for fuel production.

The introduction of hybrid powertrains does not affect the quest for the best fuel. Fuels well-suited for hybrid operation perform equally well under traditional operation.

5 Fuel Design based on Lignin Pyrolysis Oil

5.1 Introduction

Lignin accounts for roughly 40% of the energy content of lignocellulosic biomass. However, its chemical recalcitrance hampers its full exploitation. Most of today's biorefinery concepts are missing practical ways to valorize lignin. Fast pyrolysis is an easy and well-established way to liquefy lignin [190, 191]. In general, fast pyrolysis leads to three fractions: char, liquid, and gas. The liquid fraction, so called bio-oil, consists of numerous different aromatic and non-aromatic compounds. As this liquid is not suited as fuel for ICEs, an upgrading is indispensable [191–193]. Therefore, HDO has previously been studied to reduce the oxygen content of the compounds and/or to achieve saturation by hydrogen addition [194].

Within this chapter, the question of optimum upgrading is discussed using the ICE model in combination with a reaction network.

Lignin-derived pyrolysis oil is a mixture of several hundred components. The exact composition depends on the origin of the biomass and on the applied process conditions. In prior studies, the main building blocks (shown in Fig. 5.1) and the side chains (listed in Figs. 5.2 to 5.5) have been identified [194–196]. The number of identified substances varies between different studies. Although the occurrence of up to 400 different compounds has been reported [51], the number of exactly identified molecules is in the range of 50. Therefore the number of studied side chains is increased by extrapolation based on the functional groups present in the literature.

All possible combinations of main building blocks and side chains lead to a mixture of 276 different compounds. In this study all combinations of main building blocks and side chains have been taken into account, although the presence of not all of them has been verified experimentally in literature. The reason for this is threefold: First, within the vast amount of different components they may be present but not detected so far. Second, even if they are not present, (minor) changes in the process conditions could possibly favor their production. Third, this systematic approach may allow the identification of possible trends.

Contents of this chapter have been published or submitted: [91, 189]

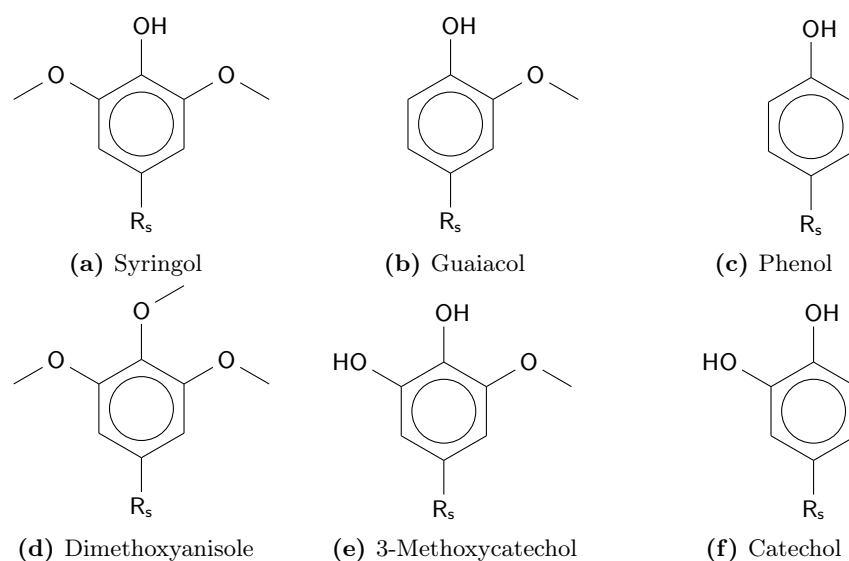


Figure 5.1: Main building blocks of lignin pyrolysis oil components. R_s denotes a side chain as introduced in Figs. 5.2 to 5.5. Names are given assuming H as side chain.

5.2 Upgrading

As pyrolysis oil is not suited for direct usage in SI ICEs, upgrading is required [51, 197]. HDO is considered to be the most promising way of converting pyrolysis oil into fuels [51, 197]. Hydrogen is added to remove oxygen from the molecules, to hydrogenate double bonds and aromatic rings. Applying these HDO reactions [17] to the side chains leads to the reaction pathways shown in Figs. 5.2 to 5.5. For the main building blocks, the reactions proceed via the pathways depicted in Fig. 5.6. Other reactions such as demethylation or decarboxylation are thus not considered herein, as these reactions do not produce new side chains. On the other hand, these reactions lower the carbon efficiency and are therefore not desirable.

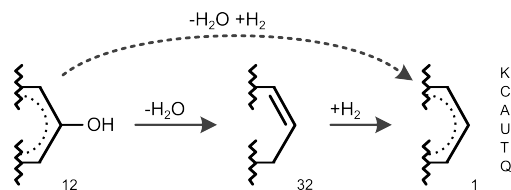


Figure 5.2: HDO upgrading pathway of a hydroxy group. The dashed arrow indicates the upgrading of phenolic compounds. The numbers represent the ID of the respective side chain. The letters identify the main building blocks in combination with which the respective side chain were reported in the literature.

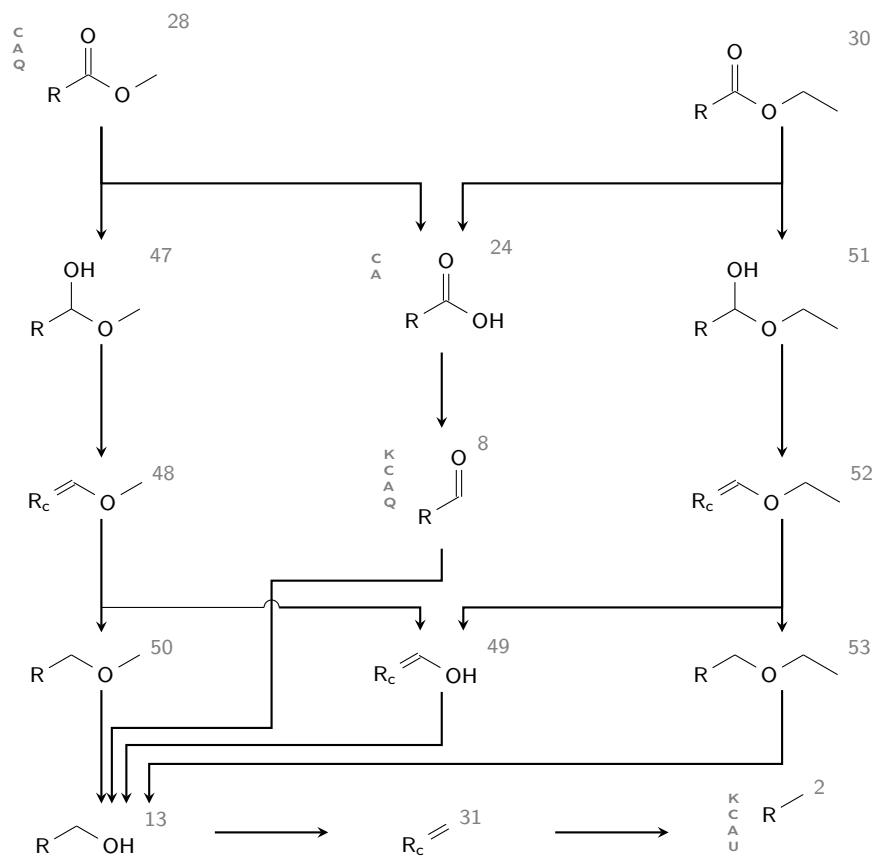


Figure 5.3: HDO upgrading pathway of different side chains leading to a final chain length of 1 C atoms. R denotes any ring structure according to Fig. 5.6, while R_c stands for aliphatic rings only. The numbers represent the ID of the respective side chain. The letters identify the main building blocks in combination with which the respective side chain were reported in the literature.

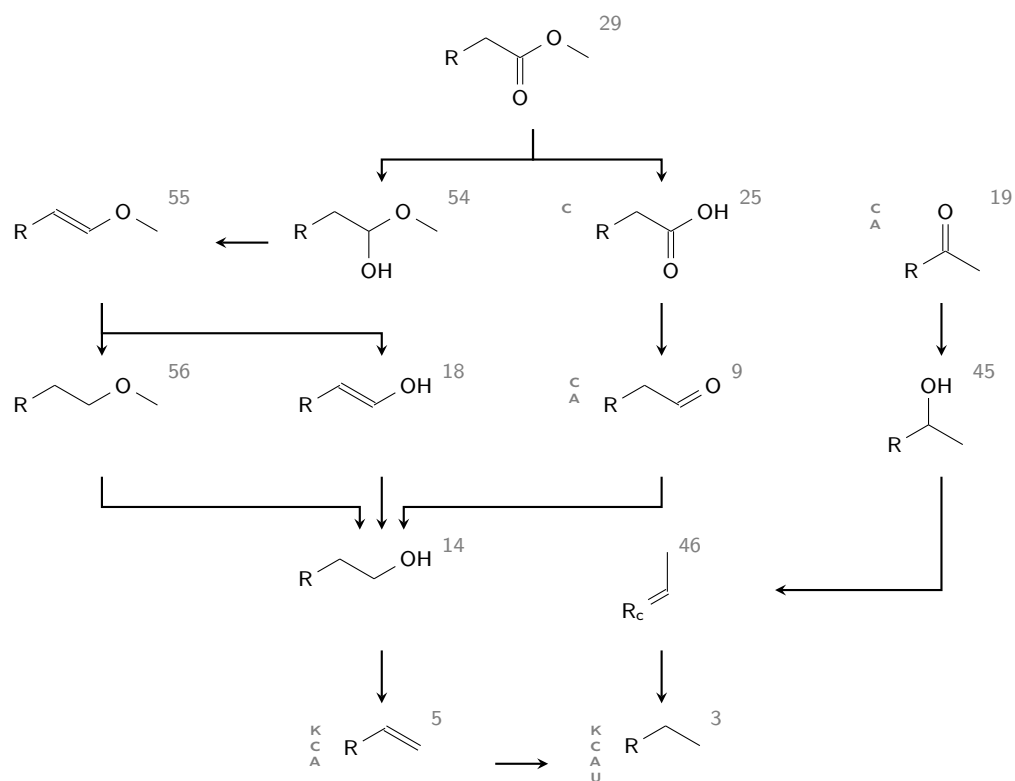


Figure 5.4: HDO upgrading pathway of different side chains leading to a final chain length of 2 C atoms. R denotes any ring structure according to Fig. 5.6, while R_c stands for aliphatic rings only. The numbers represent the ID of the respective side chain. The letters identify the main building blocks in combination with which the respective side chain were reported in the literature.

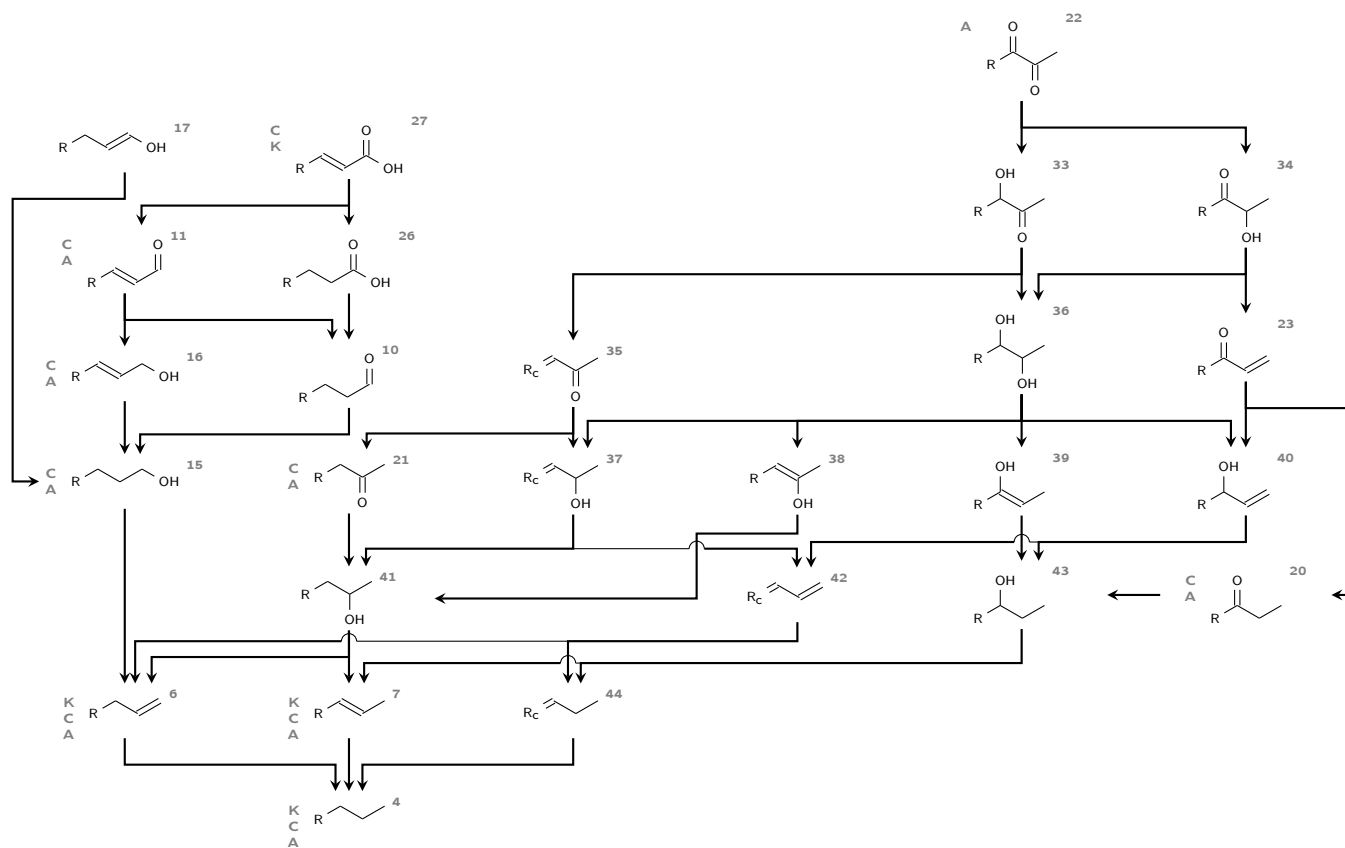


Figure 5.5: HDO upgrading pathway of different side chains leading to a final chain length of 3 C atoms. R denotes any ring structure according to Fig. 5.6, while R_c stands for aliphatic rings only. The numbers represent the ID of the respective side chain. The letters identify the main building blocks in combination with which the respective side chain were reported in the literature.

For aliphatic rings, dehydration may generate double bonds within the ring or on its substituents. These side chains are only considered in conjunction with aliphatic rings. In the case of aromatic rings, these intermediate steps (e.g. in Fig. 5.2 shown with a dashed arrow) are skipped. Considering every possible combination of side chain and main building block, 1679 different molecules need to be evaluated as fuel. To facilitate the reference to the respective compounds, the following naming convention is introduced: the main building blocks are identified by a combination of letters whereas the side chains are numbered. The corresponding labels are shown in Figs. 5.2 to 5.6, e.g. methylcyclohexane is denoted as N2.

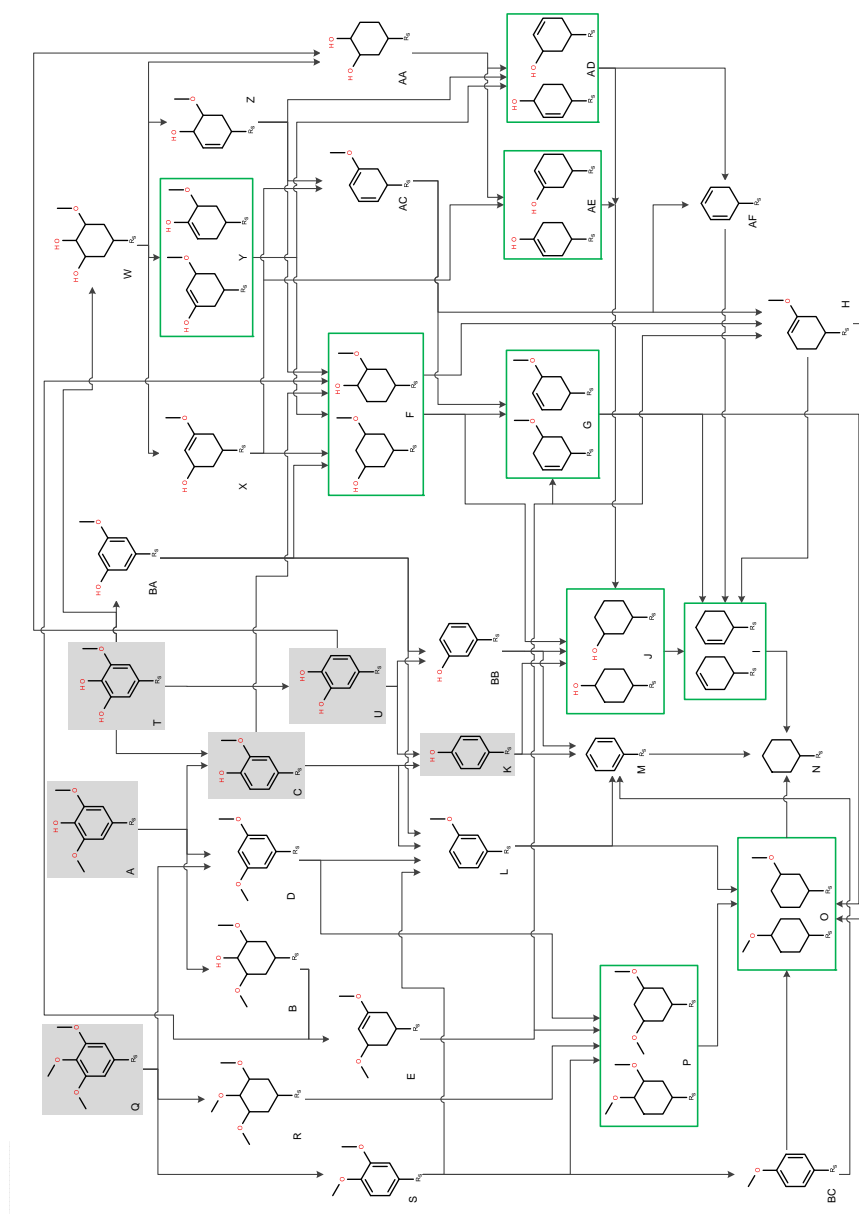


Figure 5.6: HDO reaction network of the main building blocks. The main building blocks identified in lignin pyrolysis oil [194–196] are shaded in gray (see Fig. 5.1). Fragments framed in green represent compounds whose structures cannot be distinguished by means of Group Contribution Methods. R_s denotes any side chain shown in Figs. 5.2 to 5.5.

5.3 Method

The suitability of a given compound as replacement for gasoline was judged using the ICE model. As criteria, the efficiency, the specific CO₂ emissions at 2000 rpm and full load (2 bar charging pressure) as well as the consumption over the WLTC were evaluated.

Due to the lack of experimental data for most of the studied compounds, all properties of interest were estimated using GCMs as discussed in Section 2.4. In Fig. 5.6 isomers that are identical for the applied GCMs are marked with a green frame. These isomers differ by the position of the substituents on the ring.

As the fuel must be liquid during operation, thresholds regarding the melting point (T_{melt}) and the boiling point (T_{boil}) were specified. Two different ranges were defined based on the climate of Central Europe: For all-year fuels: $T_{\text{melt}} \leq 253 \text{ K}$ and $T_{\text{boil}} \geq 333 \text{ K}$, and for summer fuels: $T_{\text{melt}} \leq 273 \text{ K}$ and $T_{\text{boil}} \geq 333 \text{ K}$. The estimated properties of all compounds meeting these requirements were used as input parameters for the SI ICE model.

5.4 Results and Discussion

5.4.1 Compliance with Boundary Conditions

Fig. 5.7, shows the boiling and the melting points of all compounds. The red horizontal line represents the threshold of the boiling point, while the vertical red solid and dashed line show the limit of the melting point for all-year and summer fuel, respectively. Among the 1679 compounds, 202 compounds satisfy the conditions as all-year fuel and 133 compounds are suited for summer operation only.

5.4.2 Group Influences

To discuss the influence of the functional groups on the accordance with the previously defined thresholds, the number of molecules following the criteria is plotted against the number of each specific functional group present in the molecule (Fig. 5.8). Based on this analysis it becomes evident that all $-\text{COOH}$ groups need to be removed. With the exception of $-\text{OCH}_x$ groups, where a maximum of one oxygen-containing group per molecule is allowed. $-\text{CHO}$ groups are only suited for summer fuels. The influence of double bonds on the melting point and thereby the boundary conditions is less pronounced. In summary, the presence of hydrogen bonds in these molecules have a strong influence on the melting point. It mostly determines whether a compound is still liquid in the temperature range of interest. All compounds have boiling points above 333 K.

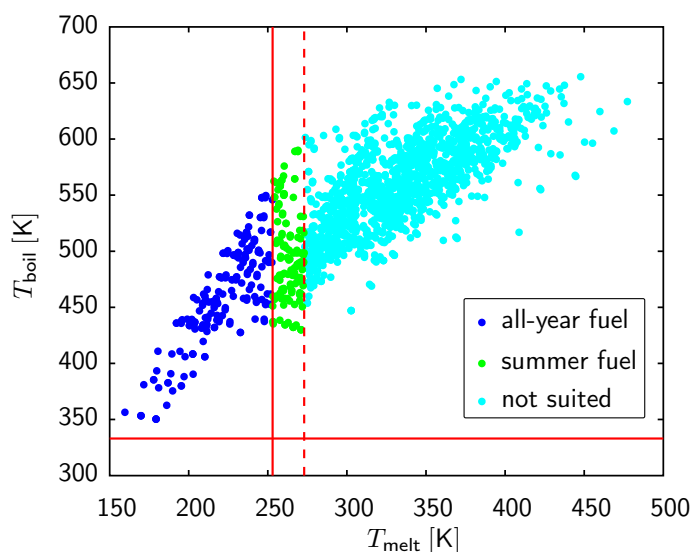


Figure 5.7: Estimation of melting and boiling points of the studied compounds. Dark blue: compounds suited as all-year fuel, green: fulfilling only summer fuel specifications and light blue: not compliant within any of the ranges. Red lines: temperature thresholds.

5.4.3 Optimized Selections

The compounds fulfilling the different criteria (efficiency, specific CO_2 emissions, and consumption) best are shown in Fig. 5.9. It is important to note that the suitability of a compound as fuel depends on its performance in the engine. The compounds that are present in all selections consequently represent a compromise of the three criteria and are not necessarily the best overall performers. 276 different molecules were identified as lignin pyrolysis oil components and their suitability as pure fuel was subsequently analyzed.

The total number of compounds was reduced to 30 (45), 21 (28) and 5 (14) in the case of efficiency (η), specific CO_2 emissions ($e_{\text{CO}_2, \text{FL}}$) and consumption as optimization criteria for all-year suitability (values for summer fuels in parenthesis). The structures in Fig. 5.9 suggest aromatics to be favorable in terms of consumption. This can be attributed to their high LHV as well as their high RON. On the other hand, molecules with a higher degree of saturation are advantageous regarding specific CO_2 emissions as the fraction of carbon atoms present is reduced, leading to lower specific CO_2 emissions. $-\text{COO}-$ groups are beneficial regarding all three criteria. $>\text{CO}$ and $-\text{OCH}_3$ groups improve the efficiency and lower specific CO_2 emissions ($-\text{OCH}_3$ groups are always attached to non-aromatic rings). The presence of $-\text{OH}$ groups improves the suitability as SI fuel. However, due to their impact on the melting point, they are only suitable for summer operation.

Table 5.1 summarizes the performance parameters together with the average amount of H_2 added for each mixture. Minimum, average and maximum values are reported.

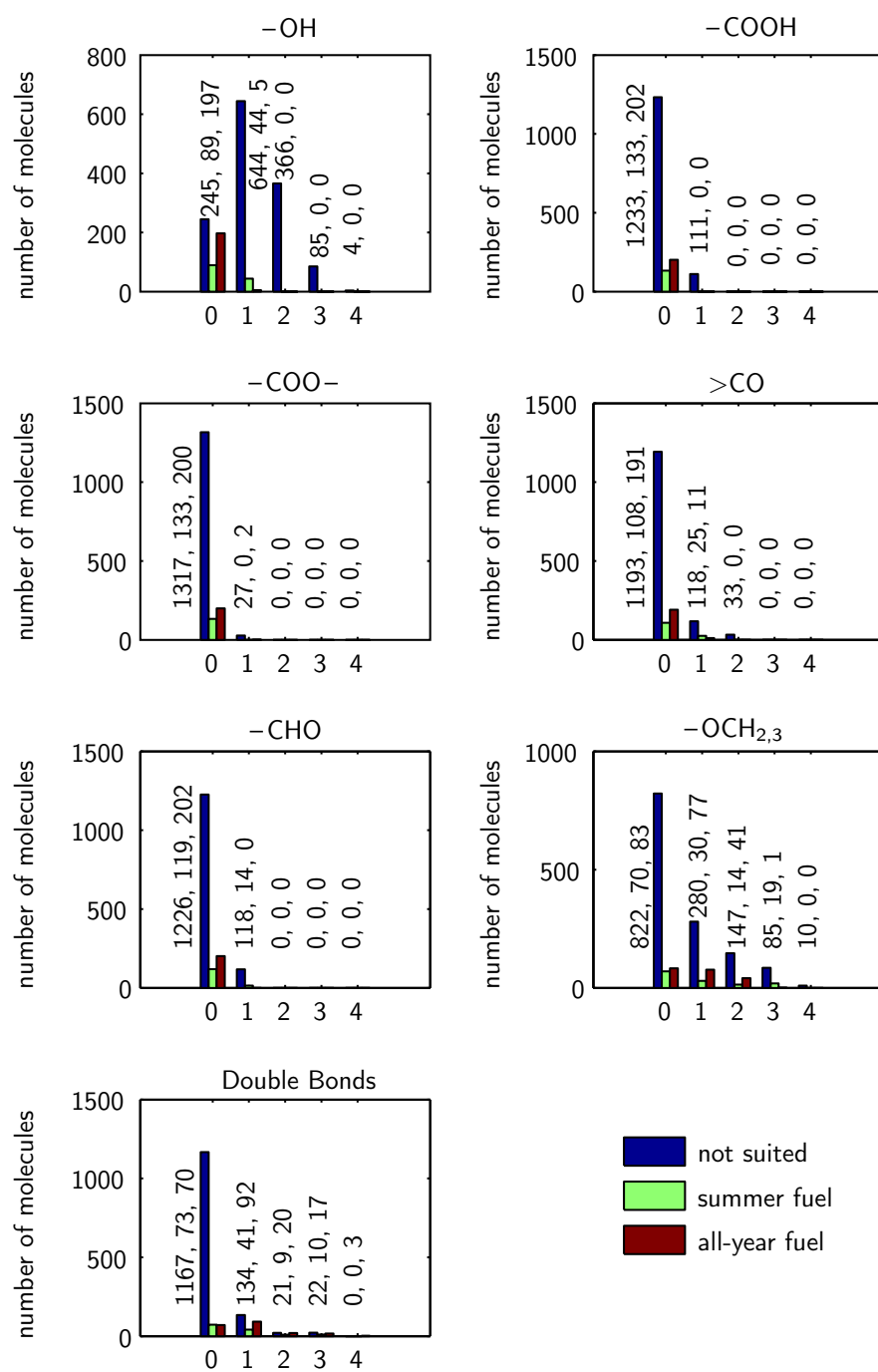


Figure 5.8: Histograms for the different functional groups categorized according to the three temperature ranges. The y-axis shows the number of molecules satisfying the criteria; the x-axis, the occurrence per molecule. The numbers show the values for each category in the following order: not suited, summer fuel, all-year fuel.

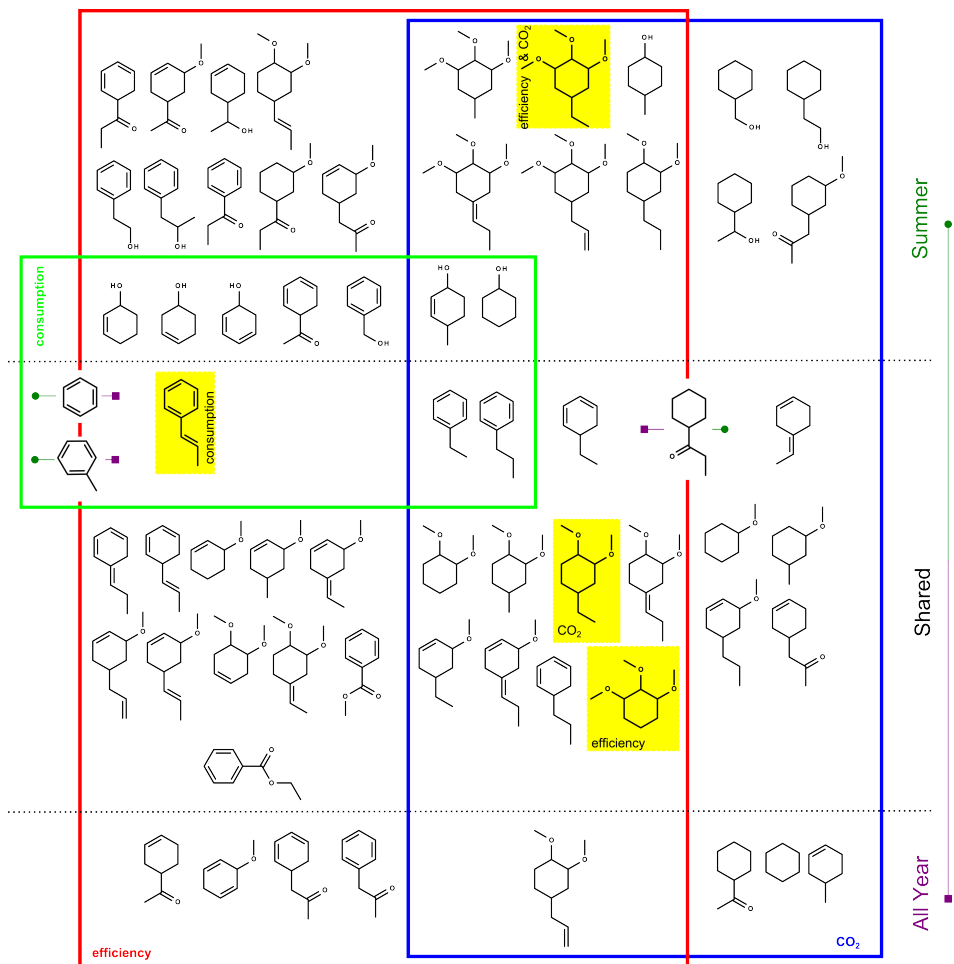


Figure 5.9: Euler diagram showing the selection of compounds with either optimized efficiency (red), specific CO₂ emissions (blue) or consumption (green). On top: summer fuels (green dots), in the middle: shared compounds, at the bottom: compounds only present in all-year fuel mixtures (violet squares). The best performing molecules are highlighted in yellow together with the parameter they optimize.

An overall summary of the results for each compound can be found in Table C.1 in the Appendix. These values are compared to the established fuels as listed in Table 4.3. As a reference, full HDO of the lignin pyrolysis oil to cyclohexane derivatives requires on average $7.05 \text{ mol}_{\text{H}_2}/\text{mol}_{\text{oil}}$ (minimum 4, maximum $10 \text{ mol}_{\text{H}_2}/\text{mol}_{\text{oil}}$). In terms of H_2 addition, roughly 50% to 70% of the maximum is needed, with all-year fuels requiring less H_2 addition than summer fuels. The amount of H_2 added for optimized selections increases in the following order: consumption < efficiency < specific CO_2 emissions. Minimum efficiency is, with one exception, higher than for gasoline. Average efficiency is in the order of *sec*-butanol for the summer fuel selections, for the all-year case it is slightly lower. Minimum CO_2 emissions are similar to *sec*-butanol and on average similar to gasoline. Only the consumption-optimized selections have a minimum CO_2 emissions in the range of gasoline. An optimization for consumption shows values below 2-phenylethanol with maximum values comparable to gasoline.

5.4.4 Single Compounds

Concerning single compounds, the best performing molecules as indicated in Fig. 5.9 are listed together with their performance values in Table 5.2. In any case, minimum consumption is achieved with β -methylstyrene (M7). Efficiency and CO_2 emissions are optimized in the summer mixture with 1,2,3-trimethoxy-5-ethylcyclohexane (R3). In the all-year mixture, efficiency is maximized with 1,2,3-trimethoxycyclohexane (R1), and CO_2 emissions are minimized with 1,2-dimethoxy-4-ethylcyclohexane (P3).

5.4.5 Influence of Selected Groups

Based on these findings, the influence of the different groups on the performance as fuel is investigated. Cyclohexane (N1) is chosen as base molecule, to which the selected groups ($-\text{CH}_3$, $-\text{CHO}$, $-\text{COCH}_3$, $-\text{COOCH}_3$, $-\text{OCH}_3$, $-\text{OH}$) are subsequently attached. At first the influence on the different input properties (x_i) is calculated:

$$\Delta x_i = x_i - x_{i,\text{N1}} \quad (5.1)$$

Based on these deviations, the averaged absolute difference ($\overline{\Delta x_i}$) is used to determine the local sensitivities around cyclohexane. By combining the local derivative with the difference in the input property it is possible to estimate its influence on efficiency ($\delta\eta_i$).

$$\delta\eta_i = \frac{\eta(x_{i,\text{N1}} + 0.5\overline{\Delta x_i}) - \eta(x_{i,\text{N1}} - 0.5\overline{\Delta x_i})}{\Delta x_i} (x_i - x_{i,\text{N1}}) \quad (5.2)$$

Fig. 5.10 presents the results of this investigation. The changes in viscosity, vapor pressure and enthalpy of vaporization for cyclohexanol are most prominent, whereas the influence of the viscosity on the efficiency is non-existent. The opposite is true for changes in heat capacity, autoignition temperature/RON and density, where even small

Table 5.1: Summary of the performance parameters (efficiency (η_{FL}), specific CO₂ emissions ($e_{\text{CO}_2,\text{FL}}$) both at full load, and consumption (c), specific CO₂ emissions ($e_{\text{CO}_2,\text{D}}$) based on the WLTC), including the average H₂ required for production of the different selections of compounds starting from lignin pyrolysis oil. std: standard deviation.

criteria		η_{FL} [%]	$e_{\text{CO}_2,\text{FL}}$ [g/kWh]	c [l/100km]	$e_{\text{CO}_2,\text{D}}$ [g/km]	$\frac{\text{mol H}_2}{\text{mol oil}}$ [-]
all-year						
η	min	34.3	0.72	6.9	184	1.00
	mean	36.6	0.78	8.0	197	4.22
	max	39.0	0.90	9.4	232	7.00
	std	0.9	0.05	0.6	12	1.46
CO ₂	min	31.1	0.72	7.1	184	1.00
	mean	36.3	0.76	8.0	193	4.89
	max	39.0	0.83	9.4	207	7.00
	std	1.3	0.03	0.6	7	1.24
c	min	34.3	0.79	6.9	202	1.00
	mean	35.7	0.83	7.2	211	3.90
	max	36.2	0.90	7.9	232	7.00
	std	0.7	0.03	0.3	9	1.26
summer fuel						
η	min	34.9	0.69	6.9	174	1.00
	mean	37.3	0.78	7.8	196	3.86
	max	40.2	0.90	9.4	227	8.00
	std	1.2	0.05	0.6	13	1.46
CO ₂	min	34.9	0.69	7.1	174	1.00
	mean	36.9	0.75	7.9	189	4.86
	max	40.2	0.80	9.4	204	8.00
	std	1.4	0.02	0.5	6	1.22
c	min	34.3	0.77	6.9	196	1.00
	mean	36.2	0.82	7.1	207	3.89
	max	36.8	0.90	7.9	232	7.00
	std	0.4	0.03	0.2	7	1.31

Table 5.2: Performance of the molecules when optimizing engine performance. Lowest consumption: β -methylstyrene (M7). Maximum efficiency and minimum CO₂ emissions in summer fuel mixtures: 1,2,3-trimethoxy-5-ethylcyclohexane (R3). Maximum efficiency in all-year fuel mixtures: 1,2,3-trimethoxycyclohexane (R1), minimum CO₂ emissions in all-year fuel mixtures: 1,2-dimethoxy-4-ethylcyclohexane (P3).

molecule	η_{FL} [%]	η_{PL} [%]	P_{FL} [kW]	$e_{CO_2,FL}$ [kg/kWh]	ε_{CR} [-]	η_{cyc} [%]	$e_{CO_2,D}$ [g/km]	c [l/100km]
M7	36.2	21.8	78.7	0.83	11.8	22.4	211	6.9
P3	37.7	22.6	82.3	0.72	11.3	17.9	184	8.3
R1	39.0	23.3	86.6	0.73	13.9	24.1	185	9.4
R3	40.2	24.1	88.6	0.69	17.4	25.1	174	8.2

changes are amplified. This behavior can be explained by the fact that the viscosity influences droplet size. However, as long as the droplets evaporate in a given time, there is no influence on the efficiency. As the power requirement of the fuel pump is negligible, changes therein are not expected to be significant. Changes in vapor heat capacity lead to changes in temperature at TDC and thus influence the thermodynamic cycle. The influence of the RON can be explained by the fact that the maximum compression ratio is knock-limited. The influence of the enthalpy of vaporization is due to the fact that an increase in enthalpy of vaporization leads to lower temperatures, which is favorable in terms of knock reduction. However according to Carnot, lower temperatures also lead to lower efficiencies. Furthermore, a higher enthalpy of vaporization increases charge cooling, which in turn allows for more fuel–air mixture to be introduced into the cylinder. The influence of the enthalpy of vaporization warrants further investigations.

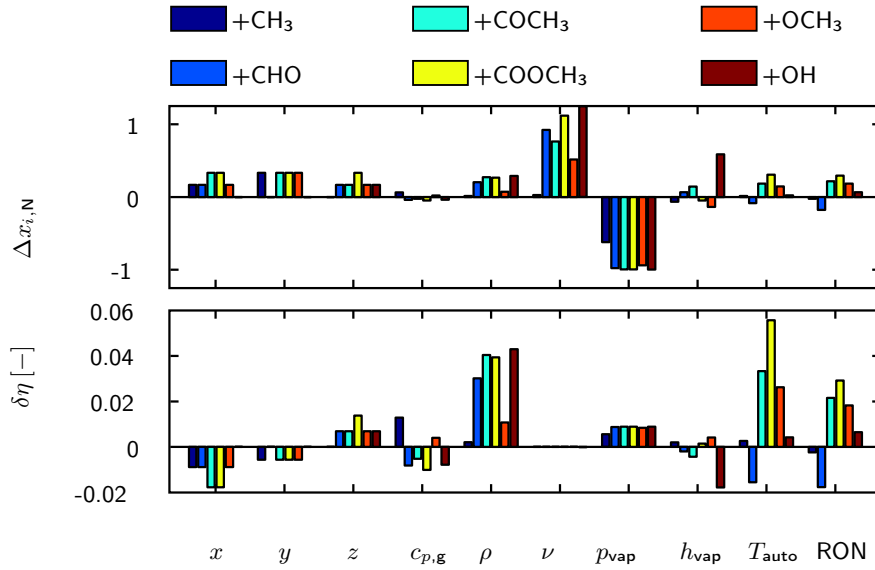


Figure 5.10: Fuel properties and efficiency dependency on functional groups attached to cyclohexane. The change in property is normalized with respect to the values of cyclohexane, except for the number of oxygens (z) that is normalized using the number of carbon atoms in cyclohexane. The change in viscosity for cyclohexanol is equal to 9.02.

5.5 Conclusion

The most suitable compounds in lignin-derived pyrolysis oil to replace gasoline could be identified, by coupling an engine model with a reaction pathways network. Fuels showing higher efficiencies than the currently-employed fuels can be produced from pyrolysis oil by selective hydrotreating. It is impossible to lower the specific CO_2 emissions compared to *sec*-butanol substantially. On the contrary, specific CO_2 emissions in the range of gasoline are expected. Yet, the consumption can be significantly reduced if the mixture is optimized for it.

The influence of selected groups ($-\text{CH}_3$, $-\text{CHO}$, $-\text{COCH}_3$, $-\text{COOCH}_3$, $-\text{OCH}_3$, $-\text{OH}$) as cyclohexane side chains on the fuel properties and efficiency was shown.

Based on these results, we derived the following design rules:

- Full HDO is not beneficial for the fuel quality. In addition, partial HDO requires less H_2 and thereby reduces process costs significantly.
- $-\text{COOH}$ groups must be completely removed to meet the required melting point ranges (besides issues with corrosion).
- Compounds with $-\text{OH}$ groups are only suitable as summer fuels.
- Structural entities with one $>\text{CO}$ group and with $-\text{OCH}_3$ groups attached to non-aromatic rings contribute to good overall performance. While $-\text{OCH}_3$ groups improve in almost all properties (except carbon and hydrogen content), $>\text{CO}$

groups lead to improvements in density and RON but worsening in heat capacity and carbon content, when compared to $-\text{OCH}_3$.

- The presence of $-\text{COO}-$ groups is advantageous as it leads to significantly higher RON.

6 Optimization of Mixtures of Established Fuels

6.1 Introduction

The introduction of fuel mixtures adds further degrees of freedom to the system defining the properties of the optimum fuel and thus possibly allows to overcome limitations of pure fuels. The following chapter investigates the possibilities and limitations of fuel mixtures consisting of the previously discussed compounds (Section 2.1 and Chapter 4).

In contrast to the case of pure fuels where, numerous publications propose new fuels; mixtures are rarely reported. In one of these studies, Dahmen and Marquardt [198] used CAMD methods to search for the optimum fuel and identified four different mixtures. Their algorithm focused on production pathways and aimed to identify compounds/mixtures that fulfill defined specifications. The four proposed mixtures are listed in Table 6.1.

Table 6.1: Mixtures proposed as future fuels by Dahmen and Marquardt [198].

Mixture Υ		Mixture Φ	
44 mol %	<i>n</i> -butanol	42 mol %	ethanol
31 mol %	cyclopentane	26 mol %	cyclopentanone
15 mol %	ethyl acetate	15 mol %	2-butanone
8 mol %	<i>n</i> -butane	7 mol %	1-butene
2 mol %	<i>n</i> -propanol	6 mol %	<i>n</i> -butanol
		3 mol %	cyclopentane
		1 mol %	<i>n</i> -propanol
Mixture Ψ		Mixture Ω	
45 mol %	<i>n</i> -butanol	58 mol %	ethanol
29 mol %	ethanol	27 mol %	cyclopentane
26 mol %	cyclopentane	15 mol %	DMF

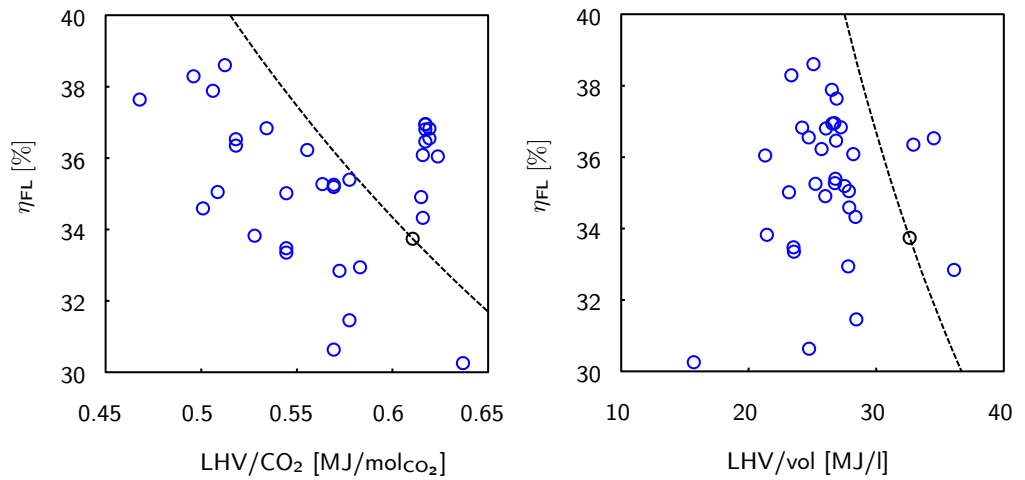
In addition to the already discussed compounds, the properties of cyclopentane, *n*-butane, cyclopentanone and 1-butene are required and listed in Table D.1. The UNIFAC method used to calculate the activity coefficients does not cover DMF. Mixture Ω could therefore not be modeled.

6.2 Algorithm

According to Fig. 4.6 on page 57, biofuels can be divided into three groups:

- (i) fuels that are better than gasoline with respect to consumption *and* CO₂ emissions
- (ii) fuels that are better than gasoline with respect to consumption *or* CO₂ emissions
- (iii) fuels worse than gasoline in both measures

As stated previously none of the considered biofuels fall into the first category. The question arises whether it is possible to design a mixture that performs better than gasoline in both measures. To investigate this question, the biofuels are once plotted regarding efficiency *vs.* energy stored per mol of CO₂ emitted (Fig. 6.1a) and once in terms of efficiency *vs.* volumetric energy density (Fig. 6.1b).



(a) Full-load efficiency *vs.* energy stored per mol of CO₂ emitted.

(b) Full-load efficiency *vs.* volumetric energy density.

Figure 6.1: Comparison of biofuels to gasoline. Blue circles: biofuels. Black circle: gasoline. Dashed black line: required efficiency to provide the same energy at the crankshaft as gasoline.

The dashed black line in both figures represents constant energy available at the crankshaft and is defined as follows:

$$\eta = \frac{\text{LHV}_{\text{gasoline}} \eta_{\text{gasoline}}}{\text{LHV}} \quad (6.1)$$

with LHV either in terms of energy per mol of CO₂ emitted or volumetric energy density. Compounds above this line are superior to gasoline with respect to CO₂ emissions (Fig. 6.1a) or consumption (Fig. 6.1b). In other words, the dashed black line defines the minimum efficiency required for a compound to outperform gasoline. These two plots allow to investigate categories (ii) and (iii). However, no statement about

category (i) is possible based on Fig. 6.1. Therefore, the two plots are combined into Fig. 6.2 where the two energy parameters are plotted on the x- and y-axis, respectively.

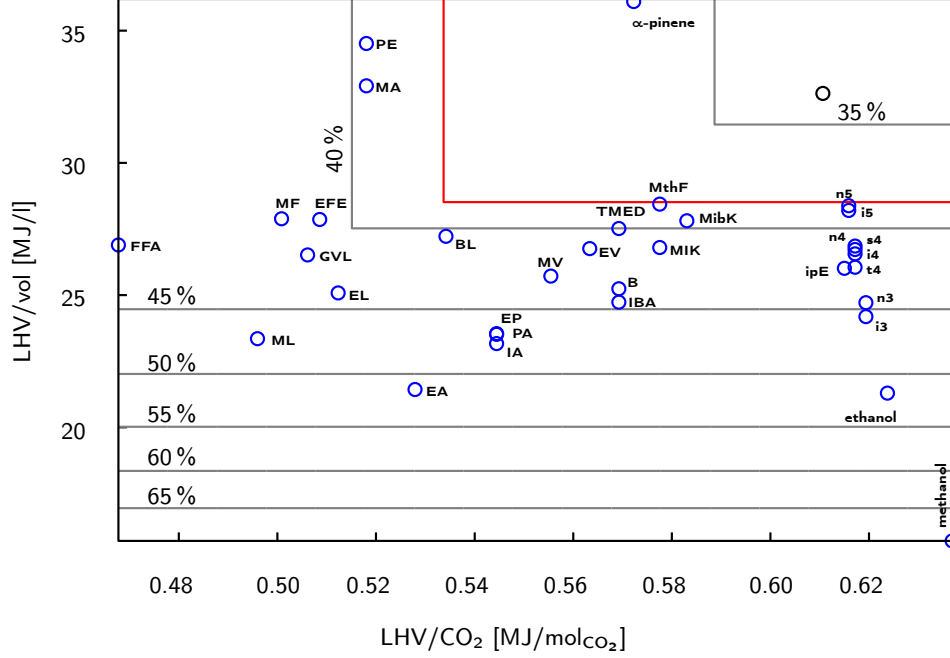


Figure 6.2: Comparison of the biofuels and gasoline with respect to both volumetric energy density and energy stored per CO₂ emitted. Blue circles: biofuels. Black circle: gasoline. Gray lines: constant efficiency required to provide the same energy at the crankshaft as gasoline. Red line: isoline at 38.6%.

The two hyperbolas of Fig. 6.1 are overlaid and shown in the form of isolines of constant efficiency. These isolines indicate the efficiency required (η_{req}) to deliver the same energy at the crankshaft as gasoline:

$$\eta_{\text{req}} = \max \left[\frac{(\eta_{\text{FL}} \text{LHV}/x)_{\text{gasoline}}}{\text{LHV}/x}, \frac{(\eta_{\text{FL}} \text{LHVM}^{-1}\rho)_{\text{gasoline}}}{\text{LHVM}^{-1}\rho} \right] \quad (6.2)$$

The horizontal parts of the isolines indicate regions where the volumetric energy density defines the required efficiency, whereas the vertical parts originate from the energy-per-CO₂ consideration. The red line represents the isoline at maximum efficiency achieved by the biofuels (38.6%, ethyl levulinate (EL)).

The required efficiency, as defined in Eq. (6.2), serves as a clearly defined criterion for the mixtures to achieve. An algorithm is designed to determine the mixtures satisfying the required efficiency conditions and to determine the maximum achievable efficiency. To reduce the computational effort and to avoid nonsensical options, a search-space

is defined restricted to the area requiring an efficiency below 40%. This boundary is chosen to envelop the peak efficiency of the pure components. Furthermore, efficiencies of mixtures are considered unlikely to exceed this limit. The search-space is then divided into cells of $0.01 \text{ MJ/mol}_{\text{CO}_2} \times 0.5 \text{ MJ/l}$. The task of the algorithm is to find the mixture with maximum efficiency for each of these cells.

In the first step, all possible 2 to 4 component mixtures are determined. For binary and ternary mixtures a step-size of 5 mol% is chosen. For 4 component mixtures, 20 mol% steps are employed to limit the total number of different mixtures to a manageable level. These mixtures are stored in a library alongside with their respective energy densities. The algorithm chooses a mixture as a starting point from the library and starts the efficiency maximization. At every iteration a set of mixtures is generated, and are run through the model. The mixture with the highest efficiency at full load is taken as an initial mixture for the next iteration. Once the initial mixture does not change anymore, the step size is halved, and the process is repeated. 20 mol% is chosen as the initial step size. Once 1 mol% is reached, the optimization is stopped. The starting point is then deleted from the library and the procedure is repeated with a new starting point.

6.3 Results and Discussion

The results of the optimization procedure are shown in Fig. 6.3. Depending on whether the efficiency exceeds the requirement or not the location of the optima is marked with either a black cross or a red dot. A black cross marks an optimum of a respective cell with a lower efficiency than required. A total of 78 mixtures were found, that exceed the requirement by 0.00 to 0.45 percentage points and are marked by red dots in Fig. 6.3. Their detailed compositions and performances are listed in Tables D.3 and D.4. The maximum efficiency is obtained by a mixture of 34 mol% phenylethanol, 25 mol% isopentanol, 22 mol% *n*-butanol, 10 mol% *n*-pentanol and 9 mol% methyl valerate (mixture α). Furthermore, none of the mixtures Υ , Φ and Ψ from ref. [198] (marked by magenta stars), reaches the required efficiency.

To check the performance of the identified mixtures, their consumption and specific CO₂ emissions over the WLTC are determined. As indicated in Fig. 6.4, their performance is comparable to gasoline with a slight increase in CO₂ emissions. On average, the increase is in the order of 3 g/km (1.5% higher as compared to gasoline). There are two possible explanations for this negligible deviation: firstly, the change in the ignition delay model and, secondly, the summation of numerical errors. All values for pure fuels are calculated using the original ignition delay model (Eq. (3.41) on page 30). In case of mixtures an adaption to the ignition delay model has been introduced (see Section 3.4.2.2 on page 43) for details). It is thus possible that the changes in the ignition delay model lead to differences in the compression ratio and ultimately in engine performance. However, the deviations for the mixtures in question are small and are therefore negligible. The summation of numerical errors arises from rounding errors for the efficiency and energy densities (per mol of CO₂ emitted and volumetric) of

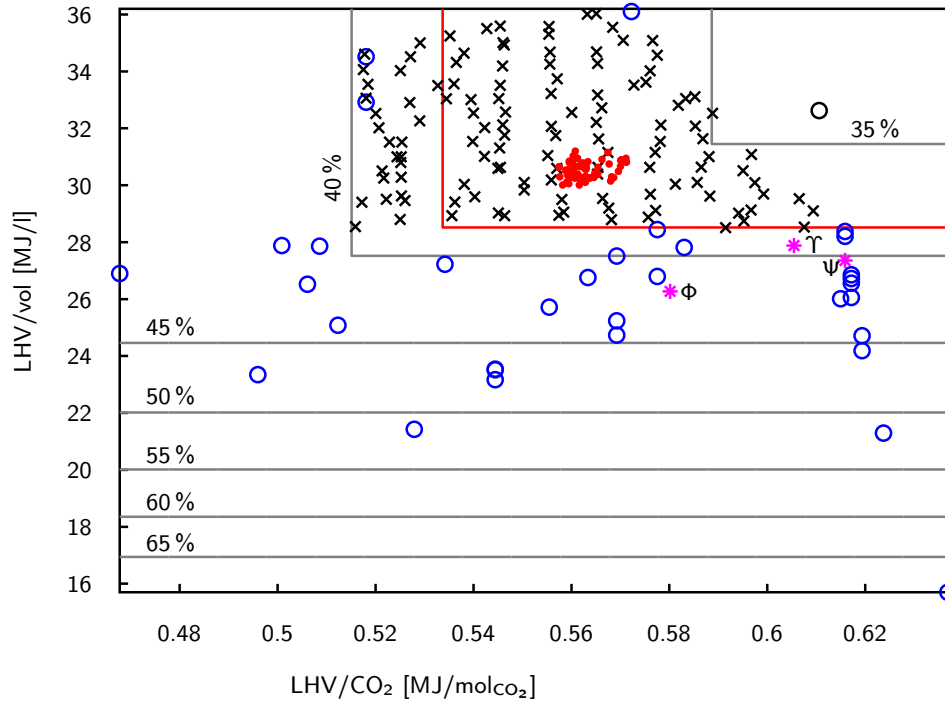


Figure 6.3: Results of the mixture optimization in terms of energy per mol CO₂ emitted and volumetric energy density. Blue circles: biofuels. Black circle: gasoline. Red dots: identified mixtures providing more energy at the crankshaft than gasoline. Magenta stars: mixtures proposed in the literature. Black crosses: mixtures with maximum efficiency within their cell, efficiency below requirement. Gray lines indicate the efficiency required to provide the same energy at the crankshaft as gasoline. Red line: isoline at 38.6%.

gasoline. These errors influence the calculation of the required efficiency, and thus the criterion of the algorithm. From the mixtures proposed in the literature, Ψ stands out with lower specific CO₂ emissions than gasoline, but increased consumption, whereas Υ and Φ show inferior performance than gasoline.

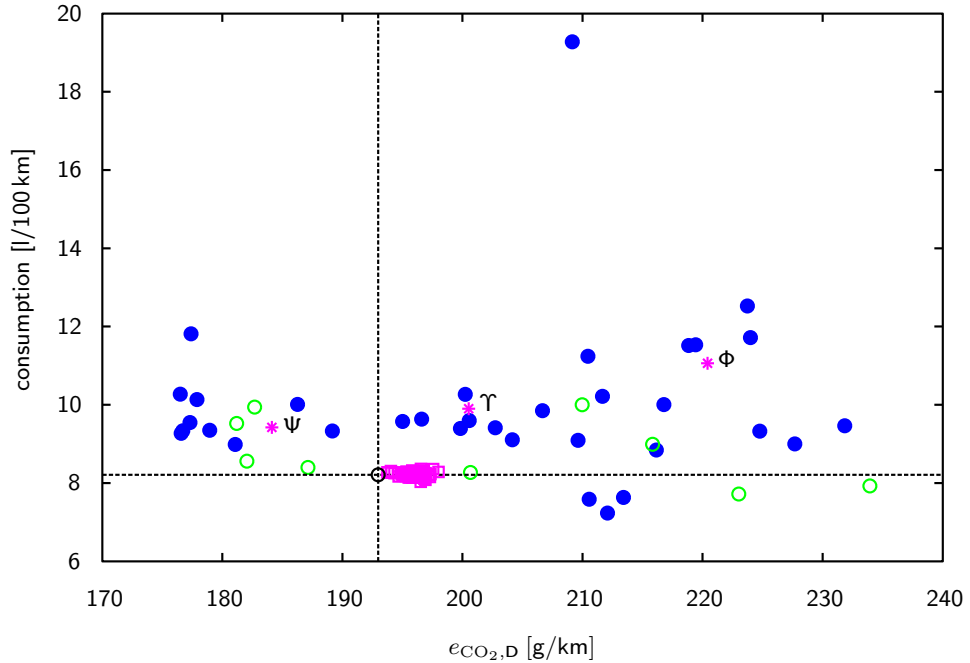


Figure 6.4: Comparison of the different mixtures and pure fuels with respect to consumption and CO₂ emissions over the WLTC. Magenta squares: identified mixtures providing more energy at the crankshaft than gasoline. Magenta stars: mixtures proposed in literature. Blue circles: biofuels. Green circles: gasoline components. Black circle: gasoline.

In Table 6.2 the performance of the mixtures from the literature (Υ , Φ and Ψ) as well as a selection of the identified mixtures (α to γ) are listed. Regarding driving cycles, only results for the WLTC are reported. Further results including values for the CADC and NEDC can be found in Table D.2. Mixture α is chosen due to having the highest difference to the required efficiency. Mixtures β and γ are chosen based on minimum consumption or minimal specific CO₂ emissions respectively. Their compositions are reported in Fig. 6.5.

A summary of the compositions of these fuel mixtures is given in Fig. 6.6. The height of the bars represents the average mixture fraction of the compound, only considering mixtures where the compound is present. The numbers shown are the number of mixtures in which the compound is present (out of 78). All but one mixture contain 2-phenylethanol, which is the compound with the highest average mole-fraction (34.2 mol %). Methyl valerate is also very common, but with smaller shares (7.2 mol %).

Table 6.2: Overview of the performance of the proposed fuel mixtures. η_{FL} efficiency at full load, η_{PL} efficiency at 2000 rpm and $P_{out} = 6.6$ kW, P_{FL} power output at full load, $e_{CO_2,FL}$ specific CO₂ emissions, ε_{CR} compression ratio, η_{cyc} cycle efficiency, $e_{CO_2,D}$ CO₂ emissions per distance and c consumption over the WLTC.

mixture	η_{FL} [%]	η_{PL} [%]	P_{FL} [kW]	$e_{CO_2,FL}$ [kg/kWh]	ε_{CR} [-]	η_{cyc} [%]	$e_{CO_2,D}$ [g/km]	c [l/100km]
Υ	32.5	20.2	68.9	0.80	7.4	20.4	201	9.9
Φ	33.3	20.4	71.1	0.82	8.5	19.4	220	11.1
Ψ	35.3	21.5	74.8	0.73	11.0	21.9	184	9.4
α	36.9	22.2	80.9	0.76	12.1	22.5	196	8.3
β	36.8	22.2	80.7	0.77	12.2	22.5	200	8.2
γ	36.7	22.1	80.3	0.76	11.8	22.5	194	8.3

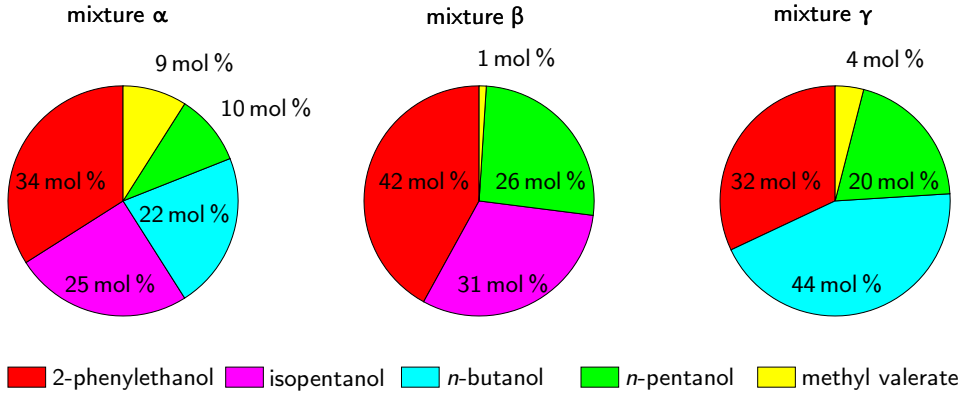


Figure 6.5: Composition of the identified mixtures.

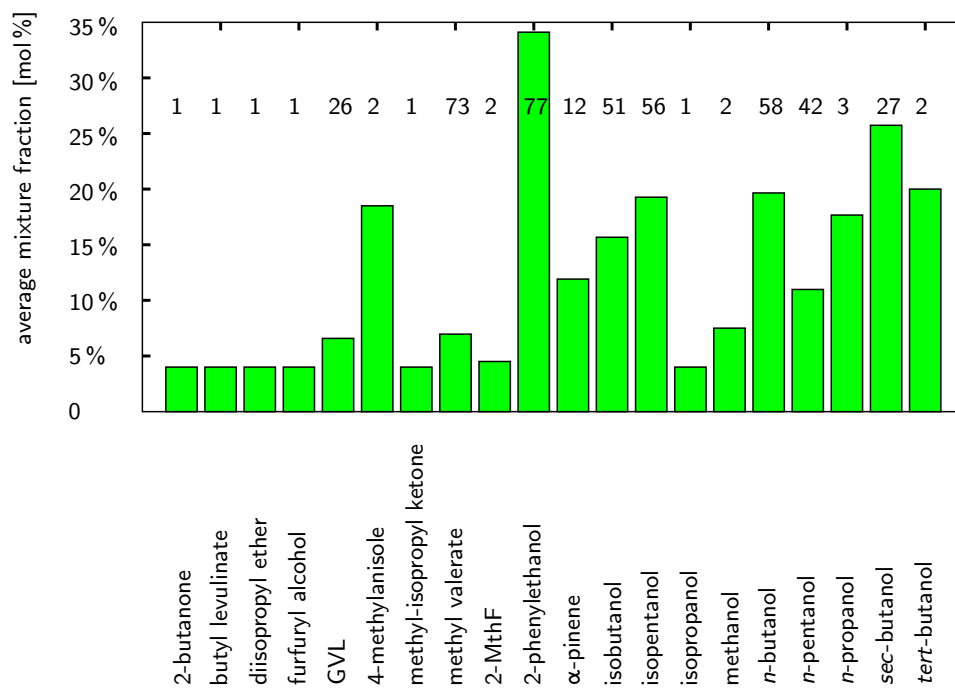


Figure 6.6: Average mole-fraction of the 78 mixtures with performance similar to gasoline. Numbers show the number of mixtures in which the compound is present.

6.4 Conclusions

As presented in this chapter, 78 mixtures of established biofuels have been identified showing identical performance as gasoline. Furthermore, three mixtures from the literature have been added to the pool of discussed fuels. Considerations about constant energy at the crankshaft with respect to CO₂ emitted and volumetric energy density have been introduced. Additional insights into the driving factors for specific CO₂ emissions and consumption have been gained. Based on these insights, it was possible to design an optimization algorithm that is able to cope with the additional degrees of freedom. This algorithm identified 78 different mixtures with almost identical performance as gasoline. No mixture could be identified with a performance superior to gasoline with respect to both specific CO₂ emissions and consumption.

As main components of these mixtures, 2-phenylethanol has been identified (average mixture content 34.1 mol %) that is present in all but one mixture. Methyl valerate (7.0 mol %), *n*-butanol (19.7 mol %) and isopentanol (19.3 mol %) are less common but still present in most mixtures with 73, 58 and 56 occurrences, respectively. These results are well-aligned with the results for pure components, in which 2-phenylethanol shows minimum consumption and butanol and pentanol isomers minimize specific CO₂ emissions. Therefore, it seems natural to mix those two to overcome the limitations of either one by the advantages of the others. More interesting is the consequent inclusion of methyl valerate. One possible explanation might be its high density leading to lower volumetric consumption.

7 Systematic Fuel Design using the reverse Group Contribution Method (rGCM)

The aim of the rGCM is to find the optimal fuel for an SI ICE. For all practical purposes it can be assumed that the number of possible candidates is infinite. It is, therefore, necessary to design a systematic approach for searching molecules that fulfill *a priori* defined specifications. However, as stated before, these specifications are unknown for SI fuels. The standards currently in place evolved based on the fossil feedstocks used nowadays, and they do not necessarily reflect the specifications for the best suited fuel.

This chapter addresses the algorithm used to determine the optimal fuel for an SI ICE.

7.1 Concept

To reverse the well-known GCMs (see Section 2.4) it is required to solve an underdetermined system of equations (7 equations for the properties, excluding constraints, and roughly 50 to 200 groups). Additionally, the target value of each property is unknown. These two problems are overcome by introducing an optimization procedure using the ICE model presented in Chapter 3, to assess the different options. In order to reduce the number of possibilities to consider and to reflect the composition of biomass, the algorithm is limited to molecules consisting of carbon, hydrogen and oxygen atoms.

An overview of the whole algorithm is given in Fig. 7.1. First, the algorithm randomly selects a starting point which is subsequently checked for feasibility. Entering the loop, all points reachable by a single mutation to the initial point are determined. These mutations include addition and subtraction of groups. Afterwards, the properties of the initial point (x_i) are estimated using the GCMs presented in Section 2.4. These values are then used in combination with the ICE model to calculate the grading criteria (χ). Using finite differences and additional model evaluation, it is also possible to estimate the first derivative of the grading criteria at this point ($\frac{\Delta\chi}{\Delta x_i}$). Based on these results the grading criteria are estimated for each of the possible points, and they are categorized according to this estimation. Starting with the highest ranked point, the following procedure is conducted to determine an initial point for the next iteration: The chosen point is run through the engine model, and its grade is calculated. If the calculated grade is higher than the current initial point, the initial point for the next iteration is found. Otherwise, the next point is taken, and the procedure continues. This procedure

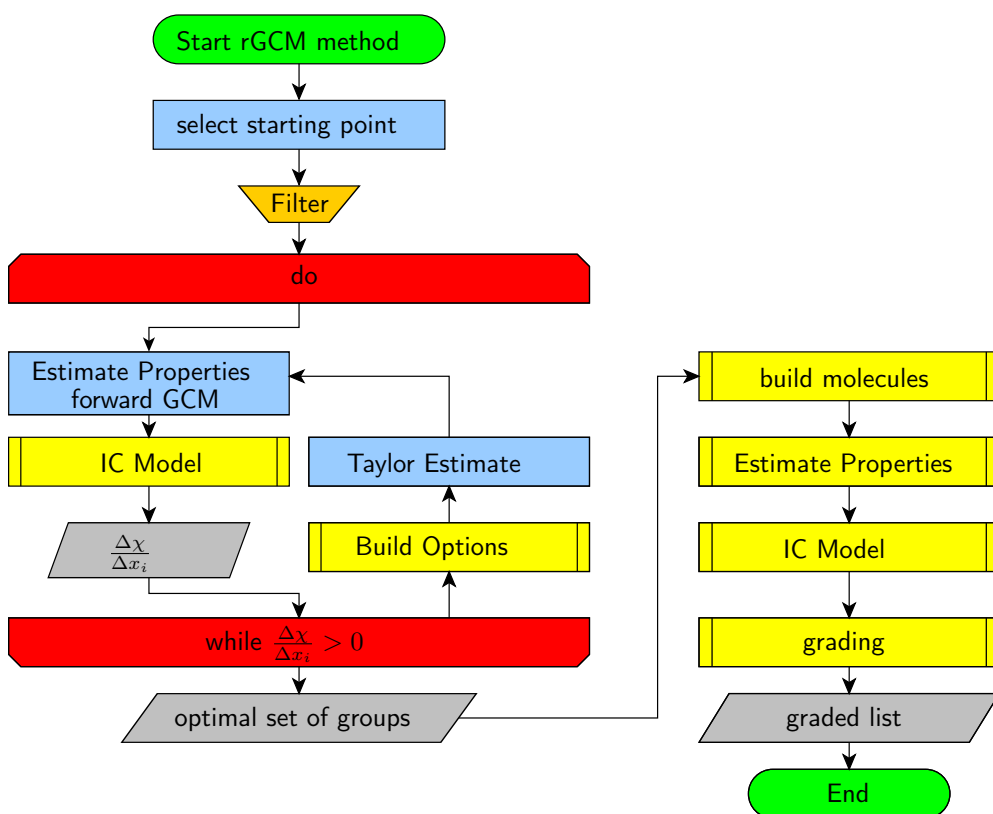


Figure 7.1: Flow sheet of the rGCM algorithm, showing the most important steps of the algorithm.

is repeated until the finite differences indicate that a local maximum has been reached.

As a result of this loop, a selection of groups with optimal fuel performance was found. Based on this selection, all possible molecular structures were derived. Knowing the exact structure, the properties of these isomers were estimated as accurately as possible and evaluated using the ICE model. This results in a ranked list of fuel candidates.

7.2 Adaptations

7.2.1 Group Matching

GCMs are chosen according to the discussion in Section 2.4. The GCMs reported by Hukkerikar *et al.* [97] show a significantly higher number of groups than the ones reported by Joback and Reid [96] and Nannoolal *et al.* [99]. The group definition matches for simple/small groups; however, the methods by Hukkerikar *et al.* [97] also include larger groups. Hukkerikar *et al.* [97] defined second and third level groups that cover several first level groups combined in a specific way. For the proposed algorithm, it is important that each group is independent of other groups. Therefore, the different definitions and contributions need to be unified. The second and third level groups in GCMs are designed to add on top of the first level groups and thereby increase the accuracy especially for large molecules. These additional levels carry further structural information, leading to increased complexity when designing the rGCM algorithm. The second and third level groups are consequently extended such that they include the first level groups and become independent. Extension is achieved by adding up the contribution of the different levels: e.g. $-\text{CH}(\text{CH}_3)_2$ is a second level group that consists of one $>\text{CH}-$ and two $-\text{CH}_3$ groups. The contribution ($\zeta_{\text{CH}(\text{CH}_3)_2,\text{tot}}$) of the group can thus be described by the sum of the second level contribution ($\zeta_{\text{CH}(\text{CH}_3)_2,2\text{nd}}$) and the first level contribution ($\zeta_{\text{CH},\text{CH}_3}$).

$$\zeta_{\text{CH}(\text{CH}_3)_2,\text{tot}} = \zeta_{\text{CH}(\text{CH}_3)_2,2\text{nd}} + \zeta_{\text{CH}} + 2\zeta_{\text{CH}_3} \quad (7.1)$$

The unification of the different GCMs is accomplished in a similar way. The contributions of larger groups undefined for one method are calculated based on the values of applicable smaller groups. This process may be justified by the basic assumption for GCMs: the additivity of group contributions.

7.2.2 Aromatic Rings

Although aromatic rings can be described by either aromatic carbons with (aCH) or without (aC) an attached hydrogen, their presence in an aromatic ring is a strong constraint. The reason is that exactly six of these groups are needed to build a valid aromatic ring. Thus, adding or removing a single aC group is not permitted. Different positions of substituents lead to different second level contributions. To overcome these problems and simplify the tasks of the algorithm, aromatic rings were defined as groups of their own. It is possible to define rings with zero to six open connection points. The

zero-open connection point option is equal to six aCH, better known as benzene. It is not included as a group in this context, as it has already been included in Chapter 4.

Groups with more than two open connection points require an additional termination group for every additional open connection point. An analysis of the GCM led to the conclusion that only a very limited set of aromatic compounds with five or six substituents has a melting point below -20°C . As the number of possible options grows exponentially with the number of branching points, the inclusion of these rings leads to an over-proportional number of possibilities. Under the given constraints, the overwhelming majority of them are invalid. Thus, including them would lead to a situation where the algorithm is required to generate, check and dismiss these options frequently. These compounds are evaluated separately and compared to the identified optimal compounds.

7.3 Algorithm

7.3.1 Group Classification

The groups presented in the GCMs are classified according to their structure connectivity. The first classification leads to the following distinction:

fundamental: by using the groups within this class all other groups can be described (25)

cyclic: groups used to describe aliphatic rings (35)

complex aromatic: groups used to describe substituents of aromatic rings (37)

complex: a combination of groups of the other classes (155)

The classification based on connectivity uses the number of outgoing connections for each group. Indicated by roman numerals: capital for normal connections and lowercase for aliphatic ring connections, e.g. type iil groups are groups with two aliphatic ring connections (ii) and one normal connection (I).

In Fig. 7.2 the complete list of fundamental groups including their connectivity classification is given. A number of representatives for each class is given in Fig. 7.3. The full list is shown in Appendix E.

7.3.2 Iteration Procedure

A selection of groups is defined as a number of groups together with a count of their occurrence. The algorithm works on such group selections during the optimization. To minimize the number of possible options, the fundamental groups are taken as the backbone of these selections. Every iteration starts with one selection of fundamental groups; a number of different options are then generated and tested. This procedure (in Fig. 7.1 denoted as “Build Options”) is presented in detail in the following. The overall optimization procedure is an adaptation of the pattern search algorithm [199].

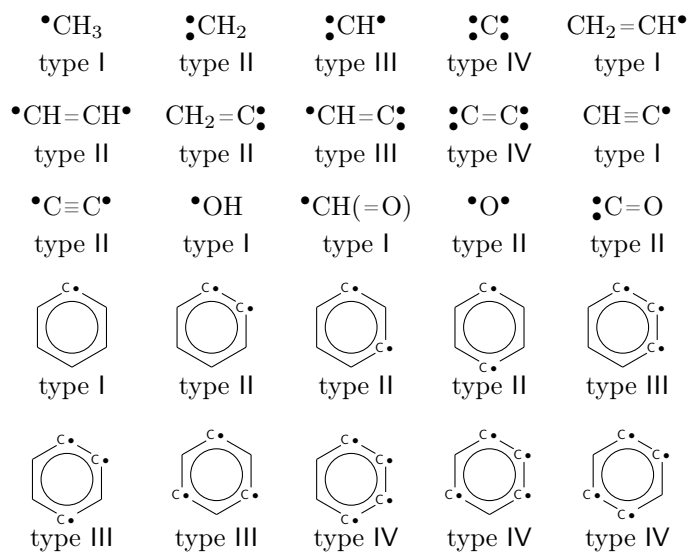


Figure 7.2: Complete list of fundamental groups. Open connection points denoted by \bullet .

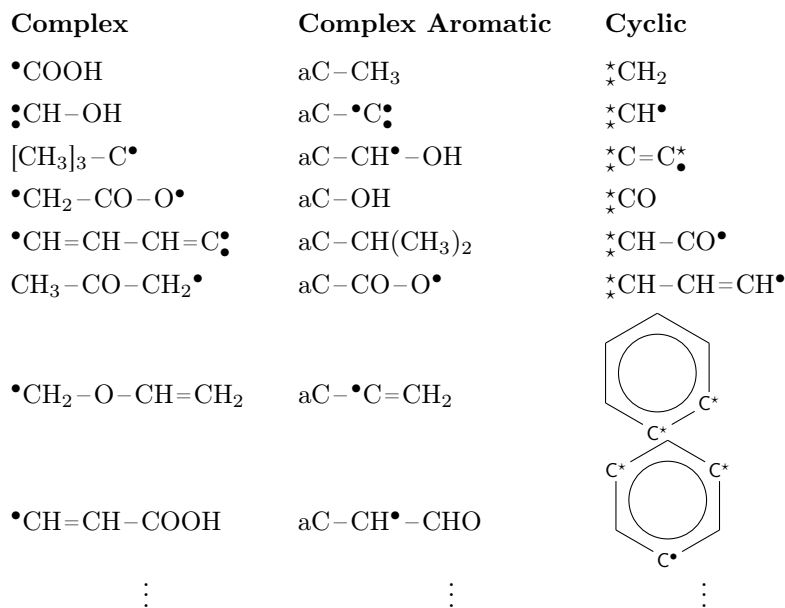


Figure 7.3: Examples for each class of groups. The full list is provided in Appendix E, \bullet denotes a non-cyclic connection point, \star denotes an open cyclic connection point, aC: denotes an aromatic Carbon.

7.3.2.1 Fundamental Options

The first task of the algorithm is to generate all possible adaptations of the initial selection of fundamental groups. This step can be further distinguished into an addition and a subtraction part. It is vital that only selections which result in at least one valid molecule are created. During the addition part, every type II group is added once. The addition of type III and IV groups requires one, and two additional type I groups respectively. Otherwise, it is not possible to generate a valid molecule based on the selection. Therefore every type III (type IV) group is, in conjunction with every type I group (combination of two type I groups), added once.

Subtraction is limited to the groups present. Type II groups can be removed without any further implication, whereas for type III and IV, one or two type I groups have to be omitted as well. Similarly to before, every possible combination has to be taken into account. Type I groups are a special case, as they cannot be added or subtracted without leading to an invalid molecular structure. To avoid this, type I groups are *replaced* instead of added/subtracted. The replacement is done such that every possible combination is generated exactly once.

7.3.2.2 Complex Aromatic Groups

The GCM of Hukkerikar *et al.* [97] differentiates between aliphatic groups and their equivalent directly attached to an aromatic ring. For example, a $-\text{CH}_3$ group attached to an aromatic carbon (aC) is not represented as $-\text{CH}_3 + \text{aC}$ but as a group of its own (aC- CH_3). To take this into account for every fundamental group selection that contains an aromatic ring, the following substitution procedure has to be applied for every aromatic carbon without an additional hydrogen (aC). Every possible combination of the available groups within the selection to complex aromatic groups is determined. Special caution must be taken that a connection between all groups is possible. The problem is that e.g. if all type I groups are directly attached to the aromatic ring and other groups are present, there is no possible molecule derivable from such a selection. In the aforementioned example, this would result in an aromatic molecule plus a fragment.

The algorithm is designed to loop through all possible combinations, which are saved as options for each fundamental group selection.

7.3.2.3 Aliphatic Rings

The implemented GCMs differentiate between groups in straight chain configuration and their equivalent in aliphatic rings. A possibility to take this into account would be to include them in the set of fundamental groups. However, as a minimum of three non-hydrogen ring atoms are required to build a ring.

Rather than building only valid selections, a different method for selections containing aliphatic ring groups was applied. Starting from a base selection of fundamental groups, the present groups are, according to Fig. 7.4, converted into ring groups. By allowing

the conversion of type I groups to type II groups, the conversion rules ensure that ring closure is possible. For the GCMs it is important how many connection points are present as well as their position within a ring.

The conversion was performed in a way that all possible combinations between cyclic and non-cyclic groups are created. After that, each option was checked according to Section 7.3.3, to guarantee that at least one valid molecule can be constructed out of it. Hence, only valid options are processed in the following steps.

7.3.2.4 Complex Groups

Each generated selection is further checked for possible combinations of present groups to complex groups, e.g. $>CO$ and $-OH$ to $-COOH$. If such a transformation is possible, the basic selection is kept (containing $>CO$ and $-OH$) and the new selection (containing $-COOH$ instead of $>CO$ and $-OH$) is added to the options. In the further process, the new option is considered as well, leading to all possible combinations of complex and other groups within the different selections.

7.3.3 Validity

There are two different kinds of conditions to be checked: Firstly, it has to be ensured that the compound is liquid and, secondly, the selection of groups must result in at least one valid molecule. To satisfy the first condition all-year round, thresholds regarding the melting point ($T_{\text{melt}} \leq 253 \text{ K}$) and the boiling point ($T_{\text{boil}} \geq 333 \text{ K}$) were specified. The second issue is less straightforward and is discussed in the following.

7.3.3.1 Group Selections without Aliphatic Ring Groups

For group selections containing no aliphatic ring groups, a termination group is required for every branching point. This can be described mathematically as follows:

$$n_I = 2 + n_{III} + 2n_{IV} \quad (7.2)$$

with the number of type α groups (n_α , $\alpha = I, III, IV$).

7.3.3.2 Group Selections Containing Aliphatic Ring Groups

As aliphatic rings can act either as branching or termination points, the situation is more complex for ring structures. The considerations have been inspired by the double bond equivalent known from organic chemistry, which cannot be applied directly in the present case. Two different scenarios are explored: Firstly, the maximum amount of type I groups (termination) possibly provided by aliphatic rings and, secondly, calculating the maximum amount of branching. A lower and an upper boundary is established. As long as the present selection of groups lies within those boundaries, it is possible to identify at least one valid molecule.

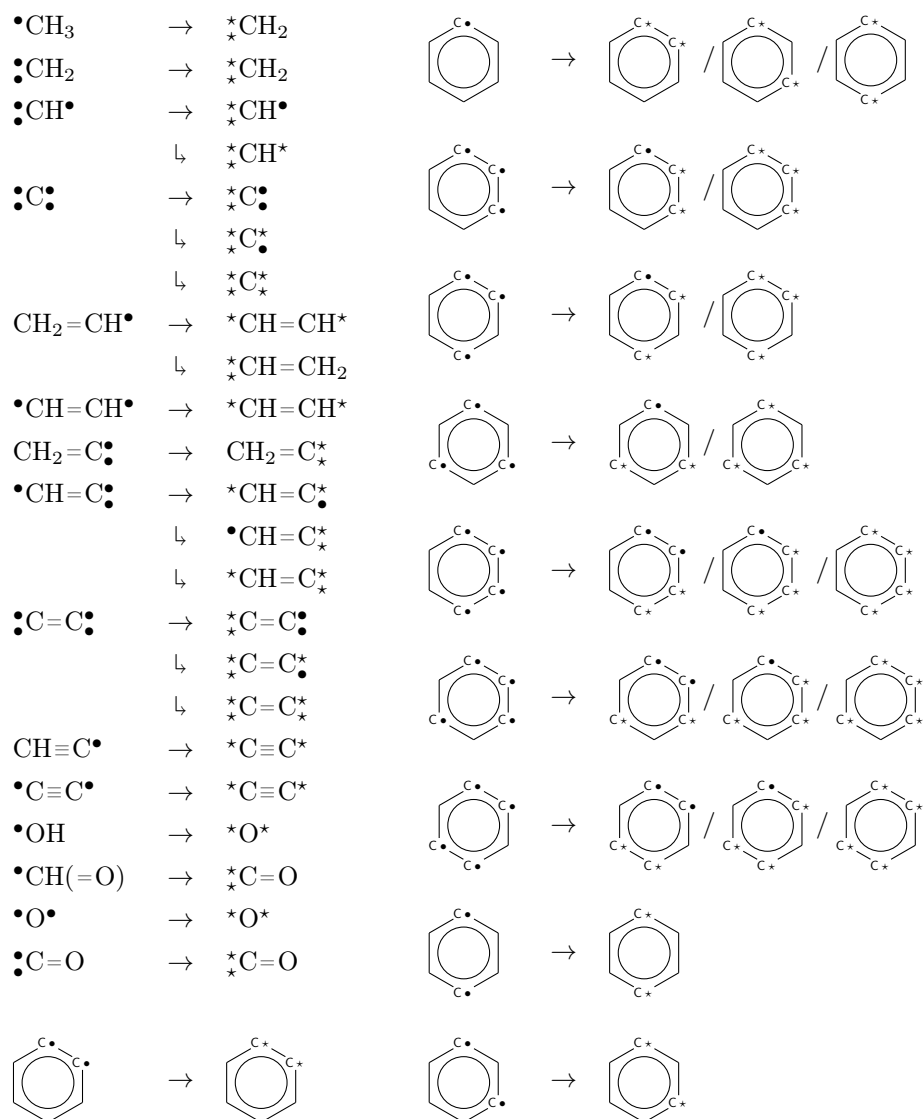


Figure 7.4: Conversion table: from fundamental to cyclic groups. \bullet denotes a non-cyclic connection point, \star denotes an open cyclic connection point

7.3 Algorithm

In any case, the number of ring connection points must be even to avoid unpaired connection points.

$$(n_{\text{iii}} + n_{\text{liii}}) \bmod 2 = 0 \quad (7.3)$$

The number of interlinked rings ($N_{\text{R,il}}$) can be calculated as follows:

$$N_{\text{R,il}} = \begin{cases} 0 & n_{\text{iii}} + n_{\text{liii}} + n_{\text{iv}} = 0 \\ \frac{1}{2}(n_{\text{iii}} + n_{\text{liii}}) + n_{\text{iv}} + 1 & \text{else} \end{cases} \quad (7.4)$$

The number of non-hydrogen atoms being part of a ring ($N'_{\text{R,m}}$) is determined on the basis of the groups present and has to be corrected for atoms which are possibly part of multiple rings:

$$N_{\text{R,m}} = \begin{cases} N'_{\text{R,m}} + (n_{\text{iii}} + n_{\text{liii}}) + \left(1 + \frac{n_{\text{iii}} + n_{\text{liii}}}{2}\right) n_{\text{iv}} & \text{for } (n_{\text{iii}} + n_{\text{liii}}) < 4 \\ N'_{\text{R,m}} + \frac{3(n_{\text{iii}} + n_{\text{liii}}) - 1}{2} + \left(1 + \frac{n_{\text{iii}} + n_{\text{liii}}}{2}\right) n_{\text{iv}} & \text{for } (n_{\text{iii}} + n_{\text{liii}}) \geq 4 \end{cases} \quad (7.5)$$

This leads to the effective number of non-hydrogen atoms taking part in rings ($N_{\text{R,m}}$). The correction is based on the fact that every type iv group is part of at least two rings. For every two type iii(l) groups an additional ring exists. Furthermore, as soon as at least four type iii(l) groups are present, some of them may take part in three rings. The smallest possible ring contains three non-hydrogen atoms. Therefore the number of non-hydrogen atoms in ring groups and the number of interlinked rings must satisfy the following condition:

$$N_{\text{R,il}} \leq \text{floor} \left(\frac{N_{\text{R,m}}}{3} \right) \quad (7.6)$$

To ensure a connection between the cyclic and the non-cyclic part of the molecule ϑ_1 is defined. It describes whether at least one connection between the interlinked rings and the rest is present.

$$\vartheta_1 = \begin{cases} 0 & \text{for } N_{\text{R,il}} = 0 \text{ OR } n_{\text{liii}} > 0 \\ 1 & \text{else} \end{cases} \quad (7.7)$$

The maximum possible number of rings (N_{R}) can now be calculated as follows:

$$N_{\text{R}} = \min \left[\text{floor} \left(\frac{N_{\text{R,members}}}{3} \right) - N_{\text{R,il}}, n_{\text{lii}} + n_{\text{liii}} - \vartheta_1 \right] \quad (7.8)$$

where the first term describes the maximum number of rings with 3 non-hydrogen atoms not interlinked with other rings, and the second term counts the number of connection points between the ring and the non-ring part of the molecule.

To determine the upper and lower boundary of type l groups provided/required by the

construction of rings, two scenarios are investigated. Firstly, as few rings as possible are built requiring as many type I groups as possible. Secondly, as many rings as possible are built providing as many type I groups as possible. The number of available and required type I groups (non-ring) is then needed to meet the boundaries set by the possibilities due to the rings.

For the first scenario the number of required type I groups ($n_{I,cyc,req}$) is given as:

$$n_{I,cyc,req} = n_{Iii} + 2n_{IIii} + n_{IIIi} - 2 \quad (7.9)$$

A value of -2 indicates a closed ring system with no outgoing connections, which is only allowed if no non-ring groups are present. -1 denotes a ring system acting like a type I group, 0 like a type II group.

Maximizing the number of provided type I groups leads to three different sub-cases: the number of rings exceeds the number of outgoing connections (*A*), the average outgoing connections per ring are between 1 and 2 (*B*) or the number of outgoing connections exceeds the number of rings by at least a factor of 2 (*C*). The number of rings acting as type I groups ($N_{R,I}$) is then given as:

$$N_{R,I} = \begin{cases} n_{Iii} & (A) N_R \geq n_{Iii} + n_{IIIi} \\ n_{Iii} - 2\vartheta_2 & (B) N_R \leq \frac{1}{2} (n_{Iii} + n_{IIIi}) \\ 0 & (C) \text{ else} \end{cases} \quad (7.10)$$

with ϑ_2 counting the number of type Iii groups used to form ring type II groups

$$\vartheta_2 = \begin{cases} 0 & n_{Iii} \leq N_R - n_{IIIi} \\ n_{Iii} - N_R + n_{IIIi} & \text{else} \end{cases} \quad (7.11)$$

The number of rings acting as type II groups ($N_{R,II}$) can be calculated as:

$$N_{R,II} = \begin{cases} n_{IIIi} & (A) \\ n_{IIIi} + \vartheta_2 & (B) \\ N_R - 1 & (C) \end{cases} \quad (7.12)$$

The amount of non-covered connection points (CP_{rest}) are defined as:

$$CP_{rest} = \begin{cases} 0 & (A) \text{ AND } (B) \\ n_{Iii} + 2n_{IIIi} - 2(N_R - 1) & (C) \end{cases} \quad (7.13)$$

7.3 Algorithm

The number of connection points of the interlinked ring structure (CP_{il}) is determined as follows:

$$CP_{il} = \begin{cases} n_{iii} & n_{iii} > 0 \\ 1 & \text{else} \end{cases} \quad (7.14)$$

Depending on the remaining connection points, the number of type I groups provided by rings need to be adjusted to obtain the maximum effective type I groups ($n_{l,cyc,eff}$)

$$n_{l,cyc,eff} = \begin{cases} N_{R,I} - CP_{il} - CP_{rest} + 4 & CP_{il} > 2 \text{ AND } CP_{rest} > 2 \\ N_{R,I} - CP_{il} + 2 & CP_{il} > 2 \text{ AND } CP_{rest} \leq 2 \\ N_{R,I} - CP_{rest} + 2 & CP_{il} \leq 2 \text{ AND } CP_{rest} > 2 \\ N_{R,I} & \text{else} \end{cases} \quad (7.15)$$

To represent a possible fuel, the following two conditions need to be satisfied:

$$n_{l,cyc,req} \leq 2 + n_{III} + n_{IV} - n_I \quad (7.16)$$

$$n_{l,cyc,eff} \geq 2 + n_{III} + n_{IV} - n_I \quad (7.17)$$

7.3.3.3 Chemical Stability

The only stability criterion employed is that O–O bonds are forbidden, excluding peroxides. To enforce this criterion, the number of –O– groups (n_O) and the number of –OH groups (n_{OH}) as the only relevant fundamental groups containing oxygen, are compared with the number of groups containing no oxygen ($n_{*,C}$).

$$n_O \leq \max [n_{II,C} + n_{III,C} + n_{IV,C} - n_{OH} + 1, 0] \quad (7.18)$$

Thus, it is possible to place every group with connection points to an oxygen atom between two groups without an open oxygen atom connection.

7.3.4 Grading

7.3.4.1 Criteria

For the optimization procedure, a grading criterion has to be defined based on the performance of the group selection as a fuel. The efficiency (η_{FL}), the specific CO₂ emissions ($e_{CO_2,FL}$) at 2000 rpm, and full load as well as the consumption (c), together with their combinations, are chosen as grading criteria for different runs. To minimize the computational time, the driving cycle simulation was omitted and only full load was simulated. To include the consumption as grading criterion, a correlation between the LHV, density (ρ), efficiency and consumption was developed based on 88 different fuels. The correlation for the estimated consumption (\hat{c}) over the WLTC is given in

the following equation:

$$\hat{c} = -33.427\vartheta^3 + 105.11\vartheta^2 - 116.98\vartheta + 54.065 \quad (7.19)$$

$$\vartheta = \eta_{\text{FL}} \text{LHV} \rho (\overline{\eta_{\text{FL}} \text{LHV} \rho})^{-1} \quad (7.20)$$

with an adjusted $R^2 = 0.981$, $F = 1520$ and a Root Mean Square Error (RMSE) of 0.291/100 km.

As the algorithm is designed to maximize the grading criteria (χ), the values for $e_{\text{CO}_2, \text{FL}}$ and \hat{c} are multiplied by -1 :

$$\chi_\eta = \eta_{\text{FL}} \quad (7.21)$$

$$\chi_c = -\hat{c} \quad (7.22)$$

$$\chi_{\text{CO}_2} = -e_{\text{CO}_2, \text{FL}} \quad (7.23)$$

In order to combine different grading criteria, the different components are normalized based on the values for gasoline.

$$\chi_\eta^{\text{N}} = \frac{\chi_\eta}{\eta_{\text{gasoline}}} = \frac{\chi_\eta}{0.337} \quad (7.24)$$

$$\chi_c^{\text{N}} = \frac{\chi_c}{c_{\text{gasoline}}} = \frac{\chi_c}{8.2} \quad (7.25)$$

$$\chi_{\text{CO}_2}^{\text{N}} = \frac{\chi_{\text{CO}_2}}{e_{\text{CO}_2, \text{gasoline}}} = \frac{\chi_{\text{CO}_2}}{0.77} \quad (7.26)$$

Summation then enables combination of the normalized grades. Three different combinations are evaluated: all, efficiency and CO_2 , as well as efficiency and consumption.

$$\chi_{\text{all}} = \chi_\eta^{\text{N}} + \chi_c^{\text{N}} + \chi_{\text{CO}_2}^{\text{N}} \quad (7.27)$$

$$\chi_{\eta, \text{CO}_2} = \chi_\eta^{\text{N}} + \chi_{\text{CO}_2}^{\text{N}} \quad (7.28)$$

$$\chi_{c, \text{CO}_2} = \chi_c^{\text{N}} + \chi_{\text{CO}_2}^{\text{N}} \quad (7.29)$$

As the efficiency is used to estimate the consumption, the combination between the two is not used as a grading criterion on its own.

7.3.4.2 Taylor Estimate

The time required to simulate all generated options exceeds by far all practical measures. In order to circumvent this issue, a three-step procedure relying on a Taylor Estimate is applied to assess the grade ($\chi_{\text{est}, j}$) of option j .

$$\chi_{\text{est}, j} = \chi_0 + \sum_i \left[\frac{\Delta \chi_i}{\Delta x_i} (x_{j, i} - x_{0, i}) \right] \quad (7.30)$$

where χ_0 is the grade and $x_{0,i}$ the i^{th} property of the initial selection. The average deviation of property i (Δx_i) is calculated based on the whole set of selections.

$$\Delta x_i = \frac{1}{n} \sum_{k=1}^n (x_{k,i} - x_{0,i}) \quad (7.31)$$

In the first step, the local derivatives of the grading criteria around the initial point are determined using finite differences.

$$\Delta \chi_i = \chi(\dots, x_{0,i-1}, x_{0,i} + \Delta x_i, x_{0,i+1}, \dots) - \chi_0 \quad (7.32)$$

In the second step, the grade of each option is estimated using Eq. (7.30) and sorted according to the estimated grade. The third step is to check the estimation by choosing the highest ranking option, and to determine the actual grade by simulation on the engine model. If the grade is higher than that of the initial option, the current option is chosen as base point for the next iteration. Otherwise, the next highest ranking option is chosen, and the check is repeated. This procedure is looped until either a point for the next iteration is found, or no option is left. The latter suggesting that a local optimum has been found and the search can be terminated.

7.3.5 Processing of Results

The algorithm identifies a selection of groups as local optimum. Based on this selection all possible molecular structures need to be derived. Due to the low level of complexity, this is performed manually. Once all possible isomers are determined, their properties are estimated using GCMs. This step is important as certain combinations of small groups require larger groups to be applied. Therefore, deviations from the properties of the identified optimum are possible. The performance at 2000 rpm and full load as well as over the driving cycles of all isomers were determined using the model. Based on the results the compounds showing top performance were identified as most promising fuel and discussed in the following section.

7.4 Results

Two different scenarios were investigated: Unrestricted and with an imposed limitation on the boiling point. The additional limitation is motivated by the fact that the main source of unburnt hydrocarbon emissions from SI DI engines is related to non-evaporated fuel. The main issue is wall impingement of the fuel spray and the formation of a fuel layer on the walls of the combustion chamber. Therefore, an upper boundary on the boiling point was introduced according to the wall temperature (470 K).

The results of the optimization are largely independent of the grading criteria, and thus no distinction is made in the discussion. Minor differences can be detected between the results depending on whether η or CO_2 is chosen as grading criterion.

The compounds resulting from the unrestricted run are denominated using capital letters (A, B, C) and are shown in summarized form in Figs. 7.5 to 7.7, an extensive list of all isomers is given in Figs. E.1 to E.4. All the different isomers presented are indistinguishable for the applied GCMs and are therefore equally well-suited.

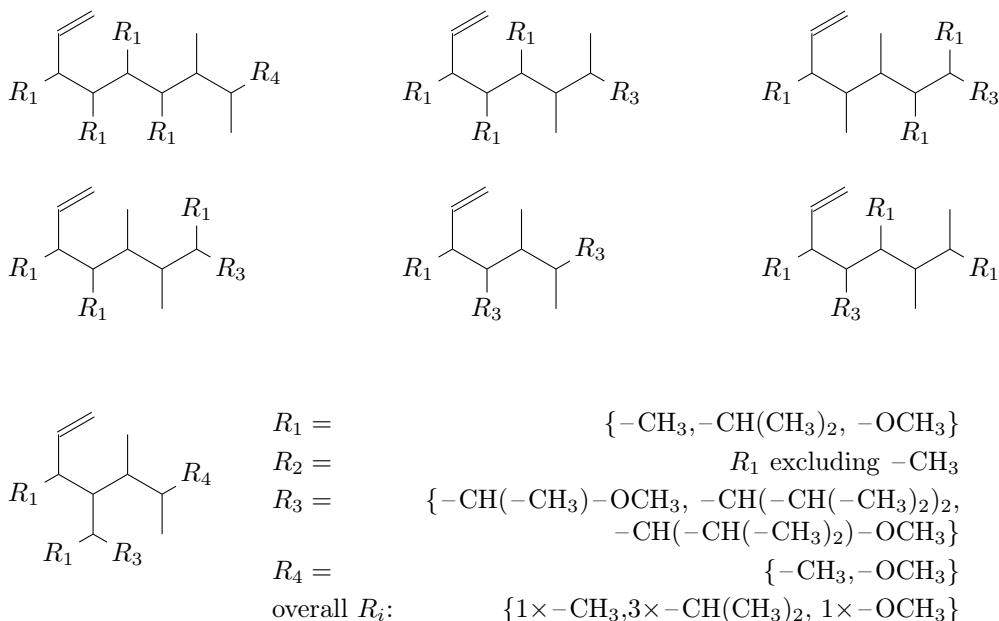


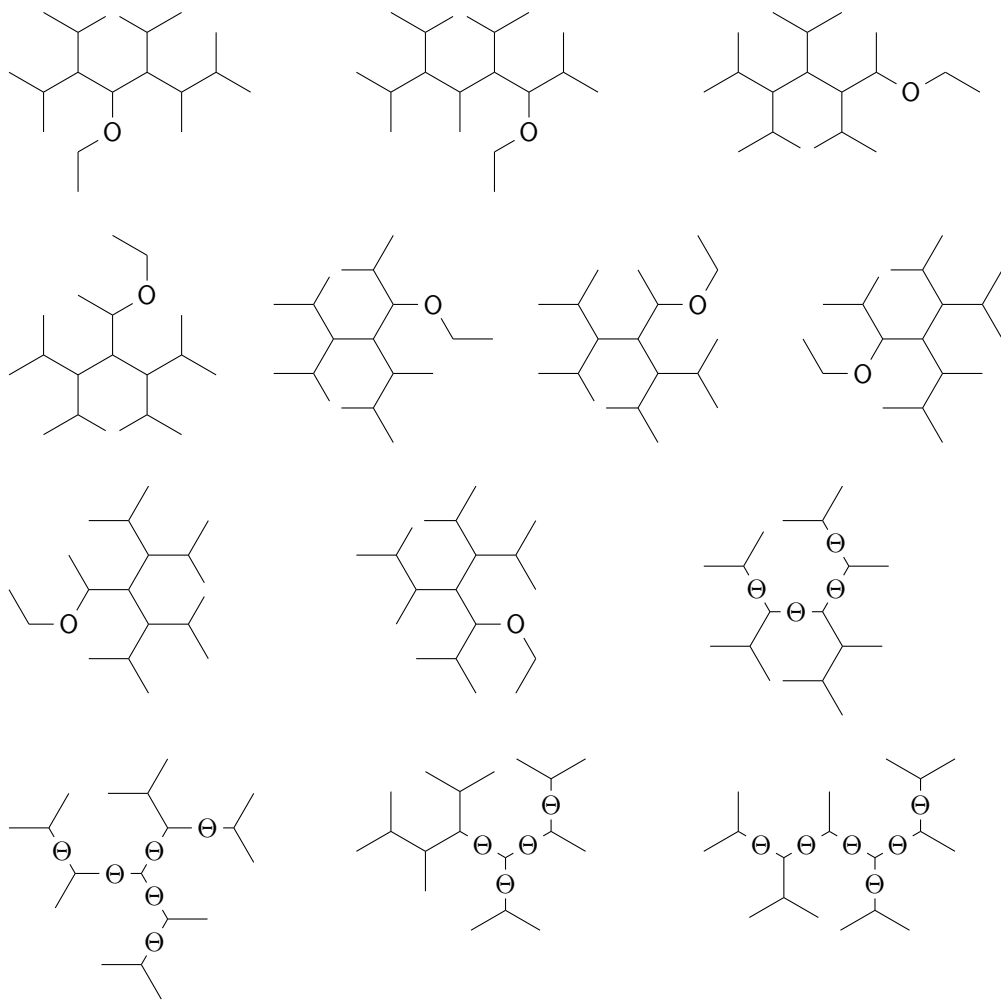
Figure 7.5: Compound A, resulting from unrestricted optimization. The options for the substituents R_1 , R_2 , R_3 and R_4 can be chosen such that for the whole molecule 1 OCH_3 , 3 $\text{CH}(\text{CH}_3)_2$ and 1 CH_3 group is present.

The molecules identified by the restricted run are shown in Fig. 7.8 and labeled using lowercase letters a to d. For all these cases, there is only one possible combination of the groups, resulting in one unique structure. Interestingly, compound b (β -methylstyrene) has already been identified in Section 5.4.4 as lignin pyrolysis oil upgrading targets to minimize consumption.

The number of publications concerning the compounds a to d is very limited. β -methylstyrene (compound b) seems to be the best-studied compound. However, no fuel-related applications could be found.

The properties, estimated according to the employed GCMs, for each of these compounds are listed in Table 7.1. For some of the compounds (A, C and a), a melting point above the limit of 253 K is reported. This originates in the different isomers tested based on the identified group selections and can lead to small changes in properties and thereby the increased melting point. However, the deviation from the limit (max. 9 K) is significantly smaller than the accuracy of the employed GCM (AAE = 15.99 K).

Compounds A, B and C show extreme values for the RON. Nevertheless, judging from



Θ: 1x-CH₂-O-

Figure 7.6: Compound B, resulting from unrestricted optimization. Θ denotes a possible placement of a -CH₂-O- group, out of which one has to be occupied.

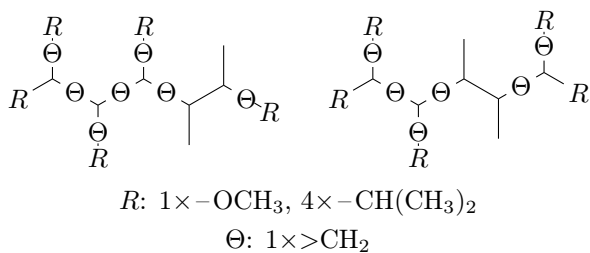


Figure 7.7: Compound C, resulting from unrestricted optimization. \ominus denotes a possible placement of a $>\text{CH}_2$ group, out of which one has to be occupied. The options for the substituent R can be chosen such that for the whole molecule 1 OCH_3 and 4 $\text{CH}(\text{CH}_3)_2$ groups are present.

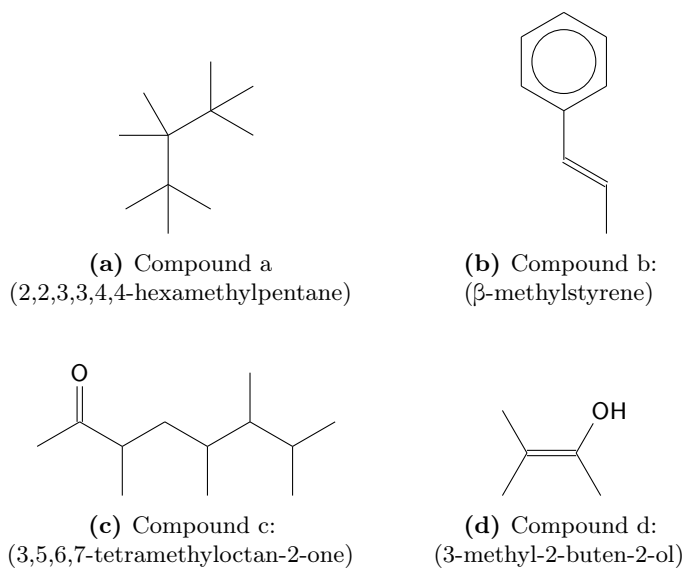


Figure 7.8: Compounds identified by the optimization with a maximum boiling point of 470 K.

Table 7.1: Properties of the identified compounds, estimated by the GCMs at standard conditions ($T = 298 \text{ K}$, $p = 0.1 \text{ MPa}$).

	formula	ρ [kg/m ³]	$c_{p,g}$ [J/(mol K)]	ν [mm ² /s]	p_{vap} [Pa]	h_{vap} [kJ/mol]	RON [-]	LHV [MJ/kg]	T_{melt} [K]	T_{boil} [K]
A	C ₂₁ H ₄₂ O	829	489	5.18	0.003	88.0	672	40.8	260	580
B	C ₁₉ H ₄₀ O	806	454	3.75	0.036	80.2	290	41.0	239	550
C	C ₂₁ H ₄₄ O	820	500	5.68	0.002	90.1	542	41.2	262	582
a	C ₁₁ H ₂₄	769	257	2.23	261	49.4	131	44.3	258	425
b	C ₉ H ₁₀	909	138	1.04	125	47.7	111	40.1	246	457
c	C ₁₂ H ₂₄ O	833	280	2.14	4	63.4	134	38.9	245	492
d	C ₅ H ₁₀ O	810	232	3.34	289	52.0	97	33.6	248	413

their highly branched structure, their RONs are expected to be high. These compounds show high boiling points and vapor pressures close to zero, making their cold start capability questionable. The high RON allows for high compression ratios, which might mitigate this issue. The increased compression ratio leads to higher temperatures in the cylinder before ignition, supporting the evaporation of less volatile compounds. For compounds with a boiling point limitation, the situation is different. Vapor pressures are still not high, but, except for compound c, within the range of established fuels. For compounds a, b, and d, there is a loose inverse correlation between the enthalpy of vaporization and the RON. This can be attributed to the fact that knocking limits peak temperature and pressure. The enthalpy of vaporization contributes to lower temperatures, whereas the RON defines the maximum allowable temperature/pressure levels before the onset of knock. A more detailed discussion is given in Section 2.3.

In Table 7.2 the performance of the identified compounds is listed; further results including the performance over the CADC and NEDC are listed in Table E.4. No difference can be observed for the unrestricted optimization. Molecules a to d show inferior performance. With respect to compression ratio, compounds A to C range close to or at the maximum of 20. In contrast, compounds a to d possess compression ratios between 11 to 15 which is the estimated range of optimum compression ratios from an engine point of view. The exact location of this optimum is not well-established and depends on the fuel [145, 200].

Table 7.2: Performance of the identified compounds. η_{FL} efficiency at full load, η_{PL} efficiency at 2000 rpm and $P_{\text{out}} = 6.6$ kW, P_{FL} power output at full load, e_{CO_2} specific CO₂ emissions, ε_{CR} compression ratio, η_{cyc} cycle efficiency, $e_{\text{CO}_2,\text{D}}$ CO₂ emissions per distance and c consumption over the WLTC.

fuel	η_{FL} [%]	η_{PL} [%]	P_{FL} [kW]	$e_{\text{CO}_2,\text{FL}}$ [kg/kWh]	ε_{CR} [-]	η_{cyc} [%]	$e_{\text{CO}_2,\text{D}}$ [g/km]	c [l/100km]
A	40.7	24.6	87.8	0.65	19.5	25.8	160	6.5
B	40.7	24.7	87.7	0.64	20.0 ^a	25.8	158	6.6
C	40.7	24.7	87.7	0.64	20.0 ^a	25.8	157	6.5
a	38.6	23.2	82.8	0.65	13.0	23.9	166	6.9
b	36.2	21.8	78.7	0.83	11.8	22.4	211	6.9
c	39.3	23.7	85.2	0.67	14.8	24.4	171	7.1
d	39.5	23.8	86.5	0.69	10.8	24.4	177	8.5

^a maximum allowed compression ratio

7.5 Conclusions

An algorithm that allows optimizing molecules with regard to their performance as gasoline replacement was developed. This so-called rGCM combines GCMs, a pattern search optimization procedure, and a thermodynamic model of an ICE. The introduction of the rGCM allowed us to identify eight different fuel candidates with optimized performance in a DISI ICE. Each of them was superior in performance compared to the established fuels including gasoline.

Two different scenarios were analyzed: Firstly, no limits were set to the boiling point and, secondly, the boiling point was limited to the cylinder wall temperature (470 K). The compounds identified within the first run (A to C) outperformed the compounds (a to d) from the second run. Considering their properties, compounds A to C could suffer from cold start problems.

The identified compounds resulted in an efficiency of 36.2% to 40.7% at full load, specific CO₂ emissions in the range of 158 g/km to 211 g/km and a consumption of 6.51/100 km to 8.51/100 km. Apart from compound b, the compounds analyzed significantly outperformed the established fuels: ethyl levulinate showed maximum efficiency (38.6%), *sec*-butanol minimum specific CO₂ emissions (177 g/km) and 2-phenylethanol minimal consumption (7.21/100 km).

It is important to note, that only performance related criteria were applied during the optimization. Other issues related to SI engine operation, such as cold start, oil dilution and emissions, have not been studied.

8 Summary, Conclusions and Outlook

8.1 Summary

This work presents a new approach to Computer Aided Molecular Design (CAMD) of fuels. It combines a custom-built engine model and established Group Contribution Methods (GCMs) with an optimization procedure. The engine model allows to compare the different compounds currently discussed as potential biofuels.

In the following sections, a summary of the results of this thesis are given, including a comparison of the findings of the different chapters and an outlook with recommendations/directions for further work on the subject.

A thermodynamic model of a Spark Ignition (SI) Direct Injection (DI) Internal Combustion Engine (ICE) was developed, focusing on fuel-related influences. Besides the Research Octane Number (RON), the model only requires readily available properties such as vapor heat capacity, liquid viscosity, liquid density, enthalpy of vaporization, vapor pressure and elemental composition as input. To determine the potential of a compound as fuel, the model optimizes the efficiency by adapting the compression ratio. For this optimization the operating point is defined by 2000 rpm and a charging pressure of 0.2 MPa. This adaptation is constrained by the occurrence of knock and a peak pressure limitation of 25 MPa. The model is publicly available at <http://fuel-simulation.psi.ch>.

Reviewing the literature, 34 compounds were identified as possible biofuels to replace gasoline. The performance of these compounds as pure fuels has been analyzed regarding efficiency, specific CO₂ emissions and consumption over various driving cycles. In summary, no compound was superior to gasoline with respect to both specific CO₂ emissions and consumption. When focusing on specific CO₂ emissions only, butanol isomers were most promising with *sec*-butanol resulting in CO₂ emissions of only 177 g/km compared to 193 g/km for gasoline. Consumption is minimized by 2-phenylethanol with 7.21/100 km compared to the 8.21/100 km of gasoline. Both compounds reduce the respective indicator by roughly 10 % compared to gasoline. Furthermore, an idealized consideration of hybrid powertrains showed a reduction potential of 40 % to 60 %, depending on the driving cycle, with respect to both consumption and specific CO₂ emissions. This reduction is unaffected by the fuel choice, thus compounds well-suited for traditional operation perform equally well under hybrid operation.

Supporting the design of lignin pyrolysis oil upgrading by Hydrodeoxygenation (HDO), the versatility of the ICE model has been used to identify the optimum

target compounds. The upgrading process was described by generalized HDO reaction pathways. GCMs were applied to estimate the required properties for each of the intermediate molecules. Subsequently, these molecules were analyzed for their suitability as fuel. Constrained by limitations to the melting and boiling points, a molecule has been identified for each of the reaction pathways, minimizing either consumption, specific CO₂ emissions or maximizing efficiency.

The mixture model was used to determine the possibilities offered by mixing the established fuels. Thereby, 78 mixtures were identified with a performance similar to gasoline. A mixture with both lower specific CO₂ emissions and lower consumption than gasoline could not be found.

To characterize the ideal SI fuel, the reverse Group Contribution Method (rGCM) algorithm was designed. It combines GCMs, the engine model and a pattern search optimization procedure. This unique combination allows to efficiently identify the best-suited molecule(s) to serve as an SI fuel. An unrestricted run led to the identification of three highly branched compounds, labeled A to C (as shown in Figs. 7.5 to 7.7 on pages 100–102). A limitation to the boiling point was defined based on considerations to reduce potentially unburnt fuel emissions. With this boundary in place, another four molecules have been found, labeled a to d (as shown in Fig. 7.8 on page 102). The molecular structure of these compounds was discussed in Chapter 7.

8.2 Conclusions

Figs. 8.1 and 8.2 summarize and compare the results of the chapters of this thesis. In general, it can be stated that the mixtures proposed in the literature blend in well with the other biofuels (Υ , Φ and Ψ). The mixtures that were identified in Chapter 6 (α to γ) perform very similarly to gasoline in terms of all measures. The exception is their efficiency, being significantly higher. The compounds identified as targets of lignin pyrolysis oil upgrading show relatively high efficiencies (except M7). At the same time, their consumption is comparable (P3, R3) or even higher than gasoline (R1). M7 was also identified as a compound with minimum consumption in the boiling-point-limited run of the rGCM. The rGCM identified compounds that show superior performance over gasoline in both CO₂ emissions and consumption. In terms of performance over the Worldwide harmonized Light vehicles Test Cycle (WLTC), molecules A, B, C, a and c outperform the established fuels with respect to both consumption and specific CO₂ emissions. Compounds a and b achieve minimum consumption for the limited boiling point scenario. However, CO₂ emissions are significantly increased for compound b. Compound d has a similar consumption compared to gasoline in conjunction with reduced specific CO₂ emissions.

By identification of compounds A to C and a to d, the task to determine the ideal SI fuel has been accomplished. These compounds optimize the performance of the presented model. However, due to the idealizations employed in the thermodynamic model, experimental tests are needed to verify their suitability as fuel. Parameters as cold start, emissions beside CO₂, toxicity, oil dilution, and storability are not considered

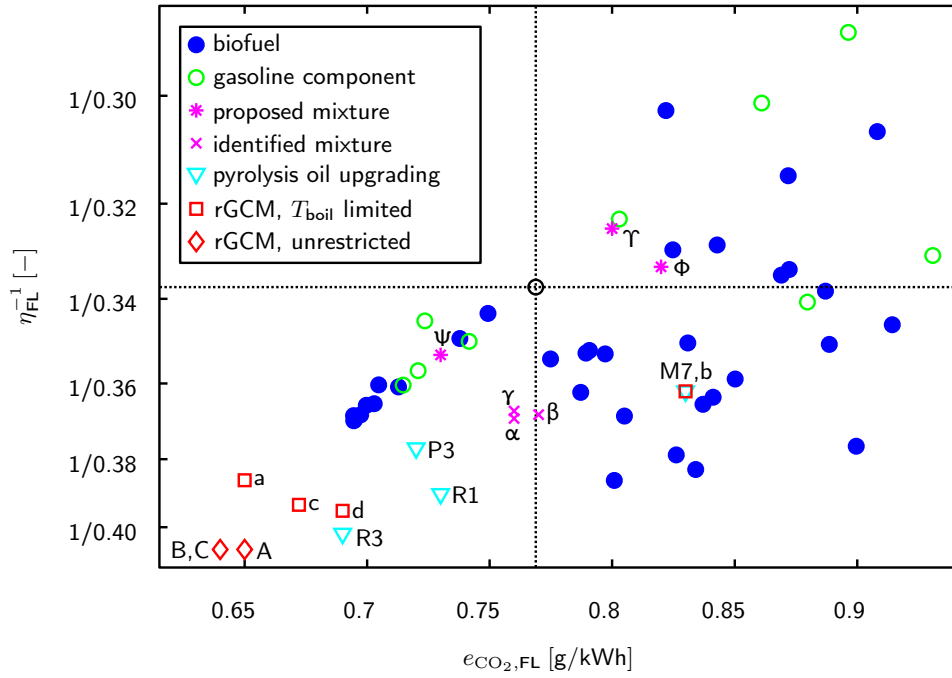


Figure 8.1: Comparison of all compounds and mixtures discussed with respect to efficiency and specific CO₂ emissions at full load. Biofuels (blue filled circles), gasoline components (green circles), gasoline (black circle). Pyrolysis oil upgrading target molecules (cyan triangles). Mixtures proposed in the literature [198] (magenta stars), identified mixtures (magenta crosses). Results of the unrestricted rGCM (red diamonds). Results of the boiling-point-limited rGCM (magenta squares).

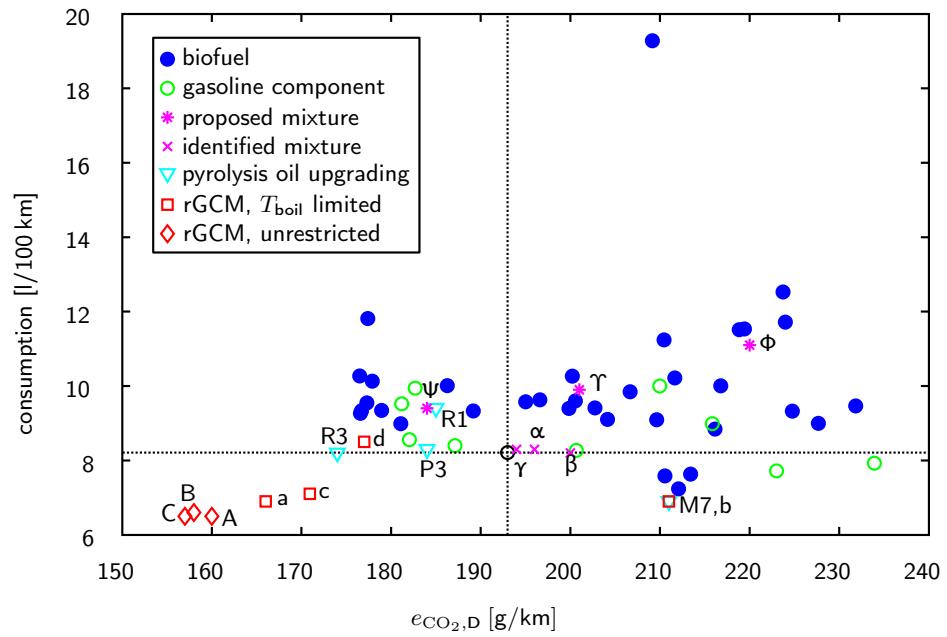


Figure 8.2: Comparison of all compounds and mixtures discussed with respect to consumption and CO₂ emissions over the WLTC. Biofuels (blue filled circles), gasoline components (green circles), gasoline (black circle). Pyrolysis oil upgrading target molecules (cyan triangles). Mixtures proposed in the literature [198] (magenta stars), identified mixtures (magenta crosses). Results of the unrestricted rGCM (red diamonds). Results of the boiling-point-limited rGCM (magenta squares).

in the model. Furthermore, once a production pathway has been developed a Life Cycle Analysis (LCA) needs to be performed to assess the sustainability of the fuels.

8.3 Outlook

The outlook is divided into three parts: A modeling section, discussing strategies to further improve the engine model. Followed by a paragraph describing further directions regarding the considered fuels and mixtures thereof. Finally, possible improvements and non-fuel related applications for the rGCM are proposed.

8.3.1 Modeling

- The model would benefit from a correlation for the ignition delay only depending on available properties. One possibility would be the substitution of the RON by the autoignition temperature or to use the derived Cetane Number (dCN). Both properties are easier to determine experimentally than the RON.
- Through extensive experimental studies, it might be possible to develop a model that links heat release during combustion to molecular properties. This approach would allow a more accurate combustion model.
- After minor improvements to the evaporation model, cold start issues could be studied. Required changes include the detailed consideration of the spray, taking into account break up and wall impingement.
- Besides engine performance, emissions are of interest when discussing future fuels. Therefore the model should be extended to include emissions, such as unburnt fuel, soot, CO, and NO_x. Other than general estimations with limited applicability, there are no applicable models known to the author which allow estimating unburnt fuel, soot or CO emissions. NO_x emissions are traditionally divided into three categories: prompt, thermal and fuel NO_x. For thermal NO_x, a well-established reaction mechanism consisting of three reactions exists. To implement this mechanism, only minor adjustments would be required. As prompt NO_x involves fuel radicals reacting with N₂ from air, deriving a generalized mechanism is difficult. The same is true for fuel NO_x that arise from fuel-bound N atoms.
- To cover further modes of operation, the model could be extended to include Exhaust Gas Recirculation (EGR) and ignition timing. EGR would require a modification to the intake modeling, whereas the ignition timing would require changes to the compression step. In this way, the possible modes of operation of the engine model could be extended.

8.3.2 Established Fuels

- Similarly to the approach discussed in Chapter 5, the mixture model can be applied to evaluate different fuel production schemes and optimize their performance.

- A detailed analysis of lignin pyrolysis oil, including mass fractions of each compound would allow simulating the oil as a mixture, instead of considering single components only. This would reflect reality and allows to gain further insight into the upgrading targets.
- The engine model could be applied to study the influence of the different fuel properties on the engine. This approach would require a detailed analysis of the p and T evolution for each case and could lead to the creation of a new dimensionless quantity for fuel characterization.
- Based on the sensitivity model it might be possible to develop a correlation between the efficiency and key fuel properties such as elemental composition, vapor heat capacity, enthalpy of vaporization and the RON. This point might benefit from/facilitates considerations on a novel dimensionless quantity as mentioned above.
- The engine model could be implemented in life cycle assessments to determine the tank-to-wheel emissions for different fuels over different driving cycles.
- It would be very interesting to test the determined mixtures on a real engine and see whether the predictions of equal performance as gasoline hold true.

8.3.3 The reverse Group Contribution Method (rGCM)

- As a next step, the identified compounds need to be experimentally tested to verify their performance as fuel. Therefore a synthesis method must be established enabling the production of the compounds in the required quantities.
- Once the ICE model is converted to Compression Ignition (CI), the best-suited replacement for Diesel-fuel could also be determined.
- By exchanging the ICE model with a similar model, it would be possible to design compounds for other applications, e.g. refrigerants and polymers.
- Including the mixture model into the rGCM, the design of fuel additives would be possible to improve existing mixtures. Similarly, the extension of the rGCM to design the perfect fuel mixture is thinkable, but the significantly increased degrees of freedom require an adequate solving strategy.
- A way to design feedstock-specific fuels would be to limit the number and types of available groups to only those derivable from the respective feedstock.

Bibliography

- [1] IPCC. *Climate change 2014 : synthesis report*. eng. Genève: IPCC, 2014. URL: <http://www.ipcc.ch/report/ar5/wg1/>.
- [2] International Energy Agency. *World Energy Balances 2017*. OECD, Aug. 31, 2017. 2 pp. ISBN: 9264278095. URL: http://www.ebook.de/de/product/29829769/world_energy_balances_2017.html.
- [3] International Energy Agency. *Renewables Information 2017*. OECD, Aug. 31, 2017. 2 pp. ISBN: 9264277765. URL: http://www.ebook.de/de/product/29828786/renewables_information_2017.html.
- [4] Bundesamt für Energie. *Schweizerische Gesamtenergiestatistik 2015*. July 12, 2016. URL: http://www.bfe.admin.ch/themen/00526/00541/00542/00631/index.html?lang=de&dossier_id=00763 (visited on 11/05/2017).
- [5] Bundesamt für Umwelt. *Kenngrossen zur Entwicklung der Treibhausgasemissionen in der Schweiz 1990-2015*. 2017. URL: <https://www.bafu.admin.ch/bafu/de/home/themen/klima/daten-indikatoren-karten/daten/treibhausgasinventar.html> (visited on 11/05/2017).
- [6] SCCER Mobility. *Auf dem Weg zu einem energieeffizienten und klimafreundlichen Schweizer Mobilitätssystem*. Research rep. Sept. 2017. URL: http://www.sccer-mobility.ch/export/sites/sccer-mobility/capacity-areas/dwn_capacity_areas/SCCER_Mobility_White_Paper_Sept2017.pdf (visited on 11/05/2017).
- [7] European Biofuels Technology Platform. *Strategic Research Agenda & Strategy Deployment Document*. CPL Press, 2008. ISBN: 978-1-872691-38-1.
- [8] M. Contestabile, G. J. Offer, R. Slade, F. Jaeger, and M. Thoennes. “Battery electric vehicles, hydrogen fuel cells and biofuels. Which will be the winner?”, *Energy & Environmental Science* 4.10 (2011), p. 3754. DOI: 10.1039/c1ee01804c.
- [9] S. Ramachandran and U. Stimming. “Well to wheel analysis of low carbon alternatives for road traffic”, *Energy & Environmental Science* 8.11 (2015), pp. 3313–3324. DOI: 10.1039/C5EE01512J.
- [10] G. T. Kalghatgi. “The outlook for fuels for internal combustion engines”, *International Journal of Engine Research* 15.4 (Mar. 2014), pp. 383–398. ISSN: 2041-3149. DOI: 10.1177/1468087414526189.
- [11] K. Nakata, S. Utsumi, A. Ota, K. Kawatake, T. Kawai, and T. Tsunooka. “The Effect of Ethanol Fuel on a Spark Ignition Engine”, *SAE Technical Paper 2006-01-3380*. SAE International, Oct. 2006. DOI: 10.4271/2006-01-3380.

-
- [12] D. Turner, H. Xu, R. F. Cracknell, V. Natarajan, and X. Chen. “Combustion performance of bio-ethanol at various blend ratios in a gasoline direct injection engine”, *Fuel* 90.5 (May 2011), pp. 1999–2006. DOI: 10.1016/j.fuel.2010.12.025.
- [13] C. Pana, N. Negurescu, M. G. Popa, A. Cernat, and D. Soare. “Aspects of the use of ethanol in spark ignition engine”, *SAE Technical Paper 2007-01-2040*. SAE International, July 2007. DOI: 10.4271/2007-01-2040.
- [14] M. K. Balki, C. Sayin, and M. Canakci. “The effect of different alcohol fuels on the performance, emission and combustion characteristics of a gasoline engine”, *Fuel* 115 (Jan. 2014), pp. 901–906. DOI: 10.1016/j.fuel.2012.09.020.
- [15] D. Gschwend, P. Soltic, A. Wokaun, and F. Vogel. “Review and Performance Evaluation of Fifty Alternative Liquid Fuels for Spark Ignition Engines”, *submitted to energy & fuels* (2018).
- [16] R. Luque, L. Herrero-Davila, J. M. Campelo, J. H. Clark, J. M. Hidalgo, D. Luna, J. M. Marinas, and A. A. Romero. “Biofuels: a technological perspective”, *Energy & Environmental Science* 1.5 (2008), p. 542. DOI: 10.1039/b807094f.
- [17] C. Wang, H. Xu, R. Daniel, A. Ghafourian, J. M. Herreros, S. Shuai, and X. Ma. “Combustion characteristics and emissions of 2-methylfuran compared to 2,5-dimethylfuran, gasoline and ethanol in a DISI engine”, *Fuel* 103 (Jan. 2013), pp. 200–211. ISSN: 0016-2361. DOI: 10.1016/j.fuel.2012.05.043.
- [18] P. S. Nigam and A. Singh. “Production of liquid biofuels from renewable resources”, *Progress in Energy and Combustion Science* 37.1 (Feb. 2011), pp. 52–68. ISSN: 0360-1285. DOI: 10.1016/j.pecs.2010.01.003.
- [19] J.-P. Lange, E. van der Heide, J. van Buijtenen, and R. Price. “Furfural – A Promising Platform for Lignocellulosic Biofuels”, *ChemSusChem* 5.1 (Jan. 2012), pp. 150–166. DOI: 10.1002/cssc.201100648.
- [20] C. Jin, M. Yao, H. Liu, C.-f. F. Lee, and J. Ji. “Progress in the production and application of *n*-butanol as a biofuel”, *Renewable and Sustainable Energy Reviews* 15.8 (Oct. 2011), pp. 4080–4106. DOI: 10.1016/j.rser.2011.06.001.
- [21] M. Thewes, M. Muther, A. Brassat, S. Pischinger, and A. Sehr. “Analysis of the Effect of Bio-Fuels on the Combustion in a Downsized DI SI Engine”, *SAE International Journal of Fuels and Lubricants* 5.1 (Aug. 2011), pp. 274–288. DOI: 10.4271/2011-01-1991.
- [22] V. Raman, V. Sivasankaralingam, R. Dibble, and S. M. Sarathy. “ α -Pinene – A High Energy Density Biofuel for SI Engine Applications”, *SAE Technical Paper 2016-01-2171* (Oct. 2016). DOI: 10.4271/2016-01-2171.
- [23] M. Hechinger. “Model-based identification of promising biofuel candidates for spark-ignited engines”. eng. PhD thesis. Düsseldorf: RWTH Aachen, 2014. ISBN: 978-3-18-394003-5.
- [24] M. Dahmen and W. Marquardt. “Model-Based Design of Tailor-Made Biofuels”, *Energy & Fuels* 30.2 (Feb. 2016), pp. 1109–1134. ISSN: 0887-0624. DOI: 10.1021/acs.energyfuels.5b02674.

- [25] S. Atsumi, T. Hanai, and J. C. Liao. “Non-fermentative pathways for synthesis of branched-chain higher alcohols as biofuels”, *Nature* 451.7174 (Jan. 2008), pp. 86–89. DOI: 10.1038/nature06450.
- [26] J. W. Turner, A. G. Lewis, S. Akehurst, C. J. Brace, S. Verhelst, J. Vancoillie, L. Sileghem, F. Leach, and P. P. Edwards. “Alcohol fuels for spark-ignition engines: Performance, efficiency and emission effects at mid to high blend rates for binary mixtures and pure components”, *Proceedings of the Institution of Mechanical Engineers, Part D: Journal of Automobile Engineering* 232.1 (Jan. 2018), pp. 36–56. DOI: 10.1177/0954407017752832.
- [27] J. R. Nichols. “The Methanol Story: A Sustainable Fuel for the Future”, *Journal of Scientific & Industrial Research* 62 (Jan. 2003), pp. 97–105. ISSN: 0022-4456.
- [28] A. Demirbas. “Fuel Alternatives to Gasoline”, *Energy Sources, Part B: Economics, Planning, and Policy* 2.3 (Aug. 2007), pp. 311–320. DOI: 10.1080/15567240600629492.
- [29] J. Pumphrey, J. Brand, and W. Scheller. “Vapour pressure measurements and predictions for alcohol–gasoline blends”, *Fuel* 79.11 (Sept. 2000), pp. 1405–1411. DOI: 10.1016/S0016-2361(99)00284-7.
- [30] D. Yao, X. Ling, and F. Wu. “Experimental Investigation on the Emissions of a Port Fuel Injection Spark Ignition Engine Fueled with Methanol–Gasoline Blends”, *Energy & Fuels* 30.9 (Aug. 2016), pp. 7428–7434. DOI: 10.1021/acs.energyfuels.6b01586.
- [31] M. Allard. “Issues Associated with Widespread Utilization of Methanol”, *SAE Technical Paper 2000-01-0005*. SAE International, Mar. 2000. DOI: 10.4271/2000-01-0005.
- [32] V. R. Surisetty, A. K. Dalai, and J. Kozinski. “Alcohols as alternative fuels: An overview”, *Applied Catalysis A: General* 404 (July 2011), pp. 1–11. DOI: 10.1016/j.apcata.2011.07.021.
- [33] B. H. Ramadan, F. J. Hamady, C. L. Gray, K. H. Hellman, and H. J. Schock. “Numerical Evaluation of A Methanol Fueled Directly-Injected Engine”, *SAE Technical Paper 2002-01-2702*. SAE International, Oct. 2002. DOI: 10.4271/2002-01-2702.
- [34] J. Yanowitz, E. Christensen, and R. L. McCormick. *Utilization of Renewable Oxygenates as Gasoline Blending Components*. Technical Report. Aug. 2011. DOI: 10.2172/1024518.
- [35] E. Christensen, J. Yanowitz, M. Ratcliff, and R. L. McCormick. “Renewable Oxygenate Blending Effects on Gasoline Properties”, *Energy & Fuels* 25.10 (Oct. 2011), pp. 4723–4733. DOI: 10.1021/ef2010089.
- [36] T. Lattimore, J. M. Herreros, H. Xu, and S. Shuai. “Investigation of compression ratio and fuel effect on combustion and PM emissions in a DISI engine”, *Fuel* 169 (Apr. 2016), pp. 68–78. DOI: 10.1016/j.fuel.2015.10.044.

-
- [37] D. Jin, K. Choi, C.-L. Myung, Y. Lim, J. Lee, and S. Park. “The impact of various ethanol-gasoline blends on particulates and unregulated gaseous emissions characteristics from a spark ignition direct injection (SIDI) passenger vehicle”, *Fuel* 209 (Dec. 2017), pp. 702–712. DOI: 10.1016/j.fuel.2017.08.063.
- [38] G. D. G. Peña, Y. A. Hammid, A. Raj, S. Stephen, T. Anjana, and V. Balasubramanian. “On the characteristics and reactivity of soot particles from ethanol-gasoline and 2,5-dimethylfuran-gasoline blends”, *Fuel* 222 (June 2018), pp. 42–55. DOI: 10.1016/j.fuel.2018.02.147.
- [39] G. Karavalakis, D. Short, R. L. Russell, H. Jung, K. C. Johnson, A. Asa-Awuku, and T. D. Durbin. “Assessing the Impacts of Ethanol and Isobutanol on Gaseous and Particulate Emissions from Flexible Fuel Vehicles”, *Environmental Science & Technology* 48.23 (Nov. 2014), pp. 14016–14024. DOI: 10.1021/es5034316.
- [40] F. C. Leach, R. Stone, D. Richardson, J. W. Turner, A. Lewis, S. Akehurst, S. Remmert, S. Campbell, and R. Cracknell. “The effect of oxygenate fuels on PN emissions from a highly boosted GDI engine”, *Fuel* 225 (Aug. 2018), pp. 277–286. DOI: 10.1016/j.fuel.2018.03.148.
- [41] T. Venugopal and A. Ramesh. “Performance, combustion and emission characteristics of a spark-ignition engine with simultaneous injection of *n*-butanol and gasoline in comparison to blended butanol and gasoline”, *International Journal of Energy Research* 38.8 (Sept. 2013), pp. 1060–1074. DOI: 10.1002/er.3113.
- [42] J. Williams, C. Goodfellow, D. Lance, A. Ota, K. Nakata, K. Kawatake, and W. Bunting. “Impact of Butanol and Other Bio-Components on the Thermal Efficiency of Prototype and Conventional Engines”, *SAE Technical Paper 2009-01-1908*. SAE International, June 2009. DOI: 10.4271/2009-01-1908.
- [43] P. Dürre. “Biobutanol: An attractive biofuel”, *Biotechnology Journal* 2.12 (Dec. 2007), pp. 1525–1534. DOI: 10.1002/biot.200700168.
- [44] S. Szwaja and J. D. Naber. “Combustion of *n*-butanol in a spark-ignition IC engine”, *Fuel* 89.7 (July 2010), pp. 1573–1582. DOI: 10.1016/j.fuel.2009.08.043.
- [45] C. Hergueta, M. Bogarra, A. Tsolakis, K. Essa, and J. Herreros. “Butanol-gasoline blend and exhaust gas recirculation, impact on GDI engine emissions”, *Fuel* 208 (Nov. 2017), pp. 662–672. DOI: 10.1016/j.fuel.2017.07.022.
- [46] M. Vojtisek-Lom, V. Beranek, J. Stolcpartova, M. Pechout, and V. Klir. “Effects of *n*-Butanol and Isobutanol on Particulate Matter Emissions from a Euro 6 Direct-injection Spark Ignition Engine During Laboratory and on-Road Tests”, *SAE International Journal of Engines* 8.5 (Sept. 2015), pp. 2338–2350. DOI: 10.4271/2015-24-2513.
- [47] F. Hoppe, U. Burke, M. Thewes, A. Heufer, F. Kremer, and S. Pischinger. “Tailor-Made Fuels from Biomass: Potentials of 2-butanone and 2-methylfuran in direct injection spark ignition engines”, *Fuel* 167 (Mar. 2016), pp. 106–117. DOI: 10.1016/j.fuel.2015.11.039.

- [48] H. Wei, D. Feng, G. Shu, M. Pan, Y. Guo, D. Gao, and W. Li. “Experimental investigation on the combustion and emissions characteristics of 2-methylfuran gasoline blend fuel in spark-ignition engine”, *Applied Energy* 132 (Nov. 2014), pp. 317–324. DOI: 10.1016/j.apenergy.2014.07.009.
- [49] M. Thewes, M. Muether, S. Pischinger, M. Budde, A. Brunn, A. Sehr, P. Adomeit, and J. Klankermayer. “Analysis of the Impact of 2-Methylfuran on Mixture Formation and Combustion in a Direct-Injection Spark-Ignition Engine”, *Energy & Fuels* 25.12 (Dec. 2011), pp. 5549–5561. ISSN: 1520-5029. DOI: 10.1021/ef201021a.
- [50] S. Gouli, E. Lois, and S. Stournas. “Effects of Some Oxygenated Substitutes on Gasoline Properties, Spark Ignition Engine Performance, and Emissions”, *Energy & Fuels* 12.5 (Sept. 1998), pp. 918–924. DOI: 10.1021/ef980002t.
- [51] G. W. Huber, S. Iborra, and A. Corma. “Synthesis of Transportation Fuels from Biomass: Chemistry, Catalysts, and Engineering”, *Chemical Reviews* 106.9 (2006). PMID: 16967928, pp. 4044–4098. DOI: 10.1021/cr068360d.
- [52] G. Tian, R. Daniel, H. Li, H. Xu, S. Shuai, and P. Richards. “Laminar Burning Velocities of 2,5-Dimethylfuran Compared with Ethanol and Gasoline”, *Energy & Fuels* 24.7 (July 2010), pp. 3898–3905. DOI: 10.1021/ef100452c.
- [53] S. Zhong, R. Daniel, H. Xu, J. Zhang, D. Turner, M. L. Wyszynski, and P. Richards. “Combustion and Emissions of 2,5-Dimethylfuran in a Direct-Injection Spark-Ignition Engine”, *Energy & Fuels* 24.5 (May 2010), pp. 2891–2899. ISSN: 1520-5029. DOI: 10.1021/ef901575a.
- [54] R. Daniel, G. Tian, H. Xu, M. L. Wyszynski, X. Wu, and Z. Huang. “Effect of spark timing and load on a DI SI engine fuelled with 2,5-dimethylfuran”, *Fuel* 90.2 (Feb. 2011), pp. 449–458. DOI: 10.1016/j.fuel.2010.10.008.
- [55] R. L. McCormick, M. A. Ratcliff, E. Christensen, L. Fouts, J. Luecke, G. M. Chupka, J. Yanowitz, M. Tian, and M. Boot. “Properties of Oxygenates Found in Upgraded Biomass Pyrolysis Oil as Components of Spark and Compression Ignition Engine Fuels”, *Energy & Fuels* 29.4 (Apr. 2015), pp. 2453–2461. DOI: 10.1021/ef502893g.
- [56] M. A. Ratcliff, J. Burton, P. Sindler, E. Christensen, L. Fouts, G. M. Chupka, and R. L. McCormick. “Knock Resistance and Fine Particle Emissions for Several Biomass-Derived Oxygenates in a Direct-Injection Spark-Ignition Engine”, *SAE International Journal of Fuels and Lubricants* 9.1 (Apr. 2016), pp. 59–70. DOI: 10.4271/2016-01-0705.
- [57] W. Leitner, J. Klankermayer, S. Pischinger, H. Pitsch, and K. Kohse-Höinghaus. “Advanced Biofuels and Beyond: Chemistry Solutions for Propulsion and Production”, *Angewandte Chemie International Edition* 56.20 (Apr. 2017), pp. 5412–5452. DOI: 10.1002/anie.201607257.
- [58] K. Alexandrino, Á. Millera, R. Bilbao, and M. U. Alzueta. “Interaction between 2,5-Dimethylfuran and Nitric Oxide: Experimental and Modeling Study”, *Energy & Fuels* 28.6 (June 2014), pp. 4193–4198. DOI: 10.1021/ef5005573.

-
- [59] B. Sirjean, R. Fournet, P.-A. Glaude, F. Battin-Leclerc, W. Wang, and M. A. Oehlschlaeger. “Shock Tube and Chemical Kinetic Modeling Study of the Oxidation of 2,5-Dimethylfuran”, *The Journal of Physical Chemistry A* 117.7 (Feb. 2013), pp. 1371–1392. DOI: 10.1021/jp308901q.
- [60] F. Geilen, B. Engendahl, A. Harwardt, W. Marquardt, J. Klankermayer, and W. Leitner. “Selective and Flexible Transformation of Biomass-Derived Platform Chemicals by a Multifunctional Catalytic System”, *Angewandte Chemie International Edition* 49.32 (June 2010), pp. 5510–5514. DOI: 10.1002/anie.201002060.
- [61] H. H. Khoo, L. L. Wong, J. Tan, V. Isoni, and P. Sharratt. “Synthesis of 2-methyl tetrahydrofuran from various lignocellulosic feedstocks: Sustainability assessment via LCA”, *Resources, Conservation and Recycling* 95 (Feb. 2015), pp. 174–182. DOI: 10.1016/j.resconrec.2014.12.013.
- [62] J. Wang, X. Wang, X. Fan, K. Yang, and Y. Zhang. “An ignition delay time and kinetic study of 2-methyltetrahydrofuran at high temperatures”, *Fuel* 186 (Dec. 2016), pp. 758–769. DOI: 10.1016/j.fuel.2016.08.104.
- [63] I. T. Horváth, H. Mehdi, V. Fábos, L. Boda, and L. T. Mika. “ γ -Valerolactone – a sustainable liquid for energy and carbon-based chemicals”, *Green Chemistry* 10.2 (2008), pp. 238–242. DOI: 10.1039/b712863k.
- [64] J. Q. Bond, D. M. Alonso, D. Wang, R. M. West, and J. A. Dumesic. “Integrated Catalytic Conversion of γ -Valerolactone to Liquid Alkenes for Transportation Fuels”, *Science* 327.5969 (Feb. 2010), pp. 1110–1114. DOI: 10.1126/science.1184362.
- [65] F. Contino, F. Foucher, F. Halter, G. Dayma, P. Dagaut, and C. Mounaïm-Rousselle. “Engine Performances and Emissions of Second-Generation Biofuels in Spark Ignition Engines: The Case of Methyl and Ethyl Valerates”, *SAE Technical Paper 2013-24-0098*. SAE International, Sept. 2013. DOI: 10.4271/2013-24-0098.
- [66] J.-P. Lange, R. Price, P. Ayoub, J. Louis, L. Petrus, L. Clarke, and H. Gosselink. “Valeric Biofuels: A Platform of Cellulosic Transportation Fuels”, *Angewandte Chemie International Edition* 49.26 (June 2010), pp. 4479–4483. DOI: 10.1002/anie.201000655.
- [67] R. L. McCormick, G. Fioroni, L. Fouts, E. Christensen, J. Yanowitz, E. Polikarpov, K. Albrecht, D. J. Gaspar, J. Gladden, and A. George. “Selection Criteria and Screening of Potential Biomass-Derived Streams as Fuel Blendstocks for Advanced Spark-Ignition Engines”, *SAE International Journal of Fuels and Lubricants* 10.2 (Mar. 2017). DOI: 10.4271/2017-01-0868.
- [68] B. G. Harvey, W. W. Merriman, and R. L. Quintana. “Renewable Gasoline, Solvents, and Fuel Additives from 2,3-Butanediol”, *ChemSusChem* 9.14 (June 2016), pp. 1814–1819. DOI: 10.1002/cssc.201600225.

- [69] F. Nadim, P. Zack, G. E. Hoag, and S. Liu. “United States experience with gasoline additives”, *Energy Policy* 29.1 (Jan. 2001), pp. 1–5. DOI: 10.1016/S0301-4215(00)00099-9.
- [70] M. Rosell, S. Lacorte, and D. Barceló. “Analysis, occurrence and fate of MTBE in the aquatic environment over the past decade”, *TrAC Trends in Analytical Chemistry* 25.10 (Nov. 2006), pp. 1016–1029. DOI: 10.1016/j.trac.2006.06.011.
- [71] M. J. Climent, A. Corma, and S. Iborra. “Conversion of biomass platform molecules into fuel additives and liquid hydrocarbon fuels”, *Green Chemistry* 16.2 (2014), p. 516. DOI: 10.1039/c3gc41492b.
- [72] S. Dutta, S. De, and B. Saha. “A Brief Summary of the Synthesis of Polyester Building-Block Chemicals and Biofuels from 5-Hydroxymethylfurfural”, *ChemPlusChem* 77.4 (Feb. 2012), pp. 259–272. DOI: 10.1002/cplu.201100035.
- [73] D. Gschwend, P. Soltic, P. Edinger, A. Wokaun, and F. Vogel. “Performance Evaluation of Gasoline Alternatives Using a Thermodynamic Spark-Ignition Engine Model”, *Sustainable Energy Fuels* 1 (9 2017), pp. 1991–2005. DOI: 10.1039/c7se00276a.
- [74] J. B. Heywood. *Internal Combustion Engine Fundamentals*. McGraw-Hill Education Ltd, July 11, 1989. 930 pp. ISBN: 0071004998. URL: http://www.ebook.de/de/product/3245366/john_b_heywood_internal_combustion_engine_fundamentals.html.
- [75] G. P. Merker, C. Schwarz, and R. Teichmann, eds. *Combustion Engines Development*. Springer Berlin Heidelberg, 2012. DOI: 10.1007/978-3-642-14094-5.
- [76] G. T. Kalghatgi. “Fuel Anti-Knock Quality – Part I. Engine Studies”, *SAE Technical Paper 2001-01-3584*. SAE International, Sept. 2001. DOI: 10.4271/2001-01-3584.
- [77] M. D. Boot, M. Tian, E. J. M. Hensen, and M. S. Sarathy. “Impact of fuel molecular structure on auto-ignition behavior – Design rules for future high performance gasolines”, *Progress in Energy and Combustion Science* 60 (May 2017), pp. 1–25. DOI: 10.1016/j.pecs.2016.12.001.
- [78] V. Mittal and J. B. Heywood. “The Shift in Relevance of Fuel RON and MON to Knock Onset in Modern SI Engines Over the Last 70 Years”, *SAE International Journal of Engines* 2.2 (Nov. 2009), pp. 1–10. DOI: 10.4271/2009-01-2622.
- [79] G. T. Kalghatgi. “Fuel Anti-Knock Quality – Part II. Vehicle Studies – How Relevant is Motor Octane Number (MON) in Modern Engines?”, *SAE Technical Paper 2001-01-3585*. SAE International, Sept. 2001. DOI: 10.4271/2001-01-3585.
- [80] T. Wallner, A. Ickes, and K. Lawyer. “Analytical Assessment of C2-C8 Alcohols as Spark-Ignition Engine Fuels”, *Lecture Notes in Electrical Engineering*. Springer Nature, Nov. 2012, pp. 15–26. DOI: 10.1007/978-3-642-33777-2_2.

-
- [81] A. M. Pourkhesalian, A. H. Shamekhi, and F. Salimi. “Alternative fuel and gasoline in an SI engine: A comparative study of performance and emissions characteristics”, *Fuel* 89.5 (May 2010), pp. 1056–1063. DOI: 10.1016/j.fuel.2009.11.025.
- [82] J. Tirkey, H. Gupta, and S. Shukla. “Integrated gas dynamic and thermodynamic computational modeling of multicylinder 4-stroke spark ignition engine using gasoline as a fuel”, *Thermal Science* 13.3 (2009), pp. 113–130. DOI: 10.2298/tsci0903113t.
- [83] A. Djouadi and F. Bentahar. “Combustion study of a spark-ignition engine from pressure cycles”, *Energy* 101 (Apr. 2016), pp. 211–217. DOI: 10.1016/j.energy.2016.02.013.
- [84] Y. Shen, J. Bedford, and I. S. Wichman. “Thermodynamic modeling of direct injection methanol fueled engines”, *Applied Thermal Engineering* 29.11-12 (Aug. 2009), pp. 2379–2385. DOI: 10.1016/j.applthermaleng.2008.12.002.
- [85] S. Ramachandran. “Rapid Thermodynamic Simulation Model of an Internal Combustion Engine on Alternate Fuels”, *IMECS 2009: International Multi-Conference of Engineers and Computer Scientists, Vols I and II*. Ed. by O. Castillo, C. Douglas, D. D. Feng, and J. A. Lee. 2009, pp. 2146–2151. ISBN: 978-988-17012-2-0.
- [86] D. Mehrnoosh, H. A. Asghar, and M. A. Asghar. “Thermodynamic model for prediction of performance and emission characteristics of SI engine fuelled by gasoline and natural gas with experimental verification”, *Journal of Mechanical Science and Technology* 26.7 (July 2012), pp. 2213–2225. DOI: 10.1007/s12206-012-0303-0.
- [87] J. A. Caton. “Implications of fuel selection for an SI engine: Results from the first and second laws of thermodynamics”, *Fuel* 89.11 (Nov. 2010), pp. 3157–3166. DOI: 10.1016/j.fuel.2010.05.005.
- [88] J. A. Caton. “A Cycle Simulation Including the Second Law of Thermodynamics for a Spark-Ignition Engine: Implications of the Use of Multiple-Zones for Combustion”, *SAE Technical Paper 2002-01-0007*. SAE International, Mar. 2002. DOI: 10.4271/2002-01-0007.
- [89] J. A. Caton. “Use of a Cycle Simulation Incorporating the Second Law of Thermodynamics: Results for Spark-Ignition Engines Using Oxygen Enriched Combustion Air”, *SAE Technical Paper 2005-01-1130*. SAE International, Apr. 2005. DOI: 10.4271/2005-01-1130.
- [90] J. A. Caton. “A Thermodynamic Evaluation of the Use of Alcohol Fuels in a Spark-Ignition Engine”, *SAE International Journal of Fuels and Lubricants* 2.2 (Nov. 2009), pp. 1–19. DOI: 10.4271/2009-01-2621.
- [91] D. Gschwend, S. Müller, A. Wokaun, and F. Vogel. “Optimum Fuel for Spark Ignition Engines from Lignin Pyrolysis Oil”, *Energy & Fuels* (July 2018). DOI: 10.1021/acs.energyfuels.7b03472.

- [92] A. Burcat and B. Ruscic. *Third millenium ideal gas and condensed phase thermochemical database for combustion (with update from active thermochemical tables)*. - ANL-05/20. English. Tech. rep. Chemistry and Technion - Israel Institute of Technology, 2005. URL: <https://www.osti.gov/scitech/biblio/925269-third-millenium-ideal-gas-condensed-phase-thermochemical-database-combustion-update-from-active-thermochemical-tables>.
- [93] S. A. Channiwala and P. P. Parikh. "A unified correlation for estimating HHV of solid, liquid and gaseous fuels", *Fuel* 81.8 (May 2002), pp. 1051–1063. ISSN: 0016-2361. DOI: 10.1016/s0016-2361(01)00131-4.
- [94] A. R. Katritzky, M. Kuanar, S. Slavov, C. D. Hall, M. Karelson, I. Kahn, and D. A. Dobchev. "Quantitative Correlation of Physical and Chemical Properties with Chemical Structure: Utility for Prediction", *Chemical Reviews* 110.10 (Oct. 2010), pp. 5714–5789. DOI: 10.1021/cr900238d.
- [95] C. Nieto-Draghi, G. Fayet, B. Creton, X. Rozanska, P. Rotureau, J.-C. de Hemptinne, P. Ungerer, B. Rousseau, and C. Adamo. "A General Guidebook for the Theoretical Prediction of Physicochemical Properties of Chemicals for Regulatory Purposes", *Chemical Reviews* 115.24 (Dec. 2015), pp. 13093–13164. ISSN: 1520-6890. DOI: 10.1021/acs.chemrev.5b00215.
- [96] K. G. Joback and R. C. Reid. "Estimation of Pure-Component Properties from Group-Contributions", *Chemical Engineering Communications* 57.1-6 (July 1987), pp. 233–243. DOI: 10.1080/00986448708960487.
- [97] A. S. Hukkerikar, B. Sarup, A. Ten Kate, J. Abildskov, G. Sin, and R. Gani. "Group-contribution+ (GC+) based estimation of properties of pure components: Improved property estimation and uncertainty analysis", *Fluid Phase Equilibria* 321 (May 2012), pp. 25–43. ISSN: 0378-3812. DOI: 10.1016/j.fluid.2012.02.010.
- [98] S. R. S. Sastri and K. K. Rao. "A new group contribution method for predicting viscosity of organic liquids", *The Chemical Engineering Journal* 50.1 (Oct. 1992), pp. 9–25. DOI: 10.1016/0300-9467(92)80002-R.
- [99] Y. Nannoolal, J. Rarey, and D. Ramjugernath. "Estimation of pure component properties. Part 4: Estimation of the saturated liquid viscosity of non-electrolyte organic compounds via group contributions and group interactions", *Fluid Phase Equilibria* 281.2 (July 2009), pp. 97–119. DOI: 10.1016/j.fluid.2009.02.016.
- [100] R. Gani and E. Brignole. "Molecular design of solvents for liquid extraction based on UNIFAC", *Fluid Phase Equilibria* 13 (Jan. 1983), pp. 331–340. DOI: 10.1016/0378-3812(83)80104-6.
- [101] L. Constantinou, K. Bagherpour, R. Gani, J. Klein, and D. Wu. "Computer aided product design: problem formulations, methodology and applications", *Computers & Chemical Engineering* 20.6-7 (June 1996), pp. 685–702. DOI: 10.1016/0098-1354(95)00202-2.

-
- [102] R. Gani. “Chemical product design: challenges and opportunities”, *Computers & Chemical Engineering* 28.12 (Nov. 2004), pp. 2441–2457. DOI: 10.1016/j.compchemeng.2004.08.010.
- [103] F. De Vleeschouwer, P. Geerlings, and F. De Proft. “Molecular Property Optimizations with Boundary Conditions through the Best First Search Scheme”, *ChemPhysChem* 17.10 (Mar. 2016), pp. 1414–1424. DOI: 10.1002/cphc.201501189.
- [104] R. Gani, C. Jiménez-González, and D. J. Constable. “Method for selection of solvents for promotion of organic reactions”, *Computers & Chemical Engineering* 29.7 (June 2005), pp. 1661–1676. DOI: 10.1016/j.compchemeng.2005.02.021.
- [105] A. Papadopoulos and P. Linke. “A Unified Framework for Integrated Process and Molecular Design”, *Chemical Engineering Research and Design* 83.6 (June 2005), pp. 674–678. DOI: 10.1205/cherd.04349.
- [106] A. I. Papadopoulos and P. Linke. “Multiobjective molecular design for integrated process-solvent systems synthesis”, *AIChE Journal* 52.3 (2006), pp. 1057–1070. DOI: 10.1002/aic.10715.
- [107] H.-C. Cheng and F.-S. Wang. “Trade-off optimal design of a biocompatible solvent for an extractive fermentation process”, *Chemical Engineering Science* 62.16 (Aug. 2007), pp. 4316–4324. DOI: 10.1016/j.ces.2007.05.010.
- [108] A. Giovanoglou, J. Barlatier, C. S. Adjiman, E. N. Pistikopoulos, and J. L. Cordiner. “Optimal solvent design for batch separation based on economic performance”, *AIChE Journal* 49.12 (Dec. 2003), pp. 3095–3109. DOI: 10.1002/aic.690491211.
- [109] A. I. Papadopoulos, M. Stijepovic, and P. Linke. “On the systematic design and selection of optimal working fluids for Organic Rankine Cycles”, *Applied Thermal Engineering* 30.6-7 (May 2010), pp. 760–769. DOI: 10.1016/j.applthermaleng.2009.12.006.
- [110] N. V. Sahinidis, M. Tawarmalani, and M. Yu. “Design of alternative refrigerants via global optimization”, *AIChE Journal* 49.7 (July 2003), pp. 1761–1775. DOI: 10.1002/aic.690490714.
- [111] K. C. Satyanarayana, J. Abildskov, and R. Gani. “Computer-aided polymer design using group contribution plus property models”, *Computers & Chemical Engineering* 33.5 (May 2009), pp. 1004–1013. DOI: 10.1016/j.compchemeng.2008.09.021.
- [112] R. Vaidyanathan and M. El-Halwagi. “Computer-Aided Design of High Performance Polymers”, *Journal of Elastomers & Plastics* 26.3 (July 1994), pp. 277–293. DOI: 10.1177/009524439402600306.
- [113] S. Hada, C. C. Solvason, and M. R. Eden. “Characterization-Based Molecular Design of Biofuel Additives Using Chemometric and Property Clustering Techniques”, *Frontiers in Energy Research* 2.20 (2014). ISSN: 2296-598X. DOI: 10.3389/fenrg.2014.00020.

- [114] M. Dahmen, M. Hechinger, J. V. Villeda, and W. Marquardt. "Towards Model-Based Identification of Biofuels for Compression Ignition Engines", *SAE International Journal of Fuels and Lubricants* 5.3 (Sept. 2012), pp. 990–1003. DOI: 10.4271/2012-01-1593.
- [115] D. Gschwend, D. Scholz, P. Soltic, S. Müller, and F. Vogel. "Simulation Tool for a Quick Evaluation of Molecules as Gasoline Alternatives", 5th International Conference - Tailor-Made Fuels from Biomass. June 21, 2017.
- [116] W. Bandel, G. K. Fraidl, P. E. Kapus, H. Sikinger, and C. N. Cowland. "The Turbocharged GDI Engine: Boosted Synergies for High Fuel Economy Plus Ultra-low Emission", *SAE Technical Paper 2006-01-1266*. SAE International, Apr. 2006. DOI: 10.4271/2006-01-1266.
- [117] K. Boulouchos. *Lecture Documents: IC-Engines and Propulsion Systems I*. Ed. by K. Boulouchos. ETH Zürich, Switzerland. Aerothermochemistry and Combustion Systems Laboratory, ETH Zurich 5, Fall Semester 2014.
- [118] American Petroleum Institute. *Technical Data Book - Petroleum Refining*. 6th ed. Apr. 1997.
- [119] J. H. Al-Fahemi, N. A. Albis, and E. A. M. Gad. "QSPR Models for Octane Number Prediction", *Journal of Theoretical Chemistry* 2014 (2014), pp. 1–6. DOI: 10.1155/2014/520652.
- [120] E. S. Blurock. "Automatic learning of chemical concepts: Research octane number and molecular substructures", *Computers & Chemistry* 19.2 (June 1995), pp. 91–99. DOI: 10.1016/0097-8485(95)00001-9.
- [121] V. Gargiulo, M. Alfè, G. D. Blasio, and C. Beatrice. "Chemico-physical features of soot emitted from a dual-fuel ethanol–diesel system", *Fuel* 150 (June 2015), pp. 154–161. DOI: 10.1016/j.fuel.2015.01.096.
- [122] T. Ihara, T. Tanaka, and K. Wakai. "Effects of octane number on autoignition and knocking phenomena in a stratified mixture", *Combustion, Explosion, and Shock Waves* 45.4 (July 2009), pp. 428–434. DOI: 10.1007/s10573-009-0053-1.
- [123] W.-Q. Han and C.-D. Yao. "Research on high cetane and high octane number fuels and the mechanism for their common oxidation and auto-ignition", *Fuel* 150 (June 2015), pp. 29–40. ISSN: 0016-2361. DOI: 10.1016/j.fuel.2015.01.090.
- [124] A. N. Ryzhov, Y. A. Strizhakova, E. A. Smolenskii, and A. L. Lapidus. "Modeling the octane numbers of alkenes by the inverse function method", *Petroleum Chemistry* 51.5 (Sept. 2011), pp. 354–362. DOI: 10.1134/s0965544111040074.
- [125] E. A. Smolenskii, A. N. Ryzhov, M. I. Milina, and A. L. Lapidus. "Modeling the octane numbers of alkenes", *Doklady Chemistry* 436.1 (Jan. 2011), pp. 5–10. DOI: 10.1134/s0012500811010034.
- [126] Design Institute for Physical Properties. *DIPPR Project 801 - Full Version*. Design Institute for Physical Property Research/AIChE, 2005; 2008; 2009; 2010; 2011; 2012; 2015. URL: <http://app.knovel.com/hotlink/toc/id:kpDIPPRPF7/dippr-project-801-full/dippr-project-801-full>.

- [127] B. E. Mitchell and P. C. Jurs. "Prediction of Autoignition Temperatures of Organic Compounds from Molecular Structure", *Journal of Chemical Information and Computer Sciences* 37.3 (May 1997), pp. 538–547. DOI: 10.1021/ci9601751.
- [128] J. A. Lazzús. "Autoignition Temperature Prediction Using an Artificial Neural Network with Particle Swarm Optimization", *International Journal of Thermophysics* 32.5 (Mar. 2011), pp. 957–973. DOI: 10.1007/s10765-011-0956-4.
- [129] P. J. Linstrom and W. G. Mallard. *NIST Chemistry WebBook. NIST Chemistry WebBook, NIST Standard Reference Database Number 69*. (retrieved July 21, 2016). Gaithersburg MD, 20899: National Institute of Standards and Technology, 2005. URL: <http://webbook.nist.gov>.
- [130] G. A. E. Godsave. "Studies of the combustion of drops in a fuel spray—the burning of single drops of fuel", *Symposium (International) on Combustion* 4.1 (1953). Fourth Symposium (International) on Combustion, pp. 818–830. ISSN: 0082-0784. DOI: 10.1016/S0082-0784(53)80107-4.
- [131] K. H. Kwak, D. Jung, and C. Borgnakke. "Enhanced spray and evaporation model with multi-fuel mixtures for direct injection internal combustion engines", *International Journal of Engine Research* 15.4 (Sept. 2013), pp. 488–503. ISSN: 2041-3149. DOI: 10.1177/1468087413495203.
- [132] F. P. Incropera, D. P. Dewitt, T. L. Bergman, and A. S. Lavine. *Principles of heat and mass transfer*. 7th ed. Singapore : John Wiley & Sons (Asia), 2013. ISBN: 978-0-470-64615-1.
- [133] W. E. Ranz and W. R. Marshall. "Evaporation from drops .1." English, *Chemical Engineering Progress* 48.3 (1952), pp. 141–146. ISSN: 0360-7275.
- [134] A. H. Lefebvre. *Atomization and sprays*. Boca Raton : CRC Press/Taylor & Francis, 1989. 434 pp. ISBN: 0891166033.
- [135] G. Woschni. "A Universally Applicable Equation for the Instantaneous Heat Transfer Coefficient in the Internal Combustion Engine", 76 (Feb. 1968), p. 176. DOI: 10.4271/670931.
- [136] G. F. Hohenberg. "Advanced Approaches for Heat Transfer Calculations", *SAE Technical Paper 790825* (Feb. 1979). DOI: 10.4271/790825.
- [137] M. J. Abedin, H. H. Masjuki, M. A. Kalam, A. Sanjid, S. M. A. Rahman, and B. M. Masum. "Energy balance of internal combustion engines using alternative fuels", *Renewable and Sustainable Energy Reviews* 26 (Oct. 2013), pp. 20–33. ISSN: 1364-0321. DOI: 10.1016/j.rser.2013.05.049.
- [138] M. B. Allen and E. L. Isaacson. *Numerical Analysis for Applied Science*. John Wiley & Sons, Inc., Nov. 1997. ISBN: 9780471552666. DOI: 10.1002/9781118033128.
- [139] B. Deng, J. Fu, D. Zhang, J. Yang, R. Feng, J. Liu, K. Li, and X. Liu. "The heat release analysis of bio-butanol/gasoline blends on a high speed SI (spark ignition) engine", *Energy* 60 (Oct. 2013), pp. 230–241. DOI: 10.1016/j.energy.2013.07.055.

- [140] J. C. Livengood and P. C. Wu. “Correlation of autoignition phenomena in internal combustion engines and rapid compression machines”, *Symposium (International) on Combustion* 5.1 (Jan. 1955), pp. 347–356. DOI: 10.1016/s0082-0784(55)80047-1.
- [141] A. M. Douaud and P. Eyzat. “Four-Octane-Number Method for Predicting the Anti-Knock Behavior of Fuels and Engines”, *SAE Technical Paper 780080* (Feb. 1978). DOI: 10.4271/780080.
- [142] G. Kalghatgi, K. Morganti, I. Algunaibet, M. Sarathy, and R. Dibble. “Knock Prediction Using a Simple Model for Ignition Delay”, *SAE Technical Paper 2016-01-0702*. SAE International, Apr. 2016. DOI: 10.4271/2016-01-0702.
- [143] K. S. Chen and F. P. Flynn. “Development of a Single Cylinder Compression Ignition Research Engine”, *SAE Technical Paper 650733* 650733 (1965). DOI: 10.4271/650733.
- [144] H. Nguyen-Schäfer. “Thermodynamics of Turbochargers”, *Rotordynamics of Automotive Turbochargers* (2015), pp. 21–36. ISSN: 2195-9870. DOI: 10.1007/978-3-319-17644-4_2.
- [145] M. K. Balki and C. Sayin. “The effect of compression ratio on the performance, emissions and combustion of an SI (spark ignition) engine fueled with pure ethanol, methanol and unleaded gasoline”, *Energy* 71 (July 2014), pp. 194–201. DOI: 10.1016/j.energy.2014.04.074.
- [146] R. P. Brent. “An algorithm with guaranteed convergence for finding a zero of a function”, *The Computer Journal* 14.4 (Apr. 1971), pp. 422–425. ISSN: 1460-2067. DOI: 10.1093/comjnl/14.4.422.
- [147] S. J. Pachernegg. “A Closer Look at the Willans-Line”, *SAE Technical Paper 690182* (Feb. 1969). DOI: 10.4271/690182.
- [148] A. B. Greene and G. G. Lucas. *The testing of internal combustion engines*. The English Universities Press, Ltd, 1969. ISBN: 0340053682.
- [149] G. Rizzoni, L. Guzzella, and B. M. Baumann. “Unified modeling of hybrid electric vehicle drivetrains”, *IEEE/ASME Transactions on Mechatronics* 4.3 (1999), pp. 246–257. ISSN: 1083-4435. DOI: 10.1109/3516.789683.
- [150] A. Brassat, M. Thewes, M. Müther, and S. Pischinger. “Massgeschneiderte Kraftstoffe aus Biomasse für Ottomotoren”, *MTZ - Motortechnische Zeitschrift* 72.12 (Nov. 2011), pp. 988–995. DOI: 10.1365/s35146-011-0212-2.
- [151] A. Saltelli, M. Ratto, S. Tarantola, and F. Campolongo. “Update 1 of: Sensitivity Analysis for Chemical Models”, *Chemical Reviews* 112.5 (May 2012), PR1–PR21. DOI: 10.1021/cr200301u.
- [152] M. D. McKay, R. J. Beckman, and W. J. Conover. “A Comparison of Three Methods for Selecting Values of Input Variables in the Analysis of Output from a Computer Code”, *Technometrics* 21.2 (May 1979), pp. 239–245. DOI: 10.2307/1268522.

-
- [153] F. Campolongo, A. Saltelli, and J. Cariboni. “From screening to quantitative sensitivity analysis. A unified approach”, *Computer Physics Communications* 182.4 (Apr. 2011), pp. 978–988. DOI: 10.1016/j.cpc.2010.12.039.
- [154] F. Sarrazin, F. Pianosi, and T. Wagener. “Global Sensitivity Analysis of environmental models: Convergence and validation”, *Environmental Modelling & Software* 79 (May 2016), pp. 135–152. DOI: 10.1016/j.envsoft.2016.02.005.
- [155] B. Efron and R. Tibshirani. *An introduction to the bootstrap*. Monographs on statistics and applied probability. New York: Chapman & Hall, 1993, p. 436. ISBN: 0-412-04231-2.
- [156] P. A. Vanrolleghem, G. Mannina, A. Cosenza, and M. B. Neumann. “Global sensitivity analysis for urban water quality modelling: Terminology, convergence and comparison of different methods”, *Journal of Hydrology* 522 (Mar. 2015), pp. 339–352. DOI: 10.1016/j.jhydro.2014.12.056.
- [157] UNECE, ed. *Proposal for amendments to global technical regulation No. 15 on Worldwide harmonized Light vehicles Test Procedure (WLTP)*. 2016.
- [158] T. J. Barlow, S. Latham, I. S. McCrae, and P. G. Boulter. *A reference book of driving cycles for use in the measurement of road vehicle emissions*. 2009.
- [159] *UN Vehicle Regulations - 1958 Agreement - Uniform provisions concerning the approval of vehicles with regard to the emission of pollutants according to engine fuel requirements. no. Addendum 82: Regulation No. 83, Revision 5*. 2015.
- [160] T. Schütz. *Hucho - Aerodynamik des Automobils*. 6th ed. Springer Vieweg, 2013. ISBN: 978-3-8348-2316-8. DOI: 10.1007/978-3-8348-2316-8.
- [161] J. Gmehling, B. Kolbe, M. Kleiber, and J. Rarey. *Chemical Thermodynamics*. Wiley VCH Verlag GmbH, Feb. 11, 2012. ISBN: 3527312773. URL: http://www.ebook.de/de/product/14763044/juergen_gmehling_baerbel_kolbe_michael_kleiber_juergen_rarey_chemical_thermodynamics.html.
- [162] F. Stichlmair. *Distillation*. John Wiley & Sons, Aug. 31, 1998. 544 pp. ISBN: 0471252417. URL: http://www.ebook.de/de/product/3600505/stichlmair_fair_distillation.html.
- [163] R. Wittig, J. Lohmann, and J. Gmehling. “Vapor-Liquid Equilibria by UNIFAC Group Contribution. 6. Revision and Extension”, *Industrial & Engineering Chemistry Research* 42.1 (Jan. 2003), pp. 183–188. DOI: 10.1021/ie0205061.
- [164] A. D. B. Yates, A. Swarts, and C. L. Viljoen. “Correlating Auto-Ignition Delays And Knock-Limited Spark-Advance Data For Different Types Of Fuel”, *SAE Technical Paper 2005-01-2083*. SAE International, May 2005. DOI: 10.4271/2005-01-2083.
- [165] P. L. Perez and A. L. Boehman. “Experimental Investigation of the Autoignition Behavior of Surrogate Gasoline Fuels in a Constant-Volume Combustion Bomb Apparatus and Its Relevance to HCCI Combustion”, *Energy & Fuels* 26.10 (Oct. 2012), pp. 6106–6117. DOI: 10.1021/ef300503b.

- [166] G. Kalghatgi, R. Head, J. Chang, Y. Viollet, H. Babiker, and A. Amer. “An Alternative Method Based on Toluene/*n*-Heptane Surrogate Fuels for Rating the Anti-Knock Quality of Practical Gasolines”, *SAE International Journal of Fuels and Lubricants* 7.3 (Oct. 2014), pp. 663–672. DOI: 10.4271/2014-01-2609.
- [167] M. D. Gerty and J. B. Heywood. “An Investigation of Gasoline Engine Knock Limited Performance and the Effects of Hydrogen Enhancement”, *SAE Technical Paper 2006-01-0228*. SAE International, Apr. 2006. DOI: 10.4271/2006-01-0228.
- [168] P. Risberg, G. Kalghatgi, and H.-E. Ångström. “Auto-ignition Quality of Gasoline-Like Fuels in HCCI Engines”, *SAE Technical Paper 2003-01-3215*. SAE International, Oct. 2003. DOI: 10.4271/2003-01-3215.
- [169] V. Knop, M. Loos, C. Pera, and N. Jeuland. “A linear-by-mole blending rule for octane numbers of *n*-heptane/isooctane/toluene mixtures”, *Fuel* 115 (Jan. 2014), pp. 666–673. DOI: 10.1016/j.fuel.2013.07.093.
- [170] V. Mittal and J. B. Heywood. “The Relevance of Fuel RON and MON to Knock Onset in Modern SI Engines”, *SAE Technical Paper 2008-01-2414*. SAE International, Oct. 2008. DOI: 10.4271/2008-01-2414.
- [171] T. Ott, F. Zurbriggen, C. Onder, and L. Guzzella. “Cycle-averaged efficiency of hybrid electric vehicles”, *Proceedings of the Institution of Mechanical Engineers, Part D: Journal of Automobile Engineering* 227.1 (May 2012), pp. 78–86. DOI: 10.1177/0954407012447508.
- [172] C. Pera and V. Knop. “Methodology to define gasoline surrogates dedicated to auto-ignition in engines”, *Fuel* 96 (June 2012), pp. 59–69. DOI: 10.1016/j.fuel.2012.01.008.
- [173] T. Bieleveld, A. Frassoldati, A. Cuoci, T. Faravelli, E. Ranzi, U. Niemann, and K. Seshadri. “Experimental and kinetic modeling study of combustion of gasoline, its surrogates and components in laminar non-premixed flows”, *Proceedings of the Combustion Institute* 32.1 (2009), pp. 493–500. DOI: 10.1016/j.proci.2008.06.214.
- [174] W. J. Pitz, N. P. Cernansky, F. L. Dryer, F. N. Egolfopoulos, J. T. Farrell, D. G. Friend, and H. Pitsch. “Development of an Experimental Database and Chemical Kinetic Models for Surrogate Gasoline Fuels”, *SAE Technical Paper 2007-01-0175*. SAE International, Apr. 2007. DOI: 10.4271/2007-01-0175.
- [175] L. M. Rodríguez-Antón, F. Gutiérrez-Martín, and C. Martínez-Arevalo. “Experimental determination of some physical properties of gasoline, ethanol and ETBE ternary blends”, *Fuel* 156 (Sept. 2015), pp. 81–86. ISSN: 0016-2361. DOI: 10.1016/j.fuel.2015.04.040.
- [176] R. Pischinger, M. Klell, and T. Sams. *Thermodynamik der Verbrennungskraftmaschine*. Springer-Verlag KG, Nov. 25, 2009. ISBN: 3211992766. URL: http://www.ebook.de/de/product/8476754/rudolf_pischinger_manfred_klell_theodor_sams_thermodynamik_der_verbrennungskraftmaschine.html.

-
- [177] H. Hamid. *Handbook of MTBE and Other Gasoline Oxygenates (Chemical Industries)*. ISBN: 0-8247-4058-0. CRC Press, 2004. ISBN: 0-8247-4058-0.
- [178] J. E. Anderson, U. Kramer, S. A. Mueller, and T. J. Wallington. “Octane Numbers of Ethanol - and Methanol - Gasoline Blends Estimated from Molar Concentrations”, *Energy Fuels* 24.12 (Dec. 2010), pp. 6576–6585. ISSN: 1520-5029. DOI: 10.1021/ef101125c.
- [179] G. Chen, Y. Shen, Q. Zhang, M. Yao, Z. Zheng, and H. Liu. “Experimental study on combustion and emission characteristics of a diesel engine fueled with 2,5-dimethylfuran-diesel, *n*-butanol-diesel and gasoline-diesel blends”, *Energy* 54 (June 2013), pp. 333–342. ISSN: 0360-5442. DOI: 10.1016/j.energy.2013.02.069.
- [180] US Environmental Protection Agency. *Chemistry Dashboard*. Ed. by National Center for Computational Toxicology. Oct. 2, 2017. URL: <https://comptox.epa.gov>.
- [181] J. Yanowitz, M. A. Ratcliff, R. L. McCormick, J. D. Taylor, and M. J. Murphy. *Utilization of Renewable Oxygenates as Gasoline Blending Components*. Technical Report. Feb. 2017. URL: <http://www.nrel.gov/publications>.
- [182] F. Hoppe, B. Heuser, M. Thewes, F. Kremer, S. Pischinger, M. Dahmen, M. Hechinger, and W. Marquardt. “Tailor-made fuels for future engine concepts”, *International Journal of Engine Research* 17.1 (Sept. 2015), pp. 16–27. DOI: 10.1177/1468087415603005.
- [183] A. Boretti. “Analysis of Design of Pure Ethanol Engines”, *SAE Technical Paper 2010-01-1453*. SAE International, May 2010. DOI: 10.4271/2010-01-1453.
- [184] A. Abdel-Rahman and M. Osman. “Experimental Investigation On Varying The Compression Ratio Of Si Engine Working Under Different Ethanol-gasoline Fuel Blends”, *International Journal of Energy Research* 21.1 (1997), pp. 31–40. DOI: 10.1002/(SICI)1099-114X(199701)21:1<31::AID-ER235>3.0.CO;2-5.
- [185] N. Jeuland, X. Montagne, and X. Gautrot. “Potentiality of Ethanol As a Fuel for Dedicated Engine”, *Oil & Gas Science and Technology* 59.6 (Nov. 2004), pp. 559–570. DOI: 10.2516/ogst:2004040.
- [186] M. Brusstar, M. Stuhldreher, D. Swain, and W. Pidgeon. “High Efficiency and Low Emissions from a Port-Injected Engine with Neat Alcohol Fuels”, *SAE Technical Paper 2002-01-2743*. SAE International, Oct. 2002. DOI: 10.4271/2002-01-2743.
- [187] A. M. Pourkhesalian, A. H. Shamekhi, and F. Salimi. “Performance and Emission Comparison and Investigation of Alternative Fuels in SI Engines”, *SAE Technical Paper 2009-01-0936*. SAE International, Apr. 2009. DOI: 10.4271/2009-01-0936.
- [188] TOYOTA AG. Nov. 20, 2017. URL: <https://de.toyota.ch/new-cars/prius/index.json>.

- [189] D. Gschwend, P. Soltic, S. Müller, and F. Vogel. “Simulation Tool for a Quick Evaluation of Molecules as Gasoline Alternatives – A Case Study with Bio-Oil Derived Compounds in Biorefineries”, European Biomass Conference & Exhibition. June 13, 2017.
- [190] D. C. Elliott. “Historical Developments in Hydroprocessing Bio-oils”, *Energy & Fuels* 21.3 (May 2007), pp. 1792–1815. DOI: 10.1021/ef070044u.
- [191] S.-Y. No. “Application of bio-oils from lignocellulosic biomass to transportation, heat and power generation—A review”, *Renewable and Sustainable Energy Reviews* 40 (Dec. 2014), pp. 1108–1125. DOI: 10.1016/j.rser.2014.07.127.
- [192] A. Oasmaa and S. Czernik. “Fuel Oil Quality of Biomass Pyrolysis Oils – State of the Art for the End Users”, *Energy & Fuels* 13.4 (July 1999), pp. 914–921. DOI: 10.1021/ef980272b.
- [193] A. V. Bridgwater. “Review of fast pyrolysis of biomass and product upgrading”, *Biomass and Bioenergy* 38 (Mar. 2012), pp. 68–94. DOI: 10.1016/j.biombioe.2011.01.048.
- [194] W. Mu, H. Ben, A. Ragauskas, and Y. Deng. “Lignin pyrolysis components and upgrading-technology review”, *Bioenergy Research* 6.4 (2013), pp. 1183–1204. DOI: 10.1007/s12155-013-9314-7.
- [195] C. Saiz-Jimenez and J. W. De Leeuw. “Lignin pyrolysis products: their structures and their significance as biomarkers”, *Organic Geochemistry* 10.4-6 (1986), pp. 869–876. DOI: 10.1016/S0146-6380(86)80024-9.
- [196] D. J. Nowakowski, A. V. Bridgwater, D. C. Elliott, D. Meier, and P. de Wild. “Lignin fast pyrolysis: results from an international collaboration”, *Journal of Analytical and Applied Pyrolysis* 88.1 (2010), pp. 53–72. DOI: 10.1016/j.jaap.2010.02.009.
- [197] P. M. Mortensen, J.-D. Grunwaldt, P. A. Jensen, K. G. Knudsen, and A. D. Jensen. “A review of catalytic upgrading of bio-oil to engine fuels”, *Applied Catalysis A: General* 407.1 (2011), pp. 1–19. DOI: 10.1016/j.apcata.2011.08.046.
- [198] M. Dahmen and W. Marquardt. “Model-Based Formulation of Biofuel Blends by Simultaneous Product and Pathway Design”, *Energy & Fuels* 31.4 (Mar. 2017), pp. 4096–4121. DOI: 10.1021/acs.energyfuels.7b00118.
- [199] R. Hooke and T. A. Jeeves. “"Direct Search" Solution of Numerical and Statistical Problems”, *Journal of the ACM* 8.2 (Apr. 1961), pp. 212–229. DOI: 10.1145/321062.321069.
- [200] K. Nakata, D. Uchida, A. Ota, S. Utsumi, and K. Kawatake. “The Impact of RON on SI Engine Thermal Efficiency”, *SAE Technical Paper 2007-01-2007*. SAE International, July 2007. DOI: 10.4271/2007-01-2007.
- [201] B. E. Poling, J. M. Prausnitz, and J. P. O’Connell. *The properties of gases and liquids*. 5th ed. McGraw-Hill, 2001.

- [202] P. Ghosh, K. J. Hickey, and S. B. Jaffe. “Development of a Detailed Gasoline Composition-Based Octane Model”, *Industrial & Engineering Chemistry Research* 45.1 (Jan. 2006), pp. 337–345. DOI: 10.1021/ie050811h.

List of Figures

1.1	Overview of the total energy consumption by sectors globally and for Switzerland including the energy sources used in transportation.	1
1.2	Graphical overview of the structure of this thesis.	3
2.1	Operational scheme of a DI SI engine, showing the different strokes. . .	12
2.2	Cross section through a cylinder indicating the most important geometrical features.	13
2.3	Sketch of the p - V and T - s diagrams of the Otto and Seilinger cycles. . .	13
3.1	Flow sheet representation of all considered engine parts.	22
3.2	Energy balance of an evaporating fuel droplet.	25
3.3	Droplet mass during evaporation with relation to crank angle.	26
3.4	Comparison of idealized and real engine cycles.	28
3.5	Influence of compression ratio on efficiency and knock.	33
3.6	Input–output power characteristics for gasoline operation at 2000 rpm, measured engine results <i>vs.</i> model results.	35
3.7	Measured and simulated pressure traces at $N = 2000$ rpm and different loads for gasoline operation.	36
3.8	Comparison of the model predictions with published data for different fuels and load points.	37
3.9	Convergence statistics <i>vs.</i> number of model evaluations for η_{FL} , P_{FL} and e_{CO_2}	40
3.10	Plot of sensitivity index S_i for model output $e_{CO_2,FL}$ <i>vs.</i> S_i for η_{FL} and P_{FL}	40
3.11	Comparison between the different models in terms of compression ratio <i>vs.</i> RON.	45
3.12	Comparison between the two autoignition correlations, in terms of relative error in compression ratio <i>vs.</i> volume fraction of n -heptane.	45
4.1	Distribution of total energy input at full load.	51
4.2	The three main energy flows, wall heat losses, exhaust enthalpy and power output with respect to the compression ratio.	52
4.3	Minor energy flows, fuel pump power, friction losses and after cooler with respect to the compression ratio.	53
4.4	Comparison of the different fuels with respect to CO_2 emissions and efficiency at full load.	56
4.5	Influence of carbon chain length on efficiency at full load for alcohols. . .	56

4.6	Comparison of the different fuels with respect to consumption and CO ₂ emissions over the WLTC.	57
4.7	Representation of the reduction potential for hybrid powertrains over different driving cycles.	58
5.1	Main building blocks of lignin pyrolysis oil components.	62
5.2	HDO upgrading pathway of a hydroxy group.	62
5.3	HDO upgrading pathway of different side chains leading to a final chain length of 1 C atoms.	63
5.4	HDO upgrading pathway of different side chains leading to a final chain length of 2 C atoms.	64
5.5	HDO upgrading pathway of different side chains leading to a final chain length of 3 C atoms.	65
5.6	HDO reaction network of the main building blocks.	67
5.7	Estimation of melting and boiling points of the studied compounds. . .	69
5.8	Histograms for the different functional groups categorized according to the three temperature ranges.	70
5.9	Euler diagram showing the selection of compounds with either optimized efficiency, specific CO ₂ emissions or consumption.	71
5.10	Fuel properties and efficiency dependency on functional groups attached to cyclohexane.	75
6.1	Comparison of biofuels to gasoline.	78
6.2	Comparison of the biofuels and gasoline with respect to both volumetric energy density and energy stored per CO ₂ emitted.	79
6.3	Results of the mixture optimization in terms of energy per mol CO ₂ emitted and volumetric energy density.	81
6.4	Comparison of the different mixtures and pure fuels with respect to consumption and CO ₂ emissions over the WLTC.	82
6.5	Composition of the identified mixtures.	83
6.6	Average mole-fraction of the 78 mixtures with performance similar to gasoline.	84
7.1	Flow sheet of the rGCM algorithm, showing the most important steps of the algorithm.	88
7.2	Complete list of fundamental groups.	91
7.3	Examples for each class of groups.	91
7.4	Conversion table: from fundamental to cyclic groups.	94
7.5	Compound A, resulting from unrestricted optimization.	100
7.6	Compound B, resulting from unrestricted optimization.	101
7.7	Compound C, resulting from unrestricted optimization.	102
7.8	Compounds identified by the optimization with a maximum boiling point of 470 K.	102

8.1	Comparison of all compounds and mixtures discussed with respect to efficiency and specific CO ₂ emissions at full load.	107
8.2	Comparison of all compounds and mixtures discussed with respect to consumption and CO ₂ emissions over the WLTC.	108
B.1	Correlation between RON and dCN.	145
E.1	Further isomers of Compound A.	161
E.2	Further isomers of Compound A <i>cont.</i>	162
E.3	Further isomers of Compound B.	163
E.4	Complete List of isomers of compound C.	164

List of Tables

2.1	Comparison between different frequently discussed alternative fuels. . . .	6
2.2	Overview of the chosen GCMs in combination with the respective AAE and ARE.	18
3.1	Regression results for the friction mean effective pressure equation. . . .	31
3.2	List of fuel parameters (at 298 K and 0.1 MPa) and their bounds in the Sensitivity Analysis (SA).	38
3.3	Constants for vehicle model.	41
3.4	Hybrid energy demand for standard driving cycles.	46
4.1	Gasoline and a selection of its components/additives used as reference including their properties at standard conditions ($T = 298$ K, $p = 0.1$ MPa). 49	
4.2	Investigated fuel molecules and their properties at standard conditions ($T = 298$ K, $p = 0.1$ MPa).	50
4.3	Overview of the performance of all fuels.	53
4.4	Comparison between experimentally optimized compression ratios and model predictions.	55
5.1	Summary of the performance parameters at full load and based on the WLTC, including average H ₂ requirement for production from lignin pyrolysis oil.	73
5.2	Performance of the molecules when optimizing engine performance. . . .	74
6.1	Mixtures proposed as future fuels.	77
6.2	Overview of the performance of the proposed fuel mixtures.	83
7.1	Properties of the identified compounds, estimated by the GCMs at standard conditions	103
7.2	Performance of the identified compounds.	104
A.1	Overview of the modeling constants and their values.	141
A.2	List of heat transfer deviations.	143
A.3	Main properties of the engine and test bench used to acquire validation data.	144
B.1	Further results for the discussed fuels.	146
C.1	Results for all compounds shown in Fig. 5.9.	149

D.1	Gasoline and a selection of its components/additives used as reference including their properties at standard conditions ($T = 298\text{ K}$, $p = 0.1\text{ MPa}$).	151
D.2	Further results for the discussed mixtures.	151
D.3	Mixture composition of identified mixtures.	152
D.4	Performance of identified mixtures.	154
E.1	List of complex groups.	157
E.2	List of complex aromatic groups.	158
E.3	List of cyclic groups.	158
E.4	Further results for the identified compounds.	162

Dominik Gschwend

Curriculum Vitae

Educational Background

- 2014 – 2018
April January
PhD Mechanical Engineering, ETH Zurich.
"A Systematic Search for Next Generation Transportation Fuels"
- 2011 – 2013
September November
MSc Mechanical Engineering, ETH Zurich.
- 2013 – 2013
March August
MSc Thesis, IBM Zurich Research Laboratory, Rüschlikon.
"Fundamental Investigation of Hierarchical Thermal Structures supporting In-Plane Current Delivery"
- 2012 – 2012
August December
MSc Mechanical Engineering, NTNU, Trondheim.
Exchange Semester
- 2012 – 2012
February July
Research Project, IBM Zurich Research Laboratory, Rüschlikon.
"Feasibility Analysis on Immersion Cooling of a Server Power Supply"
- 2007 – 2010
September June
BSc Mechanical Engineering, ETH Zurich.
- 2009 – 2010
September June
Focusproject, ETH Zurich.
"Development of a fully autonomous quadcopter able to locate and mark buried avalanche victims"
Award: Regional Winner, Switzerland at the European Satellite Navigation Competition 2010
- 2010 – 2010
February June
BSc Thesis, ETH Zurich.
"Development and Analysis of the Structure of a foldable Quadcopter"

Practical Experience

- 2014 – 2017
April December
PhD Student, Paul Scherrer Institute, Villigen.
 - Development of a Molecular Design Algorithm
 - Modelling of an Internal Combustion Engine in C++
 - Assistant of the professor, conducting exams and exercises
- 2010 – 2011
September June
Industrial Internship, Burckhard Compression AG, Winterthur.
FEM Simulations using ANSYS; (Structural, Modal and Thermal Analysis)
- 2009 – 2010
September June
Teaching Assistant, Institute for Mechanical Systems, ETH Zurich.
Lecture assistance in mechanics
- 2009 – 2009
September December
Teaching Assistant, Institute for Integrated Systems, ETH Zurich.
Lecture assistance in electrical engineering

List of Publications

List of Publications

1. **D. Gschwend**, A. Wokaun and F. Vogel. “A Systematic Search for Next Generation Sparkignition Fuels”. *in preparation*
2. **D. Gschwend**, A. Wokaun and F. Vogel. “Fuel Mixture Design for Sparkignition Engines based on Established Biofuels”. *in preparation*
3. **D. Gschwend**, P. Soltic, A. Wokaun and F. Vogel. “Review and Performance Evaluation of Fifty Alternative Liquid Fuels for Spark Ignition Engines”. *submitted to Energy & Fuels*
4. **D. Gschwend**, S. Müller, A. Wokaun and F. Vogel. “Optimum Fuel for Spark Ignition Engines from Lignin Pyrolysis Oil”. *Energy & Fuels*, July 2018, DOI: 10.1021/acsenergyfuels.7b03472
5. **D. Gschwend**, P. Soltic, P. Edinger, A. Wokaun and F. Vogel. “Performance Evaluation of Gasoline Alternatives using a Thermodynamic Spark-Ignition Engine Model”, *Sustainable Energy & Fuels*, Volume 1, Jan. 2017, pp. 1991–2005
6. S. Maurer, **D. Gschwend**, E. Wagner, T. Schildhauer, J. Ommen, S. Biollaz and R. Mudde. “Correlating bubble size and velocity distribution in bubbling fluidized bed based on X-ray tomography”, *Chemical Engineering Journal*, Volume 298, Aug. 2016, pp. 17–25
7. B. Burg, M. Kolly, N. Blasakis, **D. Gschwend**, J. Zürcher and T. Brunschwiler. “Steady-state low thermal resistance characterization apparatus: The bulk thermal tester”, *Review of Scientific Instruments* 86, 124903 (2015)

Patent

1. T. Brunschwiler, **D. Gschwend**, K. Matsumoto, S. Oggioni, G. Schlottig, T. Tick, J. Zürcher. “Substrate device and electric circuit arrangement having first substrate section perpendicular to second substrate section”, US Patent 9433077 B2, Jan. 19, 2015

List of Conference Contributions

1. **D. Gschwend**, P. Soltic, S. Müller, F. Vogel. “Simulation tool for a quick evaluation of molecules as gasoline alternative — a case study with bio-oil derived

- compounds in biorefineries”, *poster presentation at the European Biomass Conference & Exhibition (EUBCE) in Stockholm*, Jun. 12–15, 2017
2. **D. Gschwend**, D. Scholz, P. Soltic, S. Müller, F. Vogel. “Simulation tool for a quick evaluation of molecules as gasoline alternatives”, *presentation at the TMFB (Tailor-Made Fuels from Biomass) International Conference*, Jun. 20–22, 2017
 3. T. Brunswiler, **D. Gschwend**, S. Paredes, T. Timo, K. Matsumoto, C. Lehnberger, J. Pohl, U. Uschenderlein, S. Oggioni. “Embedded Power Insert Enabling Dual-Side Cooling of Microprocessors”, *IEEE 65th Electronic Components and Technology Conference (ECTC)*, May 26–29, 2015
 4. **D. Gschwend**, T. Tick, S. Oggioni, S. Paredes, K. Matsumoto, M. Tiwari, D. Poulikakos and T. Brunswiler. “Laminate with Thermal-Power Insert for Efficient Front-Side Heat Removal and Power Delivery” *poster presentation at 8th International Conference Integrated Power Systems (CIPS)*, Feb. 25–27, 2014

Appendix

A Internal Combustion Engine

A.1 Thermodynamic Modeling Constants

The constants involved in the ICE model are listed in Table A.1.

Table A.1: Overview of the modeling constants and their values.

name	symbol	value
ambient temperature	T_{amb}	298 K
cylinder wall temperature	\bar{T}_w	470 K
fuel injection nozzle diameter	d_{nozzle}	300 μm
peak pressure limitation	p_{peak}	25 MPa
fuel injection pressure	$p_{\text{fuel, inj}}$	20 MPa
minimum compression ratio	$\varepsilon_{\text{CR, min}}$	5
maximum compression ratio	$\varepsilon_{\text{CR, max}}$	20
minimum stepsize	$\Delta\varepsilon_{\text{CR, min}}$	0.002
	K_{p1pIII}	0.95
	$\delta_{\text{valve, III}}$	0.1
	K_{wh}	$12 (\text{m}^2/\text{s})^{0.2}$
	$K_{\text{q, tot}}$	$0.14 (\text{m}^2/\text{s})^{0.2}$

A.2 Heat Transfer – Compound dependence

Heat transfer coefficients (α) can be described by the following Nusselt number (Nu) correlation:

$$Nu = C Re^\gamma Pr^\beta \quad (\text{A.1})$$

depending on the Reynolds (Re) and Prandtl number (Pr) as well as the constants C, β, γ . Using the definitions of these dimensionless quantities, the heat transfer coefficient can be described as

$$\alpha = C \frac{k}{L} \left(\frac{pM}{RT} \frac{uL}{\mu} \right)^\gamma \left(\frac{c_p \mu}{k} \right)^\beta \quad (\text{A.2})$$

with k being the thermal conductivity of the gas, the characteristic length (L), the characteristic velocity (u) and the dynamic viscosity of the gas (μ). It is assumed that the characteristic velocity depends linearly on the mean piston speed, which introduces two new constants ($C_{1,2}$)

$$u = C_1 (c_m + C_2) \quad (\text{A.3})$$

The temperature dependence of the thermal conductivity as well as the dynamic viscosity are assumed to follow the following equations.

$$\mu = \mu_0 \left(\frac{T}{T_0} \right)^{\varepsilon_1} \quad (\text{A.4})$$

$$k = k_0 \left(\frac{T}{T_0} \right)^{\varepsilon_2} \quad (\text{A.5})$$

The constants $\varepsilon_{1,2}$ need to be determined based on measurements for each fluid. Applying all assumptions, the heat transfer coefficient can be written as

$$\alpha = \tilde{C} L^{\gamma-1} \left(\frac{M}{R} \right)^{\gamma} c_p^{\beta} \mu_0^{\beta-\gamma} k_0^{1-\beta} \left(\frac{T}{T_0} \right)^{\varepsilon_1(\beta-\gamma)+\varepsilon_2(1-\beta)} T^{-\gamma} \quad (\text{A.6})$$

$$\cdot (c_m + C_2)^{\gamma} p^{\gamma} \quad (\text{A.7})$$

$$\tilde{C} = C C_1^{\gamma} \quad (\text{A.7})$$

following the argumentation of Hohenberg [136]. L is expressed as $L = \sqrt[3]{V}$. Comparing Eq. (A.7) to the correlation from Hohenberg [136], the following identities can be deduced by means of a coefficient comparison

$$\gamma = 0.8 \quad (\text{A.8})$$

$$C_2 = 1.4 \quad (\text{A.9})$$

$$0.4 = \varepsilon_1^{(\text{air})}(\beta - \gamma) + \varepsilon_2^{(\text{air})}(1 - \beta) \quad (\text{A.10})$$

$$\Rightarrow \beta = \frac{0.4 + 0.8\varepsilon_1 - \varepsilon_2}{\varepsilon_1 - \varepsilon_2} \quad (\text{A.11})$$

$$130 = \tilde{C} \left(\frac{M_{\text{air}}}{R} \right)^{\gamma} c_{p,\text{air}}^{\beta} \mu_{0,\text{air}}^{\beta-\gamma} k_{0,\text{air}}^{1-\beta} T_0^{0.4} \quad (\text{A.12})$$

$$\Rightarrow \tilde{C} = 130 \left[\left(\frac{M_{\text{air}}}{R} \right)^{\gamma} c_{p,\text{air}}^{\beta} \mu_{0,\text{air}}^{\beta-\gamma} k_{0,\text{air}}^{1-\beta} T_0^{0.4} \right]^{-1} \quad (\text{A.13})$$

This finally leads to

$$\alpha = 130 T_0^{0.4} \left(\frac{M}{M_{\text{air}}} \right)^{0.8} \left(\frac{c_{p,\text{air}}}{c_p} \right)^{\beta} \left(\frac{\mu_{0,\text{air}}}{\mu_0} \right)^{\beta-0.8} \left(\frac{k_0}{k_{0,\text{air}}} \right)^{1-\beta}$$

$$\cdot \left(\frac{T}{T_0}\right)^{\varepsilon_1(\beta-\gamma)+\varepsilon_2(1-\beta)} T^{-0.8} V^{-0.06} p^{0.8} (c_m + 1.4)^{0.8} \quad (\text{A.14})$$

The relative deviation ($\Delta\alpha$) with respect to the correlation by Hohenberg [136] is

$$\Delta\alpha = \frac{\alpha}{\alpha^{\text{H}}} - 1 \quad (\text{A.15})$$

$$= \left(\frac{M}{M_{\text{air}}}\right)^{0.8} \left(\frac{c_{p,\text{air}}}{c_p}\right)^{\beta} \left(\frac{\mu_{0,\text{air}}}{\mu_0}\right)^{\beta-0.8} \left(\frac{k_0}{k_{0,\text{air}}}\right)^{1-\beta} \cdot \left(\frac{T}{T_0}\right)^{\varepsilon_1(\beta-\gamma)+\varepsilon_2(1-\beta)} \quad (\text{A.16})$$

The relative deviation of the heat transfer coefficient of all fuels for which data was available, the fuel–air mixtures as well as their burnt gas mixtures are calculated based on data from DIPPR and mixing rules from Poling *et al.* [201]. The results are shown in Table A.2. For each case a complete compression and succeeding expansion stroke is calculated starting at a pressure of 2 bar and a temperature of 298 K. The compression ratio was set to 10. The values for the mean and standard deviation values are taken over both strokes. The measurement accuracy claimed by Hohenberg [136] is around

Table A.2: List of heat transfer deviations, std: standard deviation, values given in %

		mean($\Delta\alpha$)	mean($ \Delta\alpha $)	std($\Delta\alpha$)
fuel–air	<i>n</i> -heptane	-7.12	10.09	8.9
	isooctane	-7.05	10.03	8.87
	benzene	-3.71	7.17	7.31
	cyclohexane	-6.51	9.55	8.62
	methanol	-12.09	15.05	11.77
	ethanol	-9.5	12.45	10.31
	<i>n</i> -butanol	-8.06	11.05	9.5
burnt	<i>n</i> -heptane	1.89	2.78	3.32
	isooctane	2.42	2.93	3.29
	benzene	1.42	2.76	3.42
	cyclohexane	2.12	2.91	3.43
	methanol	-3.6	6.85	6.96
	ethanol	-0.48	3.52	4.19
	<i>n</i> -butanol	0.96	3.29	4.14
overall		-3.52	7.17	8.65

20%. It is therefore concluded that the errors are within the measurement accuracy.

A.3 Engine Testbench Configuration

Please see Table A.3 for details of the main properties of the engine and test bench at Empa used to acquire validation data.

Table A.3: Main properties of the engine and test bench used to acquire validation data.

Engine type	four stroke, gasoline, turbocharged
Fueling	direct injection
Emission legislation	Euro 6
n_{cyl}	4
Bore B	87 mm
Stroke S	90 mm
Compression ratio ε_{CR}	10
Fuel	market fuel, fulfilling EN228, RON 98
Engine test bench	Horiba Dynas3 LI 250
Automation and DAQ system	Horiba STARS Engine
Fuel consumption measurement	AVL 730 dynamic balance
Emission bench	Horiba Mexa 9200
Cylinder pressure sensing	Kistler 6041 B sensor, water-cooled
Crank angle sensing	Kistler 2614 encoder
Indication system	Kistler KiBox

B Established Fuels

B.1 Correlation RON–dCN

To quantify the inverse correlation between dCN and RON, a fit based on literature data [34, 118–125, 181] was performed. This correlation is shown in Fig. B.1 and the resulting equation is given in Eq. (B.1).

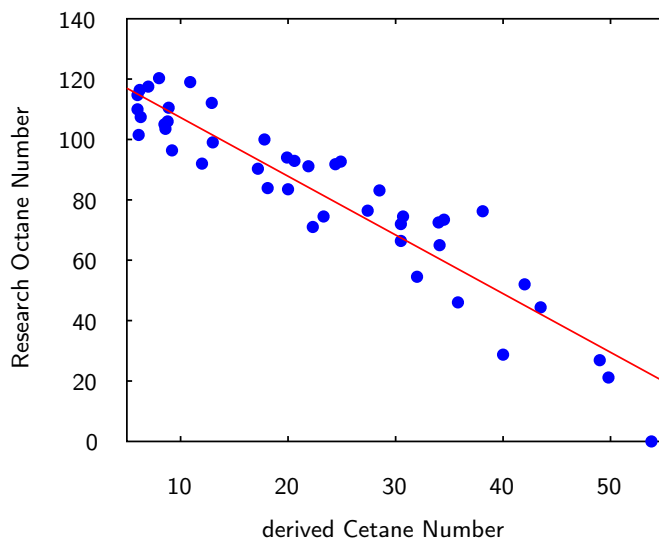


Figure B.1: Correlation between RON and dCN. Blue dots: data points, red regression line.

$$\text{RON} = 126.72 - 1.945\text{dCN} \quad (\text{B.1})$$

Number of observations: 45, Error degrees of freedom: 43

Root Mean Squared Error: 9.99

$R^2 = 0.878$, $R_{\text{adj}}^2 = 0.875$

F-statistic *vs.* constant model: 310, p -value = 2.78×10^{-21}

B.2 Results

Table B.1: Further results for the discussed fuels.

	FL		CADC			NEDC		
	p_{peak} [MPa]	T_{peak} [K]	η_{cyc} [%]	$e_{\text{CO}_2,D}$ [g/km]	c [l/100 km]	η_{cyc} [%]	$e_{\text{CO}_2,D}$ [g/km]	c [l/100 km]
gasoline	9.03	2383	24.1	198	8.4	16.1	217	9.2
isooctane	9.61	2365	24.6	187	8.8	16.5	204	9.6
1-hexene	6.63	2366	22.1	216	10.3	14.9	235	11.2
diisobutylene	10.03	2385	24.9	192	8.6	16.7	210	9.4
cyclohexane	8.64	2349	23.2	206	8.5	15.6	225	9.3
methylcyclohexane	6.11	2375	21.5	222	9.2	14.4	242	10.1
benzene	10.34	2406	23.6	240	8.1	15.8	264	8.9
toluene	11.01	2427	24.1	229	7.9	16.1	251	8.7
MTBE	11.11	2348	25.3	188	10.2	16.9	205	11.2
ETBE	11.32	2360	25.5	186	9.8	17.1	203	10.7
methanol	11.18	2206	21.5	213	19.6	14.1	237	21.9
ethanol	20.41	2147	25.8	181	12.1	17.1	201	13.4
<i>n</i> -propanol	15.83	2223	25.9	182	10.4	17.2	201	11.4
isopropanol	15.84	2227	26.1	181	10.5	17.3	199	11.6
<i>n</i> -butanol	13.51	2258	25.8	183	9.6	17.2	202	10.5
isobutanol	14.46	2259	26.1	181	9.6	17.4	199	10.5
<i>sec</i> -butanol	14.26	2262	26.1	181	9.5	17.4	199	10.4
<i>tert</i> -butanol	13.78	2269	26.0	182	9.8	17.3	200	10.7
<i>n</i> -pentanol	9.83	2275	24.4	194	9.6	16.4	212	10.5
isopentanol	12.08	2278	25.5	186	9.2	17.1	204	10.1
2-MF	12.37	2361	24.5	238	9.7	16.3	261	10.7
DMF	12.07	2385	25.3	222	9.1	17.0	242	9.9
2-MthF	8.00	2348	22.6	223	10.3	15.3	242	11.2
GVL	16.31	2244	26.8	215	9.3	17.9	235	10.2
methyl valerate	11.80	2281	26.2	201	9.8	17.6	219	10.7
ethyl valerate	10.35	2293	25.1	206	9.9	16.9	224	10.7
methyl levulinate	16.12	2229	27.0	218	10.5	18.2	237	11.4
ethyl levulinate	16.83	2249	27.3	208	9.7	18.4	227	10.6
butyl levulinate	12.00	2301	26.0	210	9.4	17.5	229	10.2
α -pinene	8.65	2375	23.5	217	7.8	15.8	236	8.5
2-butanone	11.89	2352	24.9	206	10.6	16.8	225	11.5
methyl-isopropyl ketone	12.07	2355	25.0	202	9.9	16.8	221	10.8
diisopropyl ether	9.96	2350	24.8	191	10.3	16.6	209	11.2
ethyl furfuryl ether	10.96	2323	24.8	231	9.6	16.7	252	10.4
isobityraldehyde	7.42	2346	22.2	231	12.1	15.0	250	13.1
methyl isobutyl ketone	8.51	2346	23.5	213	10.1	15.9	231	11.0
ethyl acetate	9.90	2311	24.0	231	12.9	16.2	250	14.0
ethyl propanoate	9.08	2317	23.7	226	11.9	16.1	245	12.9
propyl acetate	9.11	2316	23.7	226	11.9	16.1	244	12.8
isopropyl acetate	10.83	2325	24.7	217	11.6	16.7	235	12.6

B.2 Results

Table B.1 — *continued*

	FL		CADC			NEDC		
	p_{peak} [MPa]	T_{peak} [K]	η_{cyc} [%]	$e_{\text{CO}_2,D}$ [g/km]	c [l/100 km]	η_{cyc} [%]	$e_{\text{CO}_2,D}$ [g/km]	c [l/100 km]
TMED	10.70	2310	24.9	206	9.7	16.8	224	10.5
furfuryl alcohol	17.61	2263	26.7	234	9.2	17.8	256	10.1
4-methylanisole	13.84	2365	25.7	219	7.8	17.2	240	8.6
2-phenylethanol	14.27	2351	25.9	217	7.4	17.2	239	8.2

C Fuel from Pyrolysis Oil

Detailed results for all studied compounds as part of the pyrolysis oil upgrading.

Table C.1: Results for all compounds shown in Fig. 5.9. Efficiency (η_{FL}) and specific CO₂ emissions ($e_{CO_2,FL}$) at full load, consumption (c) and specific CO₂ emissions ($e_{CO_2,D}$) over the WLTC. SU: summer fuel, AY: all-year fuel.

ID	η_{FL} [%]	$e_{CO_2,FL}$ [g/kWh]	c [l/100km]	$e_{CO_2,D}$ [g/km]	condition & criteria
AD1	36.5	0.79	7.3	200	SU: η, c
AD2	36.8	0.77	7.2	196	SU: η, c, CO_2
AD32	36.6	0.83	7.2	211	SU: η, c
AF19	36.7	0.83	7.1	211	SU: η, c
AF20	37.1	0.81	7.0	205	SU: η
AF21	36.9	0.81	7.4	206	AY: η
AF3	36.4	0.77	7.2	195	AY & SU: η, CO_2
AF4	36.4	0.76	7.2	193	AY & SU: η, CO_2
AF44	36.4	0.77	7.2	195	AY & SU: η
AF7	36.4	0.80	7.7	202	AY & SU: η
G1	36.2	0.78	8.7	198	AY & SU: η
G19	37.5	0.79	7.7	198	SU: η
G2	36.5	0.77	8.4	195	AY & SU: η
G21	37.5	0.78	7.9	195	SU: η
G3	36.6	0.75	7.9	191	AY & SU: η, CO_2
G32	36.5	0.82	8.5	204	AY: η
G4	35.8	0.77	8.0	194	AY & SU: CO_2
G44	36.6	0.75	7.9	191	AY & SU: η, CO_2
G46	36.8	0.75	8.0	191	AY & SU: η
G6	36.1	0.79	8.1	200	AY & SU: η
G7	36.5	0.78	8.5	198	AY & SU: η
I19	36.5	0.80	7.2	203	AY: η
I2	34.1	0.80	8.1	206	AY: CO_2
I21	36.4	0.79	7.6	201	AY & SU: CO_2
I45	36.7	0.76	7.3	194	SU: η
I46	34.3	0.79	7.7	199	AY & SU: CO_2
J1	35.2	0.77	7.6	196	SU: η, c, CO_2
J2	34.9	0.77	7.6	196	SU: η, CO_2
J32	36.5	0.79	7.3	200	SU: η, c
M1	34.3	0.90	7.9	232	AY: η, c SU: c
M13	36.5	0.86	7.3	218	SU: η, c
M14	36.7	0.83	7.2	211	SU: η
M2	34.6	0.87	7.6	221	AY: η, c SU: c

Table C.1 — *continued*

ID	η_{FL} [%]	$e_{CO_2,FL}$ [g/kWh]	c [l/100km]	$e_{CO_2,D}$ [g/km]	condition & criteria	
M20	36.7	0.85	7.4	216	SU:	η
M21	36.7	0.85	7.3	216	AY:	η
M28	37.3	0.90	8.4	227	AY & SU:	η, c, CO_2
M3	36.1	0.80	7.1	204	AY & SU:	η, c, CO_2
M30	37.5	0.86	8.1	219	AY & SU:	η, c, CO_2
M4	36.0	0.79	7.1	202	AY & SU:	η, c, CO_2
M41	37.0	0.81	7.0	206	SU:	η
M7	36.2	0.83	6.9	211	AY & SU:	η, c
N1	31.1	0.83	8.7	207	AY:	CO_2
N13	35.8	0.75	7.7	191	SU:	CO_2
N14	35.6	0.75	7.6	192	SU:	CO_2
N19	36.2	0.77	7.3	196	AY:	CO_2
N20	36.3	0.76	7.2	194	AY: η, CO_2	SU: CO_2
N45	35.4	0.76	7.6	192	SU:	CO_2
O1	35.4	0.76	8.8	193	AY & SU:	CO_2
O2	35.5	0.76	8.6	191	AY & SU:	CO_2
O20	37.5	0.76	7.7	192	SU:	η
O21	37.3	0.76	7.9	189	SU:	CO_2
P1	37.4	0.74	9.2	189	AY & SU:	η, CO_2
P2	37.7	0.73	8.8	186	AY & SU:	η, CO_2
P3	37.7	0.72	8.3	184	AY & SU:	η, CO_2
P32	37.7	0.77	9.1	195	AY & SU:	η
P4	37.1	0.73	8.3	186	SU:	η, CO_2
P44	37.7	0.72	8.3	184	AY & SU:	η, CO_2
P46	37.9	0.72	8.5	184	AY & SU:	η
P6	36.8	0.76	8.5	194	AY:	η, CO_2
P7	37.3	0.76	8.9	192	SU:	η
R1	39.0	0.73	9.4	185	AY & SU:	η, CO_2
R2	39.4	0.72	8.9	181	SU:	η, CO_2
R3	40.2	0.69	8.2	174	SU:	η, CO_2
R44	40.2	0.69	8.2	174	SU:	η, CO_2
R6	39.5	0.72	8.4	183	SU:	η, CO_2

D Mixtures

Table D.1: Gasoline and a selection of its components/additives used as reference including their properties at standard conditions ($T = 298\text{ K}$, $p = 0.1\text{ MPa}$). If not stated otherwise, the values are taken from the DIPPR database [126].

fuel	formula	ρ	$c_{p,g}$	h_{vap}	p_{vap}	ν	RON	LHV
		[kg/m ³]	[J/(mol K)]	[kJ/mol]	[kPa]	[mm ² /s]	[-]	[MJ/kg]
cyclopentane	C ₅ H ₁₀	740	83	28.5	42.1	0.56	100 ^b	43.6 ^a
<i>n</i> -butane	C ₄ H ₁₀	572	99	21.0	242.5	0.28	94 ^b	45.4 ^a
cyclopentanone	C ₅ H ₈ O	943	95	42.2	1.5	1.14	109 ^{c,d}	32.1 ^a
<i>n</i> -butene	C ₄ H ₈	586	86	22.0	301.2	0.26	97 ^e	43.6 ^a

^a estimated according to [93]; ^b [202]; ^c [34]; ^d estimated via dCN;
^e [118];

Table D.2: Further results for the discussed mixtures.

ID	FL		CADC			NEDC		
	p_{peak} [MPa]	T_{peak} [K]	η_{cyc} [%]	$e_{\text{CO}_2,\text{D}}$ [g/km]	c [l/100 km]	η_{cyc} [%]	$e_{\text{CO}_2,\text{D}}$ [g/km]	c [l/100 km]
Υ	8.65	2362	23.2	207	12.0	15.7	224	11.0
Φ	10.00	2041	22.9	219	11.0	14.2	259	13.0
Ψ	12.48	2285	25.2	188	9.6	16.7	208	17.0
α	14.22	2306	25.9	199	8.4	17.1	222	9.4
β	14.31	1988	25.9	200	8.2	17.1	223	9.1
γ	13.91	1978	25.9	198	8.5	17.2	219	9.3

Table D.3: Mixture composition of identified mixtures, values given in mol%.

ID	2-butanone	butyl levulinate	diisopropyl ether	furfuryl alcohol	GVL	4-methylanisole	methyl isopropyl ketone	methyl valerate	2-MthF	2-phenylethanol	α -pinene	isobutanol	isopentanol	isopropanol	methanol	<i>n</i> -butanol	<i>n</i> -pentanol	<i>n</i> -propanol	<i>sec</i> -butanol	<i>tert</i> -butanol
1	0	0	0	0	0	0	0	0	0	41	0	19	0	0	0	19	0	0	21	0
2	0	4	0	0	0	0	0	0	0	26	14	32	9	0	9	0	0	6	0	0
3	0	0	0	0	0	0	0	0	0	39	0	20	0	0	0	20	0	0	21	0
4	0	0	0	0	0	0	0	10	0	22	15	0	10	0	6	0	0	0	37	0
5	0	0	0	0	0	0	0	10	0	23	15	0	4	0	0	0	6	0	42	0
6	0	0	0	0	0	0	0	10	0	22	15	0	4	0	0	0	6	0	43	0
7	0	0	0	0	0	0	0	10	0	22	15	0	2	0	0	0	8	0	43	0
8	0	0	0	0	0	0	0	10	0	23	15	0	4	0	0	0	4	0	44	0
9	0	0	0	0	0	0	0	10	0	23	15	0	2	0	0	0	6	0	44	0
10	0	0	0	0	0	0	0	10	0	38	0	0	28	0	0	24	0	0	0	0
11	0	0	0	0	0	0	0	11	0	39	0	9	18	0	0	0	23	0	0	0
12	0	0	0	0	0	0	0	14	0	36	0	18	0	0	0	0	0	0	32	0
13	0	0	0	0	7	0	0	1	0	37	0	9	19	0	0	16	11	0	0	0
14	0	0	0	0	0	0	0	1	0	42	0	0	31	0	0	26	0	0	0	0
15	0	0	0	0	0	0	0	20	0	36	0	0	25	0	0	0	19	0	0	0
16	0	0	0	0	0	0	0	21	0	35	0	0	22	0	0	11	11	0	0	0
17	0	0	0	0	0	0	0	24	0	34	0	0	24	0	0	0	18	0	0	0
18	0	0	0	0	0	32	0	0	0	0	10	0	18	0	0	0	0	0	40	0
19	0	0	0	0	0	0	0	4	0	32	0	0	0	0	0	44	20	0	0	0
20	0	0	0	0	0	0	0	4	0	35	0	0	18	0	0	0	0	43	0	0
21	0	0	0	0	0	0	0	5	0	39	0	20	0	0	0	15	0	0	21	0
22	0	0	0	0	0	0	0	5	5	35	0	18	0	0	0	18	0	0	19	0
23	0	0	0	0	0	0	0	5	0	35	0	18	0	0	0	18	5	0	19	0
24	0	0	0	0	0	0	0	5	0	35	5	18	0	0	0	18	0	0	19	0
25	0	0	0	0	0	0	0	5	0	35	0	18	5	0	0	18	0	0	19	0
26	0	0	0	0	0	0	0	5	0	37	0	19	0	0	0	19	20	0	0	0
27	0	0	0	0	0	0	0	5	0	37	0	19	20	0	0	19	0	0	0	0
28	0	0	0	0	0	0	0	5	0	37	0	19	0	0	0	19	0	0	20	0
29	0	0	0	0	0	0	0	0	0	33	0	24	0	0	0	0	0	0	43	0
30	0	0	0	0	0	0	0	5	0	37	0	19	0	0	0	19	0	0	0	20
31	0	0	0	0	0	0	0	5	0	37	0	39	0	0	0	19	0	0	0	0
32	0	0	0	0	0	0	0	5	0	39	0	15	0	0	0	20	0	0	21	0
33	0	0	0	0	0	0	0	5	0	39	0	20	0	0	0	20	0	0	16	0
34	0	0	0	0	0	0	0	5	0	38	0	20	0	0	0	37	0	0	0	0
35	0	0	0	0	0	0	0	5	0	38	0	0	20	0	0	37	0	0	0	0
36	0	0	0	0	0	0	0	5	0	38	0	0	0	0	0	37	0	0	20	0
37	0	0	0	0	0	0	0	5	0	38	0	0	0	0	0	37	0	0	0	20

Table D.3 — *continued*

ID	2-butanone	butyl levulinate	diisopropyl ether	furfuryl alcohol	GVL	4-methylanisole	methyl isopropyl ketone	methyl valerate	2-MthF	2-phenylethanol	α -pinene	isobutanol	isopentanol	isopropanol	methanol	<i>n</i> -butanol	<i>n</i> -pentanol	<i>n</i> -propanol	<i>sec</i> -butanol	<i>tert</i> -butanol
38	0	0	0	0	0	0	0	5	0	37	0	19	0	0	0	39	0	0	0	0
39	0	0	0	0	0	0	0	5	0	38	0	0	32	0	0	20	5	0	0	0
40	0	0	0	0	0	0	0	5	0	38	0	5	32	0	0	20	0	0	0	0
41	0	0	0	0	0	0	0	5	0	38	0	0	32	0	0	20	0	0	5	0
42	0	0	0	0	0	0	0	5	0	38	0	0	32	0	0	25	0	0	0	0
43	0	0	0	0	0	0	0	5	0	41	0	0	35	0	0	19	0	0	0	0
44	0	0	0	0	0	0	0	6	0	35	0	35	0	0	0	0	0	0	24	0
45	0	0	0	0	0	0	0	6	0	35	0	55	0	0	0	0	0	0	4	0
46	0	0	0	0	0	0	0	6	0	36	0	58	0	0	0	0	0	0	0	0
47	0	0	0	0	7	0	0	6	0	34	0	9	15	0	0	17	12	0	0	0
48	0	0	0	0	11	0	0	6	0	33	0	9	17	0	0	14	10	0	0	0
49	0	0	0	0	7	0	0	6	0	33	0	13	17	0	0	14	10	0	0	0
50	4	0	0	0	7	0	0	6	0	33	0	9	17	0	0	14	10	0	0	0
51	0	0	4	0	7	0	0	6	0	33	0	9	17	0	0	14	10	0	0	0
52	0	0	0	0	7	0	4	6	0	33	0	9	17	0	0	14	10	0	0	0
53	0	0	0	0	7	0	0	6	4	33	0	9	17	0	0	14	10	0	0	0
54	0	0	0	0	7	0	0	6	0	33	0	9	17	0	0	14	10	4	0	0
55	0	0	0	0	7	0	0	6	0	33	4	9	17	0	0	14	10	0	0	0
56	0	0	0	0	7	0	0	6	0	33	0	9	17	4	0	14	10	0	0	0
57	0	0	0	0	7	0	0	6	0	33	0	9	17	0	0	14	10	0	4	0
58	0	0	0	0	7	0	0	6	0	33	0	9	17	0	0	14	14	0	0	0
59	0	0	0	0	7	0	0	6	0	33	0	9	17	0	0	18	10	0	0	0
60	0	0	0	0	7	5	0	6	0	30	0	9	18	0	0	15	10	0	0	0
61	0	0	0	0	7	0	0	6	0	30	5	9	18	0	0	15	10	0	0	0
62	0	0	0	4	2	0	0	6	0	35	0	9	18	0	0	15	11	0	0	0
63	0	0	0	0	7	0	0	6	0	35	0	9	18	0	0	15	10	0	0	0
64	0	0	0	0	7	0	0	6	0	32	0	9	19	0	0	16	11	0	0	0
65	0	0	0	0	7	0	0	6	0	37	0	9	19	0	0	11	11	0	0	0
66	0	0	0	0	2	0	0	6	0	37	0	9	19	0	0	16	11	0	0	0
67	0	0	0	0	7	0	0	6	0	34	0	9	20	0	0	12	12	0	0	0
68	0	0	0	0	2	0	0	6	0	34	0	9	20	0	0	17	12	0	0	0
69	0	0	0	0	7	0	0	6	0	34	0	4	20	0	0	17	12	0	0	0
70	0	0	0	0	7	0	0	6	0	34	0	9	20	0	0	17	7	0	0	0
71	0	0	0	0	7	0	0	6	0	33	0	9	21	0	0	14	10	0	0	0
72	0	0	0	0	0	0	0	8	0	23	15	0	4	0	0	0	6	0	44	0
73	0	0	0	0	0	0	0	8	0	32	0	0	40	0	0	0	0	0	0	0
74	0	0	0	0	0	0	0	8	0	32	0	0	40	0	0	0	0	0	20	0
75	0	0	0	0	0	0	0	9	0	34	0	0	25	0	0	22	10	0	0	0

Table D.3 — *continued*

ID	2-butanone	butyl levulinate	diisopropyl ether	furfuryl alcohol	GVL	4-methylanisole	methyl isopropyl ketone	methyl valerate	2-MthF	2-phenylethanol	α -pinene	isobutanol	isopentanol	isopropanol	methanol	<i>n</i> -butanol	<i>n</i> -pentanol	<i>n</i> -propanol	<i>sec</i> -butanol	<i>tert</i> -butanol	
76	0	0	0	0	0	0	0	9	0	34	0	10	25	0	0	22	0	0	0	0	0
77	0	0	0	0	0	0	0	9	0	34	0	0	25	0	0	22	0	0	10	0	0
78	0	0	0	0	0	0	0	9	0	34	0	0	25	0	0	32	0	0	0	0	0

Table D.4: Performance of identified mixtures.

ID	η_{FL}	η_{PL}	P_{FL}	$e_{CO_2,FL}$	ε_{CR}	WLTC			CADC			NEDC		
						η_{cyc}	$e_{CO_2,D}$	c	η_{cyc}	$e_{CO_2,D}$	c	η_{cyc}	$e_{CO_2,D}$	c
	[%]	[%]	[kW]	[kg/kWh]	[—]	[%]	[g/km]	[l/100km]	[%]	[g/km]	[l/100km]	[%]	[g/km]	[l/100km]
1	36.9	22.1	80.9	0.77	12.5	22.6	197	8.1	26.0	201	8.3	17.1	224	9.2
2	36.4	22.1	79.7	0.77	11.5	22.4	196	8.1	25.7	200	8.3	17.1	221	9.2
3	36.9	22.1	80.9	0.77	12.5	22.5	196	8.2	26.0	200	8.3	17.1	223	9.3
4	36.2	22.0	79.1	0.77	10.9	22.3	195	8.3	25.6	200	8.5	17.0	220	9.3
5	36.2	21.8	79.1	0.77	10.8	22.3	195	8.2	25.6	200	8.4	17.1	220	9.2
6	36.2	21.8	79.0	0.77	10.7	22.3	195	8.2	25.6	200	8.4	17.0	220	9.3
7	36.1	21.8	79.0	0.77	10.7	22.3	195	8.2	25.6	200	8.4	17.0	220	9.3
8	36.2	21.8	79.1	0.77	10.8	22.3	195	8.2	25.6	200	8.4	17.1	220	9.3
9	36.2	21.8	79.1	0.77	10.8	22.3	195	8.2	25.6	200	8.4	17.1	220	9.3
10	36.9	22.2	80.9	0.77	12.1	22.6	196	8.2	26.0	200	8.3	17.1	223	9.3
11	36.8	22.1	80.7	0.77	11.8	22.5	197	8.2	25.9	201	8.3	17.1	223	9.2
12	36.9	22.2	81.2	0.77	12.3	22.6	197	8.3	26.0	201	8.5	17.2	223	9.4
13	36.9	22.2	81.0	0.77	12.3	22.6	197	8.1	26.0	201	8.3	17.1	223	9.2
14	36.8	22.2	80.7	0.77	12.2	22.5	197	8.0	25.9	200	8.2	17.1	223	9.1
15	36.8	22.2	80.9	0.77	11.7	22.6	197	8.3	26.0	201	8.4	17.1	223	9.3
16	36.9	22.2	81.1	0.77	12.0	22.6	196	8.3	26.0	200	8.5	17.2	223	9.4
17	36.8	22.2	80.9	0.77	11.7	22.5	198	8.4	25.9	202	8.5	17.1	223	9.5
18	36.5	22.0	79.7	0.77	11.4	22.5	195	8.2	25.8	199	8.4	17.2	220	9.2
19	36.7	22.1	80.3	0.76	11.8	22.5	194	8.3	25.9	198	8.5	17.2	219	9.3
20	36.8	22.1	80.9	0.77	12.7	22.5	197	8.4	25.9	200	8.5	17.1	224	9.5
21	36.9	22.2	81.0	0.77	12.5	22.6	197	8.2	26.0	201	8.4	17.1	223	9.3
22	36.8	22.2	80.9	0.77	12.3	22.5	196	8.3	25.9	200	8.4	17.1	223	9.4
23	36.9	22.2	81.0	0.76	12.5	22.6	195	8.3	26.0	199	8.4	17.1	222	9.4
24	36.8	22.1	80.6	0.77	12.1	22.5	196	8.2	25.9	200	8.3	17.1	223	9.3

Table D.4 — *continued*

ID	η_{FL}	η_{PL}	P_{FL}	$e_{CO_2,FL}$	ε_{CR}	WLTC			CADC			NEDC		
						η_{cyc}	$e_{CO_2,D}$	c	η_{cyc}	$e_{CO_2,D}$	c	η_{cyc}	$e_{CO_2,D}$	c
	[%]	[%]	[kW]	[kg/kWh]	[-]	[%]	[g/km]	[l/100km]	[%]	[g/km]	[l/100km]	[%]	[g/km]	[l/100km]
25	36.9	22.2	81.0	0.76	12.5	22.6	195	8.3	26.0	199	8.4	17.1	221	9.4
26	36.8	22.2	80.7	0.76	12.2	22.3	198	8.3	25.8	201	8.4	17.0	224	9.4
27	36.9	22.2	80.9	0.76	12.3	22.6	195	8.2	26.0	199	8.3	17.1	222	9.3
28	36.9	22.2	81.0	0.76	12.5	22.6	196	8.2	26.0	200	8.4	17.1	223	9.4
29	36.9	22.1	80.8	0.76	12.4	22.6	194	8.3	26.0	198	8.5	17.1	220	9.4
30	36.9	23.5	80.9	0.77	12.4	22.6	196	8.3	26.0	200	8.4	17.1	223	9.4
31	36.9	22.2	81.0	0.77	12.5	22.6	196	8.2	26.0	200	8.4	17.1	223	9.4
32	36.9	22.2	81.0	0.77	12.5	22.6	197	8.2	26.0	201	8.4	17.1	224	9.3
33	36.9	22.2	81.0	0.77	12.5	22.6	197	8.2	26.0	201	8.4	17.1	224	9.3
34	36.8	22.1	80.9	0.77	12.4	22.6	197	8.2	26.0	201	8.4	17.1	223	9.3
35	36.8	22.2	80.8	0.77	12.2	22.5	197	8.2	25.9	200	8.3	17.0	223	9.3
36	36.8	22.2	80.8	0.77	12.3	22.5	197	8.2	26.0	201	8.4	17.1	224	9.3
37	36.8	22.2	80.8	0.77	12.2	22.5	197	8.3	25.9	201	8.4	17.1	224	9.4
38	36.8	22.2	80.8	0.77	12.3	22.5	196	8.2	26.0	200	8.4	17.1	223	9.4
39	36.8	22.2	80.7	0.76	12.0	22.5	196	8.2	25.9	200	8.3	17.1	222	9.2
40	36.8	22.2	80.7	0.76	12.1	22.4	197	8.2	25.8	201	8.4	17.1	223	9.3
41	36.8	22.2	80.7	0.76	12.0	22.6	196	8.1	26.0	200	8.3	17.1	222	9.2
42	36.8	22.2	80.7	0.76	12.0	22.6	196	8.1	26.0	200	8.3	17.1	222	9.2
43	36.8	22.1	80.7	0.77	12.0	22.5	197	8.1	25.9	201	8.2	17.1	223	9.2
44	36.9	22.2	81.0	0.76	12.4	22.6	195	8.3	26.0	199	8.5	17.1	222	9.4
45	36.8	22.2	80.9	0.76	12.3	22.6	196	8.3	26.0	200	8.5	17.1	222	9.5
46	36.8	22.2	80.8	0.77	12.3	22.6	196	8.3	26.0	200	8.5	17.1	223	9.4
47	37.0	22.3	81.2	0.77	12.3	22.6	196	8.2	26.1	200	8.4	17.2	222	9.3
48	37.0	22.3	81.3	0.77	12.4	22.7	197	8.2	26.1	201	8.4	17.2	223	9.3
49	37.0	22.3	81.2	0.76	12.3	22.6	196	8.3	26.0	200	8.4	17.1	223	9.4
50	36.9	22.2	81.1	0.77	12.2	22.6	196	8.3	26.0	200	8.4	17.2	223	9.4
51	36.9	22.2	81.0	0.76	12.0	22.6	196	8.3	26.0	200	8.4	17.2	222	9.4
52	36.9	22.2	81.1	0.77	12.2	22.6	196	8.3	26.0	200	8.4	17.2	223	9.4
53	36.9	22.1	81.0	0.77	12.2	22.6	196	8.2	26.0	200	8.4	17.1	223	9.4
54	37.0	22.3	81.2	0.76	12.4	22.7	196	8.2	26.1	200	8.4	17.2	222	9.4
55	36.8	22.2	80.8	0.77	12.0	22.6	197	8.1	26.0	201	8.3	17.1	223	9.2
56	37.0	22.2	81.2	0.76	12.3	22.6	196	8.3	26.1	200	8.4	17.2	222	9.4
57	37.0	22.3	81.2	0.76	12.3	22.5	197	8.3	26.0	200	8.4	17.1	222	9.4
58	37.0	22.2	81.1	0.76	12.3	22.5	196	8.3	26.0	200	8.4	17.1	222	9.4
59	37.0	22.3	81.2	0.76	12.3	22.6	195	8.2	26.1	199	8.4	17.2	222	9.3
60	36.9	22.2	81.1	0.77	12.2	22.6	197	8.2	26.0	201	8.4	17.2	223	9.3
61	36.8	22.1	80.7	0.76	11.9	22.5	196	8.2	25.9	200	8.4	17.1	222	9.3
62	37.0	22.2	81.2	0.77	12.3	22.6	196	8.2	26.1	200	8.3	17.2	223	9.3
63	37.0	22.3	81.2	0.77	12.3	22.5	197	8.2	26.0	201	8.4	17.1	223	9.3
64	37.0	22.2	81.2	0.76	12.3	22.6	195	8.2	26.1	199	8.4	17.2	222	9.4
65	37.0	22.2	81.2	0.77	12.3	22.6	197	8.1	26.1	201	8.3	17.2	224	9.2

Table D.4 — *continued*

ID				WLTC					CADC			NEDC		
	η_{FL}	η_{PL}	P_{FL}	$e_{CO_2,FL}$	ε_{CR}	η_{cyc}	$e_{CO_2,D}$	c	η_{cyc}	$e_{CO_2,D}$	c	η_{cyc}	$e_{CO_2,D}$	c
	[%]	[%]	[kW]	[kg/kWh]	[-]	[%]	[g/km]	[l/100km]	[%]	[g/km]	[l/100km]	[%]	[g/km]	[l/100km]
66	36.9	22.2	81.0	0.76	12.3	22.6	196	8.1	26.0	199	8.3	17.2	222	9.3
67	37.0	22.2	81.1	0.77	12.3	22.6	196	8.2	26.0	200	8.4	17.2	222	9.3
68	36.9	22.2	81.0	0.76	12.2	22.6	195	8.2	26.0	199	8.4	17.1	221	9.3
69	37.0	22.2	81.1	0.77	12.3	22.5	197	8.2	26.0	200	8.4	17.2	223	9.3
70	37.0	22.3	81.2	0.77	12.3	22.6	196	8.2	26.1	200	8.4	17.2	222	9.3
71	37.0	22.2	81.2	0.76	12.3	22.5	196	8.3	26.0	200	8.4	17.1	222	9.4
72	36.2	21.8	79.0	0.77	10.8	22.3	195	8.2	25.6	200	8.4	17.1	220	9.2
73	36.5	22.1	80.0	0.76	11.3	22.4	194	8.3	25.7	199	8.5	17.2	219	9.3
74	36.6	22.0	80.3	0.76	11.5	22.6	194	8.3	25.9	198	8.5	17.2	218	9.3
75	36.9	22.2	80.9	0.76	12.1	22.5	196	8.3	25.9	199	8.4	17.1	222	9.4
76	36.9	22.3	80.9	0.76	12.2	22.6	195	8.3	26.0	199	8.4	17.1	221	9.4
77	36.9	22.2	80.9	0.76	12.1	22.6	195	8.3	26.0	199	8.4	17.2	221	9.4
78	36.9	22.2	80.8	0.76	12.1	22.6	195	8.3	26.0	199	8.4	17.1	221	9.4

E The reverse Group Contribution Method

E.1 List of Groups

Table E.1: List of complex groups. • denotes a noncyclic connection point.

•COOH	CH ₃ -CO•	•CH ₂ -CO•
•CH-CO•	•C•-CO•	CH ₃ -CO-O•
•CH ₂ -CO-O•	•CH-CO-O•	•C•-CO-O•
CHO-O•	•CO-O•	CH ₃ -O•
•CH ₂ -O•	•CH-O•	•C•-O•
•O-CH ₂ -CH ₂ -OH	•O-CH•-CH ₂ -OH	•O-CH ₂ -CH•-OH
•O-CO-O•	CH ₂ =CH-O•	•CH=CH-O•
•C=CH-O•	•CH-O-CH•	CH ₃ -(CH ₃ -)CH•
[CH ₃] ₃ -C•	•CH(-CH ₃)-CH(-CH ₃)•	•CH(-CH ₃)-C[-CH ₃] ₂ •
•C[-CH ₃] ₂ -C[-CH ₃] ₂ •	•C=C•-•C=C•	•CH=C•-•C=C•
CH ₂ =C•-•C=C•	•CH=CH-•C=C•	CH ₂ =CH-•C=C•
•CH=C•-CH=C•	CH ₂ =C•-CH=C•	•CH=CH-CH=C•
CH ₂ =CH-CH=C•	CH ₂ =C•-CH=CH•	•CH=CH-CH=CH•
CH ₂ =CH-CH=CH•	CH ₂ =C•-•C=CH ₂	CH ₂ =CH-•C=CH ₂
CH ₂ =CH-CH=CH ₂	CH ₃ -•C=C•	CH ₃ -CH=C•
CH ₃ -CH=CH•	CH ₃ -•C=CH ₂	CH ₃ -CH=CH ₂
•CH ₂ -•C=C•	•CH ₂ -CH=C•	•CH ₂ -CH=CH•
•CH ₂ -•C=CH ₂	•CH ₂ -CH=CH ₂	•CH-•C=C•
•CH-CH=C•	•CH-CH=CH•	•CH-•C=CH ₂
•CH-CH=CH ₂	•C•-•C=C•	•C•-CH=C•
•C•-CH=CH•	•C•-•C=CH ₂	•C•-CH=CH ₂
•CH-CHO	•C•-CHO	CH ₃ -CO-CH ₂ •
CH ₃ -CO-CH•	CH ₃ -CO-•C•	•CH-CO-OH
•C•-CO-OH	CH ₃ -CO-O-CH•	CH ₃ -CO-O-•C•
•CO-O-CO•	•CH-OH	•C•-OH
CH ₃ -CO-C•-OH	CH ₃ -CO-CH•-OH	CH ₃ -CO-CH ₂ -OH
OH-C•-CO-O•	OH-CH•-CO-O•	OH-CH ₂ -CO-O•
OH-C•-C•-OH	OH-CH•-C•-OH	OH-CH ₂ -C•-OH
OH-CH•-CH•-OH	OH-CH ₂ -CH•-OH	OH-CH ₂ -CH ₂ -OH
HOOC-CH•-COOH	HOOC-CH ₂ -COOH	HOOC-CH•-CH•-COOH
HOOC-CH ₂ -CH•-COOH	HOOC-CH ₂ -CH ₂ -COOH	HO-CH•-COOH
HO-CH ₂ -COOH	CH ₃ -O-CH•-COOH	CH ₃ -O-CH ₂ -COOH
•COO-CH•-CH•-OCO•	•COO-CH ₂ -CH•-OCO•	•COO-CH ₂ -CH ₂ -OCO•

Table E.1 — *continued*

$\bullet\text{OCO}-\text{CH}^\bullet-\text{CH}^\bullet-\text{COO}^\bullet$	$\bullet\text{OCO}-\text{CH}_2-\text{CH}^\bullet-\text{COO}^\bullet$	$\bullet\text{OCO}-\text{CH}_2-\text{CH}_2-\text{COO}^\bullet$
$\bullet\text{CO}-\text{CH}^\bullet-\text{CO}-\text{O}^\bullet$	$\bullet\text{CO}-\text{CH}_2-\text{CO}-\text{O}^\bullet$	$\bullet\text{C}^\bullet-\text{O}-\bullet\text{C}=\text{C}^\bullet$
$\bullet\text{CH}-\text{O}-\bullet\text{C}=\text{C}^\bullet$	$\bullet\text{CH}_2-\text{O}-\bullet\text{C}=\text{C}^\bullet$	$\text{CH}_3-\text{O}-\bullet\text{C}=\text{C}^\bullet$
$\bullet\text{C}^\bullet-\text{O}-\text{CH}=\text{C}^\bullet$	$\bullet\text{CH}-\text{O}-\text{CH}=\text{C}^\bullet$	$\bullet\text{CH}_2-\text{O}-\text{CH}=\text{C}^\bullet$
$\text{CH}_3-\text{O}-\text{CH}=\text{C}^\bullet$	$\bullet\text{C}^\bullet-\text{O}-\text{CH}=\text{CH}$	$\bullet\text{CH}-\text{O}-\text{CH}=\text{CH}^\bullet$
$\bullet\text{CH}_2-\text{O}-\text{CH}=\text{CH}^\bullet$	$\text{CH}_3-\text{O}-\text{CH}=\text{CH}^\bullet$	$\bullet\text{C}^\bullet-\text{O}-\bullet\text{C}=\text{CH}_2$
$\bullet\text{CH}-\text{O}-\bullet\text{C}=\text{CH}_2$	$\bullet\text{CH}_2-\text{O}-\bullet\text{C}=\text{CH}_2$	$\text{CH}_3-\text{O}-\bullet\text{C}=\text{CH}_2$
$\bullet\text{C}^\bullet-\text{O}-\text{CH}=\text{CH}_2$	$\bullet\text{CH}-\text{O}-\text{CH}=\text{CH}_2$	$\bullet\text{CH}_2-\text{O}-\text{CH}=\text{CH}_2$
$\text{CH}_3-\text{O}-\text{CH}=\text{CH}_2$	$\bullet\text{C}=\text{C}^\bullet-\text{CO}-\text{O}-\bullet\text{C}^\bullet$	$\bullet\text{CH}=\text{C}^\bullet-\text{CO}-\text{O}-\bullet\text{C}^\bullet$
$\text{CH}_2=\text{C}^\bullet-\text{CO}-\text{O}-\bullet\text{C}^\bullet$	$\bullet\text{CH}=\text{CH}-\text{CO}-\text{O}-\bullet\text{C}^\bullet$	$\text{CH}_2=\text{CH}-\text{CO}-\text{O}-\bullet\text{C}^\bullet$
$\bullet\text{C}=\text{C}^\bullet-\text{CO}-\text{O}-\text{CH}^\bullet$	$\bullet\text{CH}=\text{C}^\bullet-\text{CO}-\text{O}-\text{CH}^\bullet$	$\text{CH}_2=\text{C}^\bullet-\text{CO}-\text{O}-\text{CH}^\bullet$
$\bullet\text{CH}=\text{CH}-\text{CO}-\text{O}-\text{CH}^\bullet$	$\text{CH}_2=\text{CH}-\text{CO}-\text{O}-\text{CH}^\bullet$	$\bullet\text{C}=\text{C}^\bullet-\text{CO}-\text{O}-\text{CH}_2^\bullet$
$\bullet\text{CH}=\text{C}^\bullet-\text{CO}-\text{O}-\text{CH}_2^\bullet$	$\text{CH}_2=\text{C}^\bullet-\text{CO}-\text{O}-\text{CH}_2^\bullet$	$\bullet\text{CH}=\text{CH}-\text{CO}-\text{O}-\text{CH}_2^\bullet$
$\text{CH}_2=\text{CH}-\text{CO}-\text{O}-\text{CH}_2^\bullet$	$\bullet\text{C}=\text{C}^\bullet-\text{CO}-\text{O}-\text{CH}_3$	$\bullet\text{CH}=\text{C}^\bullet-\text{CO}-\text{O}-\text{CH}_3$
$\text{CH}_2=\text{C}^\bullet-\text{CO}-\text{O}-\text{CH}_3$	$\bullet\text{CH}=\text{CH}-\text{CO}-\text{O}-\text{CH}_3$	$\text{CH}_2=\text{CH}-\text{CO}-\text{O}-\text{CH}_3$
$\bullet\text{C}=\text{C}^\bullet-\text{CHO}$	$\bullet\text{CH}=\text{C}^\bullet-\text{CHO}$	$\text{CH}_2=\text{C}^\bullet-\text{CHO}$
$\bullet\text{CH}=\text{CH}-\text{CHO}$	$\text{CH}_2=\text{CH}-\text{CHO}$	$\bullet\text{C}=\text{C}^\bullet-\text{COOH}$
$\bullet\text{CH}=\text{C}^\bullet-\text{COOH}$	$\text{CH}_2=\text{C}^\bullet-\text{COOH}$	$\bullet\text{CH}=\text{CH}-\text{COOH}$
$\text{CH}_2=\text{CH}-\text{COOH}$		

Table E.2: List of complex aromatic groups. aC denotes aromatic Carbon, \bullet denotes a noncyclic connection point.

aC-CH ₃	aC-CH ₂ \bullet	aC-CH \bullet	aC- $\bullet\text{C}^\bullet$
aC-CH=CH ₂	aC-CH=CH \bullet	aC- $\bullet\text{C}=\text{CH}_2$	aC-C $\equiv\text{CH}$
aC-C $\equiv\text{C}^\bullet$	aC-OH	aC-COOH	aC-CO \bullet
aC-CHO	aC-CO-O \bullet	aC-O-CHO	aC-O-CO \bullet
aC-O \bullet	aC-CH \bullet -O \bullet	aC-CH ₂ -O \bullet	aC-CH \bullet -OH
aC-CH ₂ -OH	aC-CH \bullet -CHO	aC-CH ₂ -CHO	aC-CH \bullet -COOH
aC-CH ₂ -COOH	aC-CH \bullet -CO \bullet	aC-CH ₂ -CO \bullet	aC-CH \bullet -O-CHO
aC-CH ₂ -O-CHO	aC-CH \bullet -O-CO \bullet	aC-CH ₂ -O-CO \bullet	aC-CH \bullet -CO-O \bullet
aC-CH ₂ -CO-O \bullet	aC-CH(CH ₃) ₂	aC-C(CH ₃) ₃	aC-CH=C \bullet
aC- $\bullet\text{C}=\text{C}^\bullet$			

Table E.3: List of cyclic groups. \bullet denotes a noncyclic connection point, \star denotes an open cyclic connection point.

$\star\text{CH}_2$	$\star\text{CH}^\bullet$	$\star\text{C}^\bullet$
$\star\text{CH}=\text{CH}^\star$	$\star\text{CH}=\text{C}^\star$	$\bullet\text{C}=\text{C}^\star$
$\star\text{C}=\text{CH}_2$	$\star\text{O}^\star$	$\star\text{CO}$
$\star\text{C}=\text{CH}^\bullet$	$\star\text{C}=\text{C}^\bullet$	$\star\text{CH}^\star$
$\star\text{C}^\bullet$	$\star\text{C}^\star$	$\star\text{C}=\text{CH}^\star$
$\star\text{C}=\text{C}^\star$	$\star\text{C}=\text{C}^\star$	$(\bullet\text{C}=\text{C}^\star)-\text{CHO}$
$(\star\text{CH}=\text{C}^\star)-\text{CHO}$	$(\star\text{C}=\text{C}^\star)-\text{CHO}$	$(\star\text{CH}=\text{C}^\star)-\text{CO}-\text{O}-\bullet\text{C}^\bullet$

E.1 List of Groups

Table E.3 — *continued*

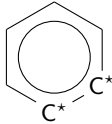
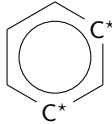
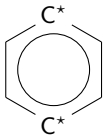
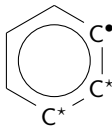
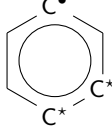
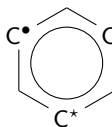
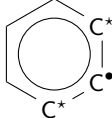
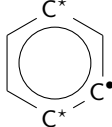
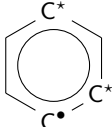
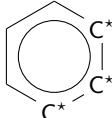
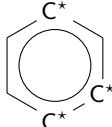
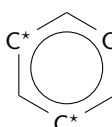
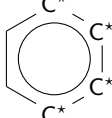
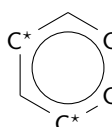
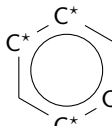
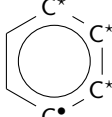
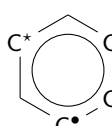
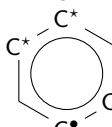
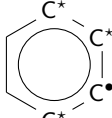
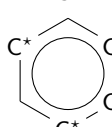
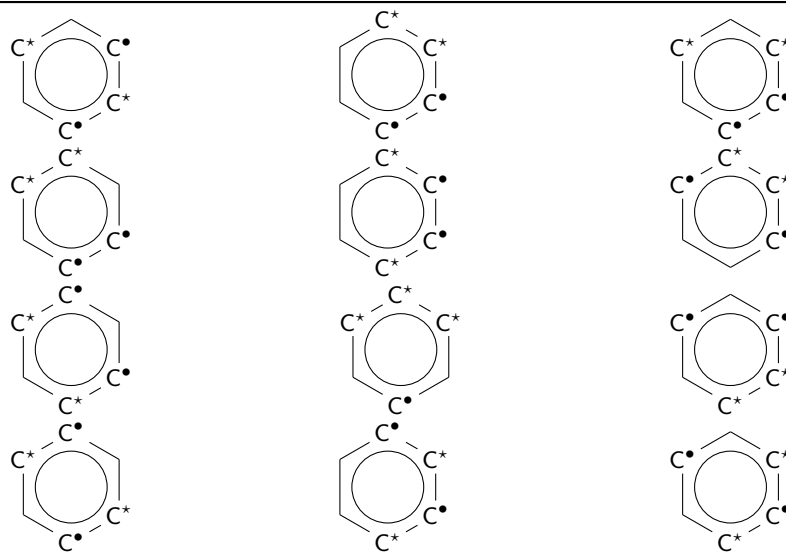
$(^*CH=C^*)-CO-O-CH_2\bullet$	$(^*CH=C^*)-CO-O-CH_2\bullet$	$(^*CH=C^*)-CO-O-CH_3$
$(^*C=C^*)-CO\bullet$	$(^*CH=C^*)-CO\bullet$	$(^*C=C^*)-CO\bullet$
$(^*C=C^*)-CH_3$	$(^*CH=C^*)-CH_3$	$(^*C=C^*)-CH_3$
$(^*C=C^*)-CH_2\bullet$	$(^*CH=C^*)-CH_2\bullet$	$(^*C=C^*)-CH_2\bullet$
$^*CH-CH_3$	$^*CH-CH_2\bullet$	$^*CH-CH_2\bullet$
$^*CH-\bullet C\bullet$	$^*CH-CH=CH\bullet$	$^*CH-CH=CH_2$
$^*CH-\bullet C=C\bullet$	$^*CH-\bullet C=CH\bullet$	$^*CH-OH$
$^*CH-COOH$	$^*CH-CO\bullet$	$^*CH-CHO$
$^*CH-O\bullet$	$^*CH-O-CHO$	$^*CH-CO-O\bullet$
$^*CH-O-CO\bullet$	$\bullet C^*-CH_3$	$^*C^*-CH_3$
$\bullet C^*-CH_2\bullet$	$^*C^*-CH_2\bullet$	$\bullet C^*-OH$
$^*C^*-OH$	$(^*C=C^*)-COOH$	$(^*CH=C^*)-COOH$
$(^*C=C^*)-COOH$		
		
		
		
		
		
		

Table E.3 — *continued*

E.2 Structure Optimization Results

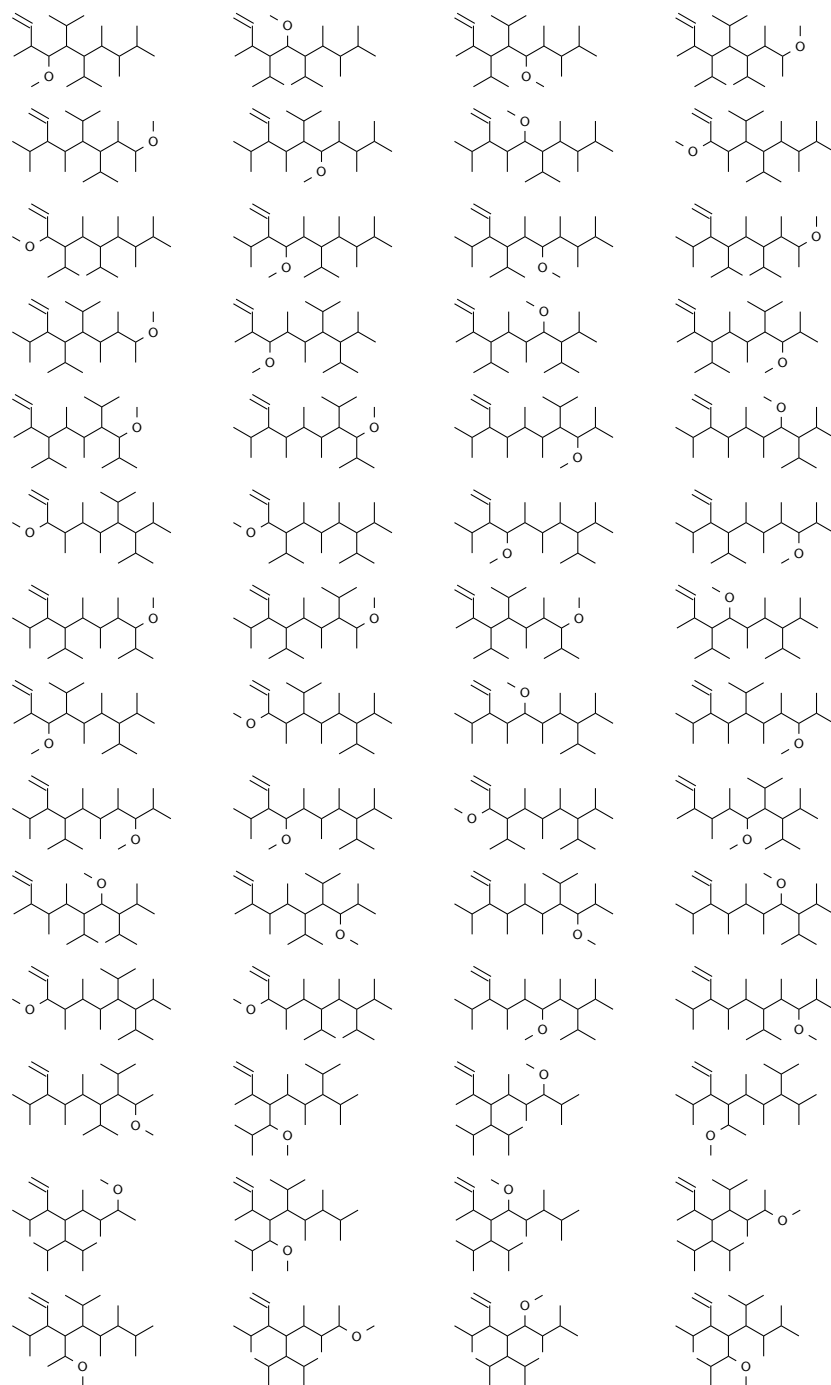
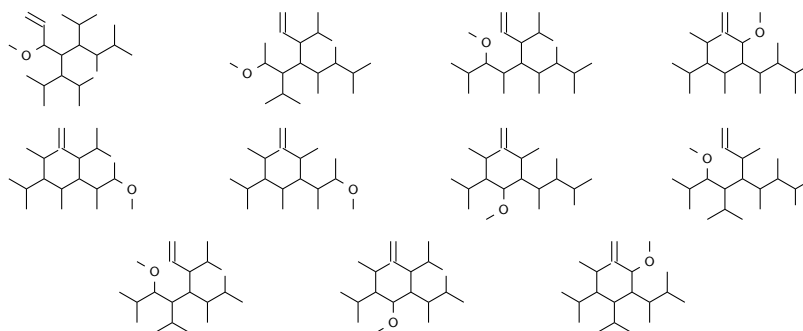


Figure E.1: Further isomers of Compound A.

Table E.4: Further results for the identified compounds.

	FL		CADC			NEDC		
	p_{peak} [MPa]	T_{peak} [K]	η_{cyc} [%]	$e_{\text{CO}_2,\text{D}}$ [g/km]	c [l/100 km]	η_{cyc} [%]	$e_{\text{CO}_2,\text{D}}$ [g/km]	c [l/100 km]
A	23.81	2319	29.5	164	6.6	19.7	180	7.3
B	23.82	2304	29.5	162	6.8	19.7	178	7.5
C	23.76	2300	29.5	161	6.7	19.7	177	7.3
a	15.52	2343	27.3	170	7.1	18.3	186	7.8
b	14.01	2042	25.6	217	7.1	17.1	239	7.8
c	17.64	2000	27.9	175	7.3	18.7	192	8.0
d	12.48	2295	27.7	182	8.8	18.9	197	9.5

**Figure E.2:** Further isomers of Compound A *cont.*

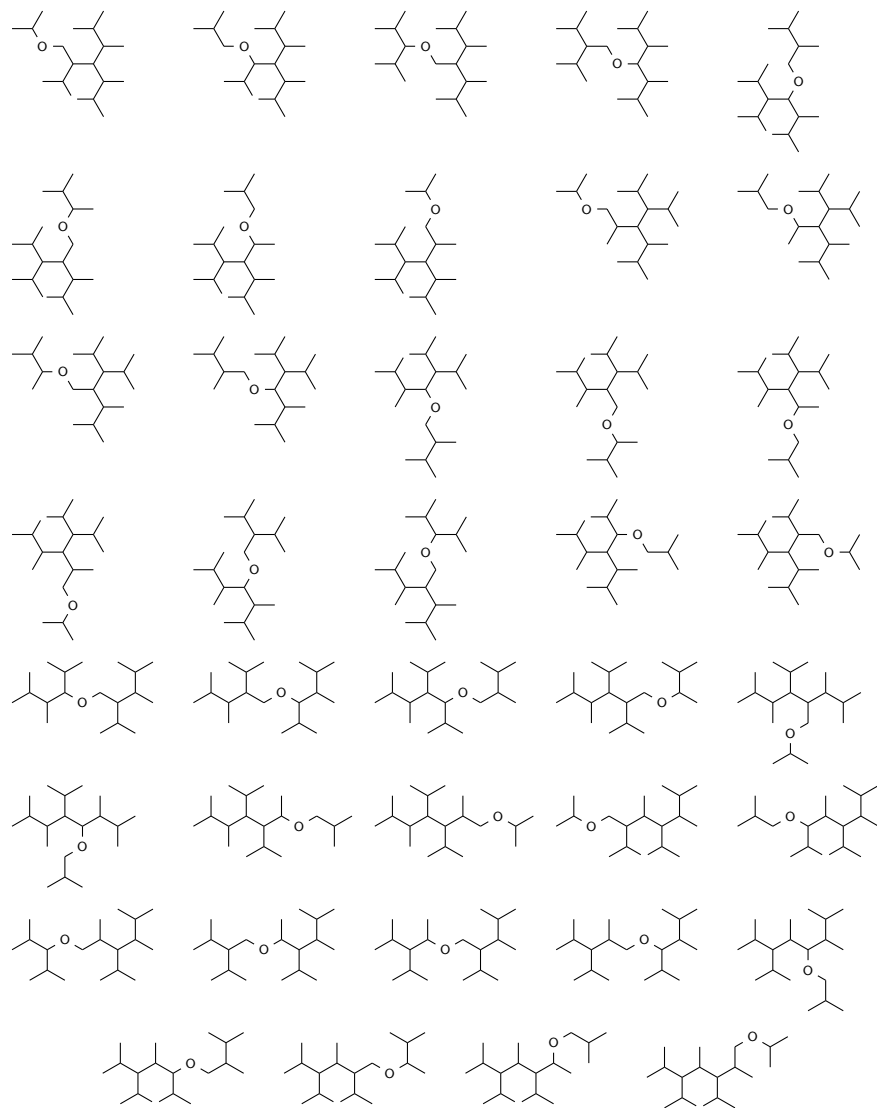


Figure E.3: Further isomers of Compound B.

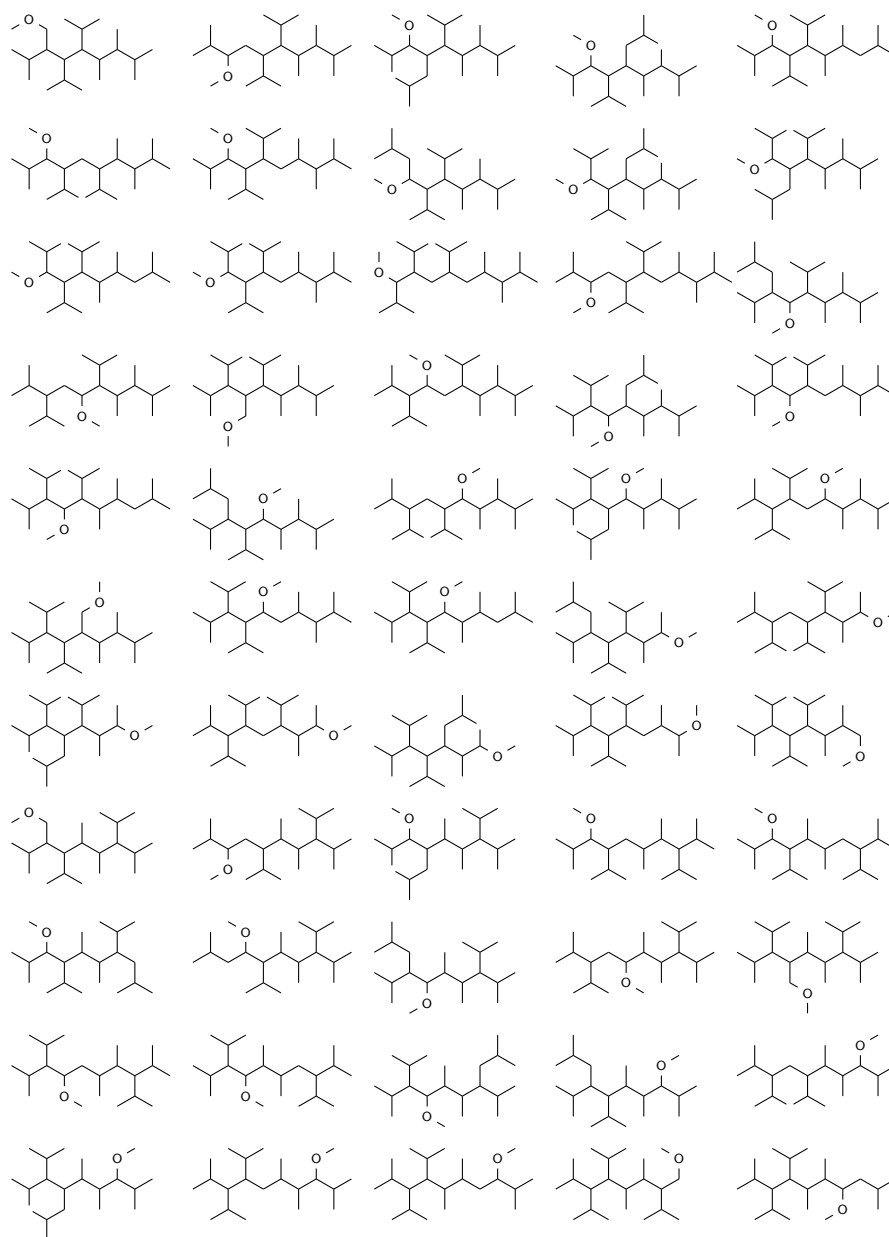


Figure E.4: Complete List of isomers of compound C.